



# University of HUDDERSFIELD

## University of Huddersfield Repository

Hamed, Moamar

Characterisation of the Dynamics of an Automotive Suspension System for On-line Condition Monitoring

### Original Citation

Hamed, Moamar (2016) Characterisation of the Dynamics of an Automotive Suspension System for On-line Condition Monitoring. Doctoral thesis, University of Huddersfield.

This version is available at <http://eprints.hud.ac.uk/id/eprint/29088/>

The University Repository is a digital collection of the research output of the University, available on Open Access. Copyright and Moral Rights for the items on this site are retained by the individual author and/or other copyright owners. Users may access full items free of charge; copies of full text items generally can be reproduced, displayed or performed and given to third parties in any format or medium for personal research or study, educational or not-for-profit purposes without prior permission or charge, provided:

- The authors, title and full bibliographic details is credited in any copy;
- A hyperlink and/or URL is included for the original metadata page; and
- The content is not changed in any way.

For more information, including our policy and submission procedure, please contact the Repository Team at: [E.mailbox@hud.ac.uk](mailto:E.mailbox@hud.ac.uk).

<http://eprints.hud.ac.uk/>

# **Characterisation of the Dynamics of an Automotive Suspension System for On-line Condition Monitoring**

**MOAMAR HAMED**

A thesis submitted to the University of Huddersfield in partial fulfilment of the requirements  
for the degree of Doctor of Philosophy

The University of Huddersfield

May 2016

## **Copyright Statement**

- I. The author of this thesis (including any appendices and/or schedules to this thesis) owns any copyright in it (the “Copyright”) and s/he has given The University of Huddersfield the right to use such copyright for any administrative, promotional, educational and/or teaching purposes.

## Abstract

As the most critical system that determines the driving performance, passenger comfort and road safety of a vehicle, the suspension system has not been found to have adequate monitoring systems available to provide early warnings of possible faults online. To fill this gap, this study has focused on the investigation of the dynamic behaviour of the suspensions upon which a new on-line condition suspension monitoring approach was proposed and verified under different conditions. Specifically, the approach quantifies the modal shapes which are obtained based on an improved modal identification applying to acceleration responses at the four corners of the vehicle. To achieve this, the research was carried out by the means of dynamic modelling, numerical simulations, optimal measurement optimisations and subspace identification improvements based on a representative vehicle system, cost-effective measurement techniques and road standards.

Firstly, a mathematical model with a seven degree-of-freedom (7-DOF) was developed in account of variable stiffness and damping coefficients, being applicable for computer simulation of the dynamic interaction between a vehicle and a road profile. To validate the proposed model during real operation, this study investigates a set of on-road experiments, to measure the acceleration of the vehicle body. Comparisons between the experimental and simulation paths demonstrated that, simulation results and measured on road results were found to be almost have similar trend.

In the simulations the modal parameters (obtained theoretically) of a vehicle are: natural frequency, damping ratio and modal shapes and their characteristics are characterised under the influence of different suspension faults and operating conditions (loads and speed). It has found that the modal shapes are more independent of operating conditions and thereby reliable as indicators of faulty suspensions, compared with modal frequency and damping which are influenced more by operating conditions. Furthermore, the modal shape difference between left and right side responses are developed as the fault severity indicator.

To obtain the modal shapes online reliably, an improved stochastic subspace identification (SSI) is developed based on an average correlation SSI. Particularly the implementation of optimal reference channels is achieved by comparing the average correlation signals which can be more efficient due to much smaller data sizes, compared with that raw data based spectrum analysis method used in original development.

On road verification based on a commercial vehicle operating in normal road conditions shows that common suspension faults including inadequate damping faults and under-inflation of the tyre, induced one of the four shock absorbers, can be detected and diagnosed with acceptable accuracy. Therefore, it can be deduced that the SSI modal shape based detection techniques are effective and therefore promising to be used to diagnose and monitor the suspension system online.

## **Declaration**

No portion of this work referred to in this thesis has been submitted in support of an application for another degree or qualification of this or any other university or other institute of learning.

*(MOAMAR HAMED)*

## **Dedication**

*In the Name of Allah, the Most Beneficent, the Most Merciful*

*To the soul of my dear father,*

*To my lovely mother, to my family, for their encouragement and continues  
support.*

## Acknowledgements

First and foremost, I would like to thank my **ALLAH** the Almighty for his helping me to finish this research and present it on time.

Secondly, I would like to thank my academic supervisors **Prof. Andrew Ball** and **Dr. Fengshou Gu** for the endless support, valuable suggestions, and their motivation, that they have afforded me all along the course of this research. Special thanks for their good support and their positive comments and continuous supervision during each stage of this thesis. They are also a source of inspiration throughout my research study and in my academic life. Most vital of all, they provided me immense knowledge and enthusiasm in various ways to achieve my target.

Besides my supervisors, I would like to pass my thanks to **Dr. Belachew Tesfa** for his support and insightful help. Thank you so much for the time you spent to help me in the first stage of this research.

Deep appreciation to my families for their support and continues help especially to my mother for her endless love and endless assistance from when I was in my first stage study till now. Last, but by no means least, my special thanks, love and deep indebtedness to my wife and my children: **Ysmen, Maoda, Amira, Abd Alaziz** and **Abd Alhadi**, for their nice smile and patience over the years of this study, also for their love and innocent smiles that have made the hardship of this task bearable. I promise you to make the coming years with much more fun. My deep love and thanks are due to my brothers, sisters, and the entire family.

# Table of Content

Copyright.....	1
<b>Abstract.....</b>	<b>2</b>
Declaration.....	4
Dedication.....	5
Acknowledgment.....	6
Table of content.....	7
List of figures.....	11
List of Tables.....	16
List of Abbreviations.....	17
List of Notations.....	19
List of publication.....	20
<b>1 CHAPTER 1: Introduction.....</b>	<b>21</b>
1.1 Background of Automotive Suspension.....	22
1.2 Historical Perspective of Suspension Systems.....	22
1.2.1 Dependent Suspension Systems.....	23
1.2.2 Independent Suspension Systems.....	23
1.3 Suspension System Functions.....	25
1.4 Suspension System Performances.....	26
1.5 Vehicle body dynamics (Bounce, pitch and roll motion).....	27
1.6 Introduction to Condition Monitoring.....	29
1.6.1 Vibration-Based Condition Monitoring.....	30
1.7 Vibration Parameters.....	31
1.8 Analysis of Surface Vibration Signal.....	33
1.8.1 Time-Domain Analysis of Vibration Signal.....	33
1.8.2 Frequency-Domain Analysis of Vibration Signal.....	34
1.9 Common Faults in Suspension Systems.....	35
1.10 Sensitivity of Model Parameters to Changes in Fault Conditions of the Suspension	38
1.11 Summary Technical Gaps and Motivation.....	39
1.12 Research Aim and Objectives.....	40
1.13 Thesis Structure and Organisation.....	41

<b>2</b>	<b>CHAPTER 2: Review of Suspension Diagnosis Methods .....</b>	<b>45</b>
2.1	Introduction .....	46
2.2	Model-Based Fault Detection and Diagnosis Methods.....	46
2.2.1	Parameter Estimation Methods .....	46
2.2.2	Observers and State Estimation .....	47
2.2.3	Parity Equations .....	47
2.3	Signal Spectrum Estimation .....	48
2.4	Fault-Diagnosis Methods .....	48
2.5	Review of Suspension Fault Diagnosis .....	48
2.6	Review on Modelling of Suspension .....	51
2.7	Effect of Tyre Pressure on Suspension Performance .....	52
2.8	Summary .....	54
<b>3</b>	<b>CHAPTER 3: Mathematical Models of a Four Wheel Vehicle.....</b>	<b>55</b>
3.1	Introduction .....	56
3.2	Suspension System Model and Dynamics .....	56
3.3	State Space Based Solutions of the Model.....	60
3.4	Assumptions and Limitations.....	61
3.5	Validation and Vehicle Dynamics Simulation Models .....	62
3.6	Theoretical Background of Impulse Response Function .....	64
3.6.1	Impulse Validation of the Model .....	65
3.7	Road Profile Excitation .....	66
3.8	Classification of Road Profiles.....	66
3.9	Calibration of the Model for Non-Stationary Inputs.....	68
3.10	Calibration of the Model for Stationary Inputs .....	69
3.10.1	Random Road Profiles .....	69
3.11	Calibration of the Model for Stochastic Subspace Identification (SSI) .....	73
3.11.1	Simulation Modal Parameters of the Vehicle by SSI .....	73
3.11.2	Measured Modal Parameters of the Vehicle by (SSI) .....	74
3.12	Summary .....	75
<b>4</b>	<b>CHAPTER 4: Simulation Results for Modal Characteristics of Suspension.....</b>	<b>77</b>
4.1	Introduction .....	78
4.2	Simulation Results for the 7-DOF Vehicle Model.....	78
4.3	Modal Shape Characteristics under Different Defects .....	80

4.3.1	Simulation of Damping Reduction .....	81
4.3.2	Simulation of Tyre Pressure Changes.....	82
4.3.3	Simulation of Spring Weakness.....	84
4.4	Suspension Performances Analysis Using Deterministic Inputs .....	85
4.5	Road Profile for Non-stationary Input .....	85
4.6	Model Simulation Conditions for Non-stationary Input .....	86
4.7	Effects of Bump's Geometry on Suspension Performance.....	86
4.8	Effects of Vehicle Speeds on Suspension Performance.....	90
4.9	Influences of the Suspension Parameters on Suspension Performance .....	91
4.9.1	Effects of Damper Faults on Suspension Performance.....	91
4.9.2	Effects of Under-Inflation Tyre on Suspension Performance.....	94
4.10	Summary .....	97
<b>5</b>	<b>CHAPTER 5: Subspace-Based System Identification and Fault Detection.....</b>	<b>98</b>
5.1	Introduction .....	99
5.2	Operational Modal Analysis (OMA) Methods .....	100
5.3	The General Stochastic Subspace Identification (SSI) Frameworks .....	102
5.4	Eigen Realisation Algorithm (ERA) and Data Correlation.....	105
5.5	Average Correlation Signal based Stochastic Subspace Identification (Acs-SSI)..	107
5.6	Summary .....	109
<b>6</b>	<b>CHAPTER 6: Performance Verification of ACS-SSI Using Simulated Datasets ..</b>	<b>111</b>
6.1	SSI Simulation Results Using Accelerations of the Body as Input .....	112
6.2	Validation under Normal Conditions .....	112
6.3	Validation under Abnormal Damping.....	118
6.4	Validation under Abnormal Spring .....	118
6.5	Summary .....	119
<b>7</b>	<b>CHAPTER 7: FRF Based Offline Identification of the Test Vehicle.....</b>	<b>120</b>
7.1	Introduction .....	121
7.2	Frequency Response Function for a Single Degree of Freedom (SDOF) System ..	121
7.3	Vibration Isolation.....	125
7.4	Transmissibility of Suspension Systems .....	126
7.5	Experimental Investigation for FRF Measurements .....	128
7.5.1	Experimental Facilities .....	129
7.5.2	Measurement Instrumentation .....	130

7.6	Test Procedures .....	132
7.7	Results and Discussion.....	134
7.7.1	Calculation of the Centre of Gravity (COG) of the Test Vehicle .....	138
7.8	Summary .....	140
<b>8</b>	<b>CHAPTER 8: On-road Experimental Investigation .....</b>	<b>141</b>
8.1	Introduction .....	142
8.2	The Effect of Tyre Pressure on Suspension Performance.....	142
8.2.1	The Test Car Specification.....	143
8.2.2	Wireless Measurement Instrumentation .....	143
8.2.3	Test Procedures .....	146
8.3	Results and Discussion.....	147
8.3.1	Influence in Time Domain .....	148
8.3.2	Influence in the Frequency Domain.....	149
8.3.3	Influence of Vehicle Speed on Suspension Response .....	150
8.4	Summary of Experimental Studies based Bumped Road.....	151
8.5	Characterisation of the Modal Responses to Different Defects .....	151
8.5.1	The Test Car Specification.....	152
8.5.2	Measurement Instrumentation .....	152
8.5.3	Test Procedures .....	154
8.6	Diagnostic Results for Suspension Defects.....	156
8.6.1	Vehicle body Vibration Responses.....	156
8.6.2	Modal Shape Based Detection Technique for Tyre Pressure Change .....	159
8.6.3	Modal Shape Based Detection Technique for Damping Variation .....	160
8.7	Summary of Experimental Studies based on Standard Roads .....	161
<b>9</b>	<b>CHAPTER 9: Conclusions and Future Work .....</b>	<b>162</b>
9.1	Thesis Objectives and Achievements.....	163
9.2	Conclusions on Characterisation of the Dynamics of an Automotive System for On-line Condition Monitoring.....	167
9.2.1	Conclusions on Suspension System Models.....	167
9.2.2	Conclusions on Experimental Studies .....	168
9.3	Novelties and Contribution to Knowledge.....	169
9.4	Future Work Recommendations for On On-Line Condition Monitoring of Suspension.....	170

## List of Figures

Figure 1-1: Hierarchy of popular suspension systems (Liu, 2008).....	24
Figure 1-2: Major components of the McPherson strut suspension system (Maher, 2011) ....	25
Figure 1-3: Sketch of a quarter car suspension .....	27
Figure 1-4: The bounce motion of the vehicle .....	28
Figure 1-5: The pitch motion of the vehicle .....	28
Figure 1-6: The roll motion of the vehicle .....	28
Figure 1-7: The three main steps in a condition monitoring system (Jardine et al., 2006) .....	29
Figure 1-8: The connection between vibration parameters.....	32
Figure 1-9: Common faults in suspension systems.....	36
Figure 1-10: Percentage of failures for different cars .....	37
Figure 1-11: Distribution of global injury by cause (Peden, 2004) .....	40
Figure 1-12: Flow chart of the modal shape based detection technique.....	42
Figure 2-1: Sketch of FDI (Patton et al., 2000) .....	47
Figure 2-2: UK Tyre Industry survey of 1072 tyres (Paine et al., 2007).....	53
Figure 3-1: Full vehicle models .....	57
Figure 3-2: Iterative process of calibrating the model .....	63
Figure 3-3: Schematic representation of linear input and output relation .....	64
Figure 3-4: Unit impulse function.....	65
Figure 3-5: Impulse response function for the four corners of the vehicle.....	65
Figure 3-6: Road Surface Profiling (Sayers & Karamihas, 1998).....	66
Figure 3-7: Road Surface Classification (ISO 8608) (Tyan et al., 2009). .....	67
Figure 3-8: Road profile in time domain .....	69
Figure 3-9: Vibration of suspension simulation and experiment for V= 8 km/h.....	69
Figure 3-10: Time domain for Random road profiles .....	71
Figure 3-11: Simulation of acceleration of the four corner of the vehicle in the time domain	71
Figure 3-12: Measured acceleration of the vehicle body (FL, FR, RL and RR) .....	72
Figure 3-13: Spectra of the vehicle body for measured and simulated vibration (FL).....	73
Figure 3-14: Mode shapes of the bounce, pitch and roll mode by SSI simulation.....	74
Figure 3-15: Measured mode shapes of the bounce, pitch and roll mode for vehicle body. ...	75
Figure 4-1: Frequency response function of the vehicle.....	79

Figure 4-2: Frequency response and mode shapes of bounce pitch and roll .....	80
Figure 4-3: Changes in natural frequency, damping ratio and mode shape for the bounce, pitch and roll modes for a damping reduction of the front left (F-L) shock absorber .....	81
Figure 4-4: Modal energy differences for bounce and pitch modes for each damper of the vehicle .....	82
Figure 4-5: Changes in the natural frequency, damping ratio and modal shape for under-inflation of the front left tyre .....	83
Figure 4-6: Modal energy differences for front and rear rolling of bounce and pitch modes .83	
Figure 4-7: Changes in the natural frequency, damping ratio and modal shape for a weakened rear right spring.....	84
Figure 4-8: Modal energy differences for bounce and pitch modes for each spring of the vehicle .....	85
Figure 4-9: Road profile in time domain plot .....	86
Figure 4-10: (a) Road profile excitation and (b) displacement of vehicle body for different bumps at vehicle speed 8 km/hr.....	87
Figure 4-11: (a) Road profile and (b) displacement of the body for different bumps at (V= 16 km/hr).....	87
Figure 4-12: Vehicle wheel's displacement with different road profile (bumps) at V= 8 km/hr .....	88
Figure 4-13: Wheel deflections for different bumps.....	89
Figure 4-14: Suspension travel for different bumps .....	89
Figure 4-15: Acceleration of the vehicle body with different road profile at (V= 8 km/hr)....	90
Figure 4-16: RMS of vehicle body with different speeds and different bumps.....	91
Figure 4-17: (a) Road profile excitation and (b) Displacement of vehicle body for different damping coefficients .....	92
Figure 4-18: Vehicle wheel's displacement with different damping coefficients .....	92
Figure 4-19: Wheel deflections for different damping coefficients .....	93
Figure 4-20: Suspension travel for different damping coefficients .....	94
Figure 4-21: Acceleration (on the left) and RMS (on the right) of the vehicle body for different damping coefficients .....	94
Figure 4-22: (a) Road profile excitation and (b) displacement of vehicle body for different tyre pressure .....	95
Figure 4-23: Vehicle wheel's displacement for different tyre pressure.....	95
Figure 4-24: Wheel deflections for different tyre pressures .....	96

Figure 4-25: Suspension travel for different tyre pressure .....	96
Figure 4-26: (a) Acceleration of the vehicle body with different tyre pressure and (b) RMS for acceleration of the body for different tyre pressure .....	97
Figure 5-1: sketch of the stochastic space model, with the $\Delta$ representing a delay (Peeters et al., 2000) .....	103
Figure 6-1: Verification of SSI model.....	112
Figure 6-2: Raw data of the displacement, velocity and acceleration of the bounce (V), pitch (P) and roll (R) of the vehicle and the four wheels (FL, FR, RL and RR) .....	113
Figure 6-3: Frequency response function of the bounce (V), pitch (P) and roll (R) of the body and the four wheels (FL, FR, RL and RR).....	114
Figure 6-4: Frequency response of the bounce (V), pitch (P) and roll (R).....	114
Figure 6-5: Correlation amplitude signals for all sensors .....	115
Figure 6-6: Stabilization diagrams for the vehicle.....	116
Figure 6-7: Mode shapes of the bounce, pitch and roll modes .....	117
Figure 6-8: Mean estimation errors of frequency and damping ratio for vertical, pitch and roll modes of the SSI model and the 7-DOF model .....	117
Figure 6-9: Estimation error for modal frequency and modal damping for different damping coefficients.....	118
Figure 6-10: Estimation error for frequency and damping for a range of spring rates .....	119
Figure 7-1: Frequency Response Function model (Irvine, 2000) .....	121
Figure 7-2: SDOF System and free-body diagram (Irvine, 2000).....	122
Figure 7-3: Bode Diagram magnitude and phase versus frequency for SDOF system .....	125
Figure 7-4: Bode diagram for different damping ratios (zeta).....	125
Figure 7-5: Vibration isolation; (a) force excitation and (b) motion excitation (Thomson, 1996) .....	126
Figure 7-6: Simplified version of the automobile suspension system .....	126
Figure 7-7: 4-Post simulator system and data acquisition layout .....	128
Figure 7-8: The test vehicle .....	129
Figure 7-9: Adjustable shock absorber from SPAX .....	130
Figure 7-10: Accelerometers and amplifier. ....	131
Figure 7-11: Data acquisition equipment (model YE6261B).....	132
Figure 7-12: (a) Sensor position on front wheels, (b) sensor position on rear wheels, and (c) sensor position on the shaker base. ....	133

Figure 7-13: Acceleration response and FRF corresponding to the vehicle body sensor 1 and the platform sensor 2.....	135
Figure 7-14: FRFs for the four corner of the vehicle.....	135
Figure 7-15: Quality factor or damping ratio by -3dB bandwidth.....	136
Figure 7-16: Natural frequency, damping ratio and transmissibility of FL-FR-RL-RR corners .....	137
Figure 7-17: Average static load of the vehicle .....	138
Figure 7-18: Force diagram of the vehicle.....	139
Figure 7-19: FRFs for the front left and front right wheel with different damping coefficients .....	140
Figure 8-1: Photo of the accelerometer and the table of specifications.....	143
Figure 8-2: Accelerometer position on the front left corner .....	144
Figure 8-3: Photo of the (DTPS) and the table of specifications.....	145
Figure 8-4: (DTPS) installed to the valve stem .....	145
Figure 8-5: Photos of the gateway and the Laptop .....	146
Figure 8-6: State diagrams of the wireless measurement system .....	146
Figure 8-7: Photo of the bump used.....	147
Figure 8-8: Sketch diagram for the bump .....	147
Figure 8-9: Time domain acceleration of the suspension and the pressure changes of the tyre when the car passes over the bump at speed of 8 km/hr.....	148
Figure 8-10: Power spectrum of vehicle body vibration with range of tyre pressures .....	149
Figure 8-11: RMS of vehicle body vibration at a range of speeds and at various tyre pressures .....	150
Figure 8-12: RMS for acceleration of the vehicle body at a range of vehicle speeds .....	151
Figure 8-13: Photo of four accelerometers (model CA-YD-104T) .....	153
Figure 8-14: Photograph of the preamplifiers.....	153
Figure 8-15: (a) Position of the front accelerometer and (b) Position of the rear accelerometer .....	155
Figure 8-16: Block diagram for the measurement system.....	156
Figure 8-17: Raw vibration signals and their spectra .....	157
Figure 8-18: Average scheme in the correlation lags domain for all sensors .....	158
Figure 8-19: Stabilization diagram of modal characteristics for baseline conditions.....	158
Figure 8-20: Mode shapes of the vehicle body .....	159
Figure 8-21: Modal energy differences corresponding to tyre pressure changes .....	160

Figure 8-22: Modal Energy Differences (MED) versus the damping changes for modes of the vehicle body ..... 161

## List of Tables

Table 1-1: Suspension faults and effects .....	37
Table 2-1: Common sensors used in laboratory vehicles (Chamseddine & Noura, 2008).....	51
Table 3-1: Vehicle parameters and values .....	62
Table 3-2: Road Roughness Classified by ISO (Tyan et al., 2009).....	67
Table 3-3: Road Roughness Expressed in Terms of $\Omega$ (Tyan et al., 2009) .....	68
Table 3-4 : Natural frequency and damping ratio for the SSI simulation.....	73
Table 3-5 : Natural frequency and damping for the measured data by SSI.....	75
Table 4-1: Natural frequency and damping ratio for the 7-dof vehicle model .....	78
Table 4-2: Model simulation conditions .....	86
Table 6-1: Frequency and damping ratio for the SSI model.....	113
Table 7-1: Specifications of the tested vehicle .....	129
Table 7-2: Specification of the accelerometers.....	131
Table 7-3: Experimental set up for damping change .....	134
Table 7-4: Natural frequency $f$ , damping ratio $\xi$ and transmissibility, TR, for four corners .....	137
Table 8-1: Experimental set up .....	146
Table 8-2: Specification of the vibration sensors .....	153
Table 8-3: Experimental setup for damping change .....	155
Table 8-4: Experimental set up for range of inflation pressures.....	156

## List of Abbreviations

CM	Condition monitoring
RMS	Root mean square
M.O.T	Ministry of transport
F-L	Front left
F-R	Front right
R-L	Rear left
R-R	Rear right
SDOF	Single-degree-of-freedom system
2-DOF	Second-degree-of-freedom system
4-DOF	Fourth-degree-of-freedom system
7-DOF	Seven degrees-of-freedom
Hz	Hertz
FDI	Fault detection and isolation
ISO	International organization for standardization
BS	British standard
AAP	Average Absorbed Power
PSD	Power spectral density
FFT	Fast Fourier transform
FT	Fourier transform
SNR	Signal-to-noise ratio
CF	Crest factor
PK	Peak value
SK	Skewness
KT	kurtosis
S	Standard deviation

CP	Power spectrum
DSA	Dynamic Signal Analyser,
FRF	Frequency response function
MR	Magneto-rheological damper
ADD	Acceleration driven damping
FTC	Fault-tolerant control
TWV	Three-wheeled vehicle
CO2	Carbon dioxide
IEA	International energy agency
WHO	World health organization
MED	Modal energy differences
P	Pitch
B	Bounce
R	Roll
SSI	Stochastic subspace identification
ACS-SSI identification	Average correlation signal based stochastic subspace
OMA	Operational modal analysis
FWD	Front wheel drive
TR	Transmissibility
COG	Centre of gravity
DTPS	dynamic tyre pressure sensor
SVD	singular value decomposition

## List of Notations

$m_s$	Vehicle body mass	[kg]
$m_f$	Mass of front suspension	[kg]
$m_r$	Mass of rear suspension	[kg]
$k_{fl}, k_{fr}$	Front spring stiffness	[N/m]
$k_{rl}, k_{rr}$	Rear spring stiffness	[N/m]
$c_{fl}, c_{fr}$	Front damping coefficient	[N.s/m]
$c_{rl}, c_{rr}$	Rear damping coefficient	[N.s/m]
$k_{tfl}, k_{tfr}$	Front tyre stiffness	[N/m]
$k_{trl}, k_{trr}$	Rear tyre stiffness	[N/m]
$I_p$	Pitch moment inertia of the body	[Kg $m^2$ ]
$I_r$	Roll moment inertia of the body	[Kg $m^2$ ]
$l_f$	Distance from front axle to the car CG	[m]
$l_r$	Distance from rear axle to the car CG	[m]
$w_f/2$	Half width of the front axle	[m]
$w_r/2$	Half width of the rear axle	[m]

## List of Publications

- **M. Hamed**, B. Tesfa, M. Aliwan, G. Li, F. Gu, and A. Ball, “The Influence of Vehicle Tyres Pressure on the Suspension System Response by Applying the Time-Frequency Approach,” in *Proceedings of the 19th International Conference on Automation and Computing (ICAC) 2013: Future Energy and Automation*, S. Qin, Y. Cao, and W. H. Chen, Eds. London, UK: Brunel University, 2013.
- **M. Hamed**, B. Tesfa, F. Gu, and A. Ball, “A study of the influence of vehicle tyre pressure on suspension system response using a full car model,” in *Proceedings of Computing and Engineering Annual Researchers’ Conference 2013 : CEARC’13*, G. Lucas, Ed. Huddersfield: University of Huddersfield, 2013, pp. 7–12.
- **M. Hamed**, B. Tesfa, F. Gu, and A. Ball, “Condition Monitoring Development for a Vehicle Suspension System Considering a Range of Vehicle Speeds and Bump Sizes,” VETO MACX\_2014 conference, Manchester University.
- **Hamed, M.**, Tesfa, Belachew, Fengshou, Gu and Ball, Andrew (2014) A study of the Suspension System for the Diagnosis of Dynamic Characteristics. In *Proceedings of the 20th International Conference on Automation & Computing, Cranfield University, Bedfordshire, UK, 12-13 September 2014*
- **Hamed, M.**, Tesfa, Belachew, Gu, Fengshou and Ball, Andrew (2014) Effects of Tyre Pressure on Vehicle Suspension Performance. In: *World Symposium on Mechanics Engineering & Applied Physics (WSMAEP’14)*, 18th - 20th June 2014, Sousse, Tunisia.

# CHAPTER 1

## INTRODUCTION

*This chapter presents a general background of automotive suspension systems. Firstly, the background and motivation of this research work are presented; secondly, existing maintenance strategies and condition monitoring techniques are discussed; and finally, the objectives and organisation of this research are outlined.*

## **1.1 Background of Automotive Suspension**

Vehicle suspension system is defined as a system of springs, shock absorbers and linkages connecting a vehicle chassis to its wheels (Liu, 2008). In past, suspension mechanisms were only installed between the chassis and the wheelbase or axles. There was hence no vibration isolation provided between the chassis and the automobile body/cabin. With increasing demand for comfort in the competitive automobile market it has now become common to provide some form of vibration isolation between the chassis and the passenger cabin. In general, suspension systems uses the idea of restoring and damping by using springs and shock absorbers (Smith & Zhang, 2009).

The suspension is required to support the vehicle body, to absorb road shocks to protect the passengers, and to provide steering control during heavy braking. Notionally, if a road was with no abnormalities, suspension would not be needed. Unfortunately, typical roads are rarely flat. Without suspension, a motor vehicle travelling at today's speeds would not only be uncomfortable, it would be unsafe for passengers and damaging to the vehicle. The suspension is designed to maximise the frictional contact between the road surface and vehicle's tyres to obtain significant and safe driving (Maher, 2011). It is also designed to provide the passengers with comfortable ride.

## **1.2 Historical Perspective of Suspension Systems**

Mechanical shock absorbers were first installed in automobiles by Mors of Germany in 1901 (Zulkifli, 2012). The early automotive suspension typically employed leaf springs as a means for isolating vibrations because they are simple, robust and cost effective. For example, Henry Ford's Model T employed one leaf spring at each axle (Fijalkowski., 2011). Even today, leaf springs are used on the suspensions of heavy vehicles and trucks (Sabarirajan., 2015). The passenger cars of today do not employ leaf springs as they have inherent limitations in low-weight applications. Coil springs and torsion bars are therefore replacing the leaf springs in current passenger vehicles. The first coil spring patent was granted to R. Tredwell in 1763 (British patent No.792) (Fijalkowski, 2011). In 1934, most automobile manufacturing companies began to use coil spring suspension for the front wheels, with each wheel suspended individually. After World War II, coil springs were installed for the front wheels in all automobiles, and until now coil springs are still used in vehicles because of their good performance (J. Wang, 2012). Torsion bar suspensions have advantages over coil springs when space is limited. Torsion bars were first employed on a 1921 Leyland vehicle. After Dr

Ferdinand Porsche standardised the torsion bar suspension system in 1933, Volkswagen started using torsion bar suspension. Indeed the current models of Volkswagen Beetle are still using the torsion bar suspension systems (Grieger & Gutzmann, 2015). Another important type of mechanical system that is used to arrest vibrations is pneumatic suspension, usually known as air suspension (J. Wang, 2012). Pneumatic suspension systems use air springs rather than the traditional mechanical coil springs or torsion bars. Generally, suspension systems can be presented as dependent and independent suspension systems. Figure 1-1 shows a diagram for the common suspension types.

### **1.2.1 Dependent Suspension Systems**

Dependent suspension generally has two main types include single or tandem axle suspension systems. the most common types for typical single axle suspensions can be as leaf spring and trailing arm suspension (Jain & Asthana, 2002; Fitch, 1994). In this type of suspension, one or more trailing arms are used to connect the wheel axle to the chassis, with swinging up and down for the rear parts of the system. Coil springs have traditionally been used in this system, but recently the conventional coil spring has been replaced with an air spring. This is powered by an air pump or compressor, which is driven either directly from the engine or electrically. This pump compresses a volume of air and uses the pressurised air as a spring. (Sternberg, 1976).

In order to obtain more weight capacity, the single axle can be extended to a tandem axle which can be carpeted by connecting some of axles close together. This advantage of increasing the capacity lead to widely using the tandem axle in heavy duty trucks and trailers (Fenton, 1996).

### **1.2.2 Independent Suspension Systems**

Independent suspension systems are based on the idea of allowing each wheel to move independently without any connection with the other side of the vehicle. This type of suspension offer superior characteristics of comfortable ride and stability. McPherson strut, trailing arm suspension and double wishbone suspension are the most modern independent suspension systems. (Jain & Asthana, 2002; Fitch, 1994). Independent trailing arm suspension and the dependent suspension have almost similar function. The difference between the two systems can be presented as each wheel hub is connected only to a trailing arm without using solid axle connecting the other wheels. Double wishbone suspension, designed to locate each wheel by using two wishbone-shaped arms (A-arms).

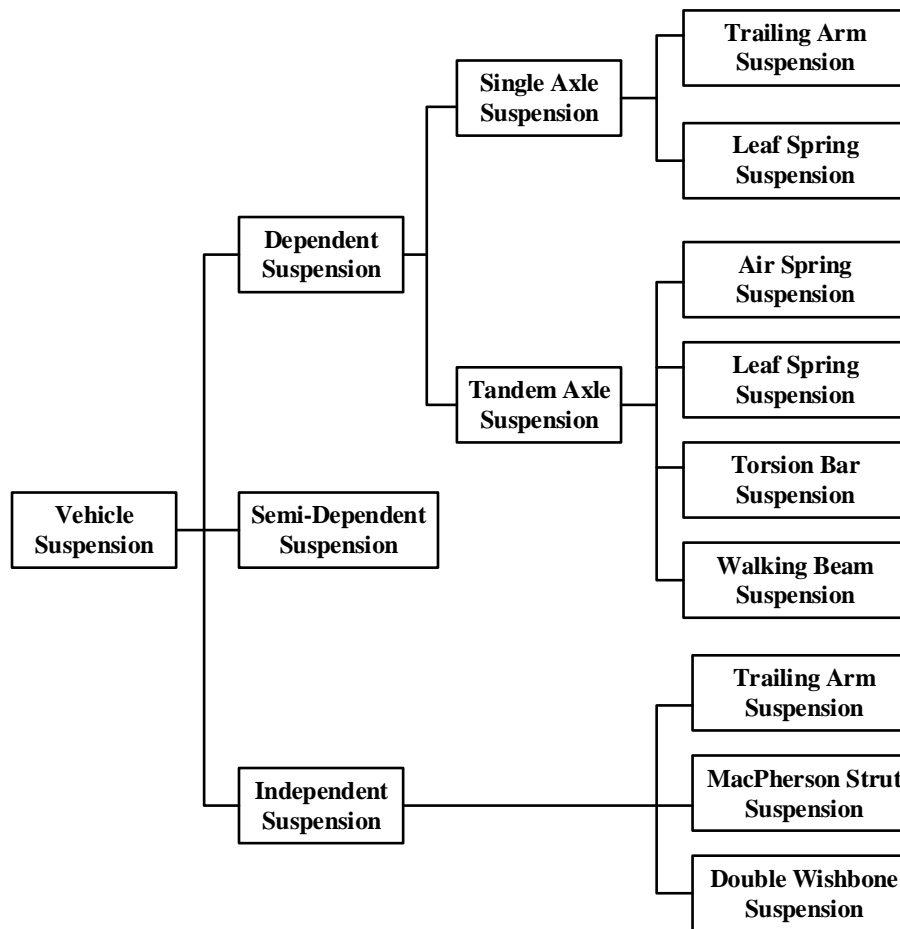


Figure 1-1: Hierarchy of popular suspension systems (Liu, 2008)

The design of this system is to enclose the damper inside a coil spring and connecting this system to the suspension arm. In fact, the McPherson strut system can show more interest as the most suspension system used in today's vehicles.

The most focus of this research will be on independent suspension and in more specific on the MacPherson Strut suspension. The McPherson strut suspension was first designed in 1940s by Earl Steele Macpherson (Andersen, 2007). Ford Vedette was first used The McPherson strut in the 1949 (Gilles, 2005). This system is popular in road vehicles because of it has advantage of compact size and also secure (Cronin, 1981) (C. Kim et al., 1999).

Figure 1-2 shows the main components of the suspension. The shock absorber, which consists of spring and damper elements, protects the vehicle from high accelerations and impact forces resulting from the road irregularities. The generated spring force depends upon the range of wheel travel. The damper's purpose is to regulate the rate of energy release from the spring. This improves road holding by ensuring the wheels do not bounce off the road. However, the resistance of the damper to sudden movements means that some components of the impact

forces reach the passenger. The selection of springs and dampers thereby represents a balance between the demands of handling and ride comfort (Matschinsky, 2000).

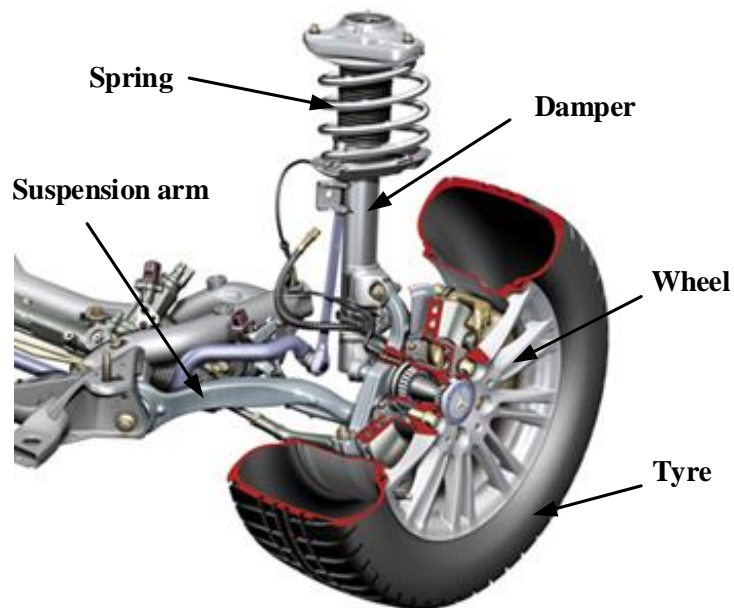


Figure 1-2: Major components of the McPherson strut suspension system (Maher, 2011)

Another form of suspension system can be classified depend on the external input to a suspension, which can be presented as Passive, Semi-active or Active suspension (Daniel Fischer & Isermann, 2004). The traditional suspension which known as passive suspension which did not consist of any controller to control the spring and the shock absorber. However the semi-active suspension system uses the idea of changing the damping rates (Patil et al., 2013). Active suspensions have a different strategies by injecting energy in to the system, In general the passenger cars today use passive suspension systems, so these are the type that will be studied in this research.

The suspension is linked to the tyres, which provide traction between the vehicle and the road while driving. Tyres are responsible to transmit all the drive and steering forces to the road through the friction of a very small contact patch (Hamed et al., 2013 & Matschinsky, 2000).

### 1.3 Suspension System Functions

The primary function of the suspension system is to maximise the stability, safety and manoeuvrability of the vehicle. The suspension system acts to maintain a good contact between the tyres and the profile surface, providing more stable vehicle, and protecting the driver and passengers from the shocks generated by uneven terrain (Lajqi & Pehan, 2012; Vivekanandan et al., 2014). The suspension system works together with the tyres, wheels, frame, suspension

linkages, wheel hubs, brake system and steering system to provide driving comfort and stability.

Suspension systems performance has more interest in recent years due to continued research and advancement in this field. A suspension system is considered to be ideal if the vehicle body is completely isolated from an uneven road and from the inertial shocks when the vehicle is cornering, braking (Lajqi et al., 2012).

The suspension system must also be able to minimise the vertical force transmitted to passengers in order to maximise their comfort and security. The objectives of using suspension systems can be achieved by minimising the acceleration of the car body. A heavily damped suspension will give a good vehicle handling, but the car operator may not be comfortable and damage may occur to the car. Conversely, low damping will give a more comfort to the passengers, but it will affect negatively the vehicle's stability. The traditional suspension of automobiles can represent a trade-off between these two conflicting criteria. Thus to optimise the balance between comfort and safety requirements at any given time, it is beneficial to adjust the damping factor dynamically with respect to a given road surface (Patil et al., 2013).

#### **1.4 Suspension System Performances**

In general, there are some factors to evaluate the performance of the suspension include ride comfort, stability and road handling (Wong, 2001). The vehicle body acceleration is related to ride quality, while road handling is can be identified by the displacement between the tyres and the vehicle body. While, the stability of a vehicle is related to how much the tyre is contacted the ground. The main concern in almost of researches is the fact that, how to improve these three parameters (Eslaminasab & Golnaraghi, 2009). Several important factors must be considered in order to analyse the vehicle's handling, stability, and ride quality. The factors of interest are the travel of suspension, wheel deflection, and the vehicle's acceleration. Each of these parameters should ideally exhibit a low amplitude in their fluctuations (Zohir, 2009; Aly & Salem, 2013; Nouby M Ghazaly, 2014;). Vehicle handling is depend on the measured distance from the suspension to the profile surface ( $z_u - z_r$ ). This manifests as movements of the wheel, as illustrated in Figure 1-3. The displacement of the vehicle body related to the vehicle wheel ( $z_s - z_u$ ) is known as Suspension travel, also illustrated in Figure 1-3. Suspension travel can be used to assess the space requirements for accommodating a suspension spring. Ride comfort quantifies the passengers' perception of the movement of the vehicle. This requires that the body acceleration is to be small. ISO: 2631-1-1997 (Mitra et al.,

2013) states that for proper road handling the wheel deflection must be around 0.051 m, while the standard suspension travel value should be close to, and not lower than, 0.127 m. It is generally accepted that the passenger feels high levels of comfort when the RMS of the body is less than  $0.315 \text{ m/s}^2$ .

According to Rehnberg (2008), there are four methods of evaluating suspension performance, that are used recently. The ISO 2631 is the most commonly used international standard for vibration evaluation. In addition, there are three other national standards which are common: the British BS 6841, the German VDI 2057, and the Average Absorbed Power (AAP). These are all largely similar to the ISO 2631-1 standard.

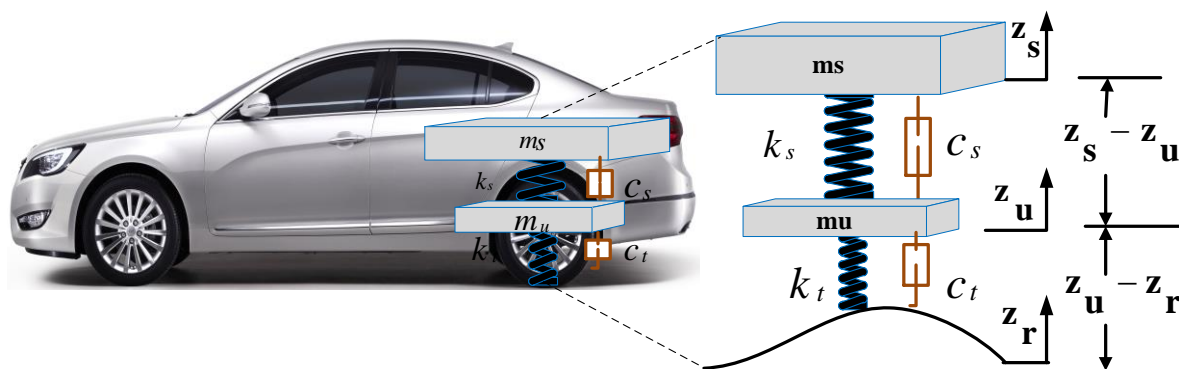


Figure 1-3: Sketch of a quarter car suspension

With today's development of using use computer software in automobiles industries, and the using of different measurement systems to assist the vehicle vibrations (Fleming, 2001; Prosser, 2007), they become easy to collect and record the data of suspension vibration during vehicle operation. In addition, condition monitoring of vehicle's systems can help in developing an effective methods to monitor the breakdown and faults in order to prevent damage of the vehicle components and increase safety. Therefore, the changes in suspension performances can be used to detect the faults and use the acquired design knowledge in future system developments for condition monitoring of suspension systems.

### 1.5 Vehicle Body Dynamics (Bounce, Pitch and Roll Motion)

The full model of the vehicle usually includes seven degrees of freedom; three relating to the vehicle body (bounce, pitch and roll) and four relating to the wheels (vertical displacement). The bounce mode is typically defined as a vertical motion of the vehicle body, experienced at the centre of gravity. This is a translation of the vehicle body along the Z-axis, as shown in Figure 1-4

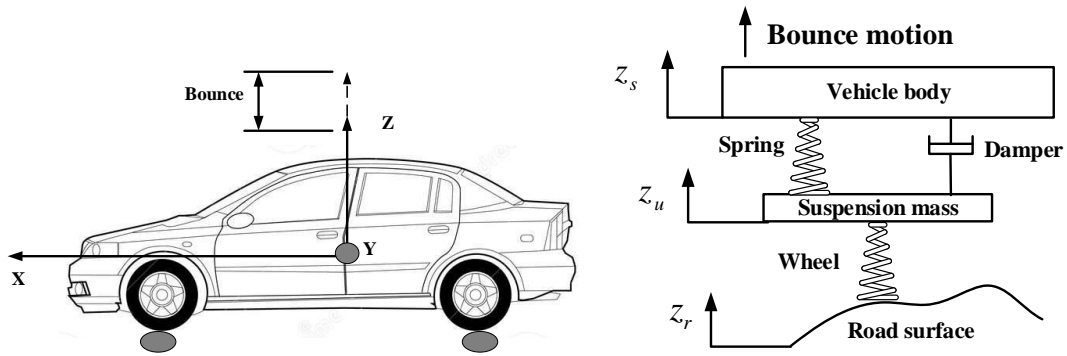


Figure 1-4: The bounce motion of the vehicle

The pitch mode is defined as a rotation of the body about a lateral axis (the Y-axis). Figure 1-5 represents the pitch inertia of the sprung mass, and shows that the front and rear ends of the vehicle are allowed to move independently. Figure 1-5 shows that the motion of the body can be represented as a 2-DOF system. The two DOFs are the pitch angle,  $\theta$ , and the vertical displacement,  $Z$ .

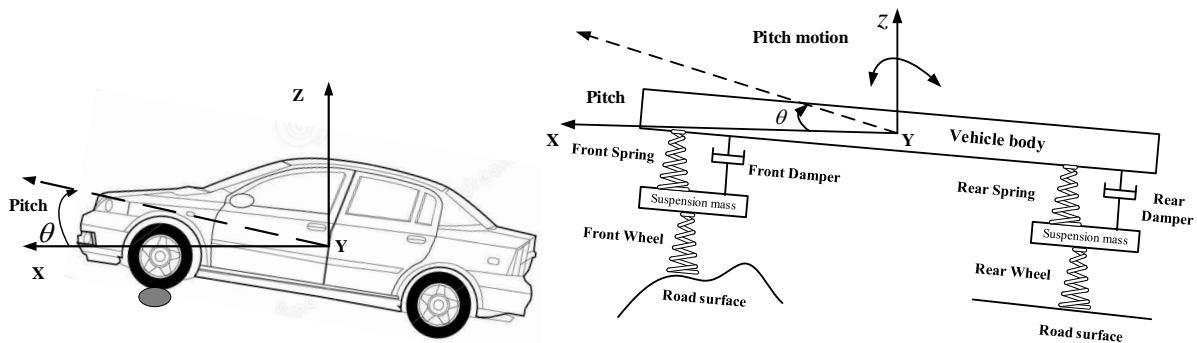


Figure 1-5: The pitch motion of the vehicle

The roll mode of the vehicle body is defined as a rotation of the vehicle around the longitudinal X-axis, as shown in Figure 1-6.

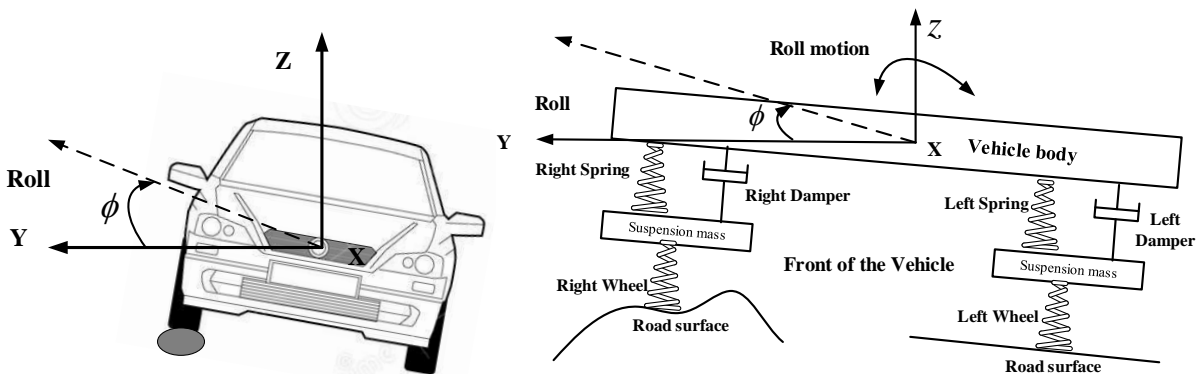


Figure 1-6: The roll motion of the vehicle

Gillespie (1985) showed that the pitch and bounce modes have a greater effect on the ride comfort than the roll mode. Additionally, the pitch was shown to be the most perceptible and hence the most annoying mode for passengers, and is therefore very important to control.

## 1.6 Introduction to Condition Monitoring

Condition monitoring can be defined as a process of continuous measurements of data to monitor the condition of a system or plant, which is then used to guide maintenance activities (Williams, Davies, & Drake, 1994). Condition monitoring concerns the gathering of data to enable better understanding of the health or condition of an item (McGrail, 1998). The condition monitoring for any machine is normally applied when this machine is in operating, and by measuring and analysing the signals which are collected in operation time, the current condition of this machine or plant will be assessed. The main objective of these processes are to decide when maintenances are needed and also to give more information about the faults and the time of occurring these faults. The assessment of the current condition of a system or item is carried out through the measuring of parameters which reflect the condition of a component.

By implementing condition monitoring, effective maintenance will be scheduled, and allows pre-emptive interventions to take place to avoid accidents before a failure occurs. The input provided to a condition monitoring activity is primarily the data obtained from various sensors. These data are used to schedule and carry out the maintenance actions, which are vital for the prevention of unforeseen stoppages and complete breakdown of the machine (Saeed, 2008). There are main three key steps for condition monitoring system: 1) Data acquisition (data collection) to indicate the condition of the system; 2) Data analysis in order to analyse the data to obtain a helpful information about the data; 3) Making the decision for Maintenance in order to recommend an efficient maintenance strategy (Zhen, 2012; Jardine, Lin, & Banjevic, 2006; Efthymiou, et al., 2012). These are shown in

Figure 1-7. Various types of data can be used for condition monitoring depending on the kinds of sensors used in the data acquisition system.

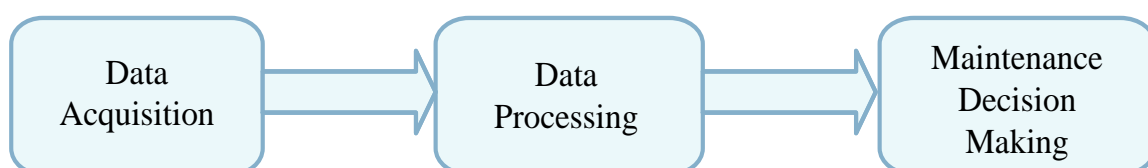


Figure 1-7: The three main steps in a condition monitoring system (Jardine et al., 2006)

The data can be measurements of vibration, acoustics, oil properties, temperature, pressure, moisture, humidity, and weather or environmental conditions. Different sensors can be used to collect each these data, such as accelerometers, pressure sensors, microphones, and acoustic emission sensors (Austerlitz, 2002; Jemielniak, 2014). Data processing is a vital step in any condition monitoring system. Its purpose is to better understand and interpret the data so that efficient maintenance policies may be proposed (Coulter, 2006). Many kinds of algorithms and techniques have been introduced to analyse the data obtained from data acquisition systems. There are numerous methods used for making maintenance decisions. Based on the types of data and the types of the sensors used for data collection, there are a variety of techniques that can, and should, be used for making maintenance decisions in a condition monitoring system (W. Wang, 2008).

- Vibration-based condition monitoring (Randall, 2011; Carden & Fanning, 2004; Fan & Qiao, 2011; Jayaswal, Wadhwani, & Mulchandani, 2008).
- Acoustic emission monitoring (Mba, 2006; Chang & Sun, 1988; Al-Ghamd & Mba, 2006).
- Acoustic-based condition monitoring (Weidong & Engineering, 2000; Gu, Li, Ball, & Leung, 2000).
- Current-based monitoring (Nandi, Toliyat, & Li, 2005; Tingtao et al., 2011).
- Visual inspection (Davies, 1998; Weidong & Engineering, 2000).
- Trend monitoring (Weidong & Engineering, 2000).

Generally, the aim of condition monitoring in vehicles is to reduce breakdowns. A commercial devices for condition monitoring to be implemented within a real vehicle includes the added goals of improving safety and reliability (Ngigi et al., 2012). Hence, an important action that must be taken is the selection of a suitable condition monitoring technique based on applicability to strongly nonlinear systems, robustness, sensitivity to disturbances, and computational performance. Subsequently, the following section (Section 1.6.1) presents a vibration-based condition monitoring technique in more detail for the purpose of condition monitoring of road vehicles.

### **1.6.1 Vibration-Based Condition Monitoring**

Vibration based condition monitoring is one of the widely used method, which based on using changes in the conditions of the system to indicate the system faults, by analysing the characteristics of the system in the time domain, frequency or modal domains, (Li, 2010). Vibration measurement is one of the common techniques used for condition monitoring, and a

powerful diagnostic for major process machinery (Jayaswal et al., 2008). The vibration signals generated by a machine are detected and analysed to determine the condition of the machine (Carden & Fanning, 2004). The correlations between mathematical models results and measured data results from the normal and up normal components, were used as early approaches for vibration monitoring. Farrar and Doubling (Weidong & Engineering, 2000) presented a compressive review in condition monitoring methods using vibration.

There are some advantages of using vibration measurements in condition monitoring (Charles R. Farrar, Doebling, & Nix, 2001). Firstly, vibrations will be as result of operating almost of machines while this machine is in operation. Secondly, the theoretical understanding of vibration mechanisms of most mechanical structures, will help to predict the characteristics of vibration responses due to particular faults. Thirdly, vibration instrumentation, such as wide using transducers and data equation system, are known to perform reliably. Finally, the availability signal processing methods and computing facilities, which can be easily analyse the vibration signals with accurate results.

## 1.7 Vibration Parameters

Machines and mechanical systems are expected to be exposed to vibration. In most cases this vibration is undesirable, and there are several problems can occur. Firstly forces and accelerations which act on the system are often indicated by the behavior of the system mass; if the mass has been moved from its original position, this motion will generate kinetic energy in the system. System stiffness is second element of the system, which is dependent upon force and displacement. In addition, damping can enable dissipation of the system's energy to control the mass vibration (Ertas, 2011). Using commercially available transducers, three parameters of vibration (displacement, velocity, and acceleration) can be measured. To understand and analyse the vibrations of any mechanical system it is helpful to know the relationship between displacement, velocity and acceleration. Displacement is defined as a measure of the distance that a vibrating body moves, while velocity is defined as a measurement of motion of a vibrating body. Acceleration is a measure of the rate of change in the velocity of a vibrating body (Ambekar, 2006). The equations representing these three parameters can be presented as:

$$x(t) = A \sin(\omega t) \rightarrow \text{Displacement} \quad 1-1$$

$$\dot{x}(t) = A \omega \cos(\omega t) \rightarrow \text{Velocity} \quad 1-2$$

$$\ddot{x}(t) = -A \omega^2 \sin(\omega t) \rightarrow \text{Accelerati on} \quad 1-3$$

To consider the physical significance of these equations, each of the above equations was plotted for one cycle in MATLAB and are shown in Figure 1-8, with zero displacement being used as the reference for time zero.

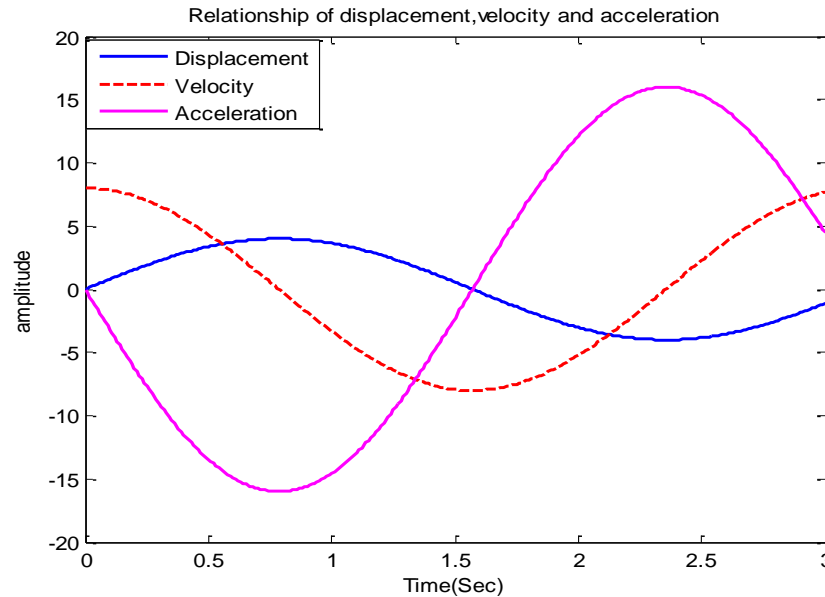


Figure 1-8: The connection between vibration parameters

- At time zero, the velocity is at its maximum value with displacement and acceleration at zero.
- 1/4 cycle later the velocity has reduced to zero with displacement at its maximum and acceleration at a maximum. In this case the mass has stopped momentarily at the peak of the cycle.
- At 1/2 cycle the velocity is at maximum value again (but in the negative direction) with displacement and acceleration again being zero and the mass passing its rest point (mean position).
- At 3/4 of the cycle the velocity has returned to zero and the displacement is at a maximum (negative) magnitude, with acceleration at a maximum in the opposite direction.
- The cycle is complete with displacement, velocity and acceleration at their original values.

The vibration signals can originate from many different sources, with each source generating its own signal. The resultant signal is the sum of the individual signals and is displayed as a composite signal. The machine condition can be determined by analysing the vibration signals

of undamaged and damaged components, and then detecting the changes (faults) by comparing between these signals.

## 1.8 Analysis of Surface Vibration Signal

The objective of the analysis of vibration signals is to obtain the vibration amplitude and the source of the vibration. Success in vibration analysis is related to the using of the data acquisition system and the processes of measuring the amplitude and frequency of the individual components' vibrations, relative phases, and trends of the overall vibration level (Shreve, 1995). Time and frequency domain techniques consist of waveform and statistical analysis (S. S. Rao, 2004).

### 1.8.1 Time-Domain Analysis of Vibration Signal

The time domain is the unprocessed signal obtained from the vibration transducer, and can be represented as a graph of vibration as a function of time. The time-domain signal is complex because it is the sum of all the individual frequency components that are present, and is a visual representation of the instantaneous value of the displacement. When performing fault diagnosis using the time-domain vibration signal, statistical methods are invariably applied. The most common statistical parameters are the root mean square (RMS), crest factor (CF), peak value (PK), skewness (SK) and kurtosis (KT) ( E. Y. Kim et al., 2007).

(RMS) is a measure of the signal energy. The RMS of variable  $X$  is the square root of the squared  $X$  value. For a set of data  $X_1, X_2 \dots X_n$ ,  $X_{RMS}$  is known as:

$$X_{RMS} = \sqrt{\frac{\sum_{i=1}^n X_i^2}{n}} \quad 1-4$$

Where  $X_i$ , is the  $i$ th value of variable  $X$ , and  $n$  is the number of data points.

The peak value (PK) is the maximum absolute value of the waveform. For a set of data  $X_1, X_2 \dots X_n$ , PK is being expressed as (E. Y. Kim et al., 2007):

$$X_{PK} = \max(|X|) \quad 1-5$$

Where,  $|X|$  the absolute value of  $X$ .

The crest factor (CF) is known as a number and sharpness of the peaks contains the signal and can be used to determine whether a signal contains repeated impulses. A high CF value

for the vibration signal would usually be an indication of a fault. The CF is the ratio of the peak value ( $X_{PK}$ ) to the RMS value ( $X_{RMS}$ ) of a waveform (E. Y. Kim et al., 2007):

$$CF = \frac{X_{PK}}{X_{RMS}} \quad 1-6$$

Kurtosis (KT) is a measure of whether the distribution of the data is peaked or relatively flat. Usually it is compared with the Gaussian or Normal distribution, for which the kurtosis is equal to 3. For data  $X_1, X_2 \dots X_n$ , the formula for kurtosis (relative to normal) is presented as (E. Y. Kim et al., 2007):

$$KT = \frac{\sum_{i=1}^n (X_i - \bar{X})^4}{(n-1)S^4} - 3 \quad 1-7$$

Where  $\bar{X}$  is the mean of data set and  $S$  is the standard deviation of the distribution, defined by (DeCoursey, 2003):

$$S = \sqrt{\frac{\sum_{i=1}^n (X_i - \bar{X})^2}{n}} \quad 1-8$$

If KT is negative then the distribution is flatter than the Gaussian, and if KT is positive it means the distribution is more peaked than the Gaussian.

### 1.8.2 Frequency-Domain Analysis of Vibration Signal

The frequency-domain of a signal (also known as a spectrum) describes the vibration signal as a function of frequency. Each component in a working machine will generate specific identifiable frequencies, and thus a given frequency spectrum can often be attributed directly to corresponding machine components (S. S. Rao, 2004).

Quefrequency domain or cepstrum analysis is the result of taking the Fourier transform of such a dB spectrum; it is the spectrum of the logarithmic power spectrum. If the power spectrum  $S_x(\omega)$  of the time signal  $x(t)$  is expressed as:

$$S_x(\omega) = |F\{x(t)\}|^2, \quad 1-9$$

then the power cepstrum,  $Cp_x(\tau)$ , is a real and can be obtained by inverse calculation of the Fourier transform of the square of the logarithm of the power spectrum of the signal (Norton & Karczub, 2003):

$$C_{P_x}(\tau) = F^{-1} \left\{ \log_{10} S_x(\omega) \right\}^2 \quad 1-10$$

Power cepstrum analysis is usually used as a complementary tool to identify components which are not readily identifiable by spectral analysis. Some of statics analysis is usually used to predict the signal contents of future events, e.g. the RMS amplitude of the time-domain vibration signal is monitored and plotted over time, and if the magnitude exceeds a certain critical level then remedial action is taken. However the vibration signal of a machine, while generated by the individual components, will also be affected by their assembly, installation and interaction.

### 1.9 Common Faults in Suspension Systems

The most common faults that can occur within the components of suspension systems are: (i) leaking or damaged shock absorbers, (ii) spring weakness, (iii) pivot and bushing wear, (iv) damaged main support member assembly, and (v) incorrect vehicle tyre inflation pressures (Hamed, Tesfa, Fengshou, & Ball, 2014). These faults are demonstrated graphically in Figure 1-9. Faults of the shock absorbers may occur in the form of any combination of the several factors: (i) seal wear, (ii) reduced oil volume caused by leakages, (iii) mount breakage and worn or extruded bushings. All of these factors can result in a reduction in shock absorber performance, causing braking distances to increase (Börner., 2002). This in turn leads to accelerated tyre wear, and reduced car handling when cornering (Weispfenning, 1997).

The spring failures can be occurred as: defects in the structure material such as inclusion in spring, also it can be as manufacturing defects, which appears as cracking, complex stress conditions and chemically induced failures. These defects can compromise the vehicle's load-carrying capacity (Prawoto, Ikeda, Manville, & Nishikawa, 2008). better contact between the wheels and the road can be as a result of using softer springs, to improve the dynamic performance of the vehicle (Sekulic & Dedovic, 2011), but an increase in the stiffness while passing over a bump leads to an increase in the pitch and roll values and also the maximum lateral and vertical acceleration of the vehicle (Zehsaz, Vakili-Tahami, & Paykani, 2014).

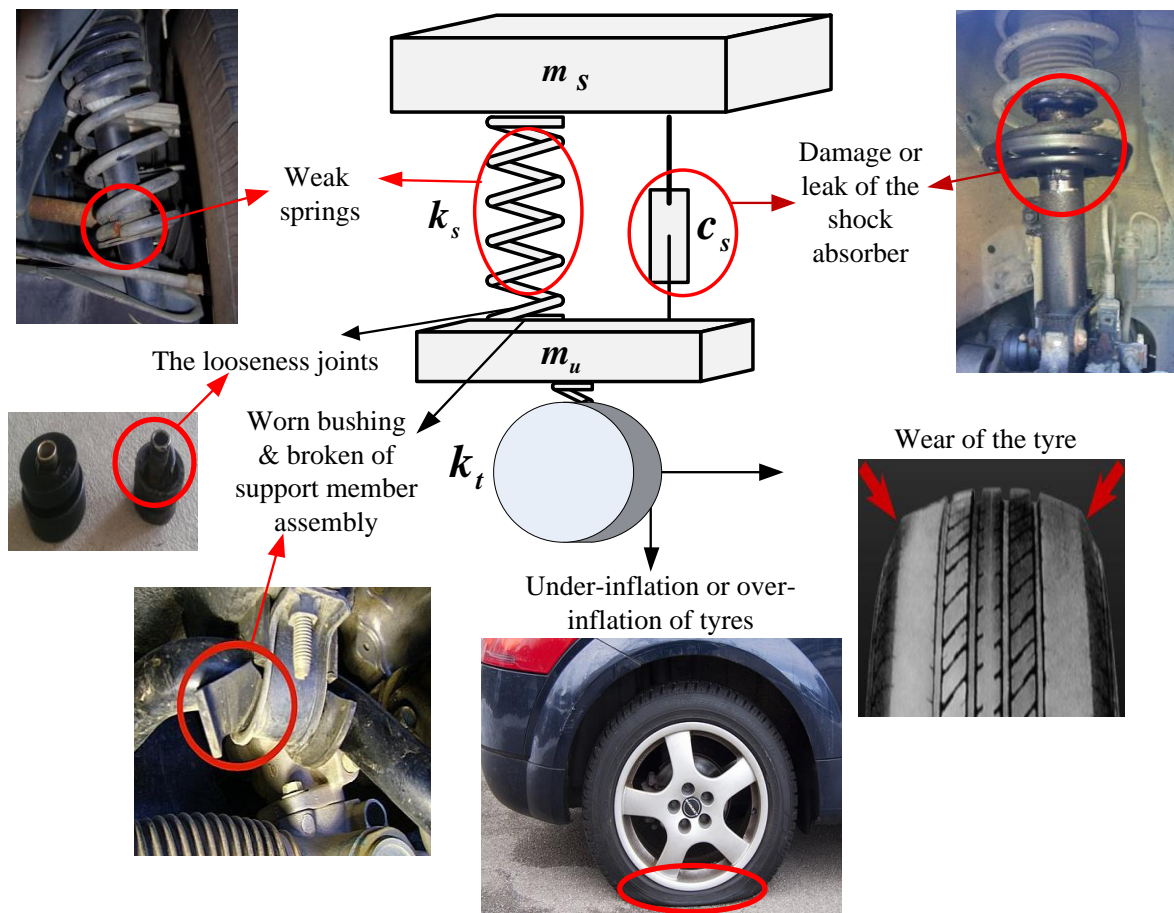


Figure 1-9: Common faults in suspension systems

The selection of a correct inflation pressure is critical to the successful operation of a tyre. If the tyre is operating at higher inflation pressure than that required, this can cause uneven tread wear, reduce the ride comfort, and decrease the stability. Similarly, Operating the tyre at under-inflation pressure can cause tread wear, destroy of the tyre's structure and can also degrade the car's performance (Daws, 2010). In addition, under-inflated tyres can cause higher fuel consumption which is responsible for environmental costs. The effects of some of these defects are summarised in Table 1-1.

Vehicle performance is often inhibited by the development of suspension faults. The early detection of abnormalities in vehicle suspension will lead to limitations of the damage inflicted on the vehicle during different conditions, and thereby improve the comfort and security of passengers.

Table 1-1: Suspension faults and effects

Fault condition	Effect
Faulty shock absorber	Uncomfortable ride, noise, vibrations, longer braking distances, tyre wear, reduced handling
Faulty coil spring	Vehicle leans toward the side, noise, uncomfortable ride, abnormal or excessive tyre wear
Air spring not inflated	Vehicle bouncing excessively, vehicle leans toward the side
Lateral rod deformation	Vehicle leans toward the side
Damage of lateral rod bushing	Vehicle leans toward the side, uncomfortable ride
Worn pivot bushing	Irregular tyre wear
Damage of trailing arm bushing	Vehicle leans toward the side, uncomfortable ride
Broken main support member assembly	Excessive driveline vibration, suspension is harsh or bumpy, looseness and cracks
Rear axle deformation	Vehicle leans toward the side
The looseness of joints	Noise
Under-inflation or over-inflation of tyre	Tyre tread wear, degraded ride comfort

The Ministry of Transport (M.O.T) in the UK checked vehicles for MOT tests of about 2.2 million vehicles in the period between October 2010 to October 2011 (John, 2010). Figure 1-10 show the percentage failure of different vehicles by category. The tests shows that the biggest failures of (19.79%) was associated with signalling and lighting problems, then suspension faults was (13.18%) and followed by tyre faults (8.75%).

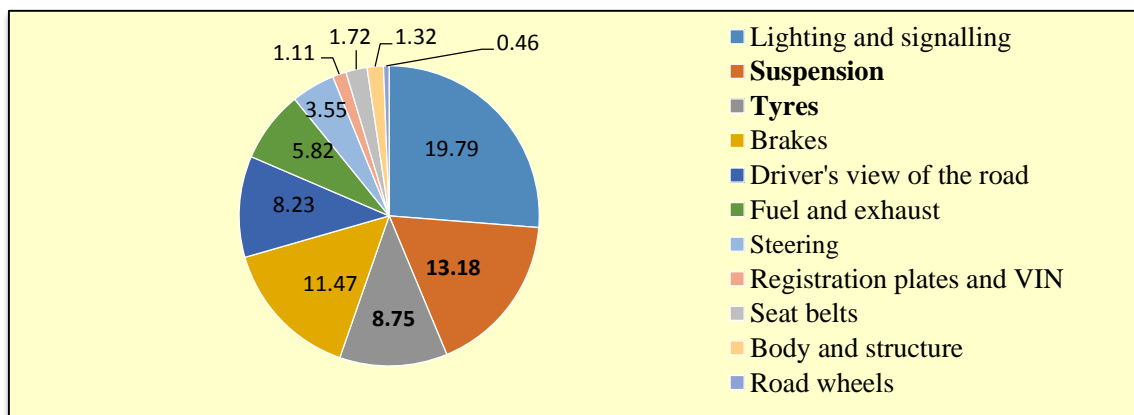


Figure 1-10: Percentage of failures for different cars

### 1.10 Sensitivity of Model Parameters to Changes in Fault Conditions of the Suspension

The complex interaction between the road surface and the vehicle has led to a need for an efficient method of fault detection in suspension systems. To solve this problem, and to enable the development of on-line condition monitoring for suspension systems, this study focused on the sensitivity of vehicle model parameters to changes in suspension fault conditions. These parameters include the natural frequency, damping ratio and modal shapes. They have been identified theoretically using the mathematical model, and also from measured vibration data using an analysis based on stochastic subspace identification (SSI). These parameters were also analysed whilst different suspension faults were simulated by (i) reducing damping coefficients, (ii) changing spring stiffness, and (iii) reducing each wheel's tyre inflation pressure.

Vehicle load conditions generally influence the damping ratio and natural frequency; and so these parameters are unsuitable for fault monitoring in suspension systems. Since the damping ratio and natural frequency depend strongly on the mass of the vehicle, the following equations suggest that a change in the vehicle mass can affect the damping and frequency values:

$$\det([M]\omega_n^2 + [K]) = 0 \quad 1-11$$

$$\omega_n = \frac{1}{2\pi} \sqrt{\frac{k}{m}} \quad 1-12$$

where  $m$  is the vehicle mass,  $k$  is the spring stiffness, and  $\omega_n$  is the system's natural frequency.

The damping ratio,  $\xi_i$  associated with each eigenvalue, is given by:

$$\xi_i = \text{real}(\lambda_i) / |\lambda_i| \quad 1-13$$

Additional parametric studies have indicated that the vehicle's mode shapes are less sensitive to the load, and more so to the suspension parameters, including damping, stiffness, and tyre inflation. This is because mode shapes are related to the inherent properties of a structure, which are independent of the applied loads and forces (Richardson et al, 1997). The mode shapes will thus be sensitive only to the boundary conditions and the system's material properties, such as damping and stiffness. Furthermore, mode shapes have no value and they therefore require no units. These facts enable the observation that modal shape based detection

can be an effective method for suspension faults diagnosis. For more details see Jazar (2014) and Richardson et al. (1997). The following equation can be used to calculate the mode shape:

$$[A - \lambda I]v = 0 \quad 1-14$$

where  $A$  is the state matrix of the system, and  $v$  is the eigenvector associated with each eigenvalue ( $\lambda$ ).

### **1.11 Summary Technical Gaps and Motivation**

This chapter has provided a general background of the design, functions, and performance of suspension systems. Condition monitoring was introduced, and some of numerous methods used for making maintenance decisions were presented including the vibration based condition monitoring method, which was adopted in this research. The common faults associated with suspension components have been discussed. The following chapter will present a comprehensive review of a common used methods for fault detection that have been used in several previous studies, in order to understand and develop an effective on-line condition monitoring system for suspensions.

Many methods of suspension system design and fault diagnosis techniques have been reported extensively in the literature review which presented in chapter 2. Model-based fault diagnosis approaches have been discussed and presented by several researches. In addition, many methods have been applied in practical suspension systems. However, on-line monitoring of a vehicle suspension under random operational conditions (on road) has not been covered by the researchers in depth. Most of the published research either develops mathematical models to analyse the performance of suspension, while others focus on the design of controllers for the suspension system to improve the suspension performance.

This study, therefore, will attempt to explore a new on-line condition monitoring approach for suspension based on comprehensive vibration modelling, optimal measurements and advanced analysis. The proposed methodology is based on a modal shape based detection technique for suspension that aims to monitor the suspension and diagnose faults when operating on the road. Due to the large number of vehicle accidents worldwide, passengers safety remains an important objective in the automotive industry moreover, good braking performance of vehicles always need for safety. It can be noted that, when the suspension system fails, the performance of the vehicle will be degraded and serious accidents may happen.

According to the World Health Organization (WHO, 2002) (Peden, 2004) road traffic injuries account for around 23% of all injury/ deaths worldwide as shown in the pie chart in Figure 1-11. Hence, to obtain the significant safety for passengers and drivers, monitoring of suspension system and detecting system faults must have more attention. Consequently, the main motivation for this research has been the introduction of on-board safety systems for road vehicles.

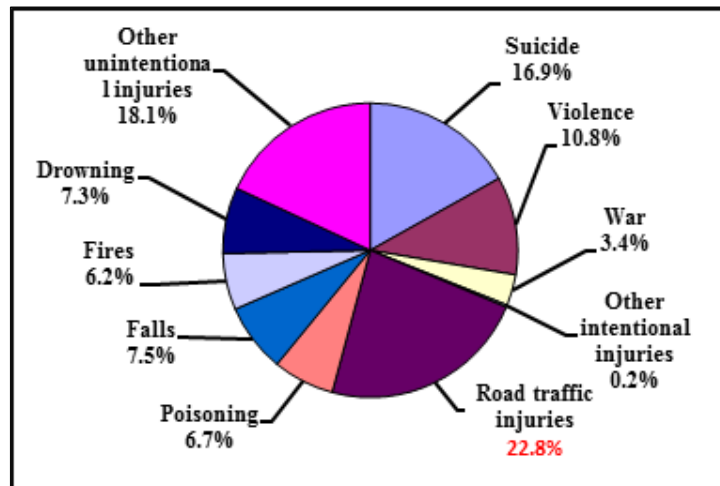


Figure 1-11: Distribution of global injury by cause (Peden, 2004)

### 1.12 Research Aim and Objectives

The main aim of this research is to investigate an on-line condition monitoring approach for vehicle suspension systems. The proposed scheme is developed based on the modal shape of the bounce and pitch modes of the vehicle, which are less sensitive to vehicle load conditions but more sensitive to key suspension parameters including stiffness, damping and tyre inflation pressures. Therefore, a modal shape based scheme is developed based on using the modal rolling energy of these two modal shapes as the diagnostic parameters for monitoring the suspension.

The research analyses the dynamics of a suspension system through numerical modelling and experimental measurements to identify the system parameters. To test the ability of the proposed method in determining the condition of suspension components and diagnosing faults, the modal parameters (obtained theoretically) of a vehicle were defined. These are the natural frequency, damping ratio and modal shapes. They are simulated using (7-DOF) model system. The modal shapes of the vehicle are then analysed under the influence of different suspension faults including damping faults and under-inflation of the tyres (see Section 4.3).

For validation purposes, experiments (see Section 8.2 and 8.4) are carried out to evaluate the technique on a vehicle subjected to different tyre inflation pressures and different damping coefficients. The results indicate that the developed method is effective for feature extraction and detection of abnormal components in a suspension system.

The research aim is accomplished by the fulfilment of the following main objectives:

- To carry out a comprehensive literature review regarding to commonly used vibration methods including methods for the detection of common faults occurring in suspension systems.
- To develop a mathematical model of a full vehicle with (7-DOF), in order to understand the vehicle dynamics, leading to the characterisation of the modal parameters of the vehicle.
- Calibrate and verify the model offline and online so that the predicted vibration responses can be in agreement with that of measurements as much as possible.
- Investigate the behaviour of modal shapes under the influence of different suspension faults (damping coefficient, spring rate and under-inflation of the tyres), making use of the virtue that modal shapes are independent of vehicle load, speed and road excitation thereby developing modal shape-based approaches for monitoring suspension systems.
- To investigate modal parameter identification technologies and develop stochastic subspace identification based approaches for the determination of the vehicle's modal parameters.
- Develop a wireless sensing system for on-line vibration and pressure measurement, which may serve to examine the influence of under-inflation pressure of the tyre on the suspension system performance.
- To evaluate experimentally the suspension models and the modal shape based detection technique proposed in this research, for different tyre pressures and damping coefficients.
- Verify and improve the proposed online condition monitoring approaches based on a modal shape deformation characteristics.
- Provide recommendations for future research to improve the performance of suspension condition monitoring.

### **1.13 Thesis Structure and Organisation**

A brief introduction for each chapter is listed here to outline the thesis. In addition, Figure 1-12 presents a flowchart of the major contents, which have been conducted in this research, for the

development, verification and validation of the proposed modal shape deformation based detection technique.

## **Chapter 2**

This chapter begins by discussing the modal based fault detection methods used in condition monitoring. A literature review regarding vibration techniques is then presented. This includes early methods such as time and frequency domains, and also more recent modal-based fault detection techniques for suspension. The motivation for the research is described in this Chapter.

## **Chapter 3**

A mathematical model that simulates vibration signals has been presented in this chapter. The model represents a 7-DOF full vehicle system. These comprise the motion of the vehicle body (bounce, pitch and roll) and the motion at each wheel. The model is used to investigate the dynamic response of the vehicle and to develop on-line condition monitoring for the suspension system.

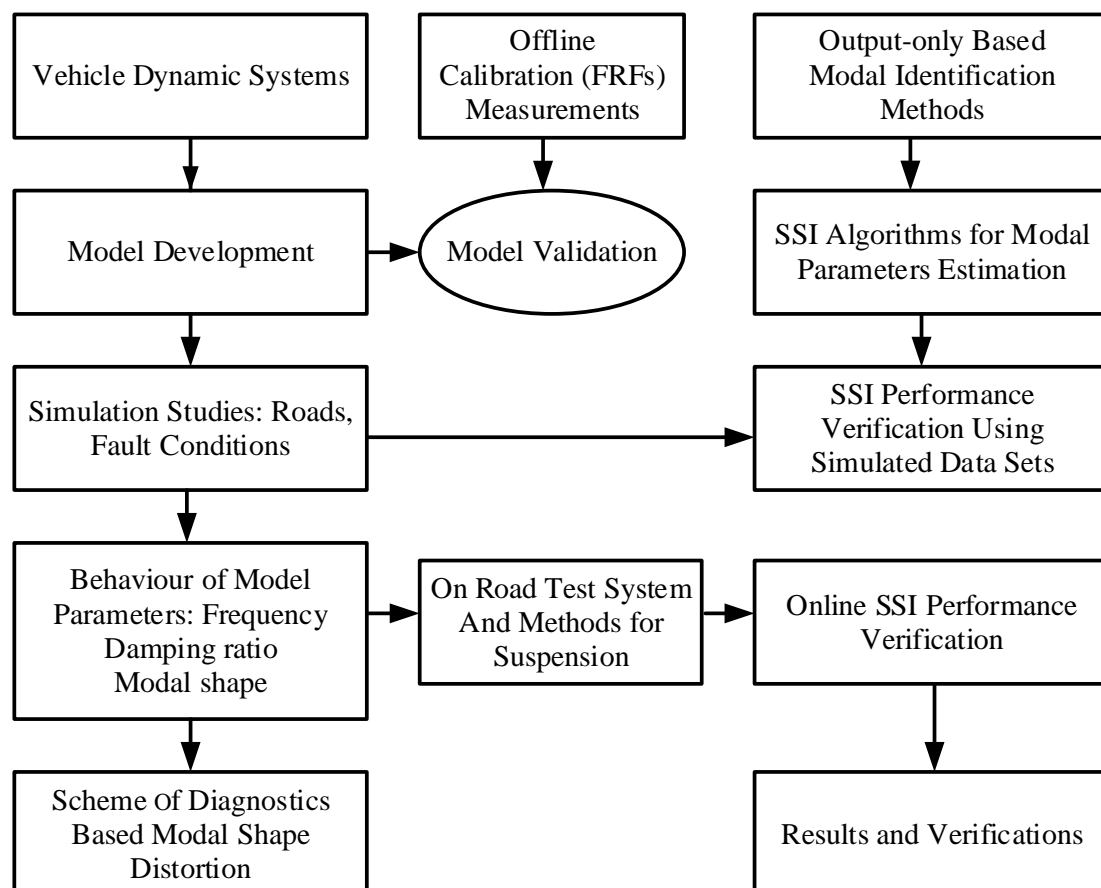


Figure 1-12: Flow chart of the modal shape based detection technique.

## **Chapter 4**

This chapter presents the simulation studies of a vehicle when driven at different velocities and across speed bumps of different profiles. Three different bump sizes were considered in this simulation. The road surface is the input to the system; when the vehicle passes over these bumps the excitation input leads to vertical vibrations in the whole system. The performance of the suspension in terms of ride quality, handling and stability of the vehicle are analysed and presented in this chapter. This is followed by a simulation analysis of the effect of changing the damping, spring weakness and under-inflation of the tyres on the suspension performance. The modal parameters of the vehicle are then obtained theoretically; the natural frequency, damping ratio and modal shapes are calculated and their characteristics are presented using a MATLAB simulation of a (7-DOF) full vehicle model. These parameters are analysed under the influence of different suspension faults. Finally, analyses are carried out to determine the energy differences for the mode shapes of the vehicle, and a new suspension fault detection technique is developed based on the observed changes.

## **Chapter 5**

This chapter introduces the stochastic subspace identification methods. In particular, an Average Correlation Signal based Stochastic Subspace Identification (ACS-SSI) method is described, which was developed recently in Chen et al. (2015) for online vehicle dynamics analysis. The general Stochastic Subspace Identification (SSI) frameworks are also described, as they allow multiple data records and data frames to be combined through an average scheme in the correlation lags domain. This suppresses random noise and non-stationary contents effectively, achieving more accurate and reliable parameter identification.

## **Chapter 6**

This chapter discussed the validation processes for the SSI model using the outputs of the 7-DOF model which are accelerations of the vehicle body as inputs to the system identification model. In this simulation, the parameters of the vehicle have been identified and presented. Furthermore, these modal parameters which have been obtained compared to the modal parameters of the 7-DOF model and they were close to each other, therefore, the SSI technique has been validated to be used for modal parameters identification of the tested vehicle.

## **Chapter 7**

This chapter presents experimental work that was carried out on the 4-post-test rig at the University of Huddersfield in order to calibrate the full vehicle model. The test was conducted to measure the vibration response of the car body and the vibration of the platform (shaker) in order to calculate the (FRF) of the vehicle. The signals of vibration were obtained for baseline

conditions and for different damping settings. During the tests, the car was induced with the simulated fault of a damaged shock absorber by replacing the front passive shock absorbers of the vehicle with adjustable shocks from SPAX Company. This test consists of three main parts: a commercial vehicle, a measurement system (vibration sensors, amplifiers, data acquisition and portable laptop) and the 4-post simulator system (shaker). In addition, this chapter describes the experimental facilities, test procedures and the FRF results.

### **Chapter 8**

This chapter presents two experimental investigations. The first experiment was conducted to test the suspension for range of tyre inflation pressures, as well as the pressure change inside the tyre, in order to analyse the tyre pressure changes effect on the suspension performance. The second experiment was conducted to evaluate the suspension model and the modal shape based detection technique, which attempt to explore an on-line condition monitoring system for suspension. The vehicle was subjected to different tyre inflation pressures and to different damping settings. The main objective of this test was to measure the acceleration of the vehicle body at the four corners of the vehicle. Experiments facilities, test procedures and results for each experiment are also included in more detail.

### **Chapter 9**

This chapter summarises the results and conclusions drawn from the research. Furthermore, suggestions are given for the future work that could be conducted in related research areas.

## **CHAPTER 2**

### **REVIEW OF SUSPENSION DIAGNOSIS METHODS**

*This chapter presents a literature review of vibration techniques used in condition monitoring of suspension systems. Relevant works are briefly reviewed in this chapter in order to obtain a general understanding of the present study.*

## **2.1 Introduction**

Consumers generally expect ensured safety, security, reliability, and comfort, from their vehicles as they do from their other products (Bertram et al., 2003). However, faults can occur on a vehicle as it can operate on harsh conditions and subject to ageing problems. In the vehicle engineering processes faults fall into the following categories: (i) soft faults - faults with sensors or actuators; (ii) process faults - where plant parameters are affected by physical/mechanical problems. Fault detection and isolation (FDI) is a field that is concerned with the detection of abnormal conditions in systems and the isolation of the subsystem in which a fault occurs. When applied to vibration data taken from dynamic structures, this process corresponds to damage detection and localisation and is achieved by detecting changes in the vibration characteristics or structural parameters of a system (Döhler, 2011). There are two main groups for FDI methods: those that do not use the mathematical model, and those that assume accurate dynamic process models (Sébastien Varrier et al., 2013; Venkatasubramanian et al., 2003). FDI selection depends on the availability of either a reliable model or a set of process measurements under the considered faulty modes of operation. The following section presents a review of the typical fault detection methods for suspension systems that have been used in previous studies. It will also discuss the influence of tyre pressure changes on the suspension performance in order to help understand the system behaviour and develop an effective on-line condition monitoring tool for suspension systems.

## **2.2 Model-Based Fault Detection and Diagnosis Methods**

The aim of detection systems is to identify faults in machines being modelled by analysing the data between different measurable signals. Many mathematical models for fault detection have been presented in the literature (Borutzky, 2014; Isermann, 1984; Frank, 1990; J. Chen & Patton, 2012; J Chen, 1999; Huang & Su, 2015). Figure 2-1 presents model-based FDI structure, where the residual is a fault indicating signal. The decision making process is to examine the residual to determine the likelihood of faults. Three basic methods are defined for model-based fault detection (Isermann, 2011; Patton, Frank, & Clark, 2000), as will be described in the coming sections.

### **2.2.1 Parameter Estimation Methods**

Parameter estimation can be used to detect faults in a process by identifying faults in the measured parameters (multiplicative faults). By comparing the reference parameters of input-

output models with the actual parameters determined by measurement, the occurrence and size of the fault can be determined (Isermann, 2011).

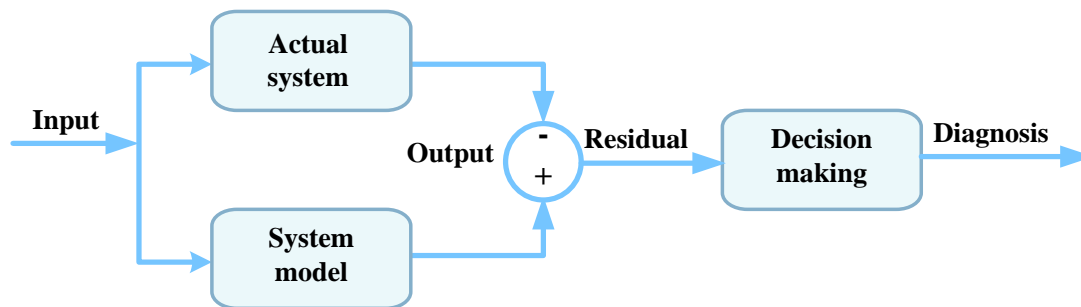


Figure 2-1: Sketch of FDI (Patton et al., 2000)

### 2.2.2 Observers and State Estimation

Estimation of the state of a system is generally known as observer. Observer theory has been discussed to estimate the linear systems, and state space equations are presented as:

$$\dot{x} = A(x) + B(u) \tag{2-1}$$

$$y = C(x) + D(u) \tag{2-2}$$

Where  $x$  is a vector of state,  $u$  is input scalar (in mechanical systems this is commonly a force or torque), and  $y$  is an output scalar. The matrices  $A$  and  $B$  describe the relationship between the state and input variables while  $C$  and  $D$  gives the relationship between the state and the output variables. This method is very useful for multiple-input/multiple-output systems. By using state or output observers, various fault schemes may be constructed. In this case the structure and parameters of the process model must be known precisely. The applicability of each method depends strongly on the specific problem being addressed, and particularly on the degree of analytical redundancy in the process measurements. Each of the schemes could be used to observe the output signals or states of the system.

### 2.2.3 Parity Equations

A relatively straight-forward approach to building residuals to indicate faults is the use of parity equations. Two basic approaches exist: (i) the output error technique; and (ii) the error method. The use of parity equations requires knowledge of a fixed parameterised model. The model acts as a reference for the measured system behaviour. Parity equation methods are strongly related to observer methods, but with simpler design. This is due to the ability to directly

produce a design from the state space equations or from the Laplace-transformed differential equations of the process (Isermann, 2011).

### **2.3 Signal Spectrum Estimation**

While model-based methods require a mathematical process model, signal-based methods do not (Isermann, 2011). To diagnose symptoms that indicate a fault, the mean, variance, domain frequencies, and other properties of the signal are calculated. For calculating the dominant frequencies a spectral signal estimation technique can be used. Alternatively, the frequency calculations can be performed directly by (FFT). However, the computational effort required to perform an FFT is quite large, and the process can hence be relatively time consuming.

### **2.4 Fault-Diagnosis Methods**

The purpose of fault diagnosis is to determine the type of fault and provide information about the fault as (the fault location, size and detection time) based on the symptoms generated by the fault-detection methods. The propagation of faults as they become observable features or symptoms follows a chain of physical cause-effect relationships. To enable fault diagnosis, experimentally trained classification methods can be applied. These can include statistical or geometrical classification methods, fuzzy clustering, neural networks, or simple pattern recognition (Isermann, 2011).

### **2.5 Review of Suspension Fault Diagnosis**

Early detection of faults in the suspension and tyre systems of road vehicles can reduce the damage inflicted on the vehicle and on other road users, in addition to improving passenger security and comfort. During a study into suspension fault detection, Isermann (2005) presented a general concept of model-based methods. In this research a time-varying parameter was calculated along with the characteristic velocity based on a mathematical model of a car.

Similarly, Marcus Börner, Straky, Weispfenning, & Isermann (2002) presented an introduction to model-based methods for vehicle suspension systems. An explanation of some of these methods was provided, including the parameter estimation method, and signal spectra estimation. This research adopted two methods to detect suspension faults. The first method is fault detection using estimation of the parameter and neural networks, based on modelling of semi-active suspension systems. The second method is used parity equations to detect faults od sensors, whereby parity equations were used to detect example sensor faults including a sensor offset fault and a sensor gain fault. The result shows that fault detection can be obtained for

both cases but they cannot be identified separately. In addition, the monitoring of tyre pressure has been provided via signal spectra analysis, and is able to detect under-inflation of the tyre of about 0.5 bars. A drawback to the method used in this study was the need for it to be continually excited to ensure a guaranteed convergence of the estimation algorithm.

Malekzadeh & Ghaffari (2015) presented a full vehicle model which used a random road as input to develop and enhance the fault detection capabilities for the active suspension system. Using this method, fault detection of suspension system was also presented. The results of this research claimed that actuator faults are well reconstructed by the simulation.

Using both full car and quarter car models, a statistical identification system was used by Metallidis, et al. (2003) to apply identification technique to non-linear suspension systems. Simulated test data was used to determine the optimal sensor location and the effectiveness of the system identification process. A model-based method has been discussed by Moncada & Marin (2011). In this research the generation of residuals was performed by comparison of real output against estimated output. This research analysed the fault detection regarding position of the sensors on a bus suspension.

Zbiri, Rabhi, & M'Sirdi (2004) presented a system designed to detect critical situations arising whilst driving; the most fundamental of these being suspension failure, over- and under-steering, and variations in tyre pressure. The main principle the system was based on was the use of a bank of observers. The researchers used identification of parameters of the suspension to detect suspension faults. For the detection of tyre pressures, variations in the derivative signals of the velocity were used.

Kashi et al., (2006) applied a model-based fault method, which relied upon theoretical information of the control system of the vehicle. To detect faults of the system, the residuals were evaluated via fault tree analysis in conjunction with a fuzzy filter. As a result of this, two variations of fault were implemented: transient and stationary. Jeppesen & Cebon (2009) presented observer-based and state-estimation techniques for fault detection in the active suspension system installed in a heavy vehicle. The sensor faults and the changing in the setting of active system were discussed.

Model based fault methods and sensor fault have been presented by Fischer et al., (2007) as tools to detect faults in the acceleration of the vehicle. In this research, signal methods and model-based methods were used to detect primarily major faults. Yetendje, Seron, & Dona (2007) applied a fault detection and identification strategy to an active suspension system.

Agharkakli, Sabet, & Barouz (2012) presented a mathematical model for passive systems. In this research, a method was presented for designing an active suspension for a passenger car, including a controller that only considers bounce motion, and the performance of the suspension was evaluated with respect to different stages of designs. Research by Ikenaga, et al. (2000) was conducted in order to improve passenger comfort and road quality. Jorge de-J, Lozoya-Santos (2012) proposed a fault detection system that could monitor the Magneto-Rheological (MR) damper condition. Their system functioned by monitoring in a quarter car model the transmissibility of semi-active suspension.

Applicative results for fault detection and control of a semi-active suspension system have been presented by Varrier et al (2013), where the control system is an extension of the “Acceleration Driven Damping” (ADD) controller for fault detection scheme to estimate the fault. A quarter vehicle model including the nonlinearities of the shock absorber were used.

The sensor faults within the system were estimated, with a particular bias toward accelerometers. The results claimed that the proposed control strategy allowed a reduction in the bad performances due to the fault. Tudon Martinez (2013) proposed a strategy to detect the faults in damping system. It was claimed that oil leakage from a damper improved passenger comfort by up to 60 % for the suspension with control system and up to 82 % for uncontrolled suspension. However, it also inhibits the vehicle’s stability.

Zhu, Xia, Chai, & Shi (2014) designed a filter to detect faults for active vehicle suspension systems. In this research some filters were designed to meets the prescribed  $H_\infty$  performance index. Breytenbach & Els (2011) discussed the ride comfort analysis for passengers. This study presented a new strategy for semi-active system known as “4 State Semi-active Suspensions”, which allow different damping for suspension. A fault-tolerant control (FTC) method for suspension was presented by Kim & Lee (2011).

The FTC which has been adopted in this research was shown to detect the faults for a closed-loop air suspension. A model-based system to detect and isolate faults in vehicle suspensions was presented by Silva et al. (2007). Bond graph modelling of the four-wheel vehicle dynamics, which has been discussed in this study, not only confirms the capability of this formalism to deal with complex physical systems, it also allows the FDI-problem in the BG domain to be solved. Mondal, Chakraborty, & Bhattacharyya (2008) discussed the fault detection of suspension system in terms of noise and parametric deflections. Simulation results of this research showed the efficacies of the FDI algorithm as well as the observer with the help using

half-car models. A full vehicle active suspension system was divided into five subsystems by Chamseddine & Noura (2008). This research was designed a local controller for each subsystem. In parallel to these controller systems, a fault diagnosis structure and local diagnosis model was designed. In addition, this research has presented the most common sensors used in laboratory vehicles, as given in Table 2-1.

Table 2-1: Common sensors used in laboratory vehicles (Chamseddine & Noura, 2008)

Sensor type	Measurements
<b>displacement transducers (LVDTs)</b>	Measure the velocity of the body and the unsprung masses.
<b>Accelerometers</b>	Measure the bounce of the vehicle body and the vertical acceleration of the suspension.
<b>Accelerometers</b>	Measure the vehicle acceleration (lateral and the longitudinal).
<b>Laser sensors</b>	Measure the bounce direction of the body and the road inputs.
<b>Gyro-meters</b>	Measure the angular velocities of pitch and roll.
<b>Load cells</b>	Measure the forces of the actuators.

## 2.6 Review on Modelling of Suspension

Numerous theoretical analyses have been carried out to develop methods that give better control of the vehicle and optimal performance of the suspension for passengers' safety and comfort. For this purpose, different models have been developed, from simple linear models with one-degree-of-freedom, through to more complex nonlinear models of rigid bodies. Simple vehicle models can provide an overall view of the vehicle behaviour under specified conditions. However, in a more detailed study by Zehsaz et al. (2014), a full model has been conducted to analyse a wide range of different manoeuvres and conditions to predict ride comfort and driving safety of the suspension. This also aided in the development of condition monitoring for suspension systems.

Rao et al. (2010) presented a three degrees of freedom model for suspension system using MATLAB. The model was used to test skyhook control strategy, and also to test other strategies for semi active suspension systems. This strategy has showed a solution for obtaining comfort ride. This approach has been also compared with the classical skyhook method to obtain further improvements in semi active suspension systems. Darus & Sam (2009) presented a full car model with passive and active suspensions. In their research the linear quadratic control (LQR)

approach was adopted for the full car model with an active system. Different types of road profile (two bumps vs single bump) have been used to compare between passive and active suspension responses. The results of this study show that, for a modelled full car of suspension systems, the amplitude of the output performance was slightly higher in the two bumps case than in the single bump case.

A mathematical model with 2-DOF and with 4-DOF have been investigated using a MATLAB tools package by Faheem et al. (2006). It was shown that both models (quarter car and half car) can be used to analyse the parameters of suspensions, and to select a suitable damping value for different suspension parameters. The quarter car model was used to with an internal solenoid-actuated valve by Eslaminasab et al (2007). In their work a new semi-active damper was designed, and two semi-active control techniques were projected. Furthermore, logical and numerical methods were developed to address the non-linearity of suspension system and the issue of response time. The experimental results were compared with the mathematical model. A quarter car model was designed by Qazi et al. (2014) to facilitate the development of a scheme for an optimal suspension controller. The result of this research was compared with different systems including a passive suspension.

Rakheja et al. (2011) used a model of in an urban bus to study the fault detection of passive suspension. The model has been used to identify the characteristics of suspension. This research adopted laboratory tests to measure the component characteristics. This research uses a three-dimensional urban bus model, to examine the performance of the vehicle. The results of this research show that, there is an agreement between the trend of the model and the data response characteristics.

In the case of a road input, Gawade et al. (2004) discussed a technique to estimate the road profile. This research considered some different road profiles of the same height. These road profiles were applied to model of a three-wheeled vehicle. The TWV model then has been validated by the measured acceleration of the vehicle while driven over a bump profile. Measuring vibration data were proposed by Wallentowitz (2003), Peters et al., (1993), Gáspár & Nadai (2007a) and Gáspár & Nadai (2007b) that are indirectly measured by sensing the acceleration of the body and wheels. The principle is to calculate the wheel displacement by numerical methods and hence replace a displacement sensor with an acceleration sensor.

## **2.7 Effect of Tyre Pressure on Suspension Performance**

The suspension is linked with the tyres, which provide traction between the vehicle and the

road while providing a flexible cushion that absorbs shock. Tyres can be considered one of the connection parts that connect the vehicle body to the wheels throughout the road surface. In addition, the wheels provide friction to allow the vehicle to perform its normal operations (Hamed, Tesfa, Gu, & Ball, 2014).

The operation of the tyre in a normal pressure is the most factor to operate the vehicle safely. If the tyre operated at higher than the recommended inflation pressure, this can cause wear to the tyre, degraded the ride comfort, and decreases stability of the vehicle. Similarly, operating tyres at lower than the normal pressure will cause the same problems, but in addition can affect the structure of the tyre. This results in tread wear and other structural fatigue and can also affect the performance of the vehicle (Daws, 2010; Hamed et al., 2014). These factors are affected by 20 percent for every 0.2 bar of tyre under-inflation (Persson & Gustafsson, 2002). The Tyre Industry Council in the UK conducts road side surveys, and found that the tyre pressure effects on the car performance are often neglected. They found from a survey of over 1000 tyres in 2002 that only 15% were correctly inflated and 72% were under inflated (Paine et al., 2007) as shown in Figure 2-2.

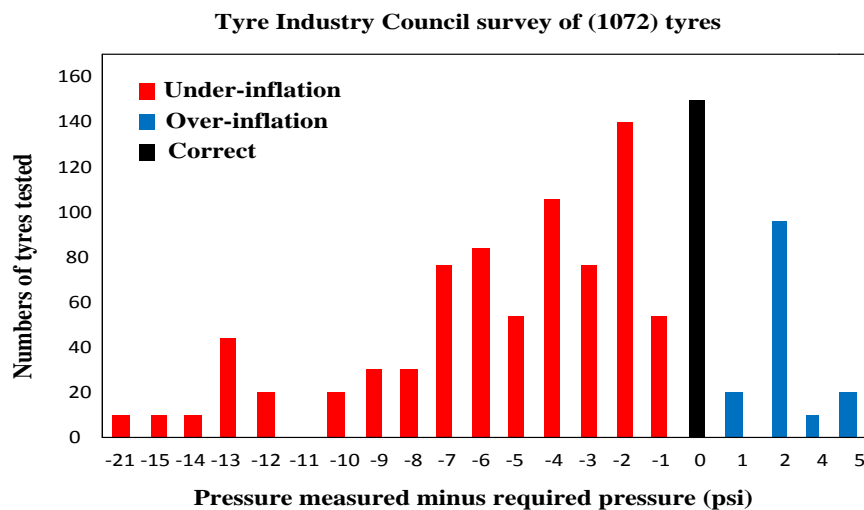


Figure 2-2: UK Tyre Industry survey of 1072 tyres (Paine et al., 2007)

According to (International Energy Agency, 2006), road transport leads to increasing energy use and carbon dioxide (CO<sub>2</sub>) emissions globally. Around 20% of a motor vehicle's fuel is estimated to be used to overcome the rolling resistance of the tyres. Therefore, the tyres are responsible for a large portion of energy consumption and CO<sub>2</sub> emissions, and additional fuel is used when tyres are under-inflated. Data presented at the 2005 International Energy Agency (IEA) Tyre Workshop indicates that on average tyres in service are under-inflated by 0.2 to 0.4 bar for passenger cars and 0.5 bar for trucks (International Energy Agency, 2006).

Rievaj, Vrábel, & Hudák (2013) presented a study into the effect of tyre pressure on stopping distance. Three different causes of improper type pressure are examined: overcrowding, under-inflation and normal value of the pressure. The study concluded that when the tyres are under-inflated the stability and the handling of the vehicle are decreased. In addition, the tyre pressure has an impact on the vehicle's driving characteristics. The influence of the tyre inflation pressure on the transient and steady state of handling dynamics for an urban bus was presented by Al-Solihat et al., (2010). They analysed a vehicle model of a three-dimensional case and concluded that an under-inflation pressure of the tyre yields (i) to increase yaw and roll motion, (ii) a notable increase in the acceleration of the vehicle body, and (iii) more deflections of the roll of the body. Persson & Gustafsson (2002) presented an indirect monitoring system for tyre pressure based on the concepts of wheel radius analysis and measuring the vibration of the wheel.

## **2.8 Summary**

This chapter has discussed the commonly used fault detection and diagnosis methods for condition monitoring. A review of literature regarding commonly used vibration techniques is then presented. This includes early condition monitoring methods such as time and frequency domains, and also more recent modal-based fault detection techniques for suspension. This chapter has given a general view to help in developing the condition monitoring for suspension, therefore, the next chapter will present a mathematical model for full vehicle system.

## CHAPTER 3

### MATHEMATICAL MODELS OF A FOUR WHEEL VEHICLE

*This chapter presents a mathematical model that allows the vibration responses of a vehicle under different suspension conditions and pave ways for fault diagnostics. Then, the linear solution of the model is also developed using state space repetitions. Finally, the model is calibrated based on frequency response analysis and impulsive response analysis.*

### 3.1 Introduction

Modelling is the representation of system information in mathematical terms so as to obtain a significant prediction of the system behaviour. In general, a quarter-car model is simple to develop and can give a general understanding about the motion of the vehicle. However, it cannot offer certain information about the full system such as the motion of the vehicle rolling and pitching. For that reason the model can be expanded into a full model by adding the four unsprung masses in each corner of the model to match the vehicle body. Subsequently, the link between the body and the wheels indicates the roll and pitch angles. The basic modelling is still the same as for the quarter-car model, but the rolling, pitching and bouncing must also be considered. This results in a vehicle with (7-DOF), comprising (3-DOF) for the vehicle body (bounce, pitch and roll) and a (1-DOF) at each corner of the vehicle. Therefore, a full vehicle model can simulate a wide range of manoeuvres and conditions (Zehsaz et al., 2014). In this research a full dynamic vehicle model was developed as presented in the next section.

### 3.2 Suspension System Model and Dynamics

A model of full-vehicle, shown in Figure 3-1 has been developed and compared to (Dong, Chen, & Zhang, 2014) model. This is a seven-degrees of freedom (7-DOF) model where the vehicle body is assumed to be a rigid with three degree of freedoms in the vertical direction (bounce), pitch motion which is the motion of the body up and down from front to the rear direction, and the roll directions which gives the longitudinal motion of the vehicle. In Figure 3-1,  $z_s$  is presented how the vehicle body is moving in the vertical direction, while  $\theta$  and  $\phi$  are the angles of pitch and roll respectively. Moreover, the model allows the inclusion of different deviations or faults on each key components of the suspension system through changing the stiffness and damping values. In addition, different types of input can be applied by using a appreciate displacement function to the wheel sets. Therefore, vibration characteristics can be understood comprehensively for subsequent fault diagnosis development.

Suspension systems of a vehicle are modelled by coil spring connected to a damper. The tyre has been presented as a single linear spring in the model.  $m_s$  is the body mass, while the front and rear suspension are illustrated as unsprung masses ( $m_f, m_r$ ).  $I_\theta$  &  $I_\phi$  are the moments of inertia for pitch and roll. The origins of the coordinate axes are assumed to be at the centre of sprung mass.  $z_{s1}, z_{s2}, z_{s3}$  and  $z_{s4}$  are the displacements of the front and rear of sprung mass.  $z_{u1}, z_{u2}, z_{u3}$  and  $z_{u4}$  are the front and rear displacements of unsprung mass.  $z_{r1}, z_{r2}$

$z_{r3}$  and  $z_{r4}$  are the disturbances of the road surface. The front and rear suspension stiffness on the left and right sides is denoted by  $k_{fl}, k_{fr}, k_{rl}$  and  $k_{rr}$ . The front and rear tyre stiffness on the left and right sides are denoted by  $k_{tfl}, k_{tfr}, k_{trl}$  and  $k_{trr}$ . The damping coefficients are presented by  $c_{fl}, c_{fr}, c_{rl}, c_{rr}$ . The equations of all motions are derived separately, resulting in the equations of the body motions.

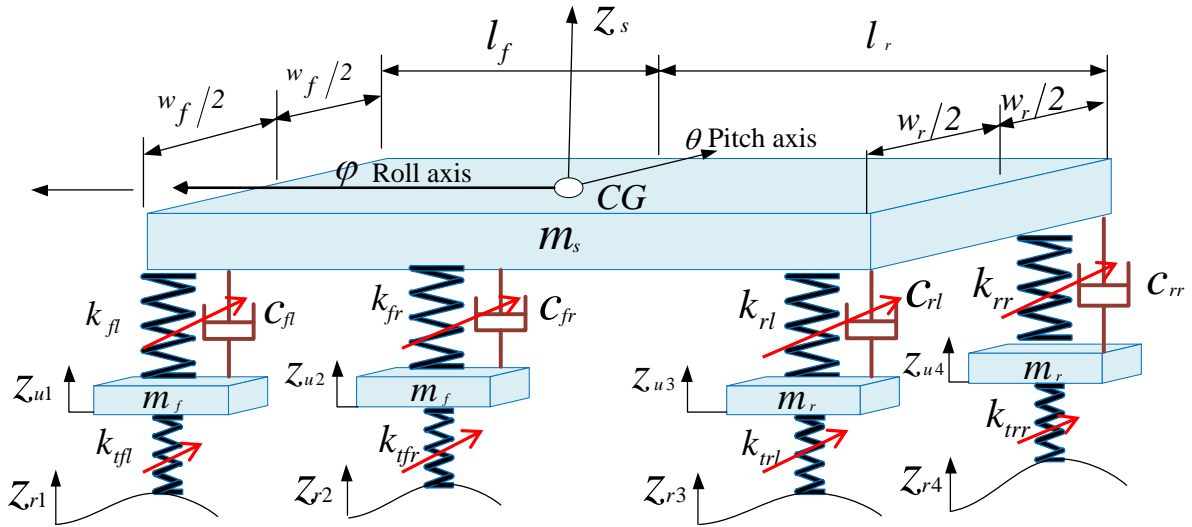


Figure 3-1: Full vehicle models

The bouncing equation of motion for the sprung mass:

$$m_s \ddot{z}_s = k_{fl}(z_{u1} - z_{s1}) + k_{fr}(z_{u2} - z_{s2}) + k_{rl}(z_{u3} - z_{s3}) + k_{rr}(z_{u4} - z_{s4}) + c_{fl}(\dot{z}_{u1} - \dot{z}_{s1}) + c_{fr}(\dot{z}_{u2} - \dot{z}_{s2}) + c_{rl}(\dot{z}_{u3} - \dot{z}_{s3}) + c_{rr}(\dot{z}_{u4} - \dot{z}_{s4}) \quad 3-1$$

Equation of motion for the pitching of the sprung mass:

$$I_p \ddot{\theta} = k_{fl} l_f (z_{u1} - z_{s1}) + k_{fr} l_f (z_{u2} - z_{s2}) + k_{rl} l_r (z_{u3} - z_{s3}) + k_{rr} l_r (z_{u4} - z_{s4}) + c_{fl} l_f (\dot{z}_{u1} - \dot{z}_{s1}) + c_{fr} l_f (\dot{z}_{u2} - \dot{z}_{s2}) + c_{rl} l_r (\dot{z}_{u3} - \dot{z}_{s3}) + c_{rr} l_r (\dot{z}_{u4} - \dot{z}_{s4}) \quad 3-2$$

Equation of motion for the rolling motion of the sprung mass:

$$I_r \ddot{\phi} = k_{fl} w_f / 2 (z_{u1} - z_{s1}) + k_{fr} w_f / 2 (z_{u2} - z_{s2}) + k_{rl} w_r / 2 (z_{u3} - z_{s3}) + k_{rr} w_r / 2 (z_{u4} - z_{s4}) + c_{fl} w_f / 2 (\dot{z}_{u1} - \dot{z}_{s1}) + c_{fr} w_f / 2 (\dot{z}_{u2} - \dot{z}_{s2}) + c_{rl} w_r / 2 (\dot{z}_{u3} - \dot{z}_{s3}) + c_{rr} w_r / 2 (\dot{z}_{u4} - \dot{z}_{s4}) \quad 3-3$$

Equation of motion for each wheel in the vertical direction:

$$m_f \ddot{z}_{u1} = -k_{fl}(z_{u1} - z_{s1}) - c_{fl}(\dot{z}_{u1} - \dot{z}_{s1}) + k_{tfl}(z_{r1} - z_{u1}) \quad 3-4$$

$$m_f \ddot{z}_{u2} = -k_{fr}(z_{u2} - z_{s2}) - c_{fr}(\dot{z}_{u2} - \dot{z}_{s2}) + k_{tfr}(z_{r2} - z_{u2}) \quad 3-5$$

$$m_r \ddot{z}_{u3} = -k_{rl}(z_{u3} - z_{s3}) - c_{rl}(\dot{z}_{u3} - \dot{z}_{s3}) + k_{trl}(z_{r3} - z_{u3}) \quad 3-6$$

$$m_r \ddot{z}_{u4} = -k_{rr}(z_{u4} - z_{s4}) - c_{rr}(\dot{z}_{u4} - \dot{z}_{s4}) + k_{trr}(z_{r4} - z_{u4}) \quad 3-7$$

The translations of the vehicle body acceleration at each corner, which is located above the four wheels of the vehicle where vibration transducers are mounted, can be represented as follows:

$$z_{s1} = z_s - l_f \theta + (w_f/2) \varphi \quad 3-8$$

$$z_{s2} = z_s - l_f \theta - (w_f/2) \varphi \quad 3-9$$

$$z_{s3} = z_s + l_r \theta + (w_r/2) \varphi \quad 3-10$$

$$z_{s4} = z_s + l_r \theta - (w_r/2) \varphi \quad 3-11$$

For efficient solutions, Equations 3-1 to 3-7 can be the in matrix format:

$$[\mathbf{M}]\ddot{\mathbf{x}} + [\mathbf{C}]\dot{\mathbf{x}} + [\mathbf{K}]\mathbf{x} = \mathbf{z} \quad 3-12$$

Where the road excitation is  $\mathbf{z} = [0 \ 0 \ 0 \ z_{r1} \ z_{r2} \ z_{r3} \ z_{r4}]^T$ , and the response vector

is  $\mathbf{x} = [z_s \ \theta \ \varphi \ z_{u1} \ z_{u2} \ z_{u3} \ z_{u4}]^T$

The mass [M], stiffness [K] and damping [C] matrixes of the full vehicle are presented as:

$$M = \begin{bmatrix} m_S & 0 & 0 & 0 & 0 & 0 & 0 \\ 0 & I_P & 0 & 0 & 0 & 0 & 0 \\ 0 & 0 & I_r & 0 & 0 & 0 & 0 \\ 0 & 0 & 0 & m_f & 0 & 0 & 0 \\ 0 & 0 & 0 & 0 & m_f & 0 & 0 \\ 0 & 0 & 0 & 0 & 0 & m_r & 0 \\ 0 & 0 & 0 & 0 & 0 & 0 & m_r \end{bmatrix}$$

$$K = \begin{bmatrix} k_{fl} + k_{fr} & (-k_{fl} - k_{fr})l_f & (k_{fl} - k_{fr})w_f/2 & -k_{fl} & -k_{fr} & -k_{rl} & -k_{rr} \\ +k_{rl} + k_{rr} & +(k_{rl} - k_{rr})l_r/2 & +(k_{rl} - k_{rr})w_r/2 & & & & \\ (-k_{fl} - k_{fr})l_f & (k_{fl} + k_{fr})l_f & -l_f w_f/2 (k_{fl} - k_{fr}) & k_{fl} l_f & k_{fr} l_f & -k_{rl} l_r & -k_{rr} l_r \\ +(k_{rl} + k_{rr})l_r & +(k_{rl} + k_{rr})l_r/2 & -l_r w_r/2 (-k_{rl} + k_{rr}) & & & & \\ (k_{fl} - k_{fr})w_f/2 & -l_f w_f/2 (k_{fl} - k_{fr}) & (k_{fl} + k_{fr})w_f/2 & -k_{fl} w_f/2 & k_{fr} w_f/2 & -k_{rl} w_r/2 & k_{rr} w_r/2 \\ +(k_{rl} - k_{rr})w_r/2 & -l_r w_r/2 (-k_{rl} + k_{rr}) & +(k_{rl} + k_{rr})w_r/2 & & & & \\ -k_{fl} & k_{fl} l_f & -k_{fl} w_f/2 & k_{fl} + k_{fl} & 0 & 0 & 0 \\ -k_{fr} & k_{fr}^* l_f & -k_{fr} w_f/2 & 0 & k_{fr} + k_{fr} & 0 & 0 \\ -k_{rl} & k_{rl}^* l_r & -k_{rl} w_r/2 & 0 & 0 & k_{rl} + k_{rl} & 0 \\ -k_{rr} & k_{rr}^* l_r & -k_{rr} w_r/2 & 0 & 0 & 0 & k_{rr} + k_{rr} \end{bmatrix}$$

$$C = \begin{bmatrix} c_{fl} + c_{fr} & (-c_{fl} - c_{fr})l_f & (c_{fl} - c_{fr})w_f/2 & -c_{fl} & -c_{fr} & -c_{rl} & -c_{rr} \\ +c_{rl} + c_{rr} & +(c_{rl} - c_{rr})l_r/2 & +(c_{rl} - c_{rr})w_r/2 & & & & \\ (-c_{fl} - c_{fr})l_f & (c_{fl} + c_{fr})l_f & -l_f w_f/2 (c_{fl} - c_{fr}) & c_{fl} l_f & c_{fr} l_f & -c_{rl} l_r & -c_{rr} l_r \\ +(c_{rl} + c_{rr})l_r & +(c_{rl} + c_{rr})l_r/2 & -l_r w_r/2 (-c_{rl} + c_{rr}) & & & & \\ (c_{fl} - c_{fr})w_f/2 & -l_f w_f/2 (c_{fl} - c_{fr}) & (c_{fl} + c_{fr})w_f/2 & -c_{fl} w_f/2 & c_{fr} w_f/2 & -c_{rl} w_r/2 & c_{rr} w_r/2 \\ +(c_{rl} - c_{rr})w_r/2 & -l_r w_r/2 (-c_{rl} + c_{rr}) & +(c_{rl} + c_{rr})w_r/2 & & & & \\ -c_{fl} & c_{fl} l_f & -c_{fl} w_f/2 & c_{fl} & 0 & 0 & 0 \\ -c_{fr} & c_{fr}^* l_f & -c_{fr} w_f/2 & 0 & c_{fr} & 0 & 0 \\ -c_{rl} & c_{rl}^* l_r & -c_{rl} w_r/2 & 0 & 0 & c_{rl} & 0 \\ -c_{rr} & c_{rr}^* l_r & -c_{rr} w_r/2 & 0 & 0 & 0 & c_{rr} \end{bmatrix}$$

Obviously these linear equations can be solved using standard methods such as the state space approach. However, to understand the details of vibration responses to different road

excitations such as nonstationary bumps and random road profiles, numerical solutions are required.

### 3.3 State Space Based Solutions of the Model

For model simulations, the model in the matrix formation of Equation 3.12 is usually represented in a state space form:

$$\dot{x} = A(x) + B(u) \quad 3-13$$

$$y = C(x) + D(u) \quad 3-14$$

where:  $x$  is a state,  $u$  is the scalar of the input, and  $y$  is the output scalar. The matrices  $A$ ,  $B$ ,  $C$  and  $D$  present the relationships between the states, input and output scalars respectively. The system matrix, which reflects the system nature, is defined as:

$$A = \begin{bmatrix} 0 & I \\ -M^{-1}K & -M^{-1}D \end{bmatrix} \quad 3-15$$

The input matrix is:

$$B = \begin{bmatrix} 0 \\ M^{-1} \end{bmatrix} \quad 3-16$$

The output matrix  $C = I$  and the feed-forward matrix  $D = 0$  with the state-space expression, the eigenvalues and eigenvectors of the system can be calculated based on:

$$[A - \lambda I]v = 0, \quad 3-17$$

Where the eigenvector for the  $i^{th}$  mode,  $v_i = [z_{si} \quad \theta_i \quad \varphi_i \quad z_{u1i} \quad z_{u2i} \quad z_{u3i} \quad z_{u4i}]$  and the corresponding natural frequency can be calculated from the eigenvalue:

$$f_i = \sqrt{|\lambda_i|} / 2\pi \quad 3-18$$

The damping ratio that is associated with each eigenvalue is given by:

$$\xi_i = \text{real}(\lambda_i) / |\lambda_i| \quad 3-19$$

Therefore, the modal shape vectors associated with the first three modes can be decomposed at the four corners of the vehicle as:

$$\begin{aligned}
v_i^1 &= v_i(1) - l_f v_i(2) + w_f / 2 v_i(3) \\
v_i^2 &= v_i(1) - l_f v_i(2) - w_f / 2 v_i(3) \\
v_i^3 &= v_i(1) + l_r v_i(2) + w_r / 2 v_i(3) \\
v_i^4 &= v_i(1) + l_r v_i(2) - w_r / 2 v_i(3)
\end{aligned}
\tag{3-20}$$

where:  $v_i^1$ ,  $v_i^2$ ,  $v_i^3$  and  $v_i^4$  are the modal shape vectors associated with the first three modes at the four corners of the vehicle,  $l_f$  is the distance from the front axle to the car CG,  $l_r$  is the distance from the rear axle to the car CG,  $w_f / 2$  is the half front width of the car and  $w_r / 2$  is the half rear width of the car.

### 3.4 Assumptions and Limitations

A 7-DOF system was used to model the full vehicle. A numerical model was developed so that the pitch, bounce, and roll motions of the vehicle could be studied. To simplify the model, the following limitations and assumptions were employed:

- Vehicle body assumed to be rigid. Three degrees of freedom assumed, in the vertical (bounce), roll and pitch directions.
- The suspension systems are assumed to consist of linear spring and damper (shock absorber) elements.
- The shock absorbers and springs connect to the vehicle model at each corner.
- The road displacement is assumed to be the input to each corner of the model.
- Each wheel has motion only in the vertical direction (1-DOF).
- Each tyre is modelled as a single linear spring.
- The motion of the bodies in the system can be approximated as linear. In actuality the suspension mass, and hence the strut and control arm, change during suspension motion.
- The dynamics of the dampers are assumed to have the same behaviour, just with different damping values.

The obtained vehicle parameters (Vauxhall ZAFIRA) can be seen in Table 3-1. These parameters include the mass of the suspension, the mass of the vehicle body, the spring stiffness and the tyre stiffness. They were obtained from the test vehicle manufacturer. The centre of gravity of the vehicle and the damping coefficients were obtained from FRF measurements of the vehicle, which were carried out on a 4-post-test rig at the Automotive Laboratory of

University of Huddersfield. The objective of this test was to perform the model calibration using the actual values of the damping and actual measurements of the vehicle. For more details see Chapter 7. The real measurements taken at the sensor positions were implemented in the model.

Table 3-1: Vehicle parameters and values

Parameters	Symbol	Value	Unit
Vehicle sprung mass	$m_s$	1480	$Kg$
Masses of front suspension	$m_f$	40.5	$Kg$
Masses of rear suspension	$m_r$	40.5	$Kg$
Front spring stiffness	$k_l, k_{fr}$	21500	$N/m$
Rear springs stiffness	$k_{rl}, k_{rr}$	19500	$N/m$
Front damping coefficients	$c_{fl}, c_{fr}$	1400	$N.s/m$
Rear damping coefficients	$c_{rl}, c_{rr}$	1400	$N.s/m$
Front tyres stiffness	$k_{tfl}, k_{tfr}$	190900	$N/m$
Rear tyres stiffness	$k_{trl}, k_{trr}$	190900	$N/m$
Moment inertia of Pitching	$I_p$	360	$Kg\ m^2$
Moment inertia of rolling	$I_r$	2200	$Kg\ m^2$
Distance from the front axle to the car CG	$l_f$	1.22	$m$
Distance from the rear axle to the car CG	$l_r$	1.58	$m$
Half front width of the car	$w_f/2$	0.702	$m$
Half rear width of the car	$w_r/2$	0.702	$m$

### 3.5 Validation and Vehicle Dynamics Simulation Models

With rapid developments in our ability to using computers and software to model physical systems, the simulation of vehicle dynamics has received increased attention from researchers in the automobile industry. Development of mathematical models of vehicles is important to give insight and understanding of the vehicle dynamics (Kutluay, 2013). An important step that

must take place after developing a model is verification. This is where the model is tested to ensure that it is correct and fulfils any agreed results.

Model validation methodology has been discussed by many researchers for individual cases, such as the dynamics identifications of the vehicles (D. J. COLE, 1992) or the acceleration of commercial vehicles (NALECZ, LU, & D'ENTREMONT, 1994). The parameter estimation and validation of the models have been developed by Salaani et al., (2007) and by Heydinger et al., (2007). These studies concluded that there are number of factors that may generate discrepancies in the validation process, including:

- Theoretical formulation of the model
- Programming
- Identification of the parameter
- Experimental layout and procedures

A half vehicle suspension model was studied by Hu (1993). The validation methodology presented by this study was based on comparing the time domain responses of a vehicle with the model's simulation. In similar studies (e.g. Heydinger et al., 2007) the validation process is presented by plotting the time domain analysis of the measured data and the model results together on the same graph . However, due to the changing of the motion of the sprung and unsprung masses, the suspension should be also analysed in the frequency domain. Figure 3-2 presents the iterative process of calibrating the model.

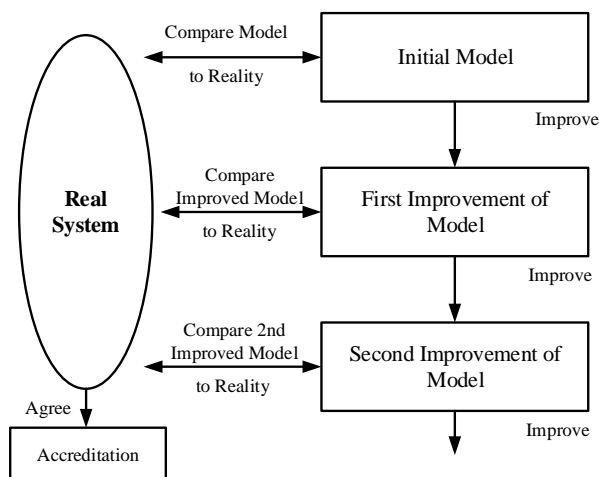


Figure 3-2: Iterative process of calibrating the model

In this research, the model is calibrated using impulse, non-stationary and stationary inputs. In order to validate the model, some iterative processes must be conducted to compare the model to the actual system behaviour, and then the discrepancies between the model and the actual

data can be conducted to obtain insights to improve the model. These processes are repeated until model the accuracy is shown to be acceptable, and finally the model will be accredited.

### 3.6 Theoretical Background of Impulse Response Function

In general, applied forces induce vibration waves that propagate within a model or support structure. The vibrations can be detected by measuring acceleration signals. If the system is considered as a linear dynamic system (i.e., the unknown forces that lead to linear acceleration), then there will be a relationship between the measured data (acceleration) and the input (force). This system is shown schematically in Figure 3-3.

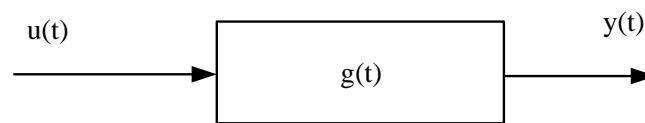


Figure 3-3: Schematic representation of linear input and output relation

Mathematically, the linear relationship of the system between the input and the output can be presented as following (Sahoo et al., 2014). For more details see (Mee, 2003).

$$y(t) = \int_0^t g(t-\tau).u(\tau)d\tau \quad 3-21$$

Where  $y(t)$  is the output signal of the model or structure as a result of applying the load,  $u(t)$  and  $g(t)$  is the system response function.

The impulse response is a process of differentiation of the step response regarding to time. The relationship between input and output for this type of systems can be expressed by applying the Laplace transform of equation 3-21:

$$Y(s) = G(s).U(s) \quad 3-22$$

Where  $Y(s)$ ,  $G(s)$  and  $U(s)$  show the Laplace transforms for  $y(t)$ ,  $g(t)$  and  $u(t)$ . It can be assumed that an input is applied to the system,  $u(t) = S\delta(t)$ , where  $\delta(t)$  is the impulse function, and  $S$  is the time integral:

$$\delta(t) = \begin{cases} 0 & \dots\dots\dots t \neq 0 \\ 1 & \dots\dots\dots t = 0 \end{cases} \quad 3-23$$

The Laplace transformation of a unit impulse function is 1, and the waveform associated with the unit impulse function can be in the form shown in Figure 3-4.

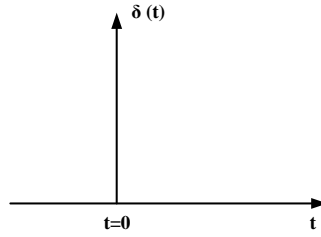


Figure 3-4: Unit impulse function

By adopting  $u(t) = S\delta(t)$  in Equation 3-21,

$$y(t) = \int_0^t g(t - \tau) \cdot S\delta(\tau) d\tau \quad 3-24$$

This equation can be presented as follows:

$$y(t) = \int_0^t g(t - \tau) \cdot S\delta(\tau) d\tau = S \int_0^t g(t - \tau) \delta(\tau) d\tau, \quad 3-25$$

Then the final result gives (Mee, 2003):

$$y(t) = Sg(t) \quad 3-26$$

### 3.6.1 Impulse Validation of the Model

Impulse inputs have been generated and applied to the mathematical model. The impulse function of the vehicle body at the four corners (FL, FR, RL and RR) is presented in Figure 3-5. It can be noted that the impulse function of the system can give more information about the response of the vehicle when subjected to an unknown force history,

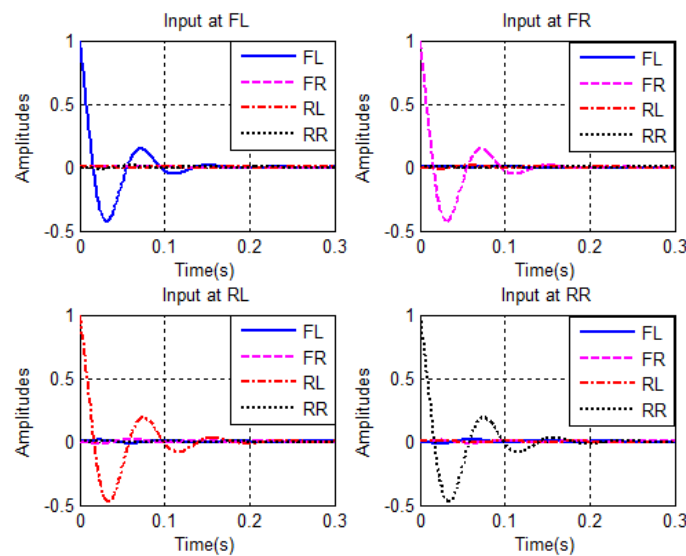


Figure 3-5: Impulse response function for the four corners of the vehicle

It can be noted from this figure that, the response of the model shows the same amplitude for the front left (FL) and front right (FR) corners and the same amplitude for the rear left (RL) and the rear right (RR) corners.

### 3.7 Road Profile Excitation

A road profile can be considered as an imaginary line representing a two-dimensional part of the road. The lateral profile line shows the super elevation and crown of the road. The grade of the road surface, roughness, and texture are presented by the longitudinal profiles (Sayers & Karamihas, 1998). Generally, all vehicles have the same road profiles, with the variations only occurring in the vehicle response. In this case, the road profiles are based on of the structure of the vehicle with different applications. Figure 3-6 shows an example for road profile. The longitudinal profile generates the pitching movement and the lateral profile presents the rolling movement of the vehicle, Guglielmino et al. (2008). The main source of excitation for vehicle simulations is the representation of the road profile.

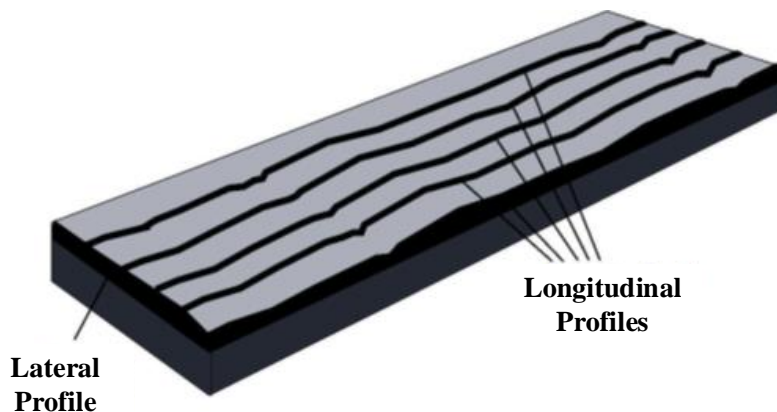


Figure 3-6: Road Surface Profiling (Sayers & Karamihas, 1998)

### 3.8 Classification of Road Profiles

The longitudinal profiles have the greatest effect on a vehicle's response, and their classifications are based on ISO 8606. ISO has classified road roughness based on power spectral density (PSD) as shown in Figure 3-7 and Table 3-2 (Tyan et al., 2009).

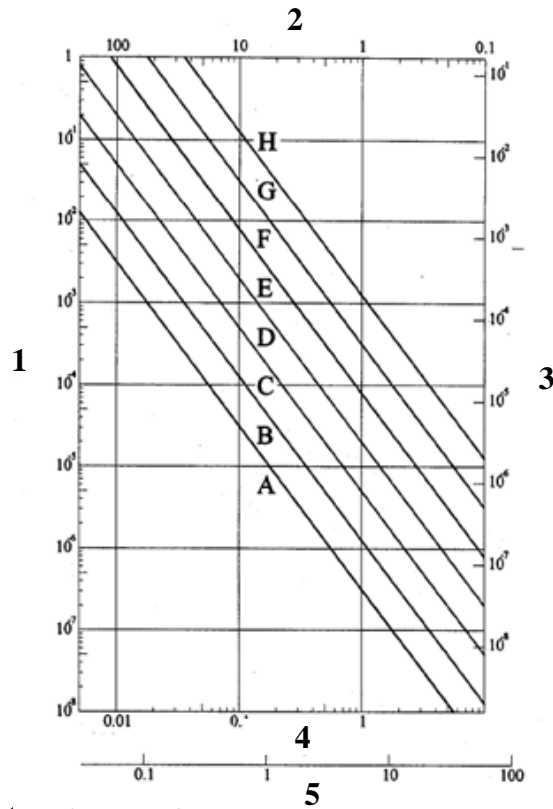


Figure 3-7: Road Surface Classification (ISO 8608) (Tyan et al., 2009).

The numbers on the axes are presented as 1: displacement PSD,  $\Phi(n)$  [ $m^3$ ], 2: wavelength,  $\lambda$  [m] 3: displacement PSD,  $\Phi(\Omega)$  [ $m^3$ ], 4: spatial frequency,  $n$  [cycle/m] and 5: angular frequency,  $\Omega$  [rad/m].

Table 3-2: Road Roughness Classified by ISO (Tyan et al., 2009)

	Degree of roughness $\Phi(\Omega_0)$ ( $10^{-6} m^2 / (cycle / m)$ ) where $n_0 = 0.1$ cycle/m		
Road class	Lower limit	Geometric mean	Upper limit
A (very good)	-	16	32
B (good)	32	64	128
C (average)	128	256	512
D (poor)	512	1,024	2,048
E (very poor)	2,048	4,096	8,192

Table 3-3: Road Roughness Expressed in Terms of  $\Omega$  (Tyan et al., 2009)

	Degree of roughness $\Phi(\Omega_0)$ ( $10^{-6} m^3$ ) where $\Omega_0 = 1 \text{ rad} / m$		
Class of the road	Lower limit	Geometric mean	Upper limit
A (very good)	-	1	2
B (good)	2	4	8
C (average)	8	16	32
D (poor)	32	64	128
E (very poor)	128	256	512

### 3.9 Calibration of the Model for Non-Stationary Inputs

In order to maximise and check the suspension model, an excitation signal should represent reality as closely as possible. In general, there are several waveforms can be used as a road profile, such as sine shape profile and square waves. In this study, the road profile is calculated according to the vehicle speed and the shape of the bump via the following equation:

$$u(p) = 1/2a * \sin(2 * \pi * f_p * t), \quad 3-27$$

where  $a$  is the height of the bump, 50 mm in this study,  $f_p$  is the effective frequency, which was calculated by considering the shape of the bump and the vehicle speed, and  $t$  is the time taken to pass over the bump. The road bump excitation signals are delayed between the front and rear wheels,  $z_{r1}$  and  $z_{r2}$ ,  $z_{r3}$  and  $z_{r4}$  according to ( $\tau = l/v$ ), where  $\tau$  is the delay in the time,  $l$  is the bump width, and  $v$  is the speed of the vehicle. A plot of road profile for the bump in time domain is presented in Figure 3-8.

To validate the model, data was collected from experiments of driving the vehicle over a bump on the premises of Huddersfield University (for more details see Section 8.2). The bump profile had dimensions of 5.80 m in width, 0.05 m in height, and 0.50 m in length. The same bump profile shown in Figure 3-8 was applied in the model. The comparison of the simulation and the experimental were performed in the time domain in terms of acceleration.

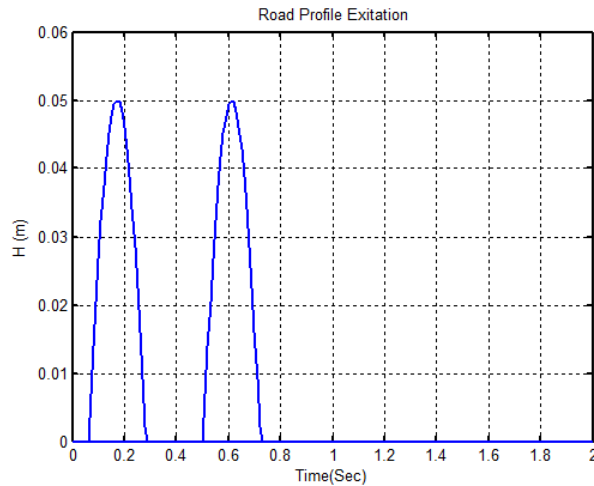


Figure 3-8: Road profile in time domain

Figure 3-9 shows the time domain analysis of the body acceleration, based on the experiments and simulation analysis. It should be conducted that the model prediction of the system behaviour matches reasonably well with the experimental data. However, a general observation from the validation was that there are some fluctuations in the period between the front and rear wheels; this period is between about 0.3 and 0.5 seconds. These fluctuations can be attributed to background noise interference which usually appear with the experimental data, and also to the simplicity of the model which assumed some factors such as aerodynamics forces and friction coefficients to be negligible.

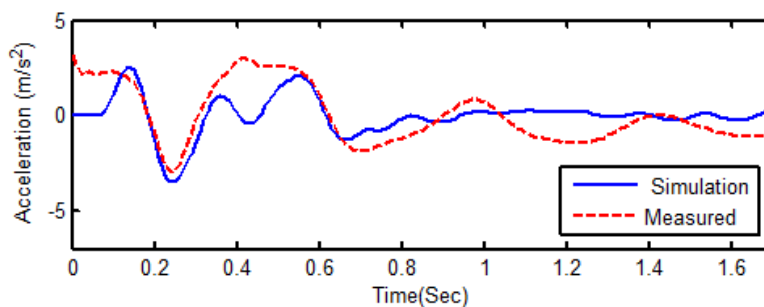


Figure 3-9: Vibration of suspension simulation and experiment for  $V= 8 \text{ km/h}$

### 3.10 Calibration of the Model for Stationary Inputs

#### 3.10.1 Random Road Profiles

The power spectral density (PSD) is the main factor to form the road profile. In order to obtain the PSD function, the measurements of the surface profile with respect to a reference plane need to be determined, then random road profiles can be calculated by a PSD in the form of (Tyan et al., 2009):

$$\Phi(\Omega) = \Phi(\Omega_0) \left( \frac{\Omega}{\Omega_0} \right)^{-\omega} \quad \text{or} \quad \Phi(n) = \Phi(n_0) \left( \frac{n}{n_0} \right)^{-\omega} \quad 3-28$$

where:  $\Omega = 2\pi/L$  (rad/m) is the angular spatial frequency,  $L$  is the wavelength,  $\Phi(\Omega_0)$  in  $m^2/(rad/m)$  is the PSD value,  $\Omega_0 = 1 \text{ rad/m}$ ,  $n = \Omega/2\pi$  is the frequency,  $n_0 = 0.1 \text{ cycle/m}$ , and  $\omega$  is the waveform,  $\omega = 2$ .

The International Organization for Standardization (ISO 8606) presented the standard for pavement roughness used in roads, where the following standard formulation has been adopted to describe pavement roughness PSD:

$$\Phi(\Omega) = \begin{cases} \Phi(\Omega_0)\Omega_1^{-2}, \dots \text{for}, 0 \leq \Omega \leq \Omega_1, \\ \Phi(\Omega_0) \left( \frac{\Omega}{\Omega_0} \right)^{-2}, \dots \text{for}, \Omega_1 < \Omega \leq \Omega_N, \\ 0, \dots \text{for}, \Omega_N < \Omega, \end{cases} \quad 3-29$$

Here the reference values of PSD at  $\Omega_0 = 1 \text{ rad/m}$ , are given by ISO 8608 as shown in

Table 3-3.  $\Omega_1 = 0.02\pi \text{ rad/m}$ , and  $\Omega_N = 6\pi \text{ rad/m}$  as suggested by ISO 8608 (Tyan et al., 2009).

In order to create a random road profile over a regime of length  $L$ . A superposition of  $N (\rightarrow \infty)$  sine waves can be assumed to be a single track for the random profile:

$$z_R(s) = \sum_{i=1}^N A_i \sin(\Omega_i s - \Phi_i), \quad 3-30$$

Where the amplitude  $A_i$  is calculated as follows:

$$A_i = \sqrt{\Phi(\Omega_i) \frac{\Delta\Omega}{\pi}}, i = 1, \dots, N. \quad 3-31$$

Here,  $\Delta\Omega \cong \frac{\Omega_N - \Omega_1}{N - 1}$  (rad/sec), following a uniform format in the period of  $[0, 2\pi]$ .

Plots of random road profiles for each corner of the tested vehicle (FL, FR, RL and RR) in the time domain are shown in Figure 3-10, which presents the random road profile for class B (good) with vehicle speed of 30 km/h. This figure presented that the signals are non-stationary, with many large local responses. In this study a 7-DOF model was investigated to simulate the response of a vehicle when operated on the road at an approximately constant speed. A random

road disturbance, which has been plotted in Figure 3-10, is assumed as the input for the model. In the simulations, the excitation input lead to vertical vibrations in the whole vehicle.

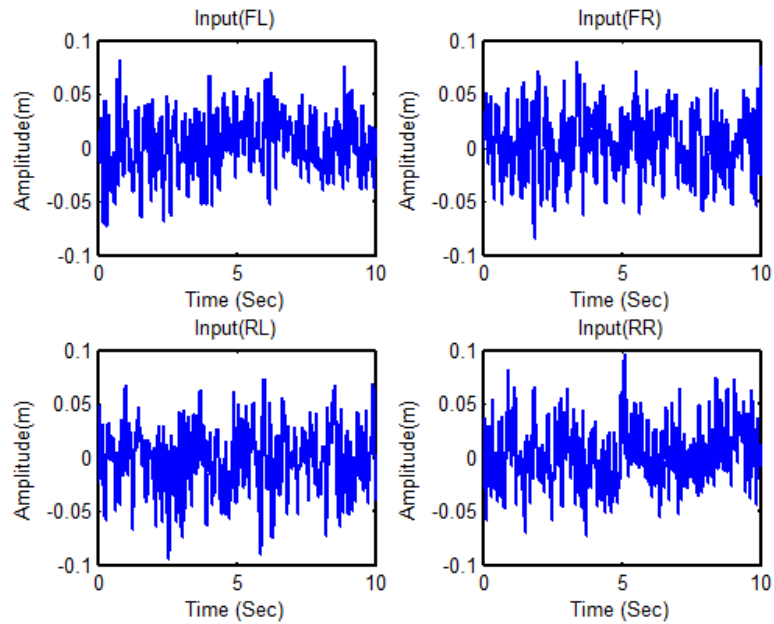


Figure 3-10: Time domain for Random road profiles

The time domain acceleration of the four corners of the vehicle (FL, FR, RL and RR) are shown in Figure 3-11. It can be noted from this figure that the acceleration responses of the vehicle are again non-stationary, with many local large responses. This is as a result of the random inputs to the system.

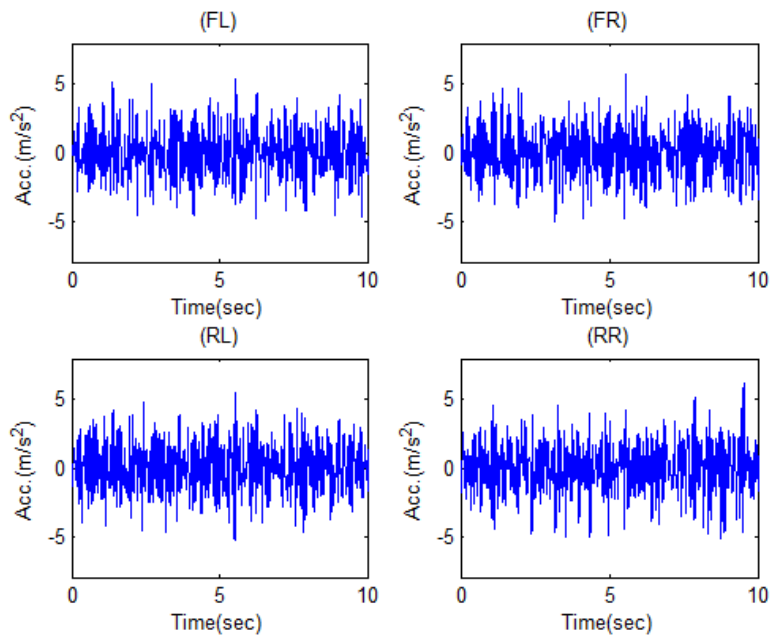


Figure 3-11: Simulation of acceleration of the four corner of the vehicle in the time domain

To validate the proposed model during real operation, this study investigates on-road tests to measure the vibration response of the vehicle body through acceleration measurements. In particular, this is done to check and evaluate the vibration response when the vehicle operates on various normal city road conditions. Figure 3-12 presents the measured vibration signals from the four accelerometers distributed on the vehicle body (for more details of the experimental setup, procedures and specifications (see Chapter 8), when the vehicle travelled on normal city roads at about 40 km. This figure shows that the signals are non-stationary, with many large local responses; the amplitude value of the acceleration signal in Figure 3-12 shows approximately the same values as the acceleration of the simulation in Figure 3-11.

To obtain the frequency response of the vehicle, the time domain results were transferred to the frequency domain. Figure 3-13 shows the spectra of the vertical accelerations of the vehicle body for the simulations and the experimental data for front left corner (FL). This figure shows that every vibration response causes a resonance frequency and generates peaks in the vicinity between 1 Hz to 4 Hz. This indicates the frequency response of the body.

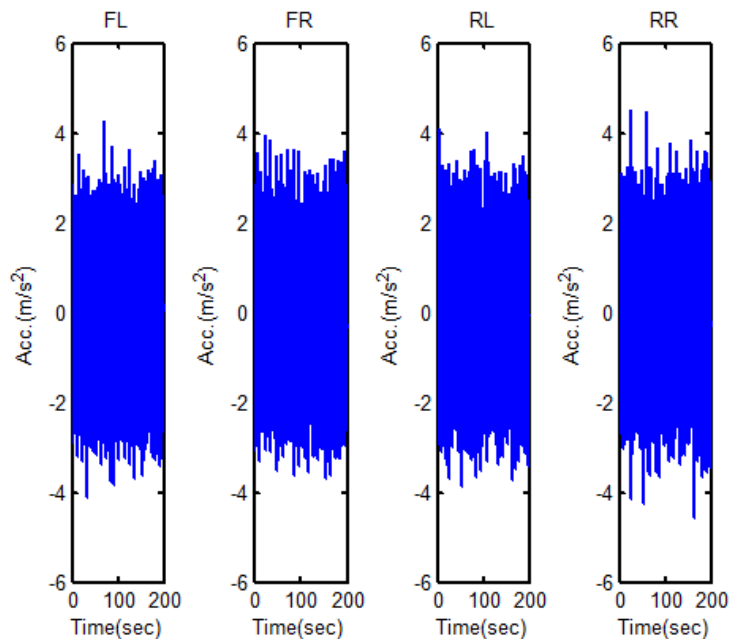


Figure 3-12: Measured acceleration of the vehicle body (FL, FR, RL and RR)

The vibration generates peak values in the frequency about 10 Hz to 13 Hz. This can be indicated that this range of high-frequency is a range of the wheels' vibration. From Figure 3-13 it can be concluded that the spectrum signatures obtained from the model shows a similar trend with the real measured data. In addition the model predicts fairly well the performance of the suspension responses.

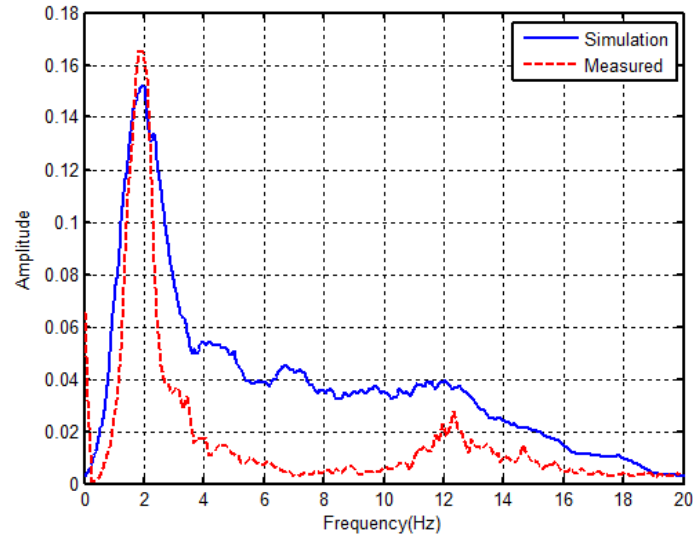


Figure 3-13: Spectra of the vehicle body for measured and simulated vibration (FL)

### 3.11 Calibration of the Model for Stochastic Subspace Identification (SSI)

#### 3.11.1 Simulation Modal Parameters of the Vehicle by SSI

The validation processes have been conducted for the SSI model by using the outputs of the 7-DOF model (responses of the vehicle body at four corners) in the base line conditions as inputs for (SSI) model, and then stochastic subspace method is implemented to identify vehicle parameters. In the simulation, the parameters of the vehicle include the bounce, pitch and roll modes have been identified. Therefore, the natural frequency  $f_i$  and damping ratio  $\xi_i$  of the bounce, pitch and roll modes of the vehicle body are shown in Table 3-4 respectively.

Table 3-4 : Natural frequency and damping ratio for the SSI simulation

Mode	Bounce	Pitch	Roll
$f_i$	1.59	1.79	2.1
$\xi_i$	0.215	0.222	0.265

Modal shapes of the bounce, pitch and roll modes of the vehicle body which were simulated by applying SSI are shown in Figure 3-14 , for baseline condition of the vehicle which mean consisted of no change in the suspension and tyre conditions.

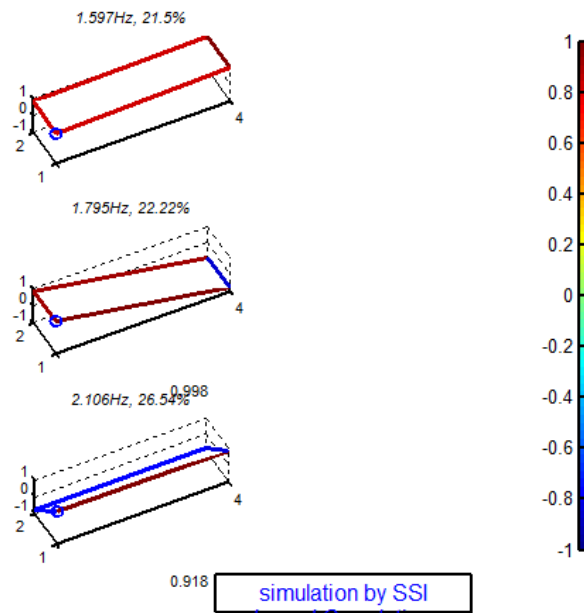


Figure 3-14: Mode shapes of the bounce, pitch and roll mode by SSI simulation.

It can be noted from Figure 3-14 that, bounce frequency is around 1.59 Hz with damping ratio of 21.5%, the bounce mode shape shows how far the vehicle's body moved in the vertical direction. Pitch frequency is in the range of 1.79 Hz with a damping ratio of about 22.22%, the pitch mode shape illustrates how the vehicle body moves up from one side and down from the other side. The roll frequency was in the range of about 2.1 Hz with a damping ratio of 26.54%. The rolling mode shape gives insight into how the vehicle body moved up and down in the longitudinal of the body, which was in the opposite direction to the pitching.

### 3.11.2 Measured Modal Parameters of the Vehicle by (SSI)

To validate the models in real operations, this study applies subspace identification method to assess the dynamic parameters of the vehicle body through vibration measurements. In particular, it is to check and evaluate if any significant vibration modes occur when the vehicle operates on normal city roads under normal conditions.

All data sets from on-road tests are processed to obtain measured modal parameters for each test case. The method used for this output-only parameter identification is an average correlation signal based stochastic subspace identification (ACS-SSI) developed recently by Z. Chen et al., (2015) for online vehicle dynamics analysis. For more details about the experimental setup, test procedures and equipment's specifications (see Chapter 8). By applying (ACS-SSI) modal parameters of the vehicle can be identified. Therefore, the natural

frequency  $f_i$  and damping ratio  $\xi_i$  of the bounce, pitch and roll modes of the vehicle body are shown in Table 3-5.

Table 3-5 : Natural frequency and damping for the measured data by SSI

Mode	Bounce	Pitch	Roll
$f_i$	1.5845	1.7110	2.3094
$\xi_i$	0.1602	0.2493	0.2577

Figure 3-15 present modal shapes of the bounce, pitch and roll modes of the vehicle body, which were obtained by applying (ACS-SSI) technique to the measured data, for baseline condition of the vehicle which mean consisted of no change in the suspension and tyre conditions. In this figure a bounce frequency is around 1.584 Hz with damping ratio of 16.04%. Pitch frequency is in the range of 1.71 Hz with a damping ratio of about 24.93% and the roll frequency was in the range of about 2.3 Hz with a damping ratio of 30.6%. The rolling mode shape gives insight into how the vehicle body moved up and down in the longitudinal of the body, which was in the opposite direction to the pitching.

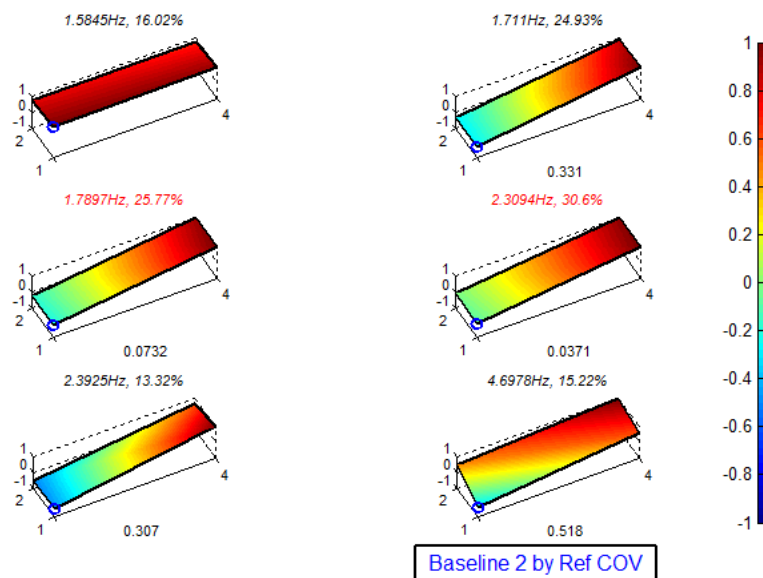


Figure 3-15: Measured mode shapes of the bounce, pitch and roll mode for vehicle body.

### 3.12 Summary

It can be summarised that, the impulse function can give a helpful information for the response of the vehicle when subjected to an unknown force history.

From stationary and non-stationary validation analysis, the simulation results and the measured results show the similar trends and acceptable agreements in the time and frequency domain. This can lead to, the developed full model can be a reliable for further research to study the online condition monitoring of the vehicle. The modal parameters which have been identified and obtained in the previous section by using measured (SSI) were compared with the (SSI) model and show an acceptable agreements.

## CHAPTER 4

### MODAL CHARACTERISTICS OF SUSPENSION SYSTEM UNDER FAULT CONDITIONS BASED ON SIMULATIONS

*This chapter presents simulation studies for examining modal characteristics of a suspension system under different conditions including different abnormal suspension cases. The seven degree-of-freedom (7-DOF) model for a full vehicle which developed in the previous chapter is solved by an impulse based standard state space method to obtain mode parameters including modal frequency, damping ratio and mode shapes. It has found that, the modal frequency and damping are influenced more by vehicle load conditions and is not suitable for monitoring faults from suspension systems. On the other hand the shapes of the bounce and pitch modes are less sensitive to the vehicle load and speed but to the suspension parameters including stiffness, damping and tyre inflation pressures.*

*Following this, the suspension performances include ride comfort, handling and stability of the vehicle were analysed based on the impulse input from a real road pump. This is followed by simulation analysis for the effects of the damping changes and the under-inflation of the tyre on the suspension performances.*

## 4.1 Introduction

As shown in the model developed in Chapter 3, vibration responses are related to the sprung mass. It means that the load of a vehicle will alter the vibration responses even if the excitation of road profiles is the same. Therefore, the direct measurement of vibration response magnitudes is not reliable for monitoring faults of the suspension systems and the feasibility of new approaches feasible must be investigated.

To identify a feasible approach that is independent of load and road conditions, a symmetric simulation study was conducted, in which the quantitative variations of modal parameters are analysed under different fault cases. Based on this study those parameters that are least influenced by load and road changes but most sensitive to faults will be selected for use in fault detection and diagnosis. Common faults in suspension system and their influences to handling and ride performance were presented using the model.

## 4.2 Simulation Results for the 7-DOF Vehicle Model

A mathematical model was investigated as a tool to predict the response of a vehicle when driven on the road. A random road disturbance, shown in Figure 3-10, is assumed as the input for the model. In the simulation, the excitation input leads to vertical vibrations in the whole vehicle. To show the fundamental characteristics of vibration modes, a commercial vehicle was examined, which has the relative parameters shown in Table 3-1. By using these parameters, the modal parameters for the 7-DOF model including the natural frequencies  $f_i$  (Hz) and damping  $\xi_i$  (%) are shown in Table 4-1, where the first three modes are bounce, pitch and roll, respectively.

Table 4-1: Natural frequency and damping ratio for the 7-dof vehicle model

Mode	Bounce	Pitch	Roll	FL-w	FR-w	RL-w	RR-w
$f_i$	1.518	1.778	2.135	10.840	10.840	11.532	11.532
$\xi_i$	0.2268	0.3297	0.3567	0.2314	0.232	0.2438	0.2439

Analysis of the frequency response function of a sprung mass is carried out for bounce (B), pitch (P), and roll (R) of the body and the vehicle wheels (FL, FR, RL and RR) respectively as shown in Figure 4-1. In this figure, the bounce, pitch and roll modes are within the frequency of 1 to 3 Hz and the wheels frequencies are around 10 to 13 Hz.

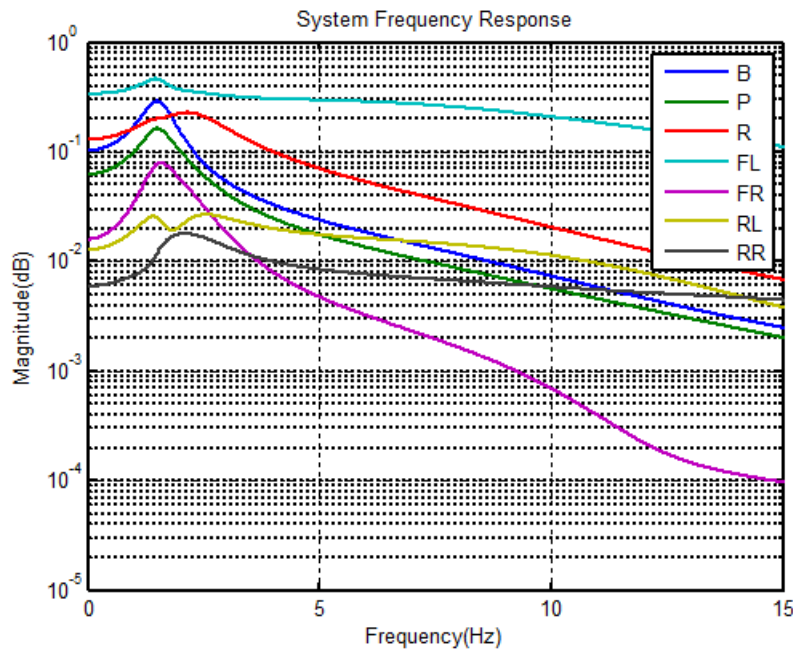


Figure 4-1: Frequency response function of the vehicle

Figure 4-2 presents (top) the responses of the body modes and (bottom) the modal shapes of the vehicle body. In Figure 4-2 the bounce frequency is around 1.51 Hz with a damping ratio of 22.68 %. The bounce mode shape shows how far the vehicle's body moved in the vertical. Pitch frequency is in the range of 1.77 Hz with a damping of 32.97 %. The pitch shape illustrates how the vehicle body moves up on one side and down on the other side. The roll frequency was in the range of about 2.13 Hz, with a damping ratio of 35.67 %. The rolling mode shape gives insight into how the vehicle body moved up and down around the longitudinal side of the body, perpendicular to the direction of pitching.

From the mode shapes in Figure 4-2, it can be noted that high relative deformations of the vehicle body occur at the front position for the bounce modes, at rear position for the pitch modes and along the sides for the roll modes. From this figure it can be seen that the body is subject to high dynamic loads at these positions.

Moreover, it can be seen that for an ideal vehicle the bounce and pitch modes should have no rolling movement, i.e. the two coordinates of the corresponding modal vector in the front and rear are the same. In other words, any difference between the two coordinates can be an indication of the asymmetry due to the abnormality in a suspension element, such as a weakened spring, hydraulic oil leakage, an under-inflated tyre or inadequate adjustment.

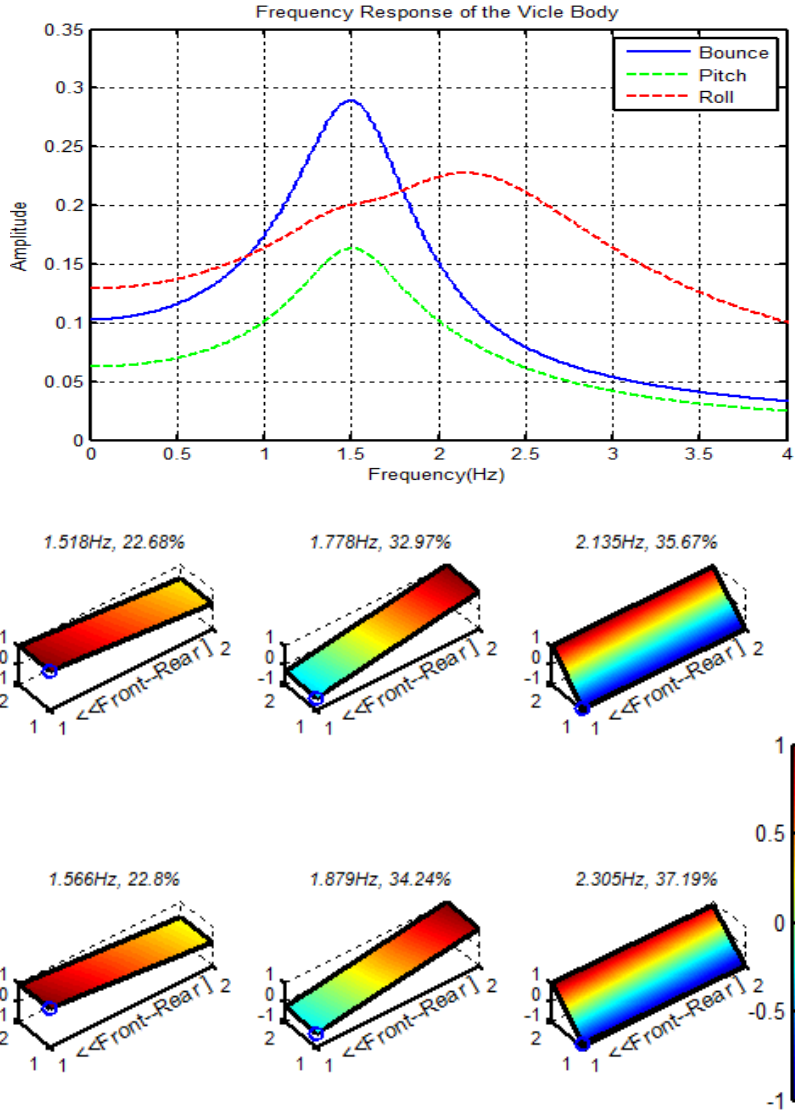


Figure 4-2: Frequency response and mode shapes of bounce pitch and roll

### 4.3 Modal Shape Characteristics under Different Defects

The eigenvector  $v$  associated with the eigenvalue  $\lambda$  is known as mode shape. The vehicle mode shapes can be obtained from the matrix  $A$ , and the energy of the mode shapes can be calculated as following procedure. For the bounce mode, the front and rear rolling differences are:

$$dE_{B12} = 2[v_1(1)^2 - v_1(2)^2] / [v_1(1)^2 + v_1(2)^2] \quad 4-1$$

$$dE_{B34} = 2[v_1(3)^2 - v_1(4)^2] / [v_1(3)^2 + v_1(4)^2]$$

And for the pitch mode:

$$dE_{P12} = 2[v_2(1)^2 - v_2(2)^2] / [v_2(1)^2 + v_2(2)^2] \quad 4-2$$

$$dE_{P34} = 2[v_2(3)^2 - v_2(4)^2] / [v_2(3)^2 + v_2(4)^2]$$

where,  $dE_{B12}$  and  $dE_{B34}$  are the rolling energies for the front and rear bouncing modes, while  $dE_{P12}$  and  $dE_{P34}$  are the rolling energies for the front and rear pitching modes. Finally, the detection and diagnostic of changes in each suspension parameter (damping coefficient, spring rate and under-inflation of the tyre) can be obtained by the modal energy difference.

### 4.3.1 Simulation of Damping Reduction

Suspension faults have been considered by reducing the damping coefficients of the (F-L), (F-R), (R-L) and (R-R) shock absorbers in 10 % increments from 20 % to 60 % of their original values. Figure 4-3 shows the changes in the natural frequency, damping ratio and modal shape for the vehicle modes for damping reduction of the front left shock absorber.

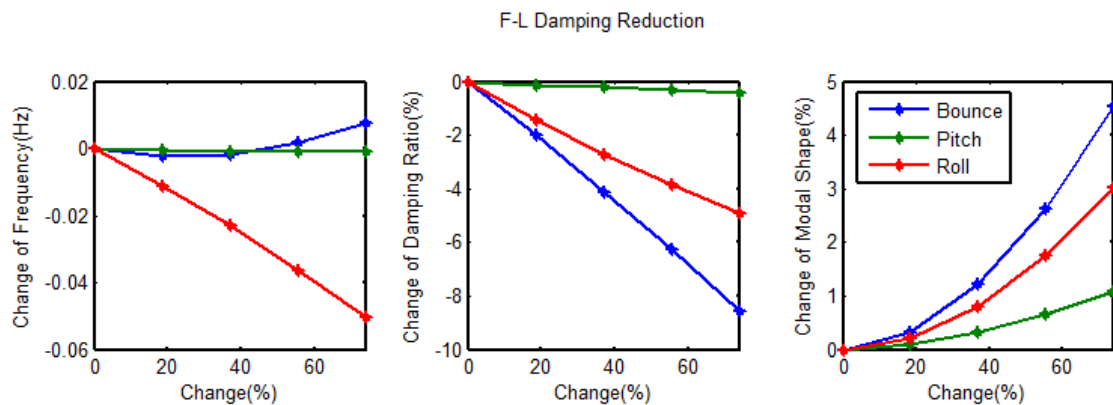


Figure 4-3: Changes in natural frequency, damping ratio and mode shape for the bounce, pitch and roll modes for a damping reduction of the front left (F-L) shock absorber

Modal Energy Differences (MED) for the front and rear rolling of the bounce and pitch modes for each of the vehicle's shock absorbers (F-L, F-R, R-L and R-R) are presented in Figure 4-4. It can be noted from this figure that the fault signature of each shock absorber has a different trend. For instance, by reducing the F-L damping coefficient the rolling energy of the front bouncing increases and the rolling energy of the rear bouncing decreases until around 50 %, when it shows a dramatic increase. It is worth noting that this trend in the simulation agrees with the experimental results presented in Section 8.6.3. For the rolling energy of the front and rear pitching in the same side (F-L), the front pitching shows an increase with the reduction in damping, while the rear pitching shows a slight decrease. An opposite trend can be seen with the front right side (F-R) for the reduction of the damping coefficients. Therefore, the fault signature of each side has its own trend and it can be effectively used for diagnostics and detection of damping faults. The influence of reducing the damping on the modal energy for

the rear left R-L and rear right R-R shock absorbers are shown in the bottom part of Figure 4-4. It can be noted that both sides show different trends and the modal energy of pitching has more significant fluctuation than the bounce energy. The modal energy of the front pitching increases in the R-L damper and decreases in the R-R side, which indicates that each side has directly opposite trends.

In summary, the key findings indicate that in each case when the damping coefficient was reduced, the fault signature has a different trend. Therefore diagnosis and fault detection of the damping change can be effectively achieved. In addition, these simulations have been validated by experimental results as shown in Section 8.6.3.

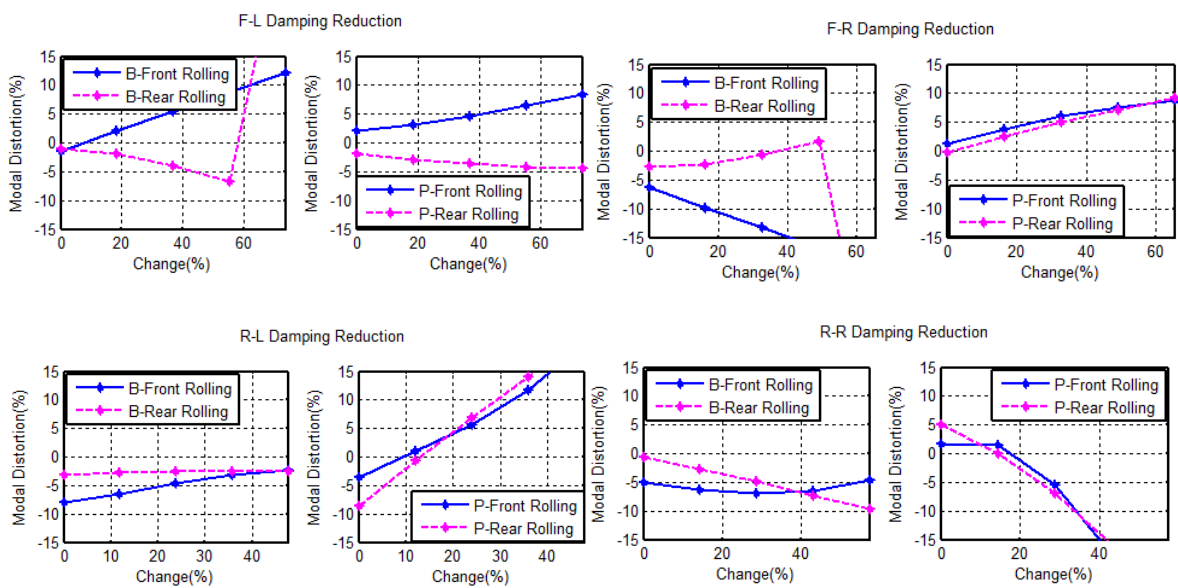


Figure 4-4: Modal energy differences for bounce and pitch modes for each damper of the vehicle

### 4.3.2 Simulation of Tyre Pressure Changes

Suspension faults have been introduced to the model by reducing the pressure of the vehicle tyre at different cases, i.e. at standard pressure (2.2 bar), and at 10 %, 20 %, 30 % and 40 % under-inflated. Figure 4-5 presents the effect of the front left tyre pressure change in the natural frequency, damping ratio and modal shape of the vehicle modes.

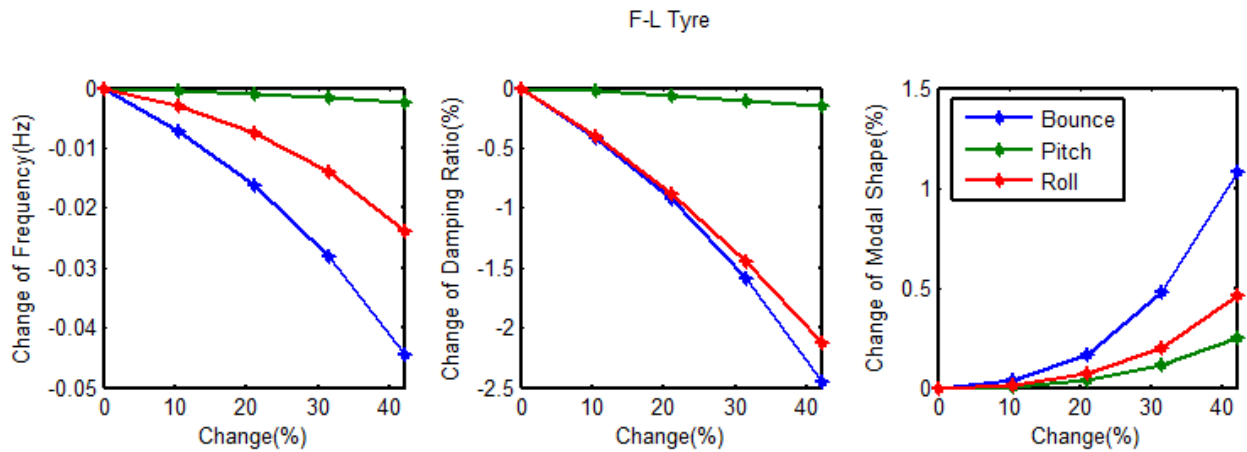


Figure 4-5: Changes in the natural frequency, damping ratio and modal shape for under-inflation of the front left tyre

Figure 4-6 presents Modal Energy Differences (MED) for front and rear rolling of the bounce and pitch modes respectively for each tyre of the vehicle. It can be noted from these figures that the fault signature of each tyre has its own trend. In this figure, rolling energy of the front and rear bouncing (B) for the front left (F-L) tyre increases steadily, and the energy of the pitching decreases slightly. Meanwhile, the energy differences of the bounce in the front right (F-R) tyre drops dramatically with under-inflation of the pressure, and the pitching energy increases slightly for front rolling and decreases in the rear rolling.

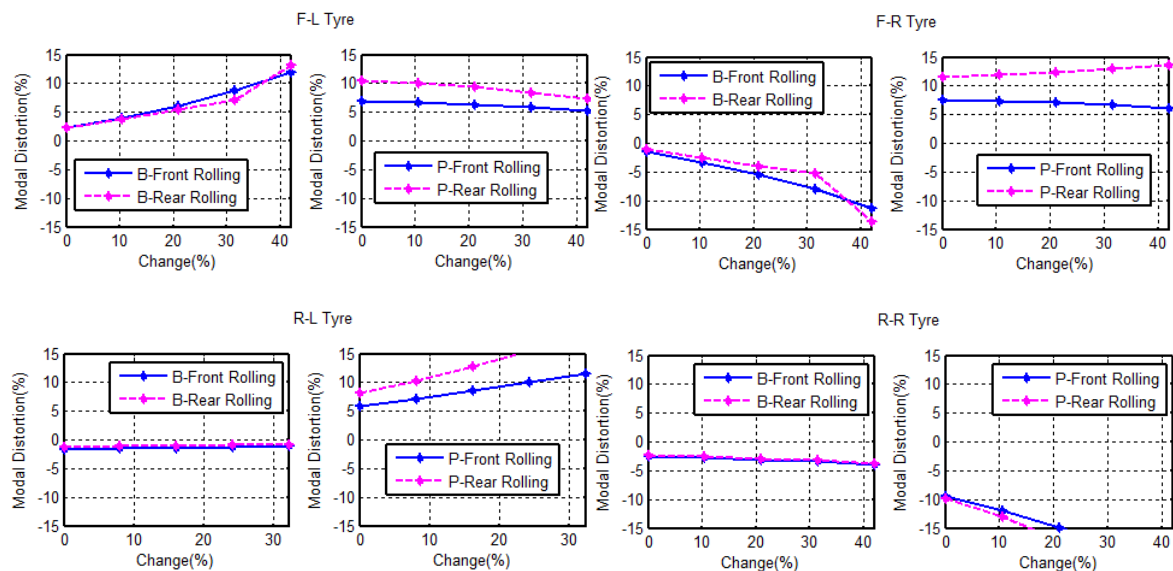


Figure 4-6: Modal energy differences for front and rear rolling of bounce and pitch modes

It can be seen that the front left and the front right tyres show opposite trends, which mean the data can be used to distinguish the under-inflation of the tyres.

For the rear tyres, the modal energy of the pitching (P) has more deflection than the bounce (B) and with opposite trends, i.e. the pitching energy rises up in the rear left and shows a dramatic decrease in the rear right, which can help in detection and diagnostic of under-inflation of each tyre separately. It can be summarised that the under-inflation of tyres can be distinguished for each side by monitoring the change of modal energy for front and rear bounce and pitch modes. Moreover, these results have been validated by experimental results as shown in Section 8.6.2.

### 4.3.3 Simulation of Spring Weakness

Suspension faults have been considered by reducing the spring stiffness in 5 % increments from 5 % to 20 % of their original values for the four corner of the vehicle springs (F-L), (F-R), (R-L) and (R-R). Figure 4-7 presents the changes in natural frequency, damping ratio and modal shape for the vehicle modes for spring weakness of the rear right spring.

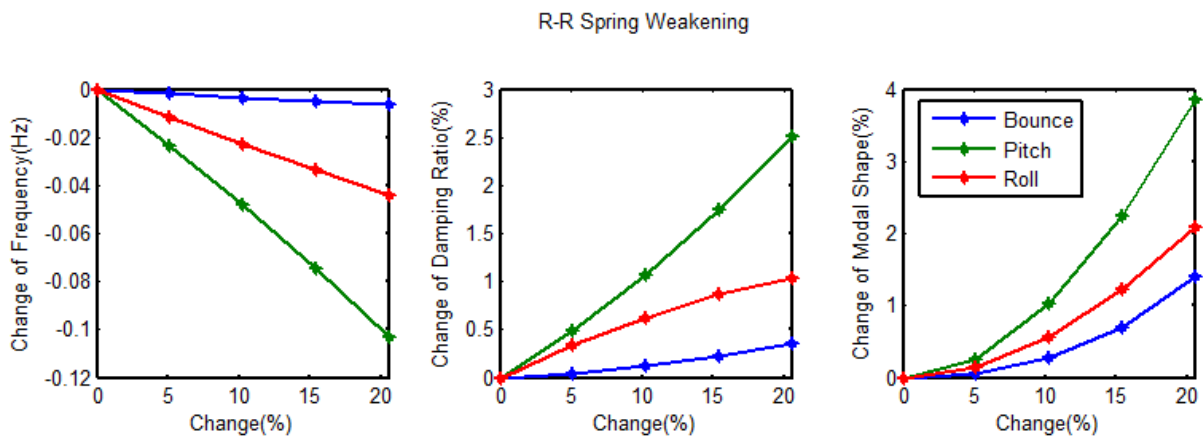


Figure 4-7: Changes in the natural frequency, damping ratio and modal shape for a weakened rear right spring

Modal Energy Differences for the front and rear rolling of bounce and pitch modes for each spring of the vehicle are shown in Figure 4-8. It can be noted from this figure that the modal energy for front left F-L and front right F-R springs have more fluctuations than the pitching modes and show opposite trends. This increases in the front left side and decreases in the front right side. Therefore, these fault signatures can be used for diagnosis of spring faults in each side.

For the rear springs, the modal energy of the pitching has more deflection than the bounce and with opposite trends, which can enable the detection and diagnosis of faults for each side. It can be summarised that the spring weakness can be distinguished effectively for each side by monitoring the change of modal energy in front and rear bounce and pitch modes.

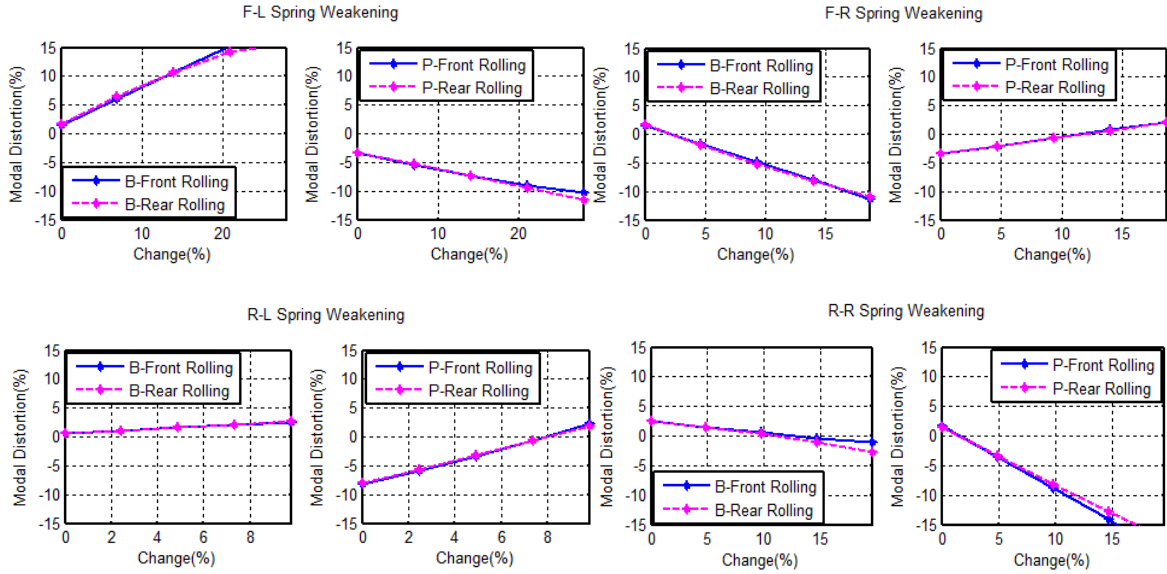


Figure 4-8: Modal energy differences for bounce and pitch modes for each spring of the vehicle

#### 4.4 Suspension Performances Analysis Using Deterministic Inputs

The performances of suspension system include ride quality; handling and vehicle stability were discussed and presented. The road conditions and vehicle speed effect and any change in suspension specifications, including the effect of damping change and under inflation of the tyre on the suspension performance has been investigated. In this research faults have been conducted to the damping systems. The faults were introduced by decreasing the damping coefficients by 25 %, 50 % and 80 %. The effect of tyre pressure on the performance of the suspension was also examined. The suspension performance parameters examined and the results of the simulation indicate that these parameters require design optimisation, as their conflicting requirements must be balanced.

#### 4.5 Road Profile for Non-stationary Input

The assumed road profile is a bump with a half a sine wave shape. This profile has been created by considering the shape of the bump and the vehicle speed via the following equation (see Section 3.8):

$$Z(p) = \frac{1}{a} \sin(2\pi f_p t), \quad 4-3$$

where  $a$  is the bump height, considered in this study to be one of 50, 70 and 100 mm,  $f_p$  is the effective frequency of the bump calculated by considering the shape of the bump in terms of the length and width and the vehicle speed, and  $t$  is the time taken to pass over the bump. The

road input excitation signals are delayed between the front and rear wheels, according to the vehicle speed and the width of the bump ( $\tau = l/v$ ), where  $l$  is the width of the bump, and  $v$  is presented the vehicle speed. The plots of road profile for three common bumps are detailed in Table 4-2 with vehicle velocity of 8 km/hr is illustrated in Figure 4-9

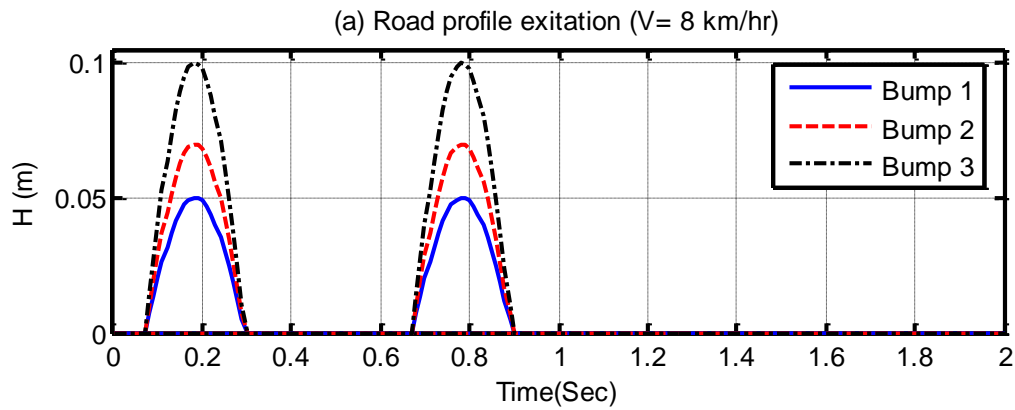


Figure 4-9: Road profile in time domain plot

#### 4.6 Model Simulation Conditions for Non-stationary Input

Three bump sizes were considered in this study (as shown in the Table 4-2): Bump 1 (500 mm width x 50 mm height), Bump 2 (500 mm width x 70 mm height), and Bump 3 (500 mm width x 100 mm height). These were each presented to the model at 8 km/hr, 16 km/hr, 24 km/hr and 32 km/hr, and also with a range of tyre pressures (see Table 4-2).

Table 4-2: Model simulation conditions

Bump sizes	Width (mm)	Height (mm)	speed (km/hr)	Tyre pressure (bar)
Bump 1	500	50	The model was run with speeds of 8, 16, 24 and 32	Standard pressure of 2.3 bar, then 1.5 bar for passenger, driver and both wheels
Bump 2	500	70		
Bump 3	500	100		

#### 4.7 Effects of Bump’s Geometry on Suspension Performance

In this study a simulation has been conducted to analyse the vehicle dynamics when driven over different speed bumps at a variety of speeds. Three bump sizes were considered in this simulation, the input of the system has been assumed to be the road disturbance, when the vehicle passes through these different bumps the excitation input leads to vertical vibrations in the whole system.

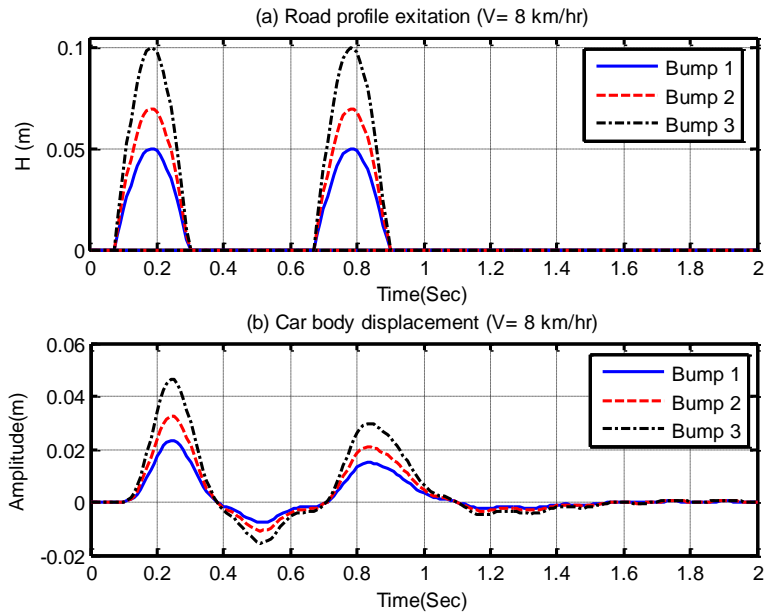


Figure 4-10: (a) Road profile excitation and (b) displacement of vehicle body for different bumps at vehicle speed 8 km/hr

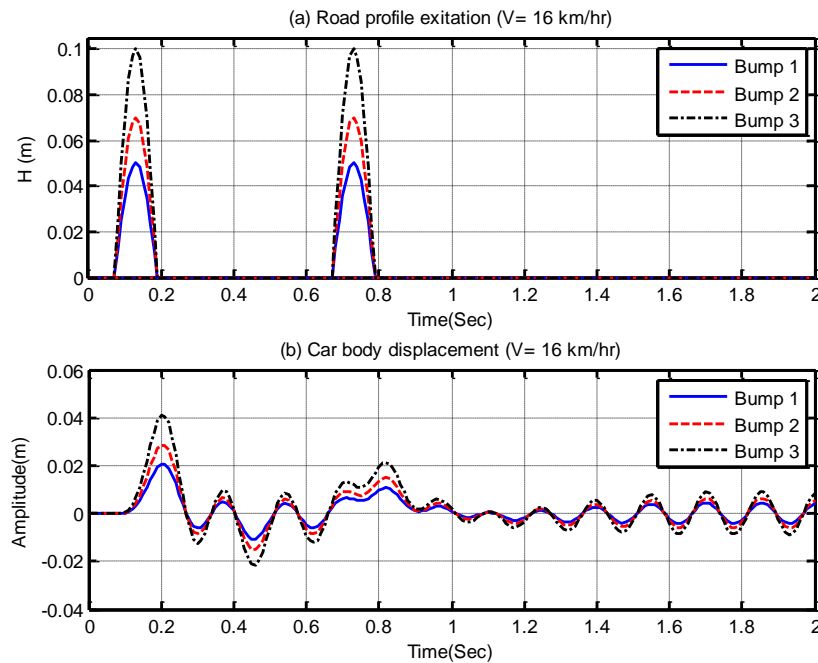


Figure 4-11: (a) Road profile and (b) displacement of the body for different bumps at ( $V= 16$  km/hr)

The plots of road profile for the three bumps, which were presented in Table 4-2, with vehicle velocities of 8 and 16 km/hr are presented in Figure 4-10 (a) and Figure 4-11 (a) for front and rear wheel of the vehicle respectively. Figure 4-10 (b) and Figure 4-11 (b) represent the displacement of the vehicle body for three bumps with vehicle velocities of 8 km/hr and 16 km/hr in time domain.

Figure 4-12 shows the displacement of the four wheels of the vehicle in time domain at the same conditions, the effect of each bump size as an amplitude value (m) that can be achieved for vehicle body and the four wheels. From these plots, the amplitude of the vehicle body and the wheels increase gradually with the increase of the bump's height.

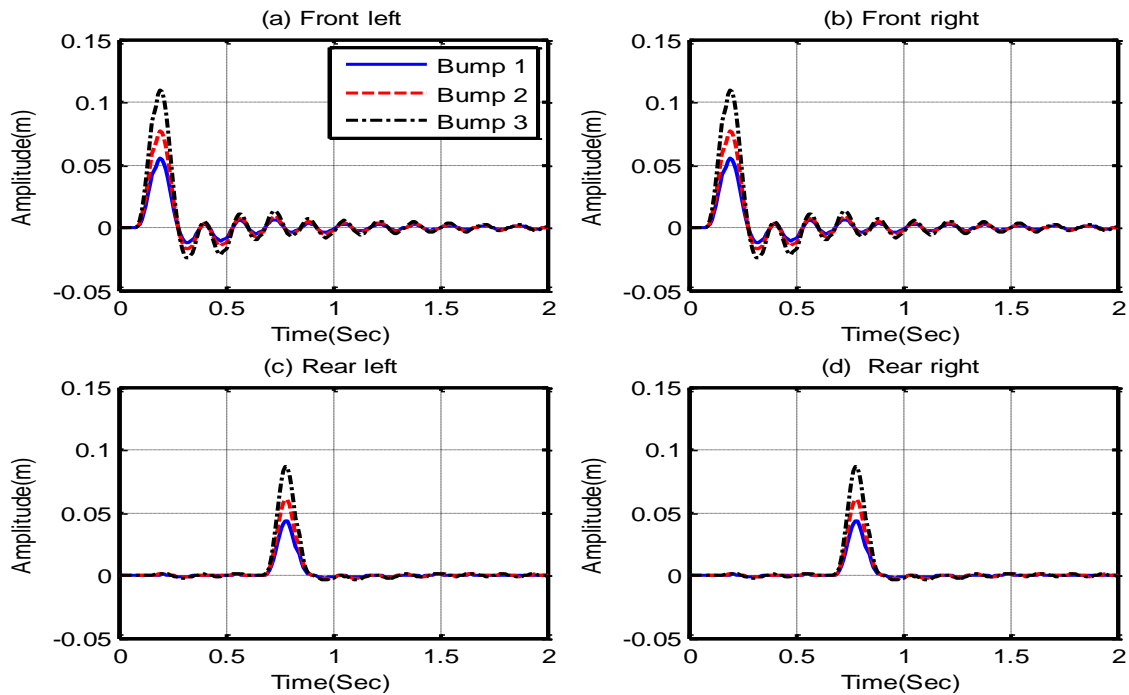


Figure 4-12: Vehicle wheel's displacement with different road profile (bumps) at  $V= 8$  km/hr

This indicates that, the performance of the suspension may be affected by this change in the geometry of bumps or road disturbances. It should be noted that, the signal was delayed between front wheel and rear wheel by the time delay which has been calculated according to vehicle speed and width of the bump as presented in (section 4.5). To analyse the vehicle performances such as of ride comfort, handling and vehicle stability, three main parameters have been analysed and presented in this section.

These parameters are the suspension travel, wheel deflection, and the body acceleration. The aim is for each of these parameters to have small amplitudes. A vehicle's handling is governed by the contact forces between the tyre and the profile surface. The wheel deflection is represented by the distance between the input and the suspension system ( $z_u - z_r$ ), the wheel deflection for this simulation was about (0.0055 m, 0.0078 m and 0.011 m) for bump1, bump 2 and bump 3 respectively as presented in Figure 4-13. This range of wheel deflection seems

to be acceptable when compared to with the agreed standard for road handling which preferred to be in the range of 0.0508 m as per ISO: 2631-1-1997 (Mitra et al., 2013).

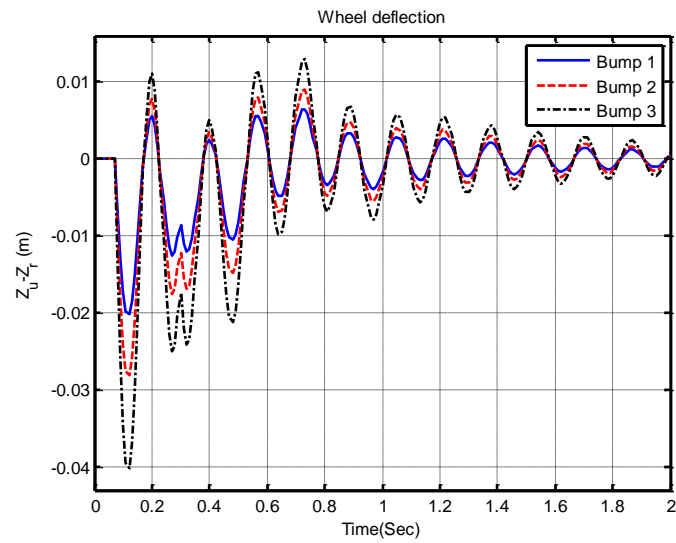


Figure 4-13: Wheel deflections for different bumps

Suspension travel is defined as a relative displacement between the vehicle body and the wheel ( $z_s - z_u$ ) as shown in Figure 4-14, the suspension travel value was about 0.023 m, 0.03 m and 0.045 m for passing the vehicle of bump1, bump 2 and bump 3 respectively. This range of suspension travel seems to be acceptable compared with the standard value which must be in the range of minimum of 0.127 m as per ISO: 2631-1-1997 (Mitra et al., 2013).

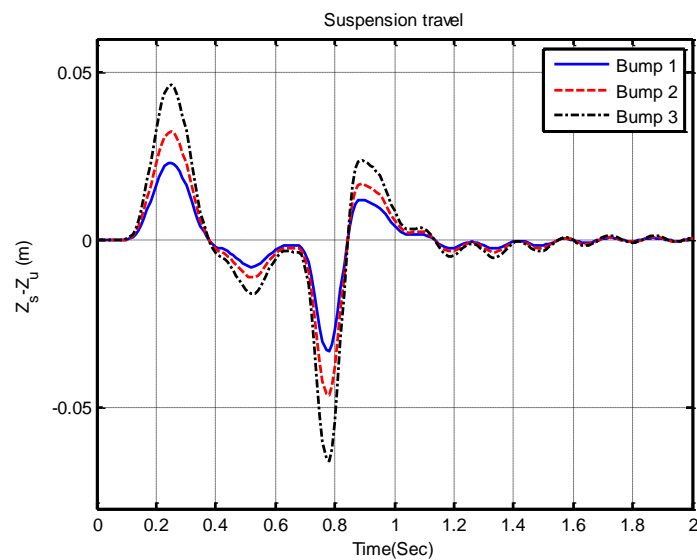


Figure 4-14: Suspension travel for different bumps

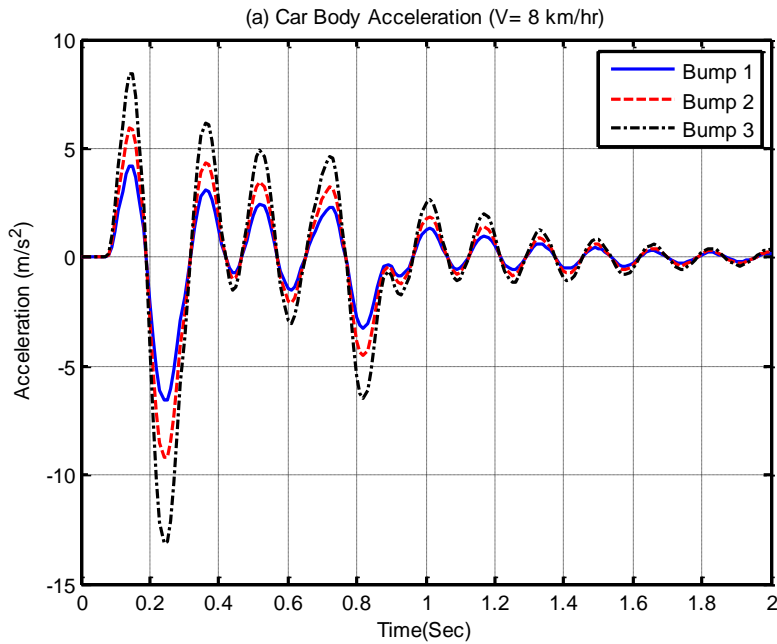


Figure 4-15: Acceleration of the vehicle body with different road profile at ( $V= 8$  km/hr)

According to ISO: 2631-1-1997 (Mitra et al., 2013), the ride comfort will be obtained if the RMS acceleration is under  $0.315$  m/s<sup>2</sup>. Ride comfort relates the passengers' perception of the body motion. The vehicle body acceleration should be relatively small for optimum comfort. Figure 4-15 shows the vehicle body acceleration. In addition, the simulated acceleration results seem to be agree with the work of other such as Agharkakli et al., (2012).

#### 4.8 Effects of Vehicle Speeds on Suspension Performance

To simulate vibration in terms of vehicle speed, the vibration can be simulated in the case of different road profiles. Figure 4-16 shows a typical RMS for acceleration of the body for different speed levels of  $8$  km/hr,  $11$  km/hr,  $16$  km/hr,  $24$  km/hr and  $32$  km/hr, with different bump size. These results indicate that the effect of vehicle speed on the acceleration was strong at a lower speed and weak in high speed. It can be clearly noted that the change of the RMS value was high with changing the speed at lower values from  $8$  to  $11$  km/hr than changing the speed at high values from  $11$  to  $16$  and from  $24$  to  $32$  km/hr which shows a slight change. In addition, the highest acceleration was found during the speed of  $16$ – $24$ km/hr. In addition, these results have been compared with (Lu, Ishikawa, Kitazawa, & Satake, 2010) and show some agreement.

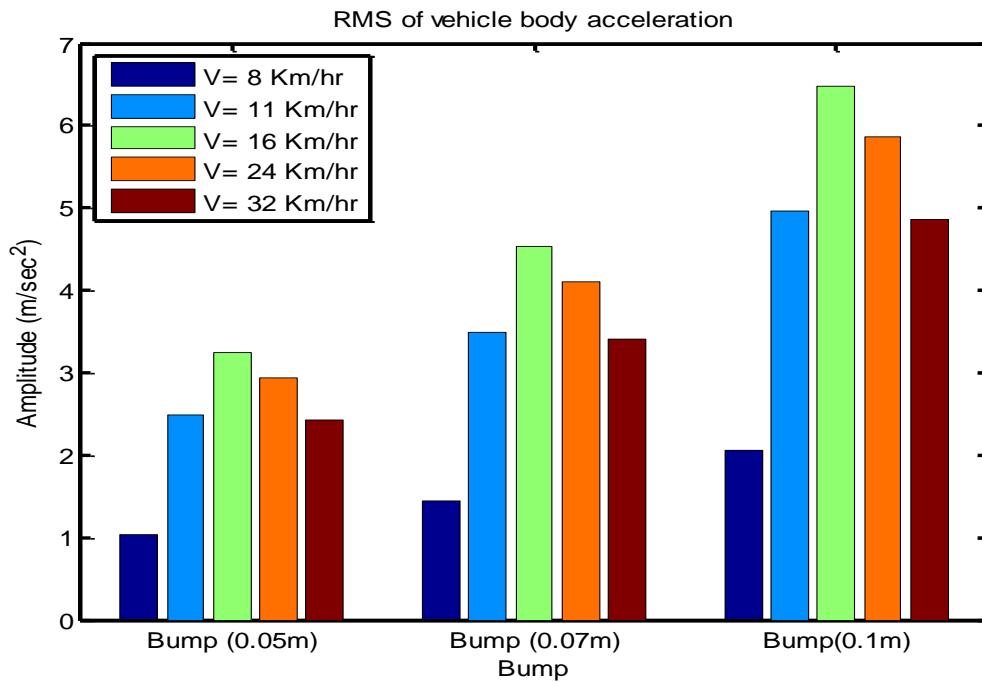


Figure 4-16: RMS of vehicle body with different speeds and different bumps

#### 4.9 Influences of the Suspension Parameters on Suspension Performance

In this study simulations were conducted to analyse the dynamics of a vehicle when the vehicle passed different speed bumps, and also to investigate the effect of damping reductions, spring weakness and incorrect inflation pressures in vehicle tyres on suspension performances. The following is the simulation analysis for the effects of the damping change, spring weakness and under-inflation of the tyre on suspension performance.

##### 4.9.1 Effects of Damper Faults on Suspension Performance

Figure 4-17(a) shows the time domain road profiles for both the front and rear wheels of the vehicle. In addition, Figure 4-17(b) shows the effect on the vehicle body response of varying the damping coefficients. These results show that increases in the damping cause a decrease the car body's relative displacement. Figure 4-18 shows the displacement of the four wheels for different damping coefficients. The results show the wheel displacement to decrease with a drop in the damping coefficient. This is indicative of the system performance being sensitive to the damping coefficients.

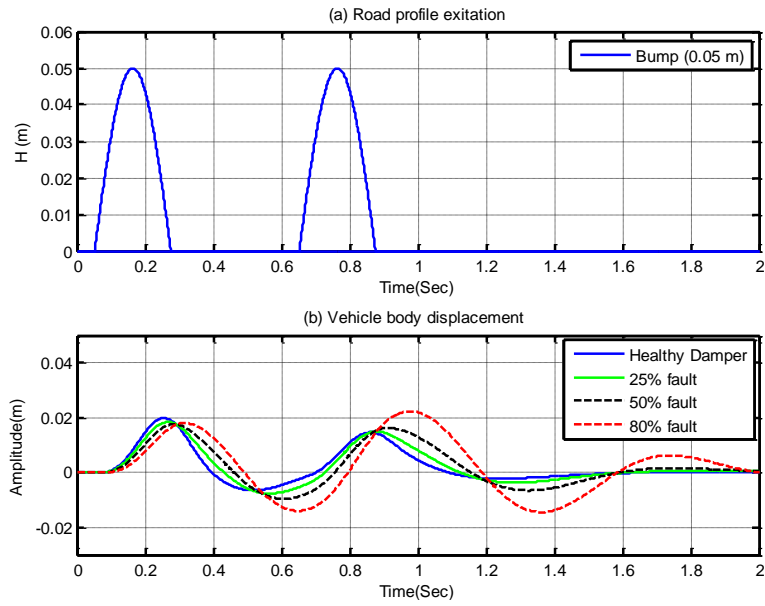


Figure 4-17: (a) Road profile excitation and (b) Displacement of vehicle body for different damping coefficients

Analysis of the suspension performances were conducted to examine the effects of different damping levels on the suspension parameters (which include handling, ride quality, and vehicle stability).

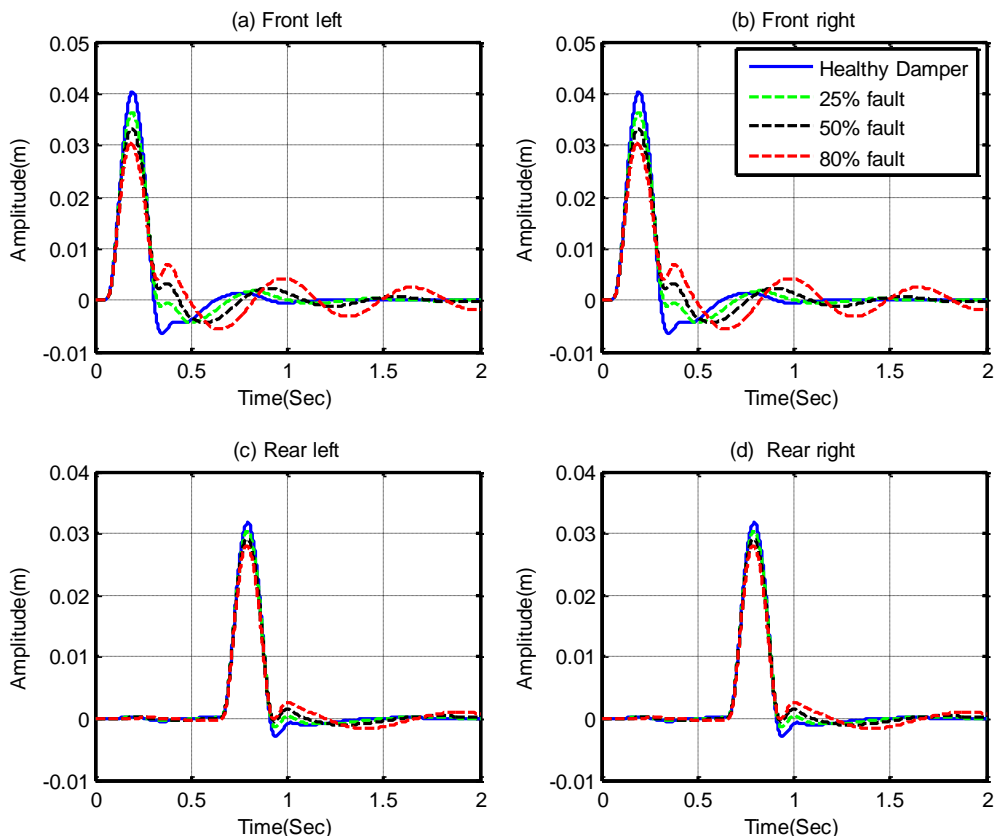


Figure 4-18: Vehicle wheel's displacement with different damping coefficients

For this simulation, the wheel deflections were approximately 0.015 m, 0.0147 m, 0.146 m and 0.0143m for a healthy, 25%, 50%, 80% faulty damper respectively, as presented in Figure 4-19. From this figure, no noticeable changes in the peak value of the wheel deflection can be observed. However, it can be noted that the vertical deflection does not decay quickly with faulty dampers, in particular, those with 80% and 50% faults. The suspension travel can be defined as a relative displacement between the vehicle body and the wheel ( $z_s - z_u$ ) as shown in Figure 4-20. From this figure, it can be observed that a higher damping coefficient provides for a lower suspension travel therefore to reduce the suspension travel a higher damping ratio is required.

In accordance with ISO: 2631-1-1997 (Mitra et al., 2013) the passenger is thought to feel highly comfortable if the RMS acceleration is below 0.315 m/s<sup>2</sup>. In Figure 4-21 (on the left) the amplitudes of the vertical acceleration were increased within the domain of the vehicle body (sprung mass) as the shock absorber damping was increased. Higher values for the shock absorber damping provided better oscillatory comfort for the passenger at excitation frequencies approximating the resonant frequency of the vehicle body. However, the vertical acceleration does not decay quickly with the reduction of the damping.

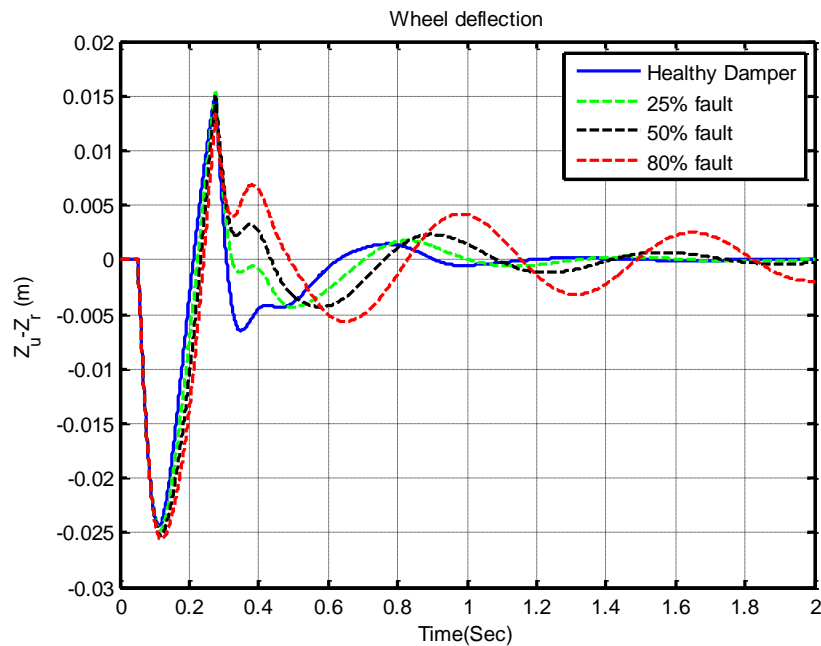


Figure 4-19: Wheel deflections for different damping coefficients

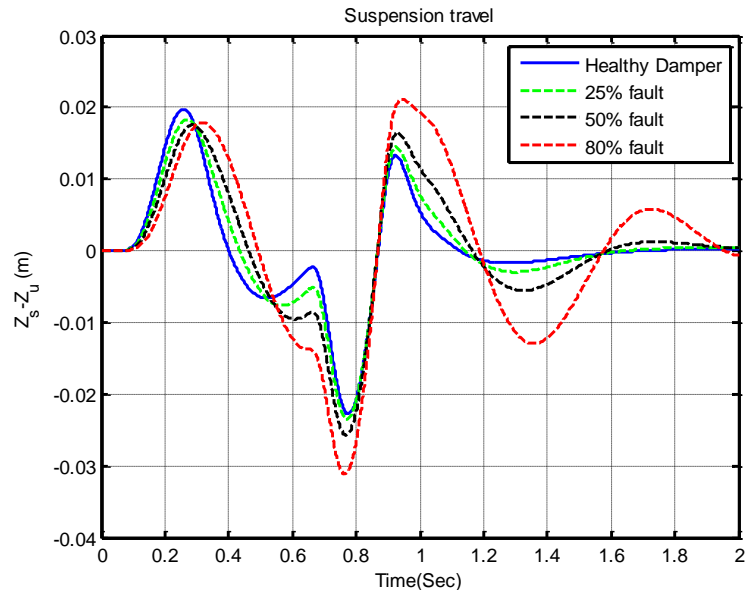


Figure 4-20: Suspension travel for different damping coefficients

Figure 4-21(right) shows an example of the RMS vehicle body acceleration with damping values: 0 % (healthy), 25 %, 50 % and 80 % faulty. These results show that the acceleration of the vehicle body decreases with decreasing damping coefficient in the cases of 25 % and 50 % faults. However, the vehicle body acceleration increases slightly for the 80 % fault condition.

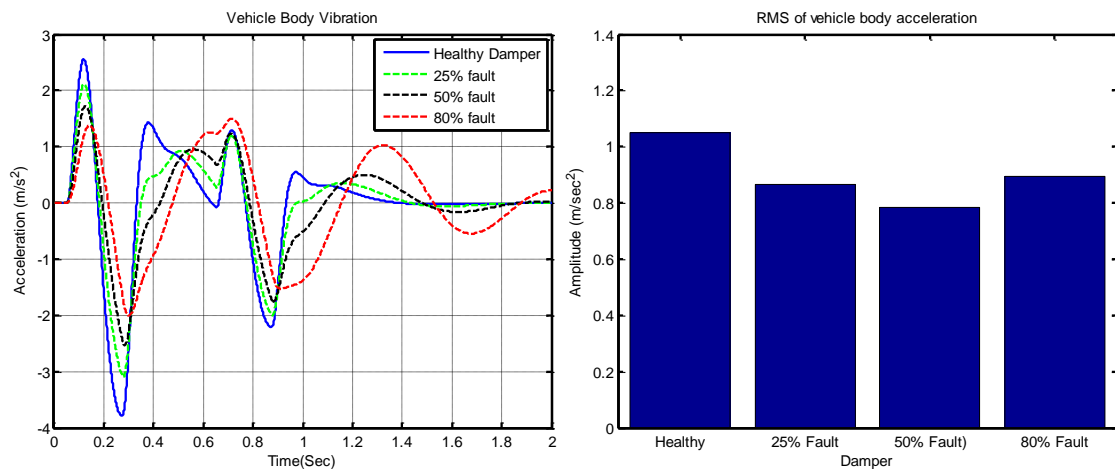


Figure 4-21: Acceleration (on the left) and RMS (on the right) of the vehicle body for different damping coefficients

#### 4.9.2 Effects of Under-Inflation Tyre on Suspension Performance

Figure 4-22(a) shows time domain the road profile for the wheels of the vehicle. The effect on the vehicle body response of varying tyre pressure is presented in Figure 4-22(b). From this figure, tyre pressure reduction causes a resulting increase in the car body's displacement.

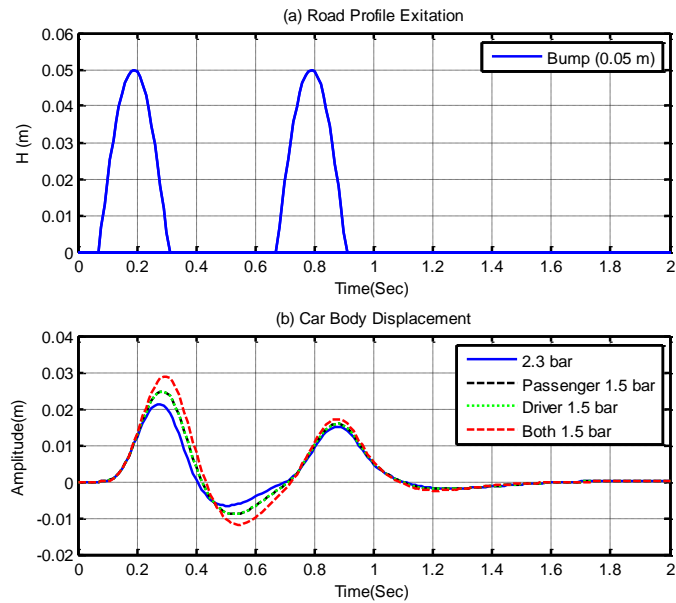


Figure 4-22: (a) Road profile excitation and (b) displacement of vehicle body for different tyre pressure

Figure 4-23 depicts the displacement of four wheels with different tyre pressures in the time domain. The results show an apparent rise in the amplitude of the front wheels when the tyre pressure value was reduced. This indicates that the performance of the suspension may be affected by under-inflated tyres which will be the focus of more detailed discussions to follow.

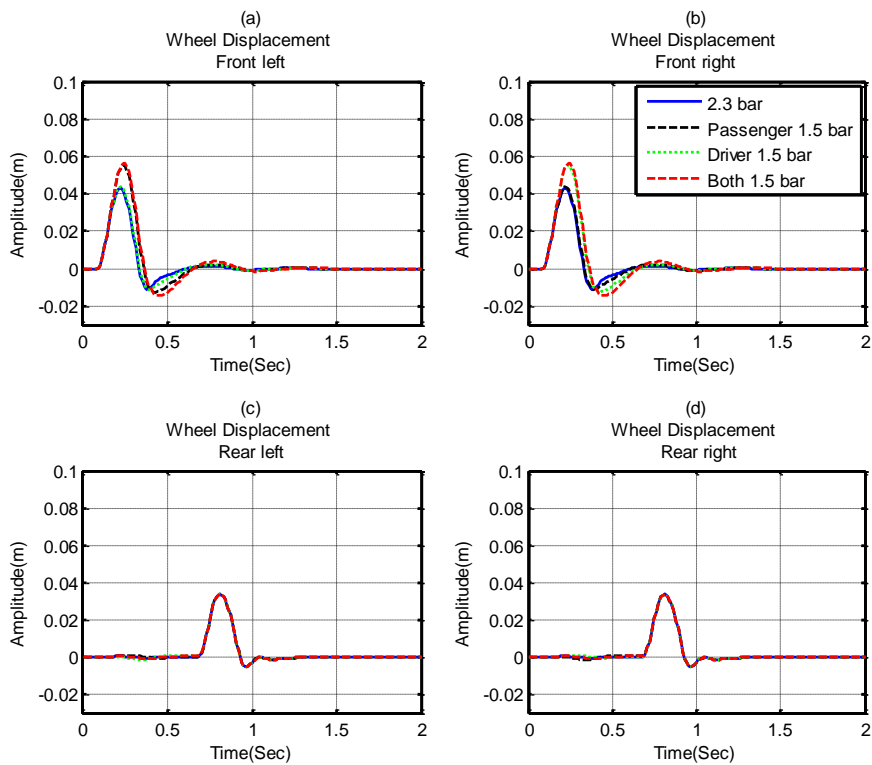


Figure 4-23: Vehicle wheel's displacement for different tyre pressure

The road handling is defined based on the contact forces between the road surface and the vehicle tyre ( $z_u - z_r$ ) and it is expressed by wheel deflection. For this simulation, the wheel deflections were approximately 0.017 m, 0.03 m, 0.013 m and 0.033 m for the standard pressure, 1.5 bar for the passenger, driver and front wheels respectively, as presented in Figure 4-24.

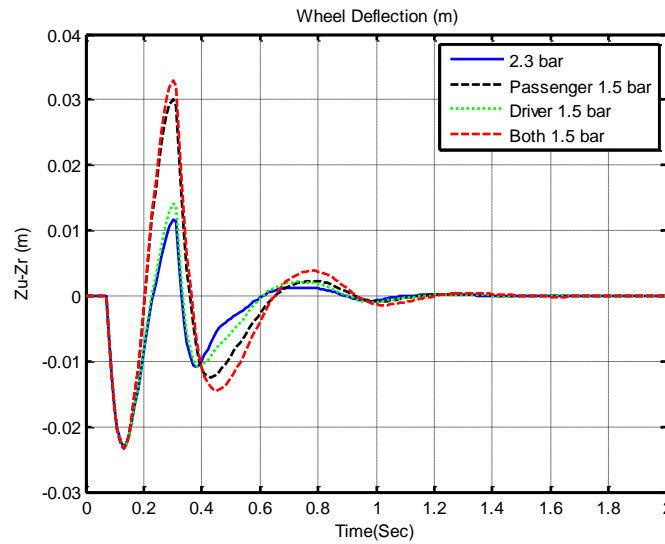


Figure 4-24: Wheel deflections for different tyre pressures

The suspension travel can be defined as a relative displacement between the vehicle body and the wheel ( $z_s - z_u$ ), in Figure 4-25 the suspension travel values are 0.021 m, 0.023 m, 0.025 m and 0.028 m for standard pressure, 1.5 bar passenger, 1.5 bar driver and 1.5 bar both wheels respectively. As it is expected the suspension travel is increasing with decreasing of tyre pressure. But this should be optimized with vehicle handling and stability.

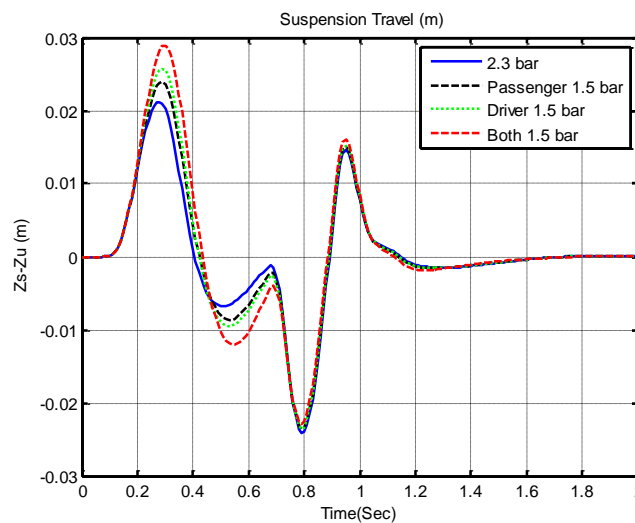


Figure 4-25: Suspension travel for different tyre pressure

Figure 4-26 (a) shows the effect of under-inflation of the tyre on the acceleration of the vehicle body. Figure 4-26 (b) shows RMS for acceleration of the vehicle at different tyre pressures. It can be noted that, the RMS value increases with the lowering of the tyre pressure, which indicated that, the ride comfort is affected negatively by under-inflation of the tyre. It can be summarized that, under-inflated tyres affect the suspension performance in conflicting criteria, it shows a slight change in terms of road handling, and however, it has a notable affect in terms of ride quality as shown in RMS plots.

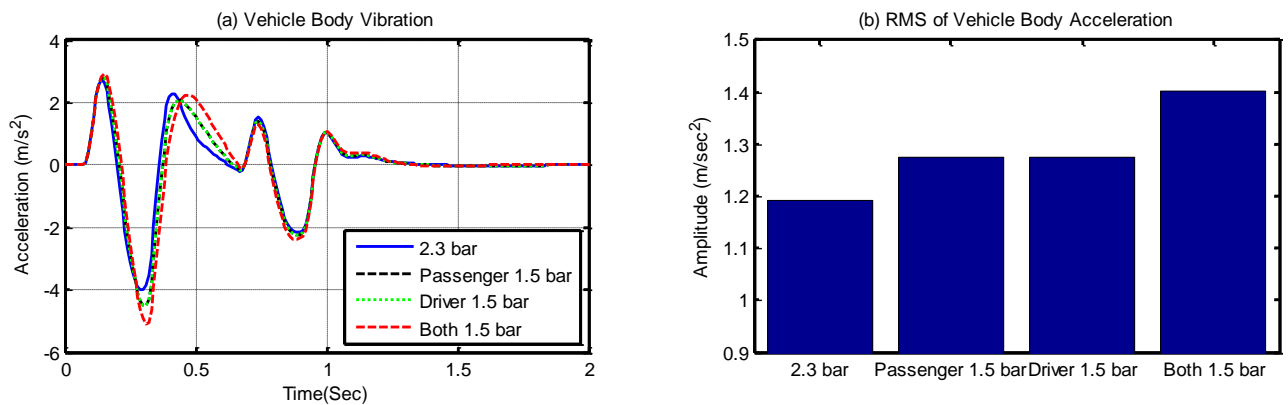


Figure 4-26: (a) Acceleration of the vehicle body with different tyre pressure and (b) RMS for acceleration of the body for different tyre pressure

#### 4.10 Summary

Simulation studies under various conditions have shown that vibration responses on four corners contain the information on suspension parameters. They show that the modal parameters, which are obtained by standard impulse method, are independent of vehicle operating conditions: load and speed, and sensitive to different the changes of faulty components. Therefore, the modal parameters can be taken as the optimal feature parameters for monitoring the suspension systems.

Subsequent studies based on real impulse of road bumps have shown that the vibration responses also changes sensitively with various faulty cases. The vibration amplitude changes may give an indication on the faults but they cannot be implemented accurately because noise influences. However, as the responses show clear correlations and interferences between the front and rear wheel excitations, it is difficult to obtain model parameters by common modal identification methods such as transient response analysis and frequency domain methods.

## CHAPTER 5

# SUBSPACE-BASED SYSTEM IDENTIFICATION AND FAULT DETECTION

*To obtain modal parameters online, this chapter investigates recent stochastic subspace identification (SSI) frameworks. An average correlation signal based stochastic subspace identification (ACS-SSI) method is concentrated more as it has been more effective and efficient for online vehicle dynamics analysis. In particular, it allows multiple data records or data frames to be combined through an average scheme in the correlation lag domain to effectively suppresses random noise and non-stationary contents, enabling more accurate and reliable identification of the modal parameters and hence achieve high performance of fault detection and diagnosis. Based these in depth understandings, it has found that it is potential to improve the method by a cross validation scheme of the correlation signals for determining optimal reference channels.*

## 5.1 Introduction

Studies made in Chapters 3 and 4 shown that it is feasible to monitor suspension system through modal parameter estimation. In particular, modal shape parameters can produce more reliable diagnostics. Therefore, this chapter focuses on developing effective modal identification methods that can be applied to online identification based on feasible or minimum number of vibration measurements.

Subspace identification methods have developed tremendously in recent years in both theory and practice because of its high performance and efficient implementation for characterising dynamics of complicated systems. Characteristics of interest to the mechanical engineer regarding this model are its vibration modes (it's eigenfrequencies) and its mode shapes (corresponding eigenvectors) (Döhler, Andersen, & Mevel, 2012).

A review of system identification for operational modal was discussed by Bart Peeters & De Roeck (2001), also an overview of subspace methods has been presented by Maia, (1997) ; Ewins, 2000 & J. Kim & Lynch (2012). In addition, input-output system identification methods for applications in structural dynamics was presented by Abdelghani et al. (1998) & Petsounis & Fassois (2001) & Antonacci et al. (2012). These critical reviews all confirms that subspace identification frameworks are more potential for online applications.

Many variants have been developed using the subspace identification framework, which include raw data SSI and covariance SSI. Of particular interesting is the average correlation signal based stochastic subspace identification (ACS-SSI) technique developed recently by Chen et al. (2015) as it has shown superior results in the identification of the dynamic properties of vehicle frames just based on online vibration measurements from road excitations.

However, their works have validated the effectiveness of ACS-SSI for the cases when the vibration responses are in a high frequency range ( $>20\text{Hz}$ ) and modal damping ratios are less than 10% which are of typical properties of vehicle frames. Alternatively, it has not been verified that the method is applicable to the scenarios of low frequency and high damping systems. Typically, the damping ratios of a suspension are about 10% to 30% and the frequency range is from 0.5 to 3 Hz. Moreover, some researchers in the review have pointed out that conventional methods may be not so effective to provide reliable results for such systems. Nevertheless, ACS-SSI is very efficient in noise suppression and computations. Therefore, this

study will focus on the verification of this new approach in conjunction with necessary improvements to the ACS-SSI in dealing with low frequency high damping scenarios.

To this end, this chapter examines the ACS-SSI by overviewing its relative background and applications. In parallel, it also investigates further its applicability and accuracy according to the theoretical basis of SSI frameworks and the signal characteristics of suspension systems, which will be included in the examination process directly for more concise clarification, rather than as a separate section which needs to recap a large amount of content.

## **5.2 Operational Modal Analysis (OMA) Methods**

In experimental modal analysis, modal parameters can be identified from vibration data (Mohanty & Rixen, 2005). Generally, ones an input is affected the system and ones the output is measured. In the most cases the input is assumed to be a stochastic process (white noise) instead of using the deterministic knowledge of the system input. Therefore, the term output-only modal analysis is used for the identification of vibrating structures.

Output-only modal analysis was first implemented in civil engineering (Bart Peeters & De Roeck, 2001) because it is difficult to generate excitations in heavy constructions such as buildings and bridges. Similarly, operational modal analysis has the positional to be useful in mechanical engineering, for example to identify the vehicle's modal parameters during operating.

There are many different stochastic identification methods that are ideal for modal parameters estimation of mechanical structures. Because of availability of output data only from the measurements in operational mechanical systems, as a result, the operational modal analysis (OMA) has the most potential to be used in estimation of the parameters for online operations of the applications. Subsequently, many techniques of OMA have the potential to be implemented in an online dynamics analysis of vehicles (Bart Peeters & De Roeck, 2001 & Mohanty & Rixen, 2005). In addition, the system identification is influenced by the characteristics of the input signal, Yang, Rakheja, & Stiharu, (1998) ; Wittbrodt, Adamic, & Wojciech, (2006) & (Eykhoff, 1974).

The modal parameters of a vehicle were estimated by Dong, Chen, & Zhang (2014) by measuring the acceleration of the vehicle based on subspace identification methods. Theoretical analysis of Dong's research has shown that when a vehicle's speed is low, the subspace method that uses accelerations of unsprung masses as inputs can give more accurate

results than the method which used road–tyre forces as inputs. A system identification technique has been used by Yang et al. (1998), to obtain the parameters of a vehicle when subjected to different cases. In this research, a pseudo-random binary sequence (PRBS) and a quasi-impulse (QI) excitation signal were used to stimulate the modes instead of using the common ramp step (RS) steering input.

Car parameter estimation was presented by Russo (2000); using the Kalman filter to study the vehicle's parameters. The dual technique was then used to estimate modal parameters of the vehicle (Wenzel, Burnham, Blundell, & Williams, 2006). The identification of modal parameters for a commercial vehicle was reported by Arıkan, Ünlüsoy, Korkmaz, & Çelebi (2008) through using structural analysis. Their experiments were used to estimate a vehicle's parameters. The results show that the identified parameters are able to identify the vehicle parameters. Subspace identification methods were used by Ming, Xiqiang, Zhang, Guan, & Yuan (2011) to estimate the vehicle the vehicle handling performance. The methods used require complex measurement systems or mathematical models for vehicle's tyre models to estimate interactions between the tyre and road surface.

In several comparative studies it was considered that reference-based stochastic subspace identification (SSI/ref) was more accurate, and efficient to identify modal parameters for OMA (Bart Peeters & De Roeck, 2001) and has been intensively implemented for ambient vibration data based modal identification. Therefore, as the road excitations considered random inputs for the vehicle, subspace methods were investigated for vehicle parameters estimation and prediction of the vehicle performances (Dong, Chen, & Zhang, 2014 & Ming, Xiqiang, Zhang, Guan, & Yuan, 2011) using data from road tests.

This research aims to obtain measured modal shapes of a vehicle to evaluate the proposed mythology of modal shape based detection techniques. The method used for this output-only modal parameter identification is an average correlation signal based stochastic subspace identification (ACS-SSI) technique developed recently by Chen et al. (2015) for online vehicle dynamics analysis. It allows multiple data records and data frames to be combined through an averaging scheme in the correlation lag domain. Thus by adopting this scheme for the measured data, the average correlation signals will be obtained and singular value decomposition (SVD) will be implemented for parameter identification. The following section gives a detailed discussion about general (SSI) frameworks.

### 5.3 The General Stochastic Subspace Identification (SSI) Frameworks

System identification techniques are usually employed to analyse data signatures and to extract structural dynamic properties of mechanical systems solely from vibration data. The extracted properties can then be used for evaluating the condition of the system. Studies have shown that among numerous system identification techniques proposed for engineering applications, the stochastic subspace identification (SSI) methods are a more robust output-only identification technique (Londono, Desjardins, & Lau, 2004; Bart Peeters, 2000).

The dynamic behaviour of suspension systems is traditionally modelled through discrete modal model approximations, which are represented as:

$$[M]\ddot{x} + [C]\dot{x} + [K]x = z \quad 5-1$$

Where,  $z = \begin{bmatrix} 0 & 0 & 0 & z_{r1} & z_{r2} & z_{r3} & z_{r4} \end{bmatrix}^T$  is the road excitation and

$x = \begin{bmatrix} z_s & \theta & \varphi & z_{u1} & z_{u2} & z_{u3} & z_{u4} \end{bmatrix}^T$  is the response vector.  $[M]$ ,  $[K]$  and  $[C]$  respectively

are the mass, stiffness and damping matrixes of the full vehicle. These will be presented in more detail in the next chapter. For system identification of discretely sampled responses, it is more convenient to reformulate the modal model into the form of a discrete-time state space model, which presented as follows:

$$X_{(k+1)} = A(x)_k + B(u)_k \quad 5-2$$

$$y_k = C(x)_k + D(u)_k \quad 5-3$$

In equations 5-2 and 5-3, matrix  $A$  is the state matrix that characterises the dynamics of the system by its eigenvalues,  $B$  is the input influence matrix that connects inputs,  $C$  is the output influence that specifies the transformation of the state, and  $D$  is matrix of transmission. The vectors  $(u)_k$ ,  $y_k$  and  $(x)_k$  are the inputs, outputs and states respectively.

The state-space model formulation of Equations 5-2 and 5-3 is entirely deterministic. However, in automotive applications, especially in the context of continuous field monitoring, it is usually impractical or impossible to measure the input excitations  $(u)_k$ . Thus, the identification

algorithms must rely on the measured outputs  $y_k$  only. In the SSI algorithm the input terms  $B(u)_k$  and  $D(u)_k$  are considered as random white noise. Thus, the system can be presented by the Reference-Based Stochastic Subspace Identification (SSI/ref). model (see Figure 5-1) (Peeters et al., 2000).

$$X_{(k+1)} = A(x)_k + w_k \quad 5-4$$

$$y_k = C(x)_k + v_k \quad 5-5$$

Where  $w_k$  and  $v_k$  are white zero-mean stochastic processes, independent of the state vector. From the stochastic state-space model formulation of Equations 5-4 and 5-5, it can be shown that the correlations of the outputs  $R_i$  can be factorised into a triplet containing the state matrices (Bart Peeters, 2000):

$$R_i = CA^{i-1}G, \quad 5-6$$

Output correlation matrices defined as,  $R_i = E[y_{k+i}y_k^T]$  here  $E$  is the operator expected. The subscript  $i$  indicates a time lag of  $(i\Delta t)$ , and  $G = E[x_{k+1}y_k^T]$  is a “next-state-output” correlation matrix.

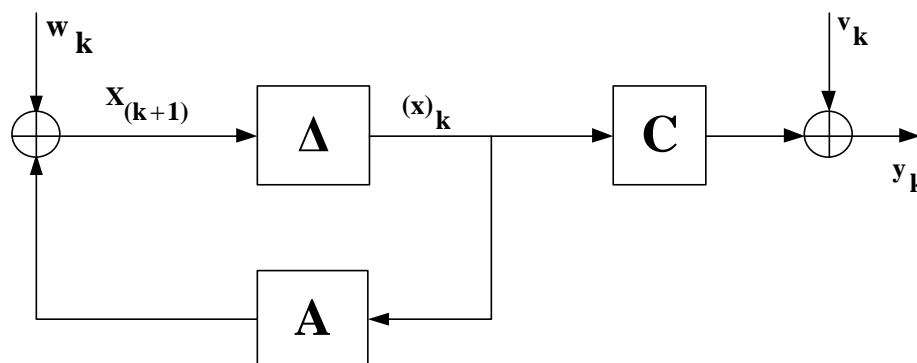


Figure 5-1: sketch of the stochastic space model, with the  $\Delta$  representing a delay (Peeters et al., 2000)

Equation 5-6 represents the basis of the correlation driven SSI algorithm. It indicates that suitable decomposition of the correlations can yield the state-space matrices, which in turn contain the structural parameters of mass, stiffness and damping. Data correlations also offer the advantages of eliminating uncorrelated noise and compressing the data while preserving

the modal information. Correlations of the data with respect to a subset of reference sensor channels computed at a sequence of different time lags may be assembled into a block Toeplitz matrix or diagonal-constant matrix, as follows:

$$\mathbf{T}_i^{ref} = \begin{bmatrix} \mathbf{R}_i^{ref} & \mathbf{R}_{i-1}^{ref} & \dots & \mathbf{R}_1^{ref} \\ \mathbf{R}_{i+1}^{ref} & \mathbf{R}_i^{ref} & \dots & \mathbf{R}_2^{ref} \\ \dots & \dots & \dots & \dots \\ \dots & \dots & \dots & \dots \\ \mathbf{R}_{2i-1}^{ref} & \mathbf{R}_{2i-2}^{ref} & \dots & \mathbf{R}_i^{ref} \end{bmatrix} \quad 5-7$$

The factorisation property of Equation 5-6 allows the block Toeplitz matrix to be factorised as follows:

$$\mathbf{T}_i^{ref} = \begin{bmatrix} \mathbf{C} \\ \mathbf{CA} \\ \dots \\ \mathbf{CA}^{i-1} \end{bmatrix} \begin{bmatrix} \mathbf{A}^{i-1}\mathbf{G}^{ref} & \dots & \mathbf{AG}^{ref} & \mathbf{G}^{ref} \end{bmatrix} = \mathbf{O}_i \mathbf{\Gamma}_i^{ref}, \quad 5-8$$

Where  $\mathbf{O}_i$  and  $\mathbf{\Gamma}_i^{ref}$  are rank  $n$  matrices known as the extended observability and reversed extended stochastic controllability matrices, respectively. The (SVD) technique is then used to reduce the block Toeplitz matrix into suitable factors as follows:

$$\mathbf{T}_i^{ref} = \mathbf{USV}^T = \begin{bmatrix} \mathbf{U}_1 & \mathbf{U}_2 \end{bmatrix} \begin{bmatrix} \mathbf{S}_1 & \mathbf{0} \\ \mathbf{0} & \mathbf{0} \end{bmatrix} \begin{bmatrix} \mathbf{V}_1^T \\ \mathbf{V}_2^T \end{bmatrix} = \mathbf{U}_1 \mathbf{S}_1 \mathbf{V}_1^T, \quad 5-9$$

Where  $\mathbf{S}_1$  is a diagonal matrix, using Equations 5-8 and 5-9, and the following so-called ‘internally balanced realisation’ may be obtained

$$\mathbf{O}_i = \mathbf{U}_1 \mathbf{S}_1^{1/2} \quad 5-10$$

$$\mathbf{\Gamma}_i^{ref} = \mathbf{S}_1^{1/2} \mathbf{V}_1^T \quad 5-11$$

The state-space  $\mathbf{A}$ , which contains the modes and eigenvalues, can be calculated by solving the observability matrix as follows:

$$\mathbf{A} = \mathbf{O}_i(1:l(i-1),:)^+ \mathbf{O}_i(l+1:li,:), \quad 5-12$$

Where  $l$  is the output channels,  $i$  is the number of rows in the block Toeplitz matrix,  $\mathbf{O}_i(1:l(i-1),:)$  and  $\mathbf{O}_i(l+1:li,:)$  respectively denote rows 1 to  $l(i-1)$  and rows  $(l+1)$ . The eigenvalue decomposition of the discrete-time state matrix  $\mathbf{A}$  yields:

$$\mathbf{A} = \mathbf{\Psi} \mathbf{\Lambda} \mathbf{\Psi}^{-1} \mathbf{1}, \quad 5-13$$

Where  $\mathbf{\Psi}$  is a complex eigenvector matrix and  $\mathbf{\Lambda}$  is diagonal matrix, these are directly related to the system poles  $\lambda_i$ , or eigenvalues of the original second order described by Equation 5-1. The system poles contain the modal frequencies  $f_i$  and damping ratios  $\zeta_i$ .

$$\lambda_i = \ln(\mu_i) / \Delta t = -\zeta_i f_i + i \sqrt{1 - \zeta_i^2} f_i \quad 5-14$$

The frequency  $f_i$ , damping ratio  $\zeta_i$ , and modal vector  $\mathbf{V}$  can be respectively calculated using matrices  $\mathbf{A}$  and  $\mathbf{C}$  as follows:

$$f_i = \frac{\lambda_i^c}{2\pi}, \quad 5-15$$

$$\zeta_i = \frac{\text{Re}(\lambda_i^c)}{|\lambda_i^c|}, \quad 5-16$$

$$\mathbf{V} = \mathbf{C} \mathbf{\Psi}, \quad 5-17$$

Where  $\mathbf{C}$  can be obtained from first  $l$  rows of  $\mathbf{O}_i$  (see Equation 5-8)

This shows that conventional SSI including Cov-SSI/ref can select modes based SVD through which a subset of modes which has significant eigenvalues. Alternatively, the modes associating with small eigenvalues are treated as noise and rejected. The limitation of this approach is that it cannot retrieve true modes when the data contains high noise content which is particularly true for the measurement from suspension systems.

#### 5.4 Eigen Realisation Algorithm (ERA) and Data Correlation

In implementing Cov-SSI, the data length cannot be infinite, rather but very short. This is particularly true for online identification which often needs to have results in real-time, and hence the correlation matrix covariance expressed in Equation 5-7 are just estimates. It means

that these estimates can have significant differences from measurement to measurement. This is especially true when data contains nonstationary effects and high noise contents. Identification results will have high uncertainties and even cannot attain convergence in completing the SSI computation, which are can be very confused when choosing the correct results because of the high variance value after an average processing.

To overcome this shortcoming, numerous research projects have been carried out over the last decades. Of particular interest are the ERA-based approaches as they can produce superior identification results with the conventional impulse response data (Lew, Juang, & Longman, 1993). Especially it is can be approached by the latest correlation data induced by white noise (Chiang & Lin, 2011a).

As shown in (C. R. Farrar & James III, 1997) the correlation signal between two responses from white noise excitations is equivalent to the impulse responses. This means that the correlation signal can be used directly for the identification of time domain. In (Pridham & Wilson, 2003; Siringoringo & Fujino, 2008) the correlation signals were employed to construct the block Hankel matrix in implementing the standard ERA based on impulse inputs, rather than white noise. These show that from the scheme of ERA based identification, the matrix in Equation 5-7 can be viewed as the impulse responses i.e. the Markov parameters in ERA. In this way, Cov-SSI is the same as ERA and the improvements made on ERA can be applied to Cov-SSI.

To reduce noise influences further, Juang, Cooper, & Wright (1987) improved conventional ERA by using correlation data of impulse responses, and named it as ERA with data correlation (ERA/DC). As shown in ERA/DC, the correlation data of the block Hankel matrix constructed from impulse responses also consists of the information of system matrix. It means that a further correlation of the matrix of Equation 5-7 can be calculated by Equation 5-18 for system identifications.

$$TT_q = T(q)T(0)^T \in \mathfrak{R}^{li \times li} \quad 5-18$$

where the zero-lag correlation  $T(0) = Y_p^{ref} Y_p^{refT}$ . According to this relationship and the way constructing the Equation 5-7, a new block Toeplitz matrix can be constructed from the further correlation data as:

$$U_{1/i}^{ref}(q) = \begin{pmatrix} TT_{q+1} & TT_{q+2} & \dots & TT_{q+b} \\ TT_{q+2} & TT_{q+3} & \dots & TT_{q+b-1} \\ \dots & \dots & \dots & \dots \\ TT_{q+a} & TT_{q+a-1} & \dots & TT_{q+a+b} \end{pmatrix} \in \mathfrak{R}^{ali \times bli} \quad 5-19$$

As this block Toeplitz matrix also contains the information of system matrix in the format as Equations 5-7, the SVD process expressed in Equations (5-7)-(5-10) can be applied to it to estimate the system matrix A and subsequently calculate modal parameters using Equations (5-15)-(5-17). However, as the effect of more noise reduction and possible nonstationary suppression due to the further correlation operations, this further correlation matrix based SSI will give more accurate results, which will be evaluated in next Chapter numerically.

### 5.5 Average Correlation Signal based Stochastic Subspace Identification (Acs-SSI).

To overcome the problem with noise influences, the output-only modal parameter identification method conducted in this research concentrates on the an average correlation signal-based stochastic subspace identification (ACS-SSI) technique which was recently developed by Chen et al. (2015) using a hybrid of the noise reduction properties of correlation function in the time or lag domain with conventional SSI techniques for online analysis of vehicle dynamics.

In ACS-SSI, correlations between sensor signals are taken as the input. This is because a correlation data sequence will be considered as the impulse of a dynamic system (Chiang & Lin, 2011b), and has been used in various time domain-based identification methods such as the eigen realisation algorithm (ERA).

Correlation signals are theoretically equivalent to impulse responses whose spectra are infinitely wide. Thus, they can be taken to be the output of a state space equation corresponding to white noise excitations, which could meets the fundamental assumption when the SSI scheme is developed originally. From this point of view, an equivalent Toeplitz matrix as expressed in Equation 5-7 can be constructed using the correlation signals instead of the raw response signals. Similarly, the covariance matrixes of the correlation signals have the form shown in Equation 5-8. Therefore, a correlation signal based Cov-SSI/ref can be implemented for system identification.

However, correlation signals estimated from one data record are often not sufficiently effective to suppress the strong noise and non-stationary influences when their contents are very high, such as the vibration responses from a vehicle suspension system. Fortunately, there are usually

multiple data records available which may be collected under similar or different operating conditions of the vehicle on road. Thus, it is expected to employ all of these records together to obtain a more reliable identification result. Traditionally, an average of power spectra across different data records is employed for noise reduction. However, as the power spectrum contains no phase information, only a limited effect of noise reduction can be attained, which is insufficient for the case of suspension identification where the measured data can contain a high noise content due to various sources including nonstationary road surfaces, power train excitations and their induced secondary responses.

Especially, the response of suspension system can be more nonstationary, this scheme of using short data segment can be more significant for the data from suspension system in reducing the nonstationarity.

As correlation signals can be calculated using a specified reference sensor for all different data records, the phase differences between these records can be preserved by these reference-based correlation signals. Thereby, an average of the correlation signals can be performed between different data records, which allow the enhancement of the regular or periodic components while suppressing the irregular random contents as the correlation signal of high lags is effective to maintain periodic signals from modal responses. Particularly, the component that associates with one of the system modes is often more significant than others and this principal response can be helpful to maintain phase consistency between those of different modes. Moreover, the autocorrelation of the reference sensor signal always has a zero phase. Therefore, the average of the autocorrelation signals from different data records effectively improves the signal to noise ratio (SNR) for the resultant correlation signals. While the cross-correlation signals maintain the relative phase connections to the reference signals, the average also enhances the desired regular components in the signal and suppresses the noise content effectively.

According to the theoretical analysis made in Chapter 4, the pitch mode often shows the more dominant response, compared with the bounce and roll modes. Thus the response characteristics satisfy the desired condition of Acs-SSI and it is possible to apply the method for identifying the modal parameters. To be more specific, the average correlation signals can be obtained based on multiple measurements or data records according to following key steps:

- Step 1. Obtain  $k$  numbers of short data segments from the measurements on  $l=4$  channels either by using multiple measurement records or by segregating a very long continuous data record into small ones.

Step 2. Take one of  $l$  channels as a reference channel and calculate the auto- and cross-correlation signals of each segment with  $N$  samples for all channels:  $i = 1, 2, 3, \dots, l$ . For instance, if channel 1 is selected as the reference channel, the average can be considered as:

$$r^{i1}(\tau) = \frac{1}{N-i} \sum_{q=0}^{N-q-1} y^i(q+\tau)y^1(q) \quad 5-20$$

Obviously this can be evaluated using the (FFT) to improve overall computing efficiency.

Step 3. Repeat Step 2 for other channels and then select the channel with highest correlation energy as the optimal reference. Obviously, this can be carried out online more efficiently by using a cross validation of much smaller correlation signals compared with that spectrum comparison or an analytical analysis suggested by Chen et al. (2015),

Step 4. Average the correlation signals from different segments to obtain the average correlation signal for each corresponding channel:

$$\overline{r^{i1}(\tau)} = \frac{1}{k} \sum_{k=1}^k r_k^{i1}(\tau) \quad 5-21$$

With this averaged correlation signals, Cov-SSI can be then implemented more reliable as the average process can significantly improve the SNR of the input data of the Cov-SSI. Consequently, more accurate, robust, and efficient identification can be obtained. Moreover, the combination of different data records make it very suitable for online implementation as the vibration measurements are often from different road conditions and may contains different levels of nonstationarity due to occasional large dents and bumps on the road surfaces. By segregating a lengthy data record into short data frames, each of which can be more pseudo-stationary the SSI framework thus can be met. Especially, the combination using 5-22 allows these short data segments to be utilised in the early stage of data analysis for more reliable implementation of SSI. This certainly more efficient compared with that implementing SSI for each data segments and taking the average of the corresponding modal parameters.

## 5.6 Summary

The general stochastic subspace identification frameworks have been examined based on the common characteristics of vibration responses from simulation studies. In particular, the ACS-SSI was preferred as it allows multiple data records and different data frames to be combined

through an average scheme in the correlation lags domain and obtains significant suppression of random noise and non-stationary content. This capability is critical in using the suspension vibration data for modal identification as the data contains weak components of mode responses due to high vibration damping effect of the system. Moreover, it is suggested that the implementation of optimal reference channels can be achieved by comparing the average correlation signals which can be more efficient due to much smaller data sizes, compared with that raw data based spectrum analysis method.

## CHAPTER 6

### PERFORMANCE VERIFICATION OF ACS-SSI USING SIMULATED DATASETS

*This chapter presents simulation validation studies for a stochastic subspace identification model, which has been implemented to identify the vehicle parameters. The output signals from the 7-DOF model have been generated as an input for the SSI model, then the parameter identification including frequency, damping and mode shape, which were obtained from SSI model, were compared to modal parameters obtained by the model, the simulation and validation process has been presented. It was observed that the SSI model result was close to the 7-DOF model results. Subsequently, the validation of the SSI model is performed.*

## 6.1 SSI Simulation Results Using Accelerations of the Body as Input

The stochastic identification technique is known as a method of an output-only by using the input of the white noise assumption (Breytenbach & Els, 2011; Russo M, 2000) and they are suitable for vibration-based health monitoring of a system (Wenzel et al., 2006; Arkan et al., 2008), where input forces are unavailable. Therefore, in this section, the outputs of the 7-DOF model (response of the vehicle body at the four corners) have been used as inputs for the SSI model, and then SSI is conducted to identify the vehicle parameters. The modal parameters of the vehicle, which have been obtained from the SSI model, were verified and validated with the 7-DOF vehicle model as presented by the sketch in Figure 6-1. Therefore, these estimated parameters can be used for the online condition monitoring of suspension by analysing the modal shape under different suspension defects.

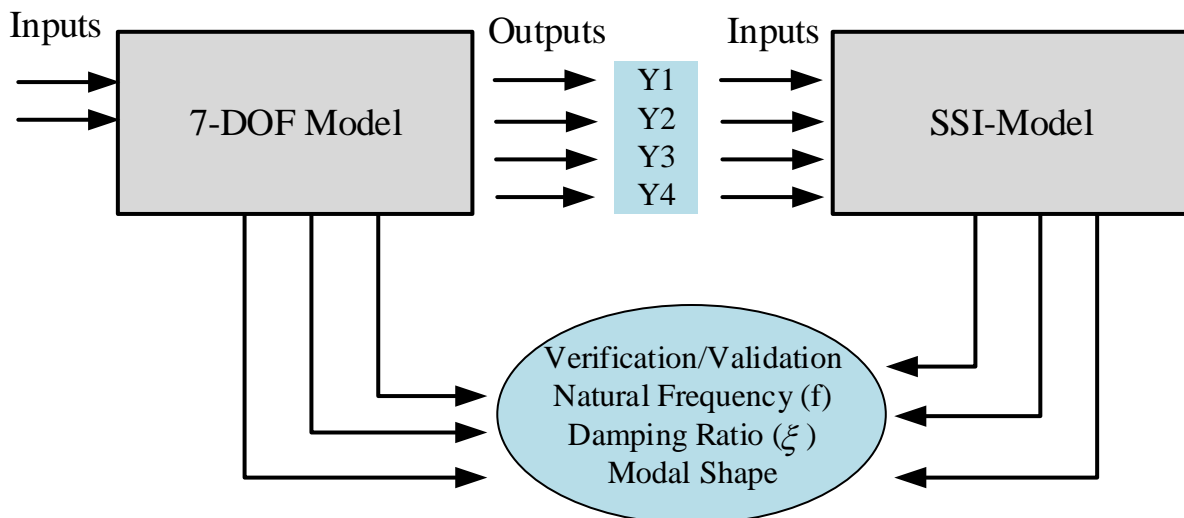


Figure 6-1: Verification of SSI model

## 6.2 Validation under Normal Conditions

The validation processes have been conducted for the SSI model by using the outputs of the 7-DOF model (responses of the vehicle body at four corners) in the base line conditions as inputs for the SSI model, and then stochastic subspace is implemented to extract vehicle parameters. The vehicle parameters, which have been identified from the SSI model, were compared with the 7-DOF model and the mean estimation error between the two models was calculated.

In the simulation, subspace identification methods can detect the bounce, modal parameters of a vehicle. Therefore, stochastic subspace identification is used to obtain the modal frequencies

$f_i$ , modal damping  $\xi_i$ , of the bounce, pitch and roll modes for normal conditions. These are shown in Table 6-1. The raw data obtained from the simulation is presented in Figure 6-2. These data are mainly the acceleration, displacement, and velocity of the body and the four wheels respectively.

Table 6-1: Frequency and damping ratio for the SSI model

Mode	Bounce	Pitch	Roll	FL-w	FR-w	RL-w	RR-w
$f_i$	1.59	1.79	2.1	11.34	11.35	12.11	12.12
$\xi_i$	0.215	0.222	0.265	0.336	0.339	0.354	0.355

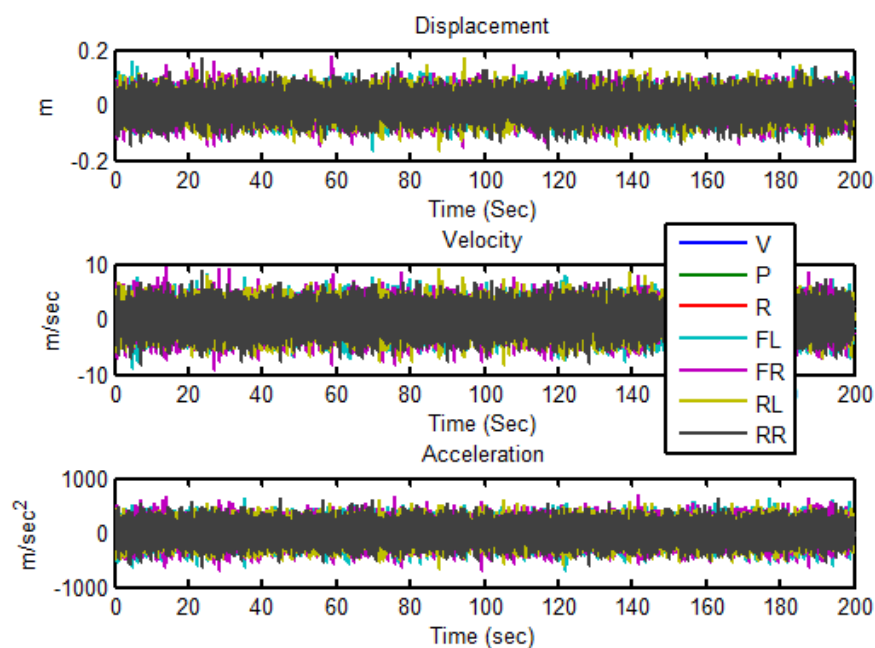


Figure 6-2: Raw data of the displacement, velocity and acceleration of the bounce (V), pitch (P) and roll (R) of the vehicle and the four wheels (FL, FR, RL and RR)

Simulation of the response function for the sprung mass has been carried out for bounce (V), pitch (P), and roll (R) of the body and the four wheels (FL, FR, RL and RR) respectively as shown in

Figure 6-3. In this figure, the bounce, pitch and roll of the body lie within the range of 1 to 3 Hz, and the wheel frequencies are around 10 to 13 Hz. From these initial results of the frequency range, the frequency range is close to that obtained from the full vehicle model. The frequency response functions of the parameters are plotted in Figure 6-4, which illustrates the vehicle displacement response of the vehicle parameters. The roll frequency has the biggest amplitude and exerts greater influence on the vehicle responses.

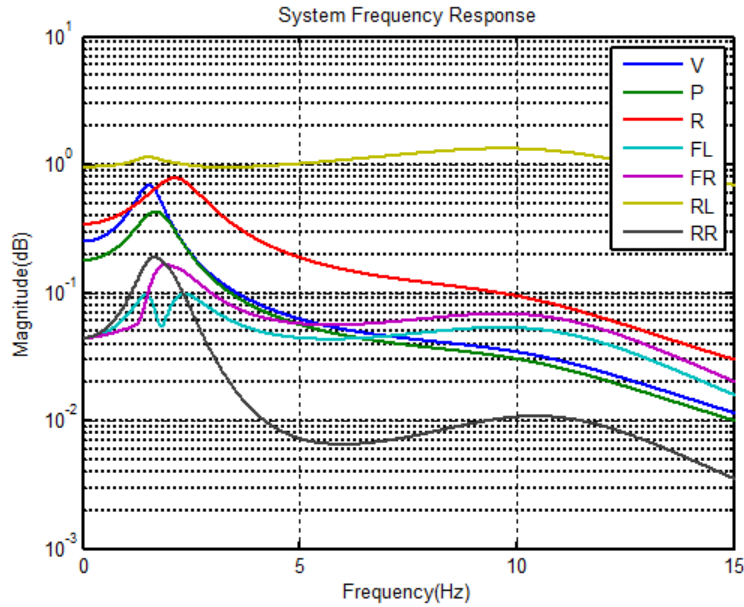


Figure 6-3: Frequency response function of the bounce (V), pitch (P) and roll (R) of the body and the four wheels (FL, FR, RL and RR)

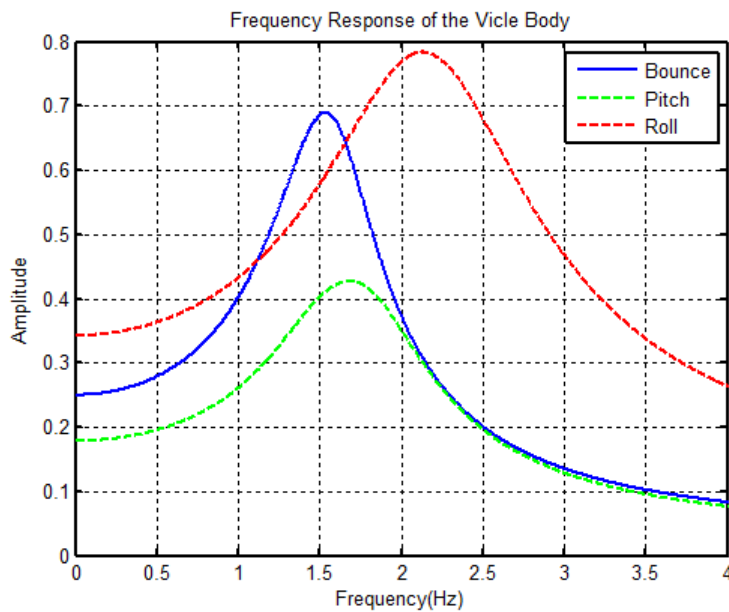


Figure 6-4: Frequency response of the bounce (V), pitch (P) and roll (R).

Theoretical analysis of the vehicle body response was carried out, whereby the accelerations of the vehicle body were generated to the SSI model. The accelerations of the body were transmitted from their centre of gravity to each corner of the vehicle, and these translations were calculated using Equations 3-8, 3-9, 3-10 and 3-11.

In order to apply the SSI algorithm, a specified reference sensor for all the data records has been selected to calculate the correlation signals; the phase information between different records can be preserved by these reference-based correlation signals. Hence, an average of the correlation signals can be performed between different data records, enhancing the regular or

periodic components by suppressing the irregular random contents. Figure 6-5 presents the correlation amplitude of each sensor with sensor number one as a reference, in order to ensure that the correct correlations are detected between all sensors at each corner. A correlation signal based Cov-SSI/ref can then be implemented for SSI.

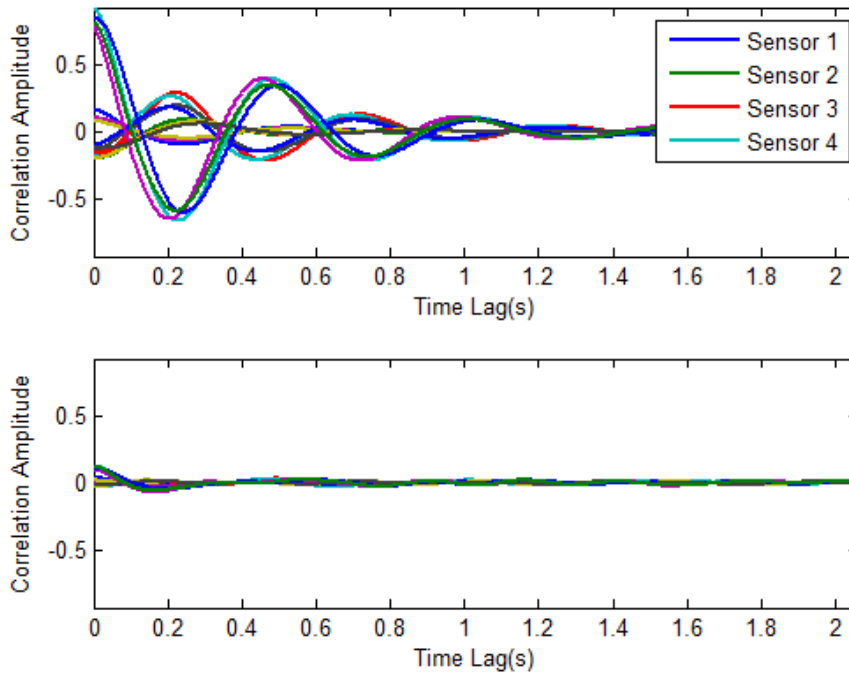


Figure 6-5: Correlation amplitude signals for all sensors

In the simulation, the sampling frequency is chosen to be 200 Hz. System poles usually have a complex pairs, which are depended on structural vibration ‘modes’. The system frequency can be obtained from the pole’s imaginary part and the damping can be calculated from the real part (Lau et al., 2007).The identification of the structure can then be presented to obtain the true modes from distinguished modes by using diagrams of stabilisation. These diagrams are known as a method to conduct the system parameters, as the structural modes will be more stable, when they come to catch the true model orders. Figure 6-6 shows a stabilisation diagram for the vehicle body, where frequencies and modal shapes are plotted with the model order. This figure illustrated that, in the range of low frequency, damping ratio, frequency and modal shape show some fluctuations. Finally, the modes become more stable, giving more accurate frequency modes of the body which can be shown in the frequency of 1.5 to 2.5 Hz.

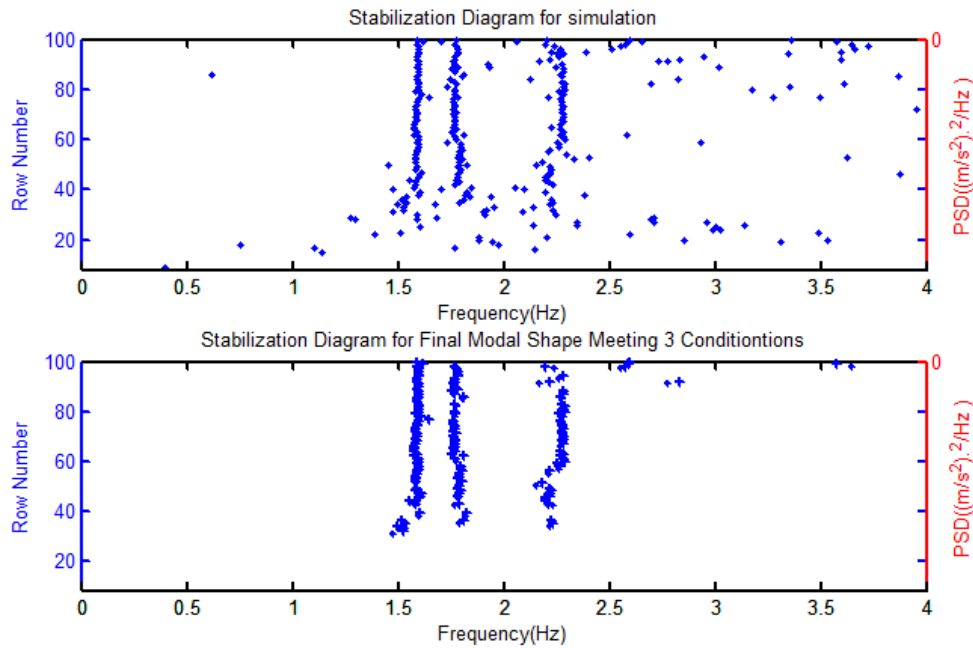


Figure 6-6: Stabilization diagrams for the vehicle

Figure 6-7 presents mode shapes of the vehicle body which were simulated by using SSI. The baseline consisted of no change in the suspension and tyre conditions. In this figure the bounce frequency is around 1.59 Hz with damping ratio of 21.50 %. The bounce mode shape shows how far the vehicle's body moved vertically. Pitch frequency is about 1.79 Hz with a damping ratio of about 22.22 %. The pitch mode shape illustrates how the vehicle body moves up front to back. The roll frequency was in the range of about 2.1 Hz with a damping ratio of 26.54 %. The rolling mode shape gives insight into how the vehicle body moved up and down about the longitudinal axis of the body, which is in the perpendicular direction of the pitching.

From Figure 6-7 it can be concluded that by using sprung mass responses as inputs, the responses of the SSI model and the 7-DOF model are similar. In general, both models results show similar trends and also almost similar values. Therefore it can be deduced that the results obtained from the model when applying the accelerations of the body as inputs were given almost similar results of vehicle modes that obtained by using the tyre force. This means that using the acceleration data of the vehicle body, which was collected by installing four accelerometers on the tested vehicle (see Section 8.4), the vehicle modes can be reliably determined. The proposed methodology, based on the 'modal shape based detection technique' for suspension systems, will be used to provide monitoring and diagnosis of the suspension during operating conditions.

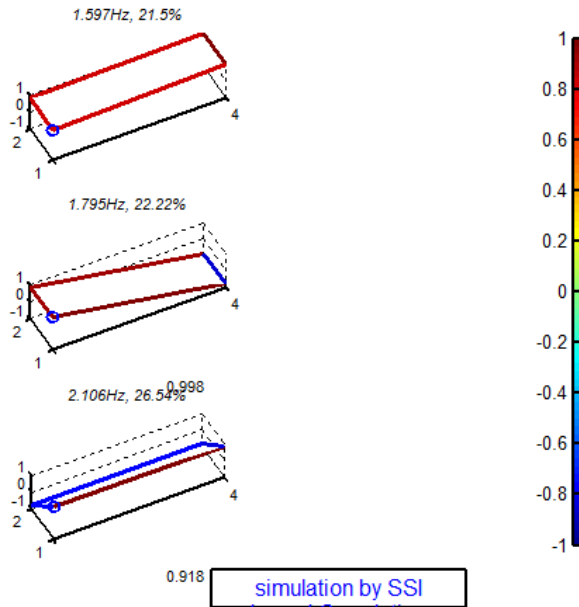


Figure 6-7: Mode shapes of the bounce, pitch and roll modes

To validate and to test the SSI model, the mean estimation error has been calculated for the parameters obtained from the SSI model and the same parameters of the 7-DOF theoretical model.

Figure 6-8 represents the mean estimation error between both models. This figure presents that the identification results produced by the stochastic subspace algorithm are reasonably accurate. The estimation error is below 4 percent for the modal natural frequency, and is almost 8 percent for the modal damping ratio, which shows more fluctuation and uncertainty than the natural frequencies. Therefore, it can be deduced that using the accelerations of the sprung mass as inputs for the SSI algorithm were produced same parameters obtained from the tyre force, and it is a reliable way to excite the vehicle parameters. Subsequently, the rolling modal energy differences between the front and rear of the bounce and pitch mode shapes can be used as reliable detection parameters by virtue of them being independent of vehicle loads and speed.

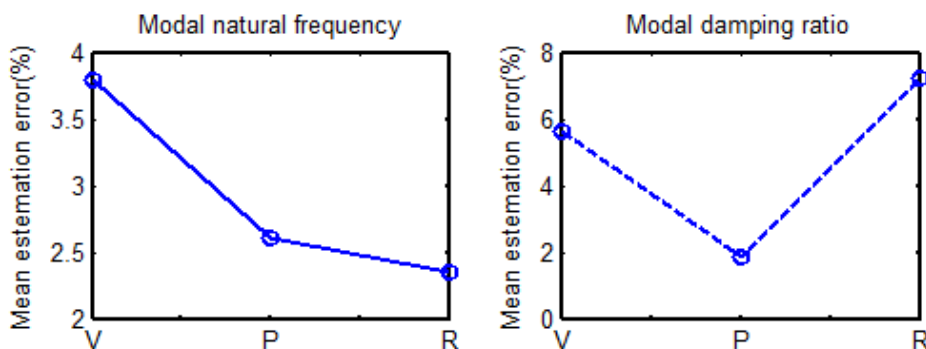


Figure 6-8: Mean estimation errors of frequency and damping ratio for vertical, pitch and roll modes of the SSI model and the 7-DOF model

### 6.3 Validation under Abnormal Damping

To validate the SSI model under abnormal conditions, suspension faults are considered in the simulation by varying the damping coefficients. Values used for each of the damping coefficients varied from 20 % to 80 % of their original values, in 20 % increments. Figure 6-9 presents estimation errors of modal natural frequency and damping ratio for different damping coefficients. This is shown for bounce (V), pitch (P) and roll (R) modes respectively.

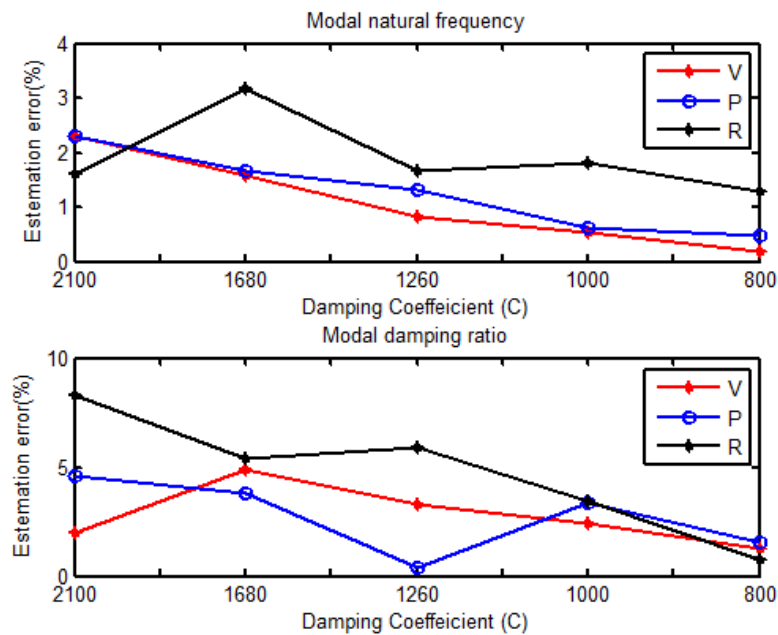


Figure 6-9: Estimation error for modal frequency and modal damping for different damping coefficients

It can be noted from this figure that the estimation error has value less than 3 percent for the modal frequency. For damping ratio, the values of error are less than 10 percent. From this figure it can be noted that the modes of bounce and pitch have lower estimation errors than the roll modes in both cases of natural frequency and damping ratio, with estimation error less than 5 percent.

### 6.4 Validation under Abnormal Spring

To validate the SSI model under the conditions of an abnormal spring, faults are considered by varying the spring rate from about 0.05 % to 0.2 % of the original values, in 0.05 % increments. In Figure 6-10 the estimation errors of the modal frequency and damping ratio for bounce (V), pitch (P) and roll (R) respectively, for a range of spring rates. In this figure, the estimation error has value of less than 8 percent for modal frequency. For damping ratio, the errors are about 10 percent. The figure also shows that the modes of bounce and pitch have lower estimation errors than the roll modes in both cases of natural frequency and damping ratio, with estimation

errors lower than 5 percent. The roll modes show more uncertainty than the bounce and pitch modes.

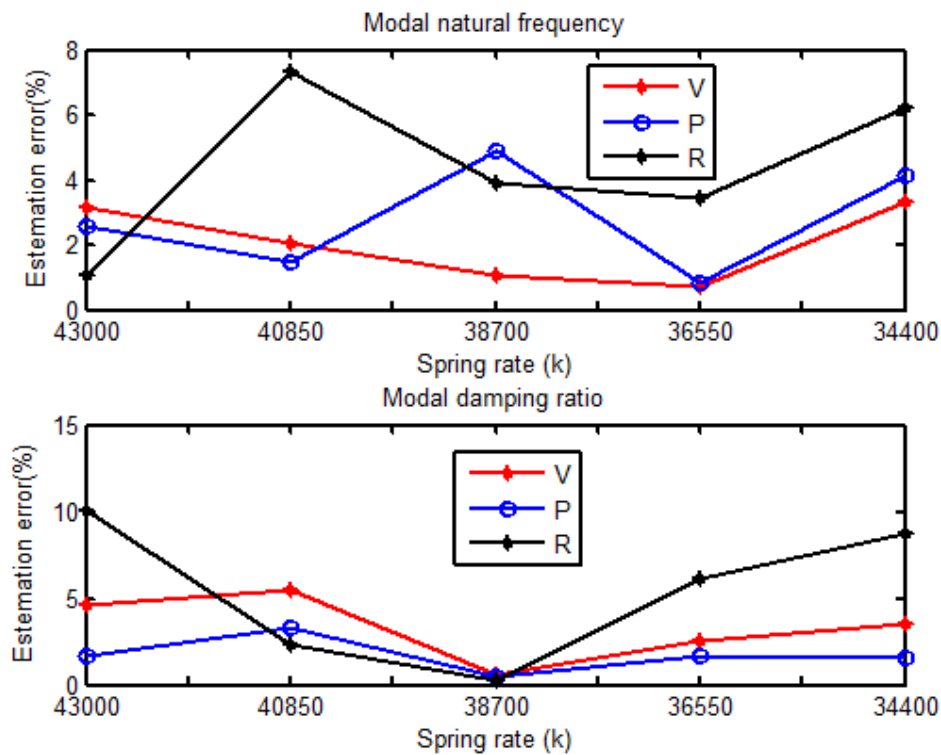


Figure 6-10: Estimation error for frequency and damping for a range of spring rates

## 6.5 Summary

The identification method is conducted estimate the vehicle parameters and also to investigate condition monitoring for suspension systems. In the system identification model, accelerations of the vehicle body which were obtained from the 7-DOF model are generated as inputs for the SSI model to perform the system identification. They are also used to validate the SSI model. In addition, the parameters of the vehicle include (natural frequencies, damping and modal shapes) for the SSI model can be effectively identified with acceptable accuracy. It was observed that the SSI model results were close to the 7-DOF model results. Subsequently, the validation of the SSI model was performed, showing that the proposed methodology can be effectively implemented for on-line condition monitoring of suspension systems.

## **CHAPTER 7**

# **FRF BASED OFFLINE IDENTIFICATION OF THE TEST VEHICLE**

*This chapter describes the experimental work carried out on a 4-post-test rig at the University of Huddersfield. The test was conducted to measure the vehicle's vibration and the vibration of the platform (shaker) in order to obtain the frequency response function (FRF) on each corner of the vehicle, which allows the suspension parameters to be estimated with a good degree of accuracy and subsequently taken as references to evaluate online experimental studies.*

## 7.1 Introduction

The analysis of FFT-based two channel digital spectra can enable measurements of a frequency response (Richardson & Formenti, 1982); (Herlufsen, 2004). An FRF is an estimation of the structure response with a particular number of DOF, per unit of excitation force which is applied with a particular input DOF. The FRF is a function or waveform that includes both a real and imaginary component that can be resolved into magnitude and phase. FRF measurements are one of effective methods to obtain the system parameters such as frequencies, mode shapes and damping ratios. An FRF Model can be considered as a linear system. Figure 7-1 represents a diagram for this system (Irvine, 2000).

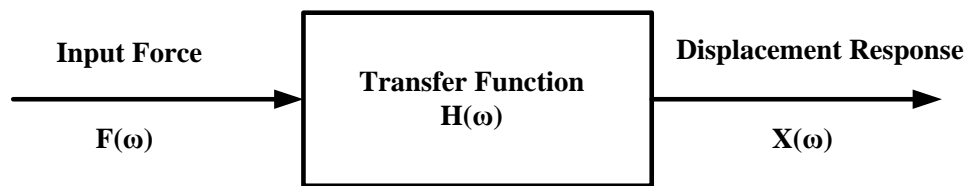


Figure 7-1: Frequency Response Function model (Irvine, 2000)

In Figure 7-1,  $F(\omega)$  is the force in the form the frequency  $\omega$ ,  $H(\omega)$  is the transfer function, and  $X(\omega)$  is the displacement. In this case, the magnitude and phase for each function can be calculated. Numerous types of spectral function then can be obtained. For simplicity, a Fourier transform can be used for each function (Irvine, 2000). By solving the following equations the relationship in Figure 7-1 can be obtained:

$$X(\omega) = H(\omega) \cdot F(\omega) \quad 7-1$$

$$H(\omega) = \frac{X(\omega)}{F(\omega)} \quad 7-2$$

To develop transfer functions for the velocity and acceleration responses the similar function can be used.

## 7.2 Frequency Response Function for a Single Degree of Freedom (SDOF) System

For simplicity, a force can be generated to a single-degree-of-freedom system (SDOF) as illustrated in Figure 7-2 (Irvine, 2000).

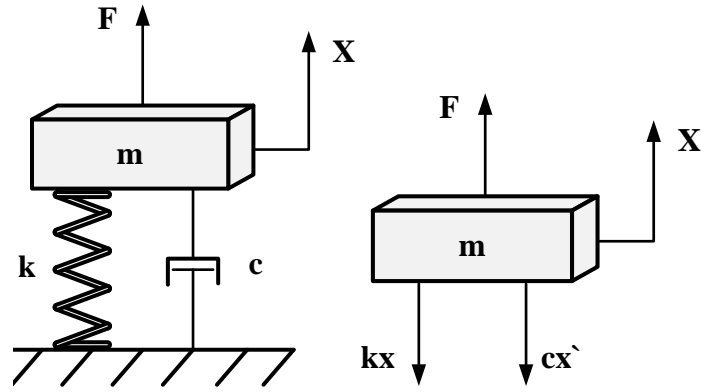


Figure 7-2: SDOF System and free-body diagram (Irvine, 2000)

In Figure 7-2,  $m$  is mass,  $c$  is damping coefficient,  $k$  is stiffness,  $x$  is absolute displacement of the mass, and  $F$  is applied force. The forces applied to the system can be presented as:

$$\Sigma F = m\ddot{x} \quad 7-3$$

$$m\ddot{x} + c\dot{x} + kx = F \quad 7-4$$

Dividing the above equation by the mass  $m$ , gives:

$$\ddot{x} + (c/m)\dot{x} + (k/m)x = F/m, \quad 7-5$$

By convention:

$$(c/m) = 2\zeta f_n \quad 7-6$$

$$(k/m) = f_n^2 \quad 7-7$$

Where  $f_n$  is frequency and  $\zeta$  is the damping, substituting these terms into Equation 7-5 gives:

$$\ddot{x} + 2\zeta f_n \dot{x} + f_n^2 x = f_n^2 F/k \quad 7-8$$

To obtain the displacement transfer function (Displacement / Force), the Fourier transform of Equation 7-8 can be calculated. By solving some relationships, the transfer function of the displacements becomes:

$$\frac{X(\omega)}{F(\omega)} = \left[ \frac{I}{k} \right] \left[ \frac{f_n^2}{f_n^2 - f^2 + j(2\xi f f_n)} \right] \quad 7-9$$

The magnitude and phase angle  $\phi$  can be used to present the transfer function as:

$$\frac{X(\omega)}{F(\omega)} = \left[ \frac{I}{k} \right] \left[ \frac{f_n^2}{\sqrt{(f_n^2 - f^2)^2 + (2\xi f f_n)^2}} \right] \quad 7-10$$

$$\frac{X(\omega)}{F(\omega)} = \left[ \frac{I/m}{\sqrt{(f_n^2 - f^2)^2 + (2\xi f f_n)^2}} \right] \quad 7-11$$

$$\phi = \arctan \left[ \frac{2\xi f f_n}{f_n^2 - f^2} \right] \quad 7-12$$

The mobility function (Velocity / Force) can be considered as

$$\frac{V(\omega)}{F(\omega)} = \left[ \frac{I}{k} \right] \left[ \frac{j f f_n^2}{f_n^2 - f^2 + j(2\xi f f_n)} \right] \quad 7-13$$

$$\left| \frac{V(\omega)}{F(\omega)} \right| = \left[ \frac{I}{k} \right] \left[ \frac{f f_n^2}{\sqrt{(f_n^2 - f^2)^2 + (2\xi f f_n)^2}} \right] \quad 7-14$$

$$\left| \frac{V(\omega)}{F(\omega)} \right| = \left[ \frac{I}{m} \right] \left[ \frac{f}{\sqrt{(f_n^2 - f^2)^2 + (2\xi f f_n)^2}} \right] \quad 7-15$$

$$\theta = \arctan \left[ \frac{-f_n^2 + f^2}{2\xi f_n} \right] \quad 7-16$$

The acceleration function (Acceleration / Force) can be presented as

$$\frac{A(\omega)}{F(\omega)} = \left[ \frac{1}{k} \right] \left[ \frac{-f^2 f_n^2}{f_n^2 - f^2 + j(2\xi f f_n)} \right] \quad 7-17$$

$$\left| \frac{A(\omega)}{F(\omega)} \right| = \left[ \frac{1}{k} \right] \left[ \frac{-f^2 f_n^2}{\sqrt{(f_n^2 - f^2)^2 + (2\xi f f_n)^2}} \right] \quad 7-18$$

$$\left| \frac{A(\omega)}{F(\omega)} \right| = \left[ \frac{1}{m} \right] \left[ \frac{-f^2}{\sqrt{(f_n^2 - f^2)^2 + (2\xi f f_n)^2}} \right] \quad 7-19$$

$$\alpha = -\pi + \arctan \left[ \frac{2\xi f f_n}{f_n^2 - f^2} \right] \quad 7-20$$

The plot of magnitude and phase versus frequency (Bode plot) is one of the common methods for presenting SDOF, as presented in Figure 7-3, at frequency range of  $f = f_n$  the magnitude will be at a maximum value and the amount of damping only will has the effect on the system response (Packard, 1997b). In this case, the frequency can be obtained from the by considering the following trends of the frequency:

- The frequency response ha a maximum amplitude.
- The input has the lags of the response by  $90^\circ$  in phase.

It can be noted that, the level of damping on a system has an effect on the magnitude of the resonant frequency of a system. To calculate the damping factor there are several methods such as the half power method. In this method, the damping can be calculated by selecting the sharpness region of the frequency peak of the system.

Figure 7-4 presents how the damping can be calculated from the width of the peak between the half-power points: points which are located a above and below the resonant peak at which the magnitude is (0.7071) times the resonant response (Packard, 1997b).

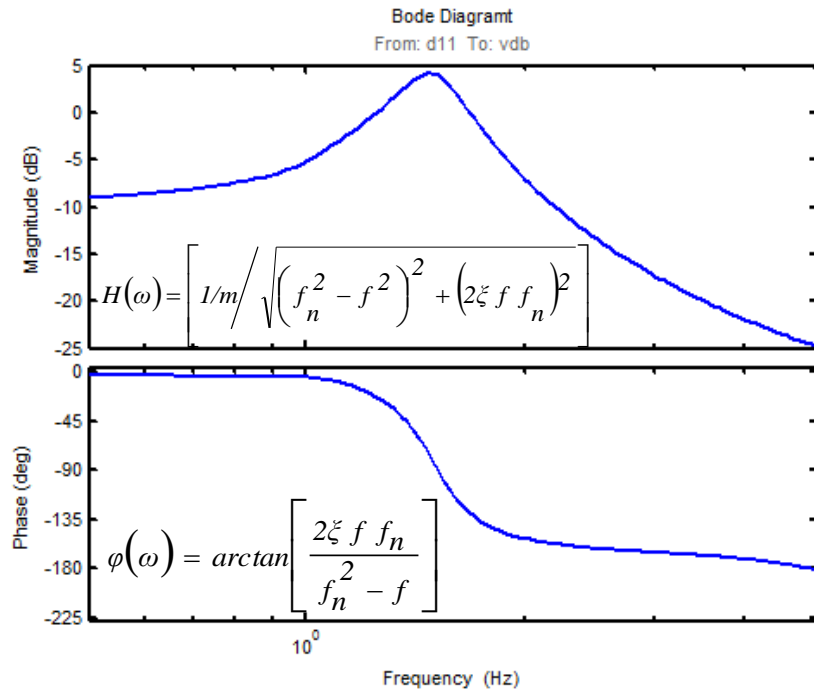


Figure 7-3: Bode Diagram magnitude and phase versus frequency for SDOF system

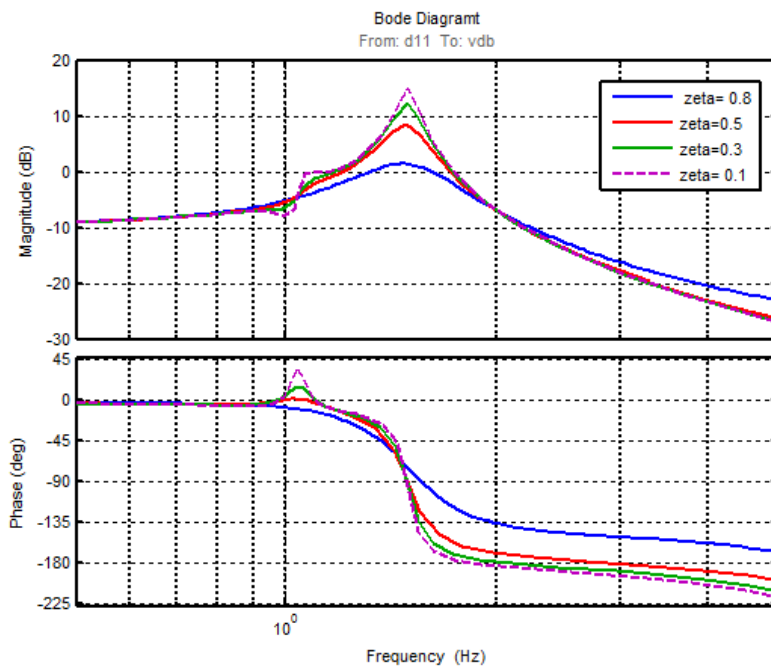


Figure 7-4: Bode diagram for different damping ratios (zeta)

### 7.3 Vibration Isolation

Vibration isolation is a process that aims to minimise or eliminate the vibration of a structure. Figure 7-5 (a) illustrates the case in which the vibration which affected the system is a force originating within the machine (force excitation). The isolator reduces the force transmitted to

the foundation. In Figure 7-5 (b) a vibrating motion is the source of vibration (motion excitation). In general, the isolator reduces the vibration transmitted to the machine.

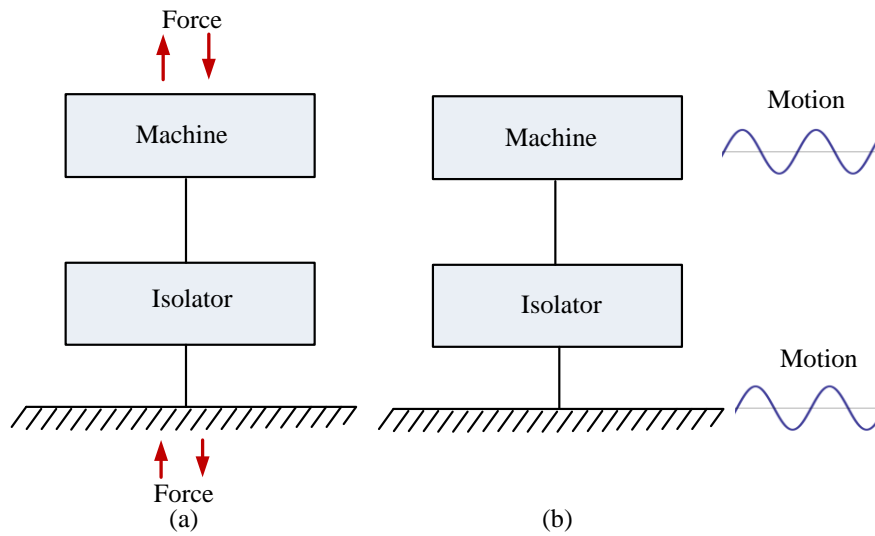


Figure 7-5: Vibration isolation; (a) force excitation and (b) motion excitation (Thomson, 1996)

#### 7.4 Transmissibility of Suspension Systems

A sketch diagram of a simplified automobile suspension is illustrated in Figure 7-6, where the input is assumed to be a sinusoidal motion. As the car is driven on the road, the tyre will produce a motion excitation to the suspension as a function of the vertical displacements. This motion will be as a rotation about the centre and also a translation through the centre. It is also assumed that the car body has a vertical motion only. The motion  $z(t)$  of the contact point of the car with the road is the input. It is considered to be sinusoidal as presented in the Equation 7-21, where the output  $x$  is the vertical motion of the body.

$$z(t) = z_0 \sin(\omega t) \tag{7-21}$$

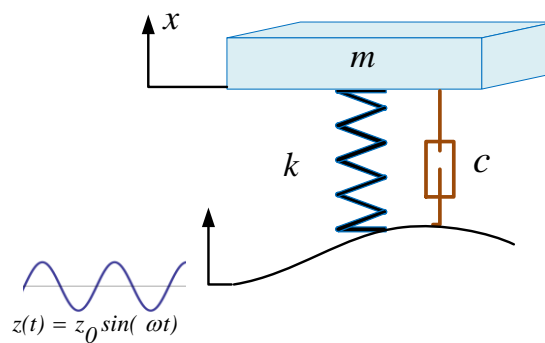


Figure 7-6: Simplified version of the automobile suspension system

The system is presented in the form of:

$$m\ddot{x} + c(\dot{x} - \dot{z}) + k(x - z) = 0, \quad 7-22$$

Or

$$m\ddot{x} + c\dot{x} + kx = c\dot{z} + kz \quad 7-23$$

Applying a Laplace transform to both sides of Equation 5.23 results in:

$$(ms^2 + cs + k)X(s) = (cs + k)z(s) \quad 7-24$$

Hence,

$$\frac{X(s)}{z(s)} = \frac{(cs + k)}{(ms^2 + cs + k)} \quad 7-25$$

The STF is then

$$\frac{X(j\omega)}{z(j\omega)} = \frac{(cj\omega + k)}{(k - m\omega^2 + jc\omega)} \quad 7-26$$

The output for the steady-state  $x(t)$  has amplitude of  $|X(j\omega)|$ , while the input is  $|z(j\omega)|$ . The transmissibility (TR) can be presented by the ratio of the displacement and is given by:

$$TR = \frac{\text{Amplitude of the output displacement}}{\text{Amplitude of the input displacement}} \quad 7-27$$

Thus

$$\frac{|X(j\omega)|}{|z(j\omega)|} = \frac{\sqrt{c^2\omega^2 + k^2}}{\sqrt{(k - m\omega^2)^2 + c^2\omega^2}} \quad 7-28$$

Substituting  $\omega_n^2 = k/m$  and  $c/m = 2\xi\omega_n$  into the Equation 7-28, and simplifying the expression results in the transmissibility being expressed as:

$$TR = \sqrt{\frac{(1 + 4\xi^2 r^2)}{(1 - r^2)^2 + 4\xi^2 r^2}}, \quad 7-29$$

Where  $r = \omega/\omega_n$  (The ratio of the frequency)

## 7.5 Experimental Investigation for FRF Measurements

The on-line condition monitoring technique presented in this research is based on a modal shape based detection technique for a suspension system. This was validated by using a 4-post-rig, which is a valuable at the University of Huddersfield. The experimental data was also used as actual parameters to validate the theoretical model, Figure 7-7 is shows a diagram of the 4-post-rig and the data acquisition layout.

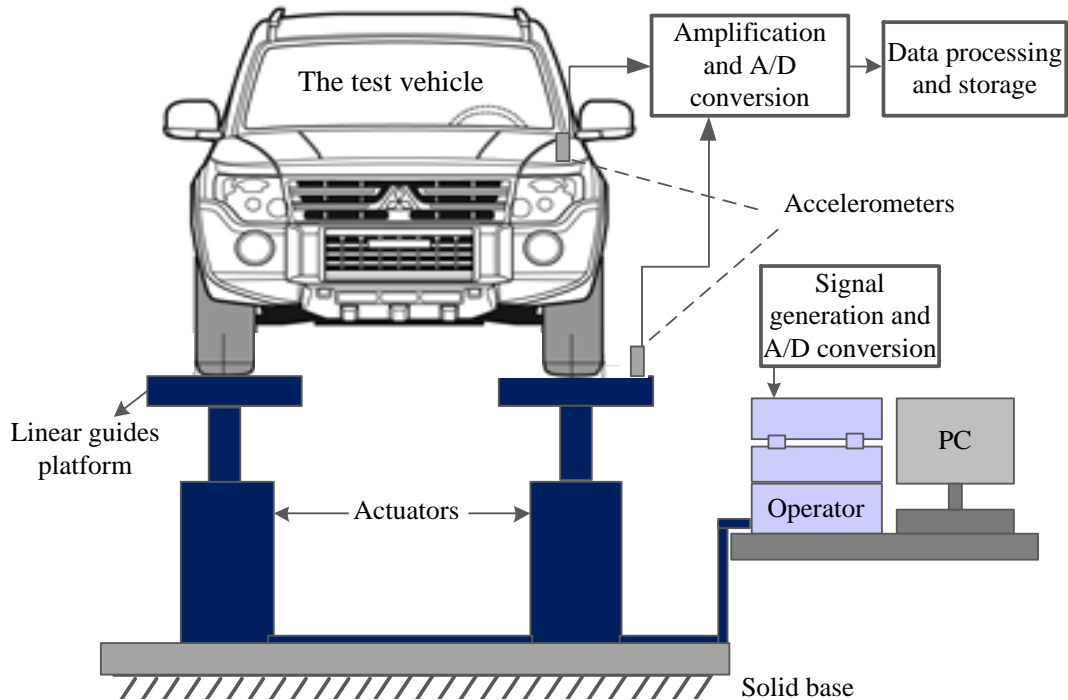


Figure 7-7: 4-Post simulator system and data acquisition layout

The objective of the experimental tests was to compute the frequency response function for each corner of the vehicle to obtain the values of the characteristic vehicle parameters including frequency, damping ratio and transmissibility of the suspension. In particular, these specific values were used in the model to obtain the optimum response of the model for validation purposes.

The data in the experiments was collected for baseline conditions and for different damping settings. During the tests, the car was induced with the fault of a damaged shock absorber by replacing the front passive shock absorbers with adjustable shocks from SPAX Company. These shock absorbers can offer a user-defined damping force, and all adjustments can be made without dismantling components. This makes it simpler, faster and easier to obtain an optimum set-up for the suspension and also makes the tests safer to perform. This test consists of three

main components: a commercial vehicle, a measurement system (vibration sensors, amplifiers, data acquisition and portable laptop), and the 4-post simulator system (shaker). The next section describes the experimental facilities and test procedures.

## 7.5.1 Experimental Facilities

### 7.5.1.1 The Test Car Specification

In this experimental study a commercial car (Vauxhall Zafira) was used. It had a 4-cylinder engine, front wheel drive, and tyre model LT245/75R16E. This is the same car that was used in the subsequent road experiments. Figure 7-8 presents a photograph of the tested vehicle that was loaded onto the 4-post-test rig, and the specifications of the vehicle are shown in the Table 7-1.



Figure 7-8: The test vehicle

Table 7-1: Specifications of the tested vehicle

Body style	MPV 5-Doors	Height	1634 mm
Driven Wheels	Front (FWD)	Wheel Base	2694 mm
Length	4317 mm	Weight	1448 kg
Width	1742 mm	Tyre model	LT245/75R16E

To measure the FRF of the suspension for different damping settings, the two front shock absorbers of the vehicle were replaced with adjustable shock absorbers (struts from SPAX

Company), as these shock absorbers can offer variable damping forces and all adjustments can be made without dismantling components. The SPAX shock absorbers have 28 increments of damping force adjustment. This allows a wide range of damping setups to suit different driving styles and road conditions. Strut-type shock absorbers (adjuster at the top) are adjustable in the rebound. To obtain the perfect setup for these shock absorbers, the manufacturer recommended initially setting all the shock absorbers to fully soft (anti-clockwise), and then changing the conditions of the shock absorber from soft to hard in 4-click increments. Figure 7-9 shows the adjustable shock absorber (SPAX).



Figure 7-9: Adjustable shock absorber from SPAX

## 7.5.2 Measurement Instrumentation

### 7.5.2.1 Accelerometers

The main function of an accelerometer is to measure mechanical motion by converting it into a voltage. Via the piezoelectric principle, the signal output is proportional to the acceleration (Cornelius & Paresh, 2004). Piezoelectric accelerometers are commonly used for measuring vibration. The design of a piezoelectric accelerometer consists of a small mass and piezoelectric crystal positioned together in a protective metal case. The working principle for this is that different forces are generated by the mass and then the vibration can be measured. These forces are in a proportional direction to the vibratory acceleration. Some sensors use an external amplifier, while others have an own internal amplifier. Piezo-electric accelerometers have the advantage of being capable to measure the low signals, with a high sensitivity. They are also relatively small in size, reliable in measuring stability and linearity, and are highly durable (Serridge & Licht, 1987).

In this research, two accelerometers were used in order to measure the vibration. These particular accelerometers are suitable for measuring the vibration because of their small mass and their wide frequency range (0.5 Hz to over 7 kHz). The sensors were connected to external charge amplifiers (YE5857A-1) to provide the power and amplify the signals. Figure 7-10 presents photographs of the accelerometer and the preamplifier, while a detailed specification of the accelerometers is given in Table 7-2.



Figure 7-10: Accelerometers and amplifier.

Table 7-2: Specification of the accelerometers

Vibration sensors	Sensor 1	Sensor 2
Model	CA-YD-104T	CA-YD-104T
Sensitivity	3.243 $pc/ms^{-2}$	3.573 $pc/ms^{-2}$
Frequency	0.5 to 7000 Hz	0.5 to 7000 Hz
Temperature	-20 to 120 °C	-20 to 120 °C

### 7.5.2.2 Data Acquisition System

A data acquisition system is a device worked to record and analyse parameters such as vibration, sound, temperature, etc. which collected from sensors and transducers. An analogue voltage signal representing a physical quantity is converted into digital data. It is then rescaled into the physical quantity according to the transducer sensitivity, so that the data can undergo meaningful analysis and be displayed appropriately. The data acquisition system of a Sinocera Model YE6231 has been used in this research. This model has 4 input channels, each channel with its own A/D (analogue/digital) converter which can be set to a sampling frequency up to

96 kHz. Converters working in parallel are synchronised, giving the possibility of the simultaneous acquisition on all four channels.



Figure 7-11: Data acquisition equipment (model YE6261B)

This type of data acquisition is ideal for monitoring vibration signals as the high sampling frequency is sufficient to capture the key information from the original analogue signal during the analogue-to-digital conversion. This data acquisition system is easily connected to a portable laptop by USB for recording and analysing the data. Figure 7-11 shows the data acquisition system.

## 7.6 Test Procedures

The two accelerometers have been fixed on the vehicle, one mounted on the vehicle body and another on the base of the platform (shaker), as illustrated in Figure 7-12. One of the main considerations regarding the accelerometers was the accessibility for installing them. The sensor mounted on the vehicle (sensor 1) was first fixed onto the front left shock absorber by gluing. Then the same sensor (1) was moved and mounted in the same position on the front right shock absorber. Figure 7-12 (a) shows the forward positions of the sensor. For measuring the vibration in the rear vehicle body, the same sensor (1) was moved and fixed on the end of

each rear corner of the car body, where the sensor could be close to the rear shock absorbers. Figure 7-12 (b) illustrates the rear positions of the sensor. Sensor (2) was fixed on the platform (shaker) to collect the acceleration of the input. This sensor was fixed to the front left platform and then moved for each corner of the platform (both sensors were used together for measuring the vibration of each corner). The accelerometer attachment to the platform was made rigid by with the use of superglue, see Figure 7-12 (c).

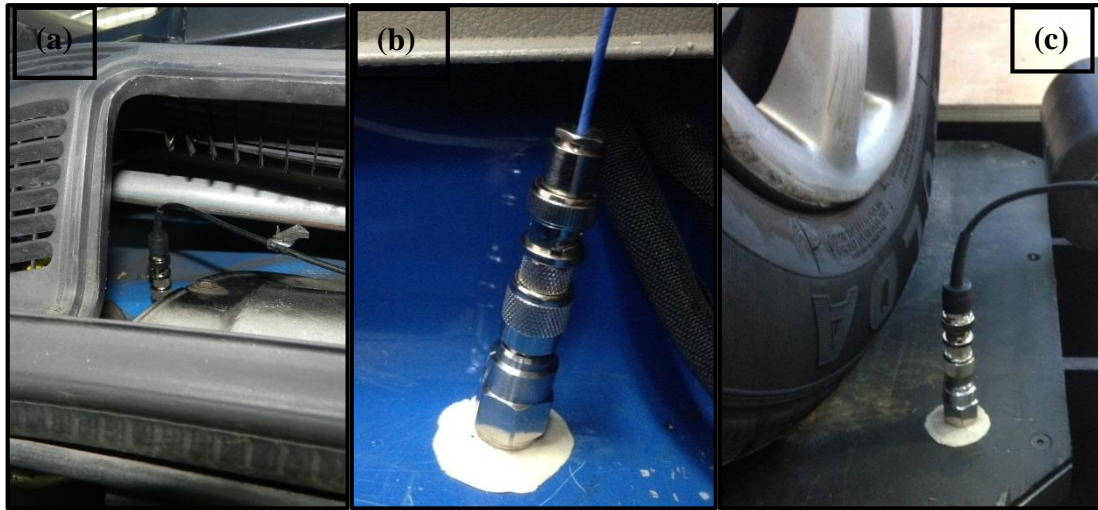


Figure 7-12: (a) Sensor position on front wheels, (b) sensor position on rear wheels, and (c) sensor position on the shaker base.

The purpose of this test is to analysis the response of the vehicle and to calculate the FRFs. For this purpose, multiple measurements were made when the oscillatory motion was generated by oscillating each platform separately. Determination of dynamic response has been made for all the vehicle wheels. The vehicle was exposed to a linear (sine sweep) frequency with about 5 mm and a frequency of 0.5 to 8 Hz. This frequency was deemed to be sufficient to include the vehicle body characteristics, and was increased at a rate of 0.03 Hz/sec. The signals were collected and measured simultaneously and the sampling rate of data acquisition was 3 kHz. For 765000 data points which were recorded in the space of 255 seconds. In this experiment, two different test conditions were examined. The first test was to measure the FRF of the vehicle, meaning the suspension was running without any induced faults and the tyre pressure of each wheel was set to a normal pressure of 2.2 bar before starting the test. The test has been conducted three times for each corner to ensure that the data is accurate and repeatable.

The second test was performed to measure the FRF of the vehicle for different damping coefficients, with the aim of evaluating on-road tests. To conduct this test for different levels

of damping, the front shock absorbers were replaced with adjustable shock absorbers as previously described (Section 7.5.1). This test was conducted by first changing the damping setting of the front left shock absorber only (Test F-L) in four cases as presented in Table 7-3. Secondly, the damping setting of the front right shock absorber only (Test F-R) was changed in four cases as shown in Table 7-3. After each test, the data acquired were viewed and imported to MATLAB for further processing.

Table 7-3: Experimental set up for damping change

(Test F-L)	Damping conditions (%)		(Test F-R)	Damping conditions (%)	
	Front left	Front right		Front left	Front right
A	Soft	Soft	A	Soft	Soft
B	2-Steps hard	Fully soft	B	Fully soft	2-Steps hard
C	4-Steps hard	Fully soft	C	Fully soft	4-Steps hard
D	Fully hard	Fully soft	D	Fully soft	Fully hard

In Table 7-3, fully soft means that the shock absorber is operating under baseline conditions. 2-steps hard, 4-steps hard and fully hard refer to decreases in the damping coefficient as a result of faults.

## 7.7 Results and Discussion

FRF measurements have been conducted between all the input/output points. Input points include the platform (shaker base), while output points include the vibrational response of the vehicle body. The vibration signals were recorded by accelerometers for 225 seconds. Baseline raw data of the acceleration response and the FRF corresponding to the vehicle body was recorded using output sensor 1, while sensor 2 focussed on the front left platform as its input (See Figure 7-13). From this figure, it can be noted that the swept frequency signal is proportional to time variations. Subsequently, the same procedures were used to measure the acceleration of the other corners of the vehicle. The FRFs of each corner were also calculated using MATLAB analysis. Figure 7-14 shows the (FRFs) for the baseline conditions of the suspension in the four corners of the vehicle. This test was conducted to identify the vehicle parameters. It can be noted from this figure that the four corners of the vehicle show significant differences in the frequency response signals. In particular, the damping value was higher in

the front left corner than the front right corner, and the values of the damping in the rear corners also produce significant differences.

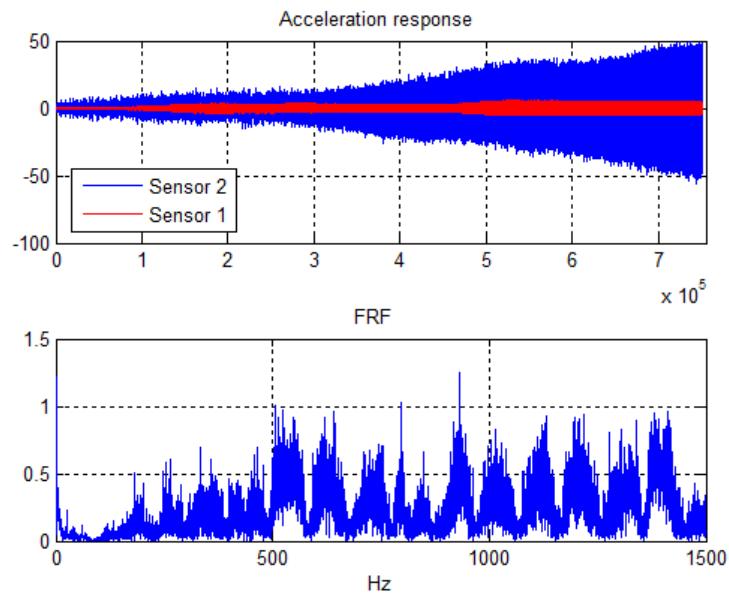


Figure 7-13: Acceleration response and FRF corresponding to the vehicle body sensor 1 and the platform sensor 2

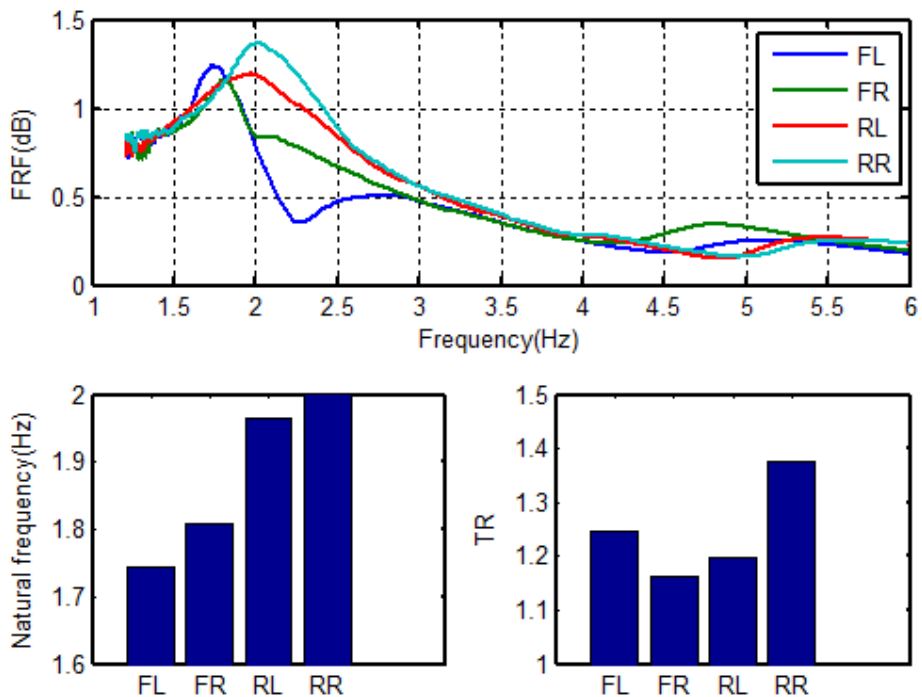


Figure 7-14: FRFs for the four corner of the vehicle

Therefore, the actual parameters of the test vehicle include the natural frequency, (which was obtained by selecting the peak value of the FRFs curves) and the transmissibility, which was calculated by Equation 7.29 for each corner (FL, FR, RL, and RR). The natural frequency and

transmissibility for each corner of the vehicle is presented in the lower plots of Figure 7-14. In addition, the Quality Factor (by -3dB) method was recognised to identify the damping ratio ( $\zeta$ ) which was calculated for each experimental data point of the frequency response function, see Figure 7-15. Damping ratio is considered to be the ratio of the energy which has been stored in the system to the dissipated energy per cycle for under-damped systems. It can be mathematically approximated as (Chouvion, 2010).

$$Q = \frac{f_r}{\Delta f} = \frac{\omega_r}{\Delta \omega} \tag{7-30}$$

Where  $f_r$  is the frequency,  $\Delta f$  is the half-power (or 3-dB) bandwidth,  $\omega_r$  is the angular frequency, and ( $\Delta \omega = 2\pi\Delta f$ ) is the angular bandwidth, the damping ratio is presented in Figure 7-16.

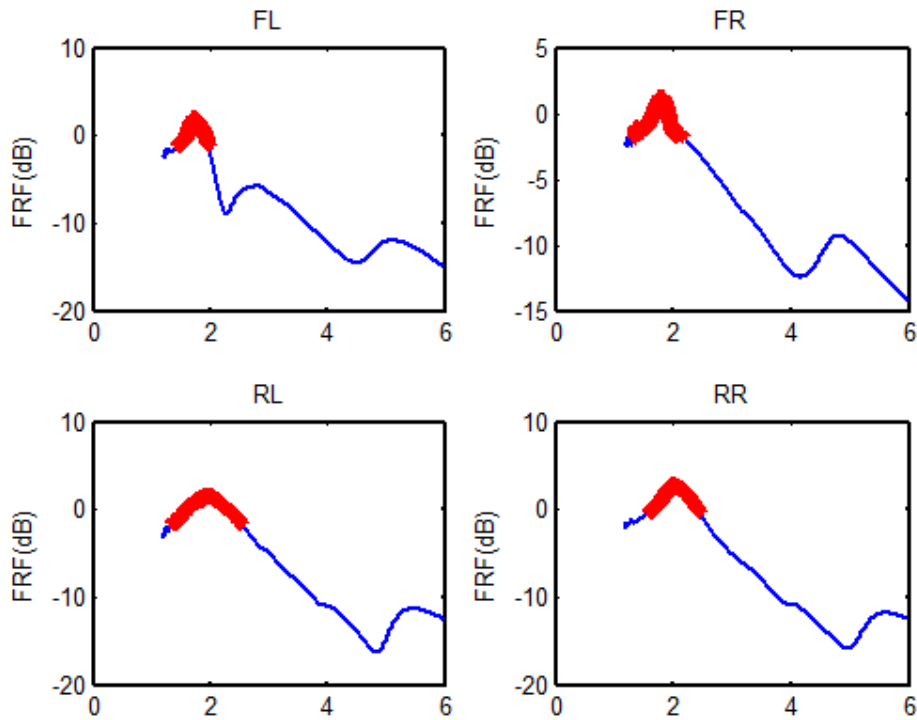


Figure 7-15: Quality factor or damping ratio by -3dB bandwidth

The actual parameters of the test vehicle were obtained, and are presented in Table 7-4. These parameters include the natural frequency, damping ratio, transmissibility and static loads of the four (FL, FR, RL and RR) corners of the test vehicle. The actual value of the damping for each corner of the vehicle was applied in the mathematical model in order to enable model refinement and direct comparison with the on-road experiments. In addition, the static load of the vehicle in each corner was used to calculate the centre of gravity of the vehicle. This has a

significant effect on the results of the simulation. The vehicle's measured centre of gravity was also applied in the mathematical model of the test vehicle, again to enable direct comparison with the on-road experiments.

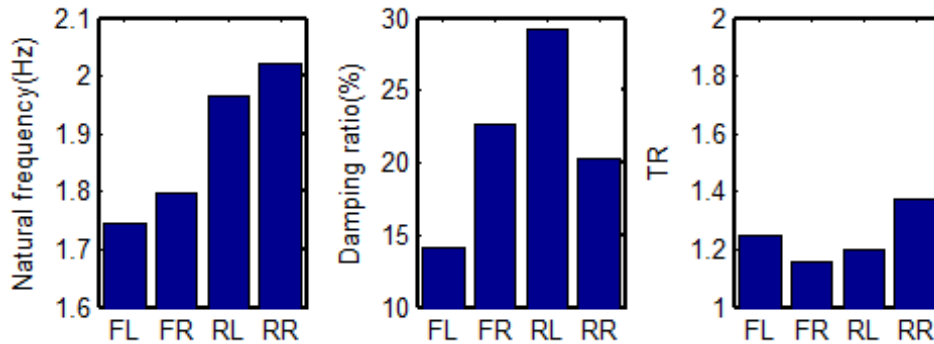


Figure 7-16: Natural frequency, damping ratio and transmissibility of FL-FR-RL-RR corners

Table 7-4: Natural frequency  $f$ , damping ratio  $\xi$  and transmissibility, TR, for four corners

Mode	FL-wheel	FR-wheel	RL-wheel	RR-wheel	Unit
$f$	1.744	1.796	1.964	2.020	HZ
$\xi$	0.141	0.227	0.292	0.202	%
TR	1.244	1.157	1.196	1.373	-
Load average	4.229	3.519	2.632	3.298	KN
Wheelbase (L)	2800				mm
Vehicle track (W)	1400				mm

It can be summarised that the actual damping values and the actual centre of gravity of the vehicle were used to refine the mathematical model, by including them as model parameters. This enables more accurate and acceptable agreements between the simulation and the measured on road results. The parameters are also presented in Table 3-1.

The static loads for the test vehicle were obtained when the vehicle was loaded over the platform of the 4-post rig. Figure 7-17 is a screenshot containing the values of the average static load for the four corners of the vehicle. It can be noted from this figure that there are significant differences in the average load distributions between the four wheels of the vehicle.



Figure 7-17: Average static load of the vehicle

From the load distribution information; the actual Centre Gravity of the test vehicle can be calculated according to the following:

### 7.7.1 Calculation of the Centre of Gravity (COG) of the Test Vehicle

By obtaining the actual force of a vehicle at each wheel, the COG of the vehicle can be calculated. The method used to calculate the centre of gravity is a simple method to find the centres of gravity as presented in (Darryl Brian, 2008). The vehicle was completely static when the forces were measured.

Figure 7-18 presents the forces which are affected on the four corners of the test vehicle.  $F_1$ ,  $F_2$ ,  $F_3$  and  $F_4$ . X and Y is the coordinates in the COG, while (L) IS the wheelbase and (W) is width of the vehicle.

Static forces and moment equations were used to find the coordinates independently of each other and to calculate COG of the body.

$$\sum M_x = (F_1 + F_2)(L - X) - (F_3 + F_4)(X) \quad 7-31$$

$$\sum M_y = (F_2 + F_4)(Y) - (F_1 + F_3)(W - Y) \quad 7-32$$

Solve the previous equations for X and Y.

$$(F_1 + F_2)L - (F_1 + F_2)X - (F_3 + F_4)X = 0 \quad 7-33$$

$$(F_1 + F_4)Y - (F_1 + F_3)W + (F_1 + F_3)Y = 0 \quad 7-34$$

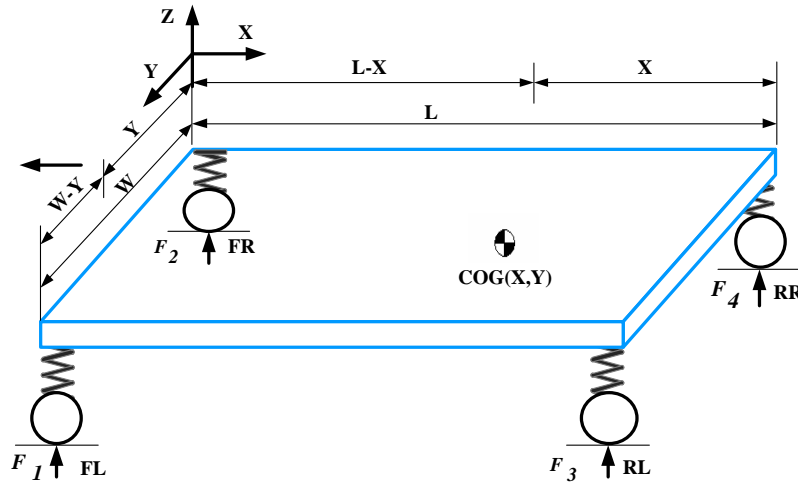


Figure 7-18: Force diagram of the vehicle

$$(F_1 + F_2)L = (F_1 + F_2 + F_3 + F_4)X \quad 7-35$$

$$(F_1 + F_3)W = (F_1 + F_2 + F_3 + F_4)Y \quad 7-36$$

$$X = \frac{(F_1 + F_2)L}{(F_1 + F_2 + F_3 + F_4)} \quad 7-37$$

$$Y = \frac{(F_1 + F_3)W}{(F_1 + F_2 + F_3 + F_4)} \quad 7-38$$

The longitudinal and lateral positions of a vehicle centre of gravity (COG) can be identified by Equations 7-37 and 7-38. Therefore, the vehicle centre of gravity can be calculated using the values of average load on each corner of the vehicle, the wheel base (L) and track of the vehicle (W), as presented in the Table 7-4.

$$X = \frac{(4229 + 3519)2800}{(4229 + 3519 + 2632 + 3298)} = 1587mm \quad 7-39$$

Where X is the distance from rear wheels to (COG)

$$Y = \frac{(4229 + 2632)1400}{(4229 + 3519 + 2632 + 3298)} = 702mm \quad 7-40$$

Where Y is the distance from right wheels to (COG)

Figure 7-19 present FRF of the vehicle body for 4 damping conditions (fully soft, 2-steps hard, 4-steps hard and fully hard). These conditions are presented in the Table 7-3. Theoretically,

when this ratio is around unity (0 dB), with no phase difference, the force between the wheel and the platform will be as the static load and the tyre deflection will be constant (Milliken & Milliken, 1995). The plots in Figure 7-19 indicate that an increase in the damping coefficient reduces the value of the response magnitude for excitation frequencies of the vehicle body. From this result, it can be deduced that, in the natural frequency range of the vehicle body, high damping is recommended. However, lower damping will provide a better ride comfort.

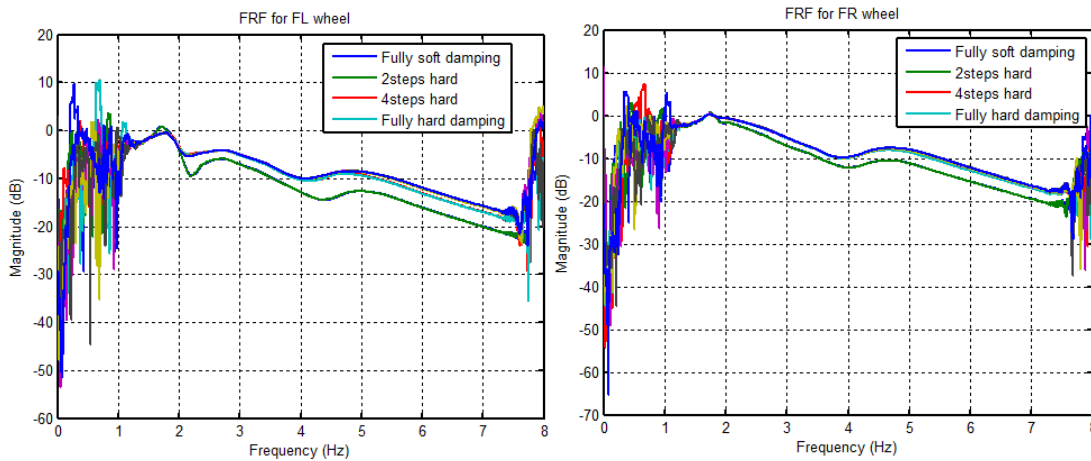


Figure 7-19: FRFs for the front left and front right wheel with different damping coefficients

## 7.8 Summary

An experimental was carried out to calculate the (FRF) of a vehicle. The purpose of this test was to obtain the actual parameters of the vehicle including the frequency, damping and transmissibility of the vehicle. The actual damping for each corner of the vehicle and the actual centre of gravity were applied to the model to enable the refinement of the mathematical model and enable direct comparison with the on-road experiments. In addition, to analyse the effects that damping changes have on the performance of the suspension response, faults were simulated in the damping systems. This was done by reducing the damping coefficient by 2-steps hard, 4-steps hard and fully hard for the front left and front right shock absorbers, as presented in Table 7-3.

The findings show the parameters of the vehicle that have been obtained. The findings also show that an increase in the damping coefficient reduces the value of the response magnitude for frequencies at the natural frequency of the vehicle body. From this it can be deduced that, in the natural frequency range of the vehicle body, high damping is recommended. However, lower damping will provide a better ride comfort in the mid to high frequency range.

## CHAPTER 8

### ON ROAD EXPERIMENTAL INVESTIGATION

*This chapter presents two experimental investigations. The first experiment was conducted to evaluate the vibration levels on special road conditions such as a speed bump. As the dynamic responses to such a bump would be for a short duration, the impulsive responses would be record and the results analysed and evaluated. In conjunction with this, the tyre pressure based monitoring method would also be evaluated. The second experiment was conducted with the test vehicle operating on a standard road to evaluate the suspension model and the modal shape based detection technique and consequently the modal shape based diagnostics.*

## **8.1 Introduction**

To evaluate the aforementioned investigations a series of experiments were carried out using a commercial vehicle operating under different road conditions. The vehicle used in these experiments was the same vehicle as that used in the 4-post tests, as detailed in Section 7.5. It was driven on typical UK suburban roads with speed limits ranging from 20 to 40 miles per hour. The passenger, who sat in the front of the vehicle alongside the driver, controlled the data collection system throughout the test. The experiments were principally organised into two main types:

The first experiment (see Section 8.2) was conducted to measure the vibration of the suspension and the pressure of tyres for a range of tyre inflation pressures, in which both vibration and dynamic pressure inside the tyre were measured simultaneously, in order to study the possibility of using impulses responses based analysis for condition monitoring. In addition, both vibration levels and pressure levels also evaluated for being an effective methods for monitoring.

The second experiment (see Section 8.4) was conducted to evaluate the suspension model and the SSI modal shape based detection technique. The experiment was to investigate the performance of the proposed online condition monitoring of the suspension system. The vehicle was subjected to different tyre inflation pressures and different damping coefficients but was driven on common roads.

For both tests, accelerations of the four corners of the vehicle were measured simultaneously and multiple data records were obtained. Thereafter, post-process was applied to obtain the vibration levels and modal shape parameters respective to each test.

## **8.2 The Effect of Tyre Pressure on Suspension Performance**

The purpose of this test was to study the effects of tyre pressure changes on suspension performance. The vehicle used was operated under ‘normal’ driving conditions and without braking when the wheels of the car passed over the bump (Hamed, Tesfa, Gu, et al., 2014). The data collected from vibration and pressure sensors was synchronised in order to identify the start point of when the wheels of the car were passing over the bump.

### 8.2.1 The Test Car Specification

In this experimental study the same vehicle as that in the 4-post-test experiments was used, for more details and specifications see Section 7.5. To investigate the effects of tyre pressure on the performance of the suspension, a wireless measurement system was used in this test. This offered a complete remote system for measurement of the pressure and vibration data

### 8.2.2 Wireless Measurement Instrumentation

The past few decades have shown a steady growth in using wireless sensors and wearable electronics (Steven R Anton, 2007). The measurement of dynamic changes of tyre pressure whilst driving is a challenge as the tyre pressure sensor rotates with the tyre. To overcome this, a wireless sensor and a node (transmitter) were assembled in the centre rim of the front left wheel to record the pressure data. The wireless measurement system comprises an accelerometer, dynamic tyre pressure sensor (DTPS), nodes (transmitters), gateway (receiver) and a laptop. Details of each component are described below:

#### 8.2.2.1 Accelerometer

The Piezo-electric accelerometer is cost-effective and commonly used for vibration measurements in the field of condition monitoring. This sensor consists of a piezoelectric crystal of small mass normally enclosed in a protective metal case (Al-Arbi, 2012). In this experimental study, one piezoelectric accelerometer (model CA-YD-104T) is fixed on the top cap of the shock absorber of the vehicle to show the vibration of the car body.

Figure 8-1 shows a photograph of the accelerometer and a table of its specifications.



Vibration sensor	
Model	CA-YD-104T
Serial number	11384
Sensitivity	$3.77 \text{ pc}/\text{ms}^{-2}$
Frequency	0.5 to 7000 Hz
Temperature	-20 to 120 °C

Figure 8-1: Photo of the accelerometer and the table of specifications

The accelerometer was fixed on the front left shock absorber. To ensure significant and stable installation of the sensor, an adapter was designed and manufactured in the University of Huddersfield. Figure 8-2 shows the accelerometer position on the vehicle body.

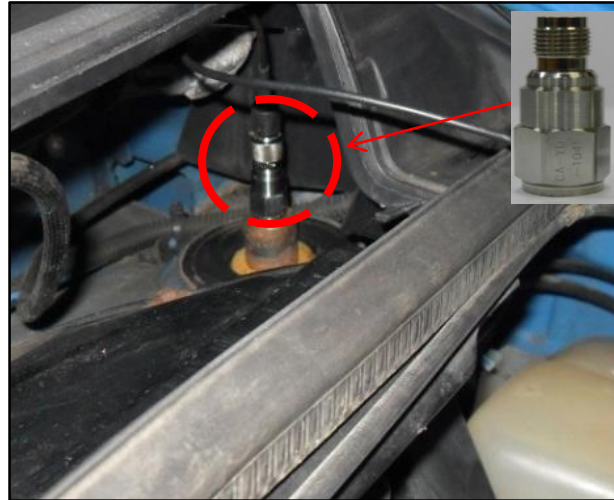


Figure 8-2: Accelerometer position on the front left corner

#### 8.2.2.2 *Dynamic Tyre Pressure Sensor (DTPS)*

The dynamic tyre pressure sensor (DTPS) has been used to measure the dynamic pressure due to the rapid interaction between the tyre and the bump. DTPS can measure these signals by sensing the change of the pressure inside the tyre due to the vibrations generated by the road geometry and tyre (Q. Wang, McDaniel, & Wang, 2012). When driving on a rough road and over bumps, DTPS data changes drastically.

In this research study, the dynamic tyre pressure sensor (DTPS) was connected to the valve stem of the front left wheel. To ensure the secure installation of the sensor, an adapter was designed and manufactured in the University of Huddersfield. This adapter was fabricated to enable tyre inflation without any damage to the sensor. Figure 8-3 is a photograph of the (DTPS) and a table of specifications. Figure 8-4 shows the position of the dynamic tyre pressure sensor (DTPS).



Dynamic tyre pressure sensor (DTPS)	
Model	CY-YD-212
Weight	10 g
Sensitivity	11.43 Pc/0.1Mpa
Response frequency	100 KHz
Temperature	-40 to 200 °C

Figure 8-3: Photograph of the (DTPS) and the table of specifications

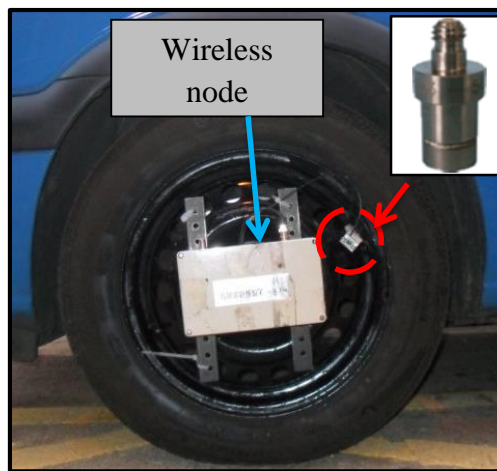


Figure 8-4: (DTPS) installed to the valve stem

### 8.2.2.3 Wireless Nodes (Transmitters) and the Gateway (Receiver)

A wireless sensor node (transmitter) was assembled and situated in the centre rim of the front left wheel as shown in the Figure 8-4. The sensor node transmits the DTPS data from the sensor to the gateway (receiver) system inside the vehicle. The other node is used for the vibration sensor positioned inside the vehicle. Each sensor node runs on one small rechargeable battery (phone battery 1.5 mA), and the batteries are recharged from energy sources regularly (after finishing the tests). The gateway (receiver) is connected to a laptop inside the car. Figure 8-5 shows photographs of the gateway and the Laptop. By displaying (Bee-Data) software, the data transmitted from the nodes will be received by the gateway (receiver) and saved in a temporary data record on the hard disk; this data then will be downloaded after completion of every test and saved into specific files. Figure 8-6 illustrates the wireless measurement system.



Figure 8-5: Photos of the gateway and the Laptop

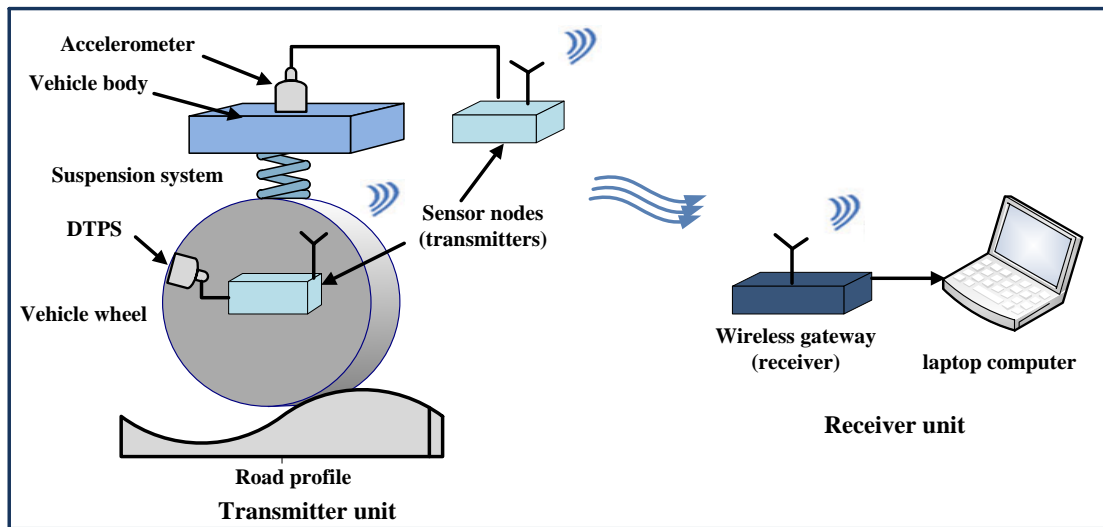


Figure 8-6: State diagrams of the wireless measurement system

### 8.2.3 Test Procedures

The experimental vehicle was operated in ‘normal’ driving conditions. The test has been conducted for four different tyre pressures with two different vehicle speed conditions as detailed in Table 8-1.

Table 8-1: Experimental set up

Tests	Wheels pressure conditions		Vehicle speed conditions
	Passenger wheel	Driver wheel	
A	Standard pressure (2.3 bar)	Standard pressure (2.3 bar)	8 km/hr, 16 km/hr
B	1.5 bar	Standard pressure	8 km/hr, 16 km/hr
C	Standard pressure	1.5 bar	8 km/hr, 16 km/hr
D	1.5 bar	1.5 bar	8 km/hr, 16 km/hr

The road profile used in this experiment is a bump which is located within the premises of The University of Huddersfield. The bump profile is 5.80 m width, 0.50 m length and 0.050 m height and this also was assumed to be the input for the model. Figure 8-7 and Figure 8-8 present a photograph and sketch diagram for the bump respectively.



Figure 8-7: Photograph of the bump used

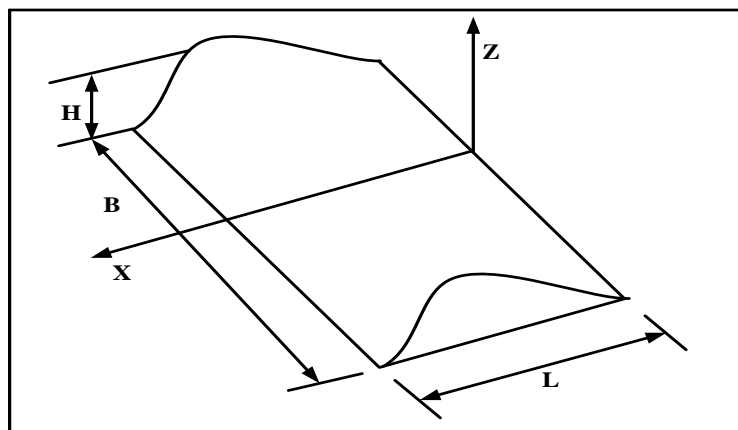


Figure 8-8: Sketch diagram for the bump

Where: (H) Height of profile [m], (B) Width of profile [m], (L) Length of the obstacle [m]

### 8.3 Results and Discussion

This section discussed the results of an experiment to examine the tyre pressure change on the performance of suspension, by measuring acceleration (vibration) of the vehicle and the dynamic pressure changes of the tyre. The experimental vehicle was driven in ‘normal’ driving conditions without applying the brake when the wheels of the car passed over the bump. The data collected from vibration and pressure sensors were synchronized together in order to specify the start point of when the wheels of the car passed over the bump, to enhance and

improve the accuracy of the vibration results, and also to understand and present the specific period for the vibration signals of interest.

### 8.3.1 Influence in Time Domain

The time-domain signal exhibits complex profiles as it is the sum of all the individual frequency components that are present. The absolute value of vibration signal in ( $m/s^2$ ) of suspension and the absolute value of dynamic pressure changes inside the front left tyre are shown in the Figure 8-9.

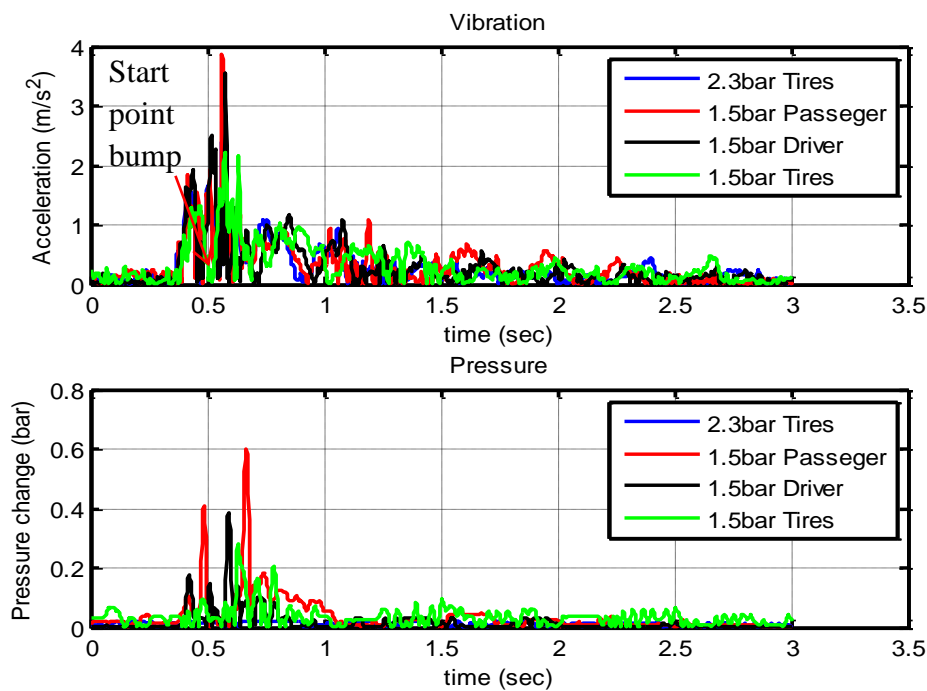


Figure 8-9: Time domain acceleration of the suspension and the pressure changes of the tyre when the car passes over the bump at speed of 8 km/hr

This figure is the time domain signal for multiple tests which have been carried out with different inflation pressures (i.e. standard pressure (2.3bar) and when the passenger wheel, driver wheel and front wheels have been lowered to 1.5 bar), and with a vehicle speed of approximately 8 km/hr. From this figure, the signals of vibration (on the top) and pressure (on the bottom) appear to share the same starting time for all tests. The red arrow in the vibration signal shows the start point when the front wheels of the car pass over the bump. Moreover, the results indicate that the amplitude of the signal increased at the instant where the front wheels of the car passed over the bump in both vibration and pressure.

### 8.3.2 Influence in the Frequency Domain

Figure 8-10 presents the acceleration spectrum analysis of the vehicle body for multiple tests which have been carried out with different tyre pressures and with a vehicle speed of approximately 8 km/hr. It is visible from this figure that every vibration causes peak values in the vicinity between 1 Hz to 3 Hz, which indicates the natural frequency of the body. In the frequency region between 10 Hz and 14Hz, the vibration response generates peak values. These frequencies support the idea that the high-frequency resonances are mainly due to the road vibration through the wheels.

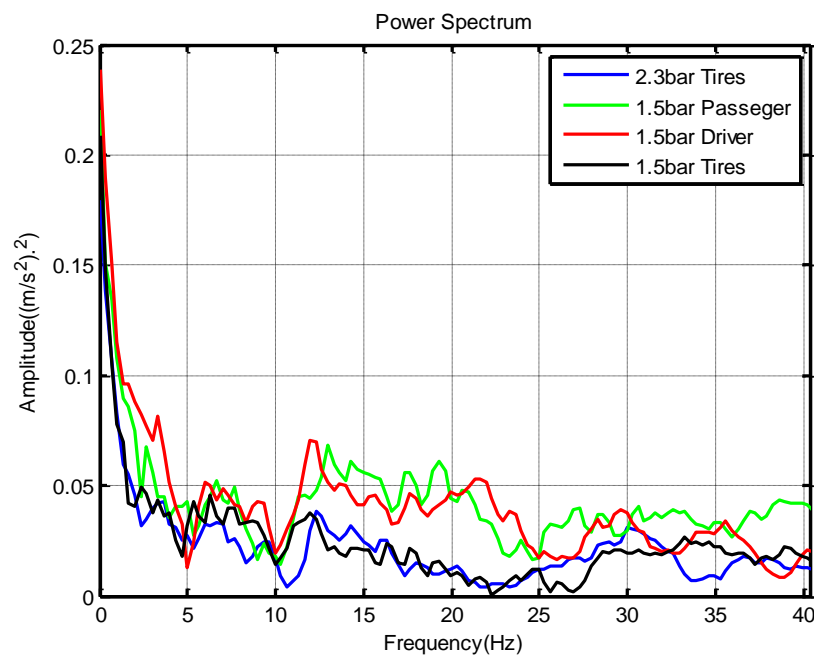


Figure 8-10: Power spectrum of vehicle body vibration with range of tyre pressures

When performing fault diagnosis using the time-domain vibration signal, statistical methods are invariably applied. The most common statistical parameters are root mean square (RMS) (E. Y. Kim et al., 2007). Figure 8-11 shows RMS for acceleration of the vehicle body at various tyre pressures with vehicle speeds of 8 km/hr and 16 km/hr. The results demonstrate that the amplitude of RMS increases in all conditions with the lowering of the tyre pressure from 2.3 bar to 1.5 bar and in all of the test cases, which indicates that the ride comfort is affected negatively by under-inflation of the tyre. It can be summarised that, under-inflated tyres affect the suspension performance in conflicting criteria. It also shows a slight change in terms of road handling and a notable affect in terms of ride quality as shown in the RMS plots. These results were validated with the model result and showed reasonable agreement.

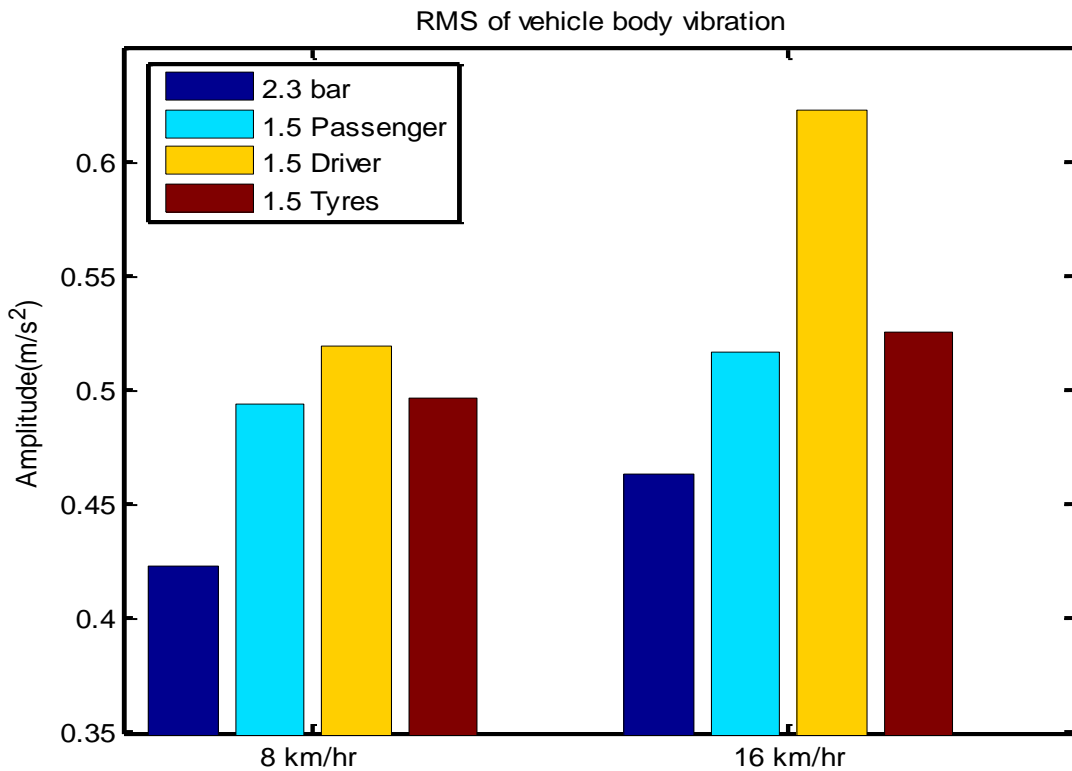


Figure 8-11: RMS of vehicle body vibration at a range of speeds and at various tyre pressures

### 8.3.3 Influence of Vehicle Speed on Suspension Response

To study vibration in relation to vehicle speed during road tests, vibrations were recorded and analysed when the wheels passed over the bump at different speeds. The influence of vehicle speeds on the suspension responses were investigated at vehicle speeds of 8 km/hr and 16 km/hr. Figure 8-12 presents RMS values and RMS differences for the acceleration of the body over a range of speeds and tyre pressures. It can be noted that the RMS value increases gradually with an increase of vehicle speed in all test conditions. These results were compared with the simulation results, which indicated that the vehicle speed has an effect on the acceleration of the vehicle body which was strongest at lower speeds and reduced at higher speeds. That means that the change of the RMS value was higher when changing the speed at lower values from 8 to 16 km/hr than it was when changing the speed at higher values from 16 to 24. There was only a slight change at 24 to 32 km/hr.

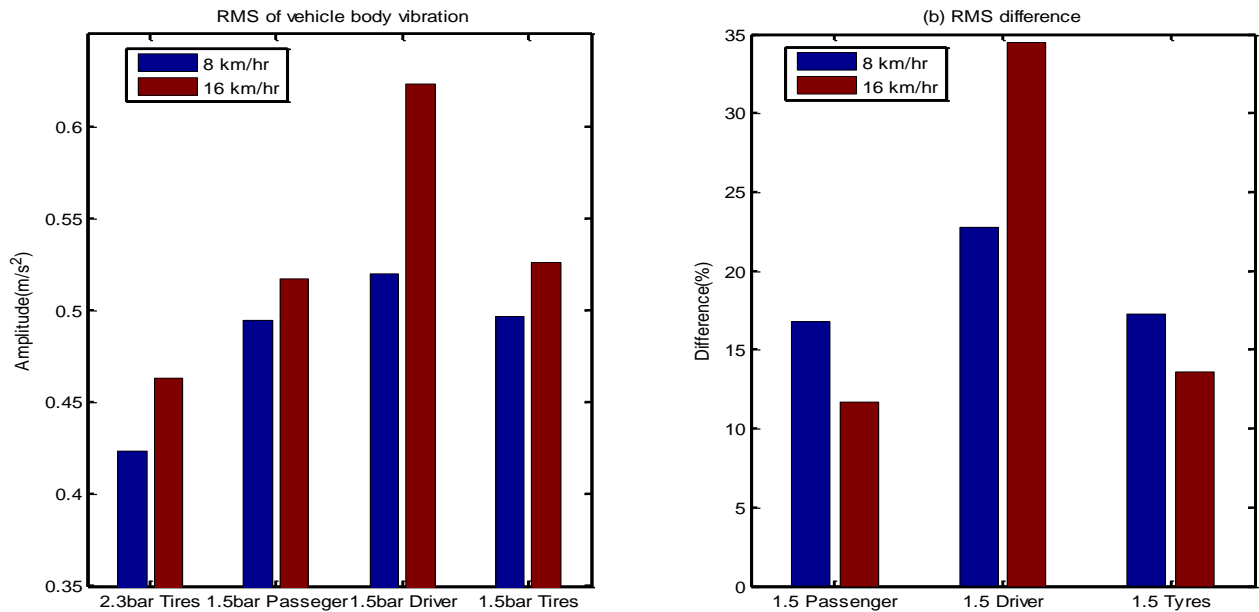


Figure 8-12: RMS for acceleration of the vehicle body at a range of vehicle speeds

#### 8.4 Summary of Experimental Studies based Bumped Road

In summary, these experimental studies show that:

- 1) The vibration increases with lower inflated tyres and increased speed when the vehicle passes the bump. This can reduce ride comfort and handling performance. However, such changes with operating conditions make it difficult to assess consistently the severity of associated problems. Therefore, it is not suitable for online monitoring.
- 2) Simple spectrum analysis could not be used as a reliable source to indicate the problems and therefore, more advanced data analysis methods are required.
- 3) Pressure based monitoring shows similar problems to that of vibration in that the changes also depend on operating conditions. Moreover, a more complicated measurement system including vehicle speed signals is required for obtaining the tyre pressure, which can be expensive. Therefore, it is also not suitable for online monitoring.

#### 8.5 Characterisation of the Modal Responses to Different Defects

In this section, experimental studies were conducted based on excitations of common roads in which vibrations of the vehicle body at each corner are based on to obtain modal parameters under different suspension conditions. This experiment was conducted for different damping coefficients (Experiment 1) and for a range of tyre inflation pressures (Experiment 2). The

same test vehicle and the same measurement system were used for both experiments (1 and 2). The purpose of this experimental is to validate the suspension model and the modal shape based detection technique. For this purpose, a number of road tests were conducted using a commercial vehicle operating in normal road conditions. The car was driven on typical UK suburban roads with speed limits from 20 to 40miles/h. During the tests the car had two people in the front seats: the driver and a passenger who controlled the data collection system.

### **8.5.1 The Test Car Specification**

In this experiment, the same vehicle was used as in the previous experiment and a photograph of the test vehicle is shown in Figure 7-8 (see Section 7.5.1). The specifications of the vehicle are shown in the Table 7-1 (see Section 7.5.1). The experimental vehicle was driven on typical UK suburban roads with speed limits from 20 to 40miles/h and on a countryside road in Huddersfield in order to avoid city centre traffic congestion. . For damping changes analysis, the two front shock absorbers of the car were replaced with adjustable shock absorbers (struts from SPAX Company) as presented in (Section 7.5.1), which was done by a MOT test qualified garage to ensure it is safe to drive .

### **8.5.2 Measurement Instrumentation**

#### **8.5.2.1 Accelerometers**

In this experimental study, four cheap piezoelectric accelerometers (model CA-YD-104T at a cost of £50 each) were used to measure the response of the vehicle body. These accelerometers are commonly used to measure the vibration of the mechanical surfaces for condition monitoring because their masses are light and do not alter the movement of the surface. These accelerometers also possess a sufficiently wide frequency range to measure automobile vibration and are of an adequate sensitivity (0.5Hz to over 7 kHz). Such a wide band accelerometer was purchased as it will be used for monitoring jointly other vehicle problems such as engine mount, brake efficiency, etc. The nominal sensitivity of the sensor is 4.0mv/m/s<sup>2</sup>, allows a large vibration such as that passing a pump to be measured while being sensitive to small vibrations of uneven road profiles. Figure 8-13 shows photograph of the accelerometers.



Figure 8-13: Photograph of four accelerometers (model CA-YD-104T)

The specification of the sensors are shown in Table 8-2. Each accelerometer was connected to an external impedance converter model YE5857A-1. The amplified output signals of these devices was then connected to the data acquisition system for converting the analogue data into digital format. Figure 8-14 shows a photograph of the preamplifiers, which has a gain of one.



Figure 8-14: Photograph of the preamplifiers.

Table 8-2: Specification of the vibration sensors

Vibration sensors	Accelerometer 1	Accelerometer 2	Accelerometer 3	Accelerometer 4
Model	CA-YD-104T	CA-YD-104T	CA-YD-104T	CA-YD-104T
Serial number	07143	11384	07213	07169
Sensitivity	$3.243 \text{ pc/ms}^{-2}$	$3.77 \text{ pc/ms}^{-2}$	$3.573 \text{ pc/ms}^{-2}$	$3.64 \text{ pc/ms}^{-2}$
Frequency	0.5 to 7000 Hz	0.5 to 7000 Hz	0.5 to 7000 Hz	0.5 to 7000 Hz
Temperature	-20 to 120 °C	-20 to 120 °C	-20 to 120 °C	-20 to 120 °C

### **8.5.2.2 Data Acquisition System**

A four data acquisition system was used to record and save the vibration data. The main function of this system is to convert the physical analogue signals into digital data and convert them into digital quantities according to transducer sensitivities. A Sinocera Model YE6231 dynamic data acquisition unit has been used in this test as presented in (Section 7.5.2) also see Figure 7-11. It operated under a continuous collection mode at a sampling frequency of 3000Hz, allowing sufficient data to be recorded during the road tests which are often carried out on many different roads for hours in order to ensure the data has stable statistics.

### **8.5.3 Test Procedures**

The test car was equipped with four vibration sensors. The accelerometers were fixed on the top caps of the four suspension struts respectively, as specified in Table 8-2 including: sensor 1 fixed on the front left shock absorber and sensor 2 connected onto the front right shock absorber. These locations were chosen as they are very close to the theoretical location and it is convenient to glue the sensors to the sensor adapters. , Sensors 3 and 4 were mounted by magnetic bases on the rear left and rear right shock absorbers respectively. The installation of all of the sensors were adjusted carefully so that they were as vertical as possible. Figure 8-15 (a) and (b) shows the front and rear position of the sensors respectively.

The output cables of these sensors were fixed to body works and then connected to the external impedance converter model YE5857A-1. All of them were passed through the drive cabinet and connected to the four channel data acquisition Model YE6231 which is controlled by a laptop inside the vehicle.

During the test, the vibration signal was collected at a sampling rate of 3000 Hz at 10 minute intervals, dependent on the traffic flow and road variations. The total data length for each tyre test was about 60 minutes which ensured that all modes of interest were sufficiently excited; these procedures were adopted for both experiments (1 and 2).

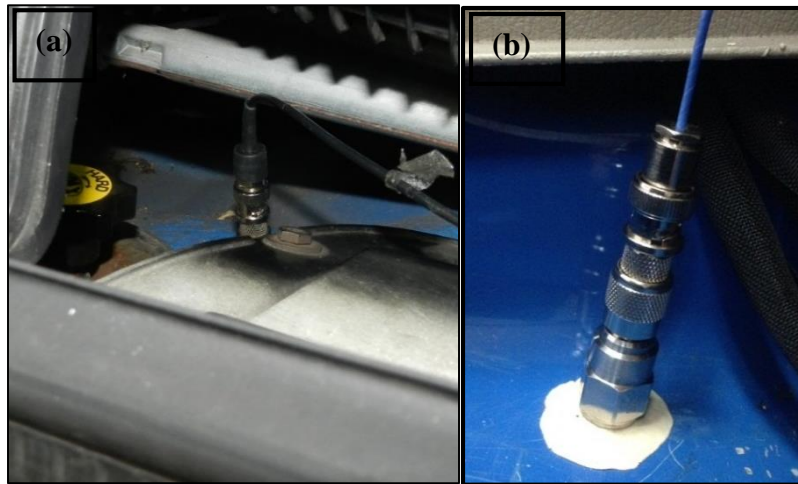


Figure 8-15: (a) Position of the front accelerometer and (b) Position of the rear accelerometer

### 8.5.3.1 Experimental Setup for Damping Change Experiment (1)

This experiment was conducted to consider the damping change. In this test the change was only made to the front left shock absorber in four cases as presented in Table 8-3 and there was no change made to the rest of vehicle’s shock absorber setting. Each test was conducted ten times and after each test the data acquired was viewed and imported to MATLAB files for further processing. In Table 8-3, “fully soft” means that the shock absorber is in the baseline conditions, 2-steps hard, 4-steps hard and fully hard refer to decreases in the damping coefficients.

Table 8-3: Experimental setup for damping change

Tests	Damping conditions		Vehicle speed
	Front left	Front right	
A	Fully soft	Fully soft	about 40 km/h
B	2-Steps hard	Fully soft	
C	4-Steps hard	Fully soft	
D	Fully hard	Fully soft	

### 8.5.3.2 Experimental Setup for Under-Inflation of the Tyre Experiment (2)

This test was conducted under three tyre inflation cases. The first one was standard pressure at 2.2bar for the car. The second and third were for lowered inflation tests in which the front left tyre was set to 1.6bar and 1.0bar respectively, and a vehicle speed of about 40km/h as presented

in Table 8-4. Therefore, detecting the pressure changes allowed an evaluation of the proposed method. In addition, the measurement system components are presented in Figure 8-16.

Table 8-4: Experimental set up for range of inflation pressures

Tests	Wheels pressure conditions	Vehicle speed
		Passenger wheel
A	Standard pressure (2.2 bar)	
B	1.6 bar	
C	1.0 bar	

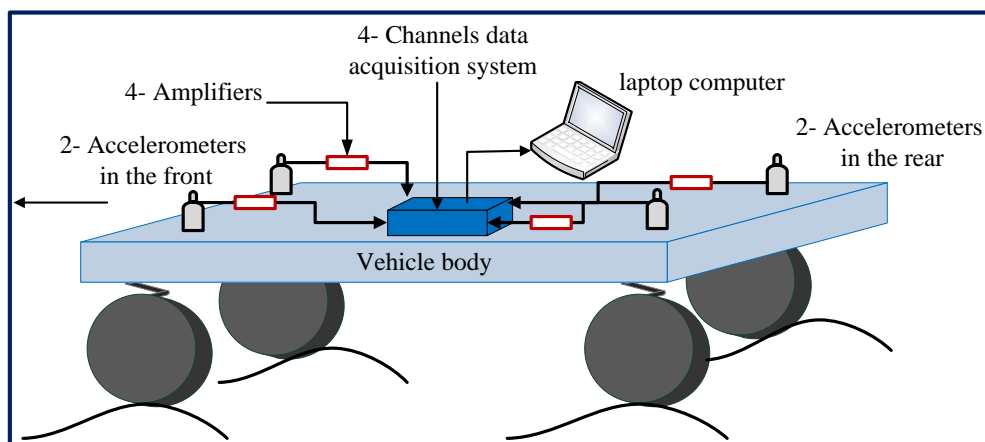


Figure 8-16: Block diagram for the measurement system

## 8.6 Diagnostic Results for Suspension Defects

### 8.6.1 Vehicle body Vibration Responses.

As presented in Table 3-1, the vehicle body used in this study was from a light commercial vehicle. Its structure had been theoretically modelled to enable on-line condition monitoring for suspension. To validate the models using real operations, this study applies an online method to identify the dynamic characteristics of the vehicle body through vibration measurements. In particular, it is to check and evaluate if any significant vibration modes occur when the vehicle operates on normal city roads under normal conditions. Figure 8-17 presents the measured vibration signals from the four accelerometers located on the vehicle body. The vehicle travelled on normal city roads at about 20-40 mile/h. Figure 8-17 shows that the signals are non-stationary with many large localised responses. Their corresponding spectra show that the energy is below 10 Hz due to the responses of suspension system effects. The range from 1 Hz to 10 Hz for the body dynamic analysis, shows much lower amplitudes and wider spread

patterns. These show that the vibration signal contains high levels of noise and interfering components. It means that the data needs to be pre-processed adequately to meet the stationary and linear conditions specified by the SSI frameworks, discussed in Chapter 5.

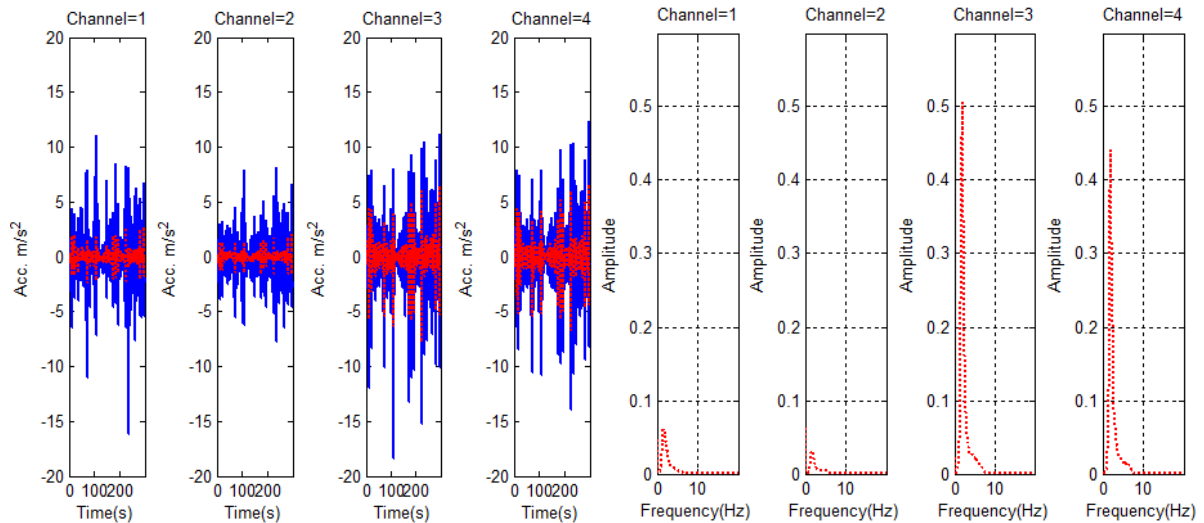


Figure 8-17: Raw vibration signals and their spectra

Therefore, all data sets from the on-road tests were processed according to the steps in Chapter 5 in order to obtain measured modal shapes for each test case. The long data records were divided into successive short segments of 2048 points in length and each of them were applied to the auto and cross correlation calculation. As there were about 10 data records, each of them being over 10,000 points, nearly 100 correlation signals can be obtained for the average correlation signals.

This average operation allows multiple data records and different data frames to be combined in the correlation lags domain. As shown in Figure 8-18, it suppresses random noise and non-stationary contents effectively and achieves clean correlation signals exhibiting high similarity to impulse responses. In addition, the figure also shows a segment of correlation signal that is excluded during the average process as it is very low in amplitude as it may come from very smooth road operation in which little suspension responses can be induced.

Thus by adopting this scheme the multiple data sets from different roads and operation conditions are combined consistently to obtain the average correlation signals to implement the singular value decomposition (SVD) for parameter identification. Moreover, a comparison of stabilisation diagrams is made between different averages applied to the correlation signals.

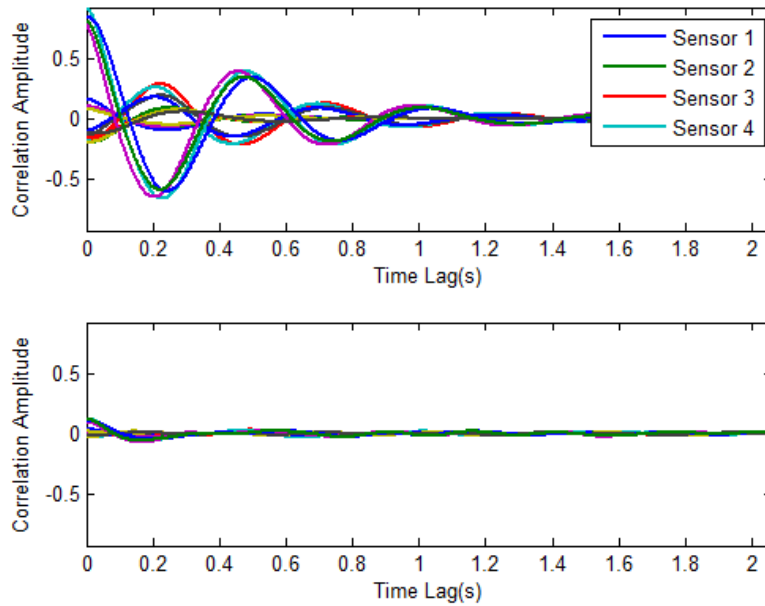


Figure 8-18: Average scheme in the correlation lags domain for all sensors

From the stabilisation diagrams in Figure 8-19 it can be seen that the spurious modes due to noise, become less with larger averages, resulting in a clearer diagram, allowing a reliable extraction of significant modes. Particularly, the potential modes at about 1.4 Hz, 1.7 Hz and 2 Hz become more stable and identifiable as shown in the bottom plot, which clearly are related to the theoretical ones. Therefore, its modal properties will be investigated for obtaining modal shapes and thereby the modal energy difference indicator to achieve system diagnostics.

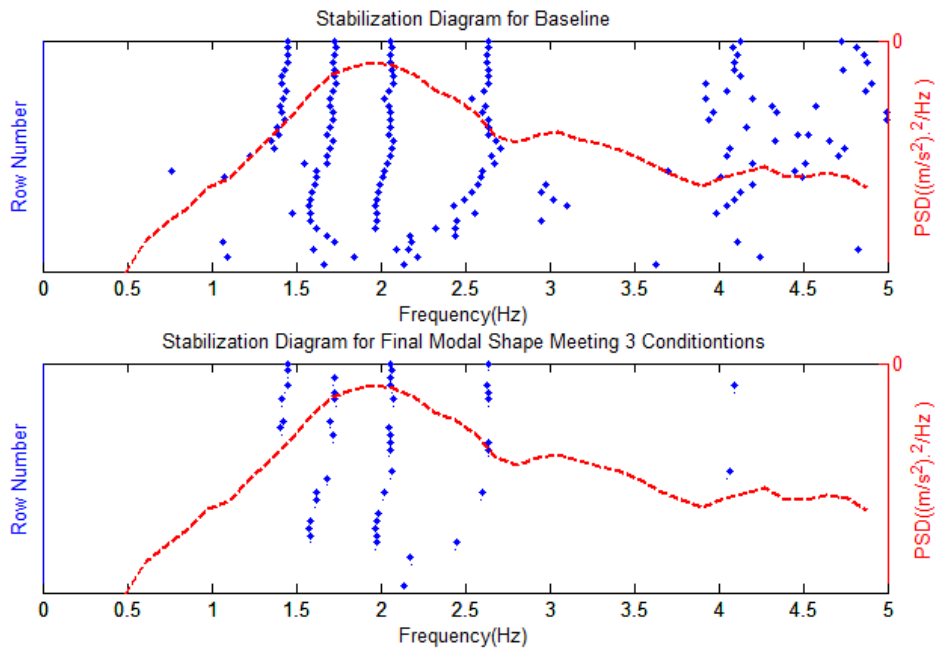


Figure 8-19: Stabilisation diagram of modal characteristics for baseline conditions

## 8.6.2 Modal Shape Based Detection Technique for Tyre Pressure Change

Figure 8-20 presents the mode shapes of the vehicle body identified by ACS-SSI for the three tyre pressure cases. It can be seen that the road excitation based identification allows only the bounce and pitch mode to be identified. However the roll motion mode is not shown as the road has rolling excitations induced, which is consistent with vehicle design requirement in that the roll mode should be stable (Yang et al., 1998). Moreover for the baseline test, the bounce and pitch motions shown in Figure 8-20 (a) and (b) are nearly the same or with little differences for both the two front coordinates and the two rear coordinates even though the road conditions are not the same between the front wheels. This shows that the car suspension system has desired dynamic characteristics. However, the modal shapes exhibit certain twists when the inflation pressure is lower on one of the tyres Figure 8-20 (c) and (d). According to the modal shapes in Figure 8-20, it can be deduced that high relative deformations of the frame occur at sensor positions of 3 and 4 (RL and RR). It indicates that the body is subject to high dynamic loads at these positions and the stiffness at this part of the body may need to be improved. As presented in the previous section, the method of (ACS-SSI) for vehicle dynamics analysis has been used. In addition, it also can be seen that either the modal frequency values or the damping amplitudes could not show a consistent results with the change in tyre pressures. To show more accurate indications, Figure 8-21 illustrates the Modal Energy Differences (MED) versus the tyre pressure changes for the front and rear rolling of the bounce and pitch modes of the vehicle body.

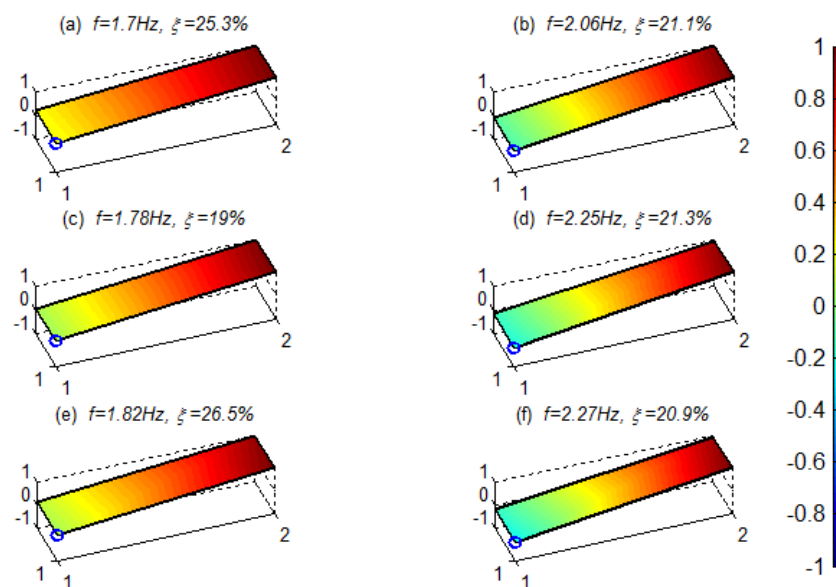


Figure 8-20: Mode shapes of the vehicle body

Front left tyre pressure was changed from baseline to 1.6bar and then to 1.0bar respectively as presented in Table 8-4. In Figure 8-21, rolling energy of front bouncing (B) shows more fluctuations with increasing of their value than the rolling energy of rear bouncing (B) modes. While, the rolling energy differences of front and rear rolling of pitch (P) modes have a slight change with a little increase on the rear modes.

These significant changes due to the change in tyre pressure dedicate that, it is possible to differentiate the small pressure change from normal pressure operations and achieve diagnosis even though no clear difference can be perceived by drivers. In addition, these results show acceptable likeness when compared to the results of the model of the same tyre (see Figure 4-6).

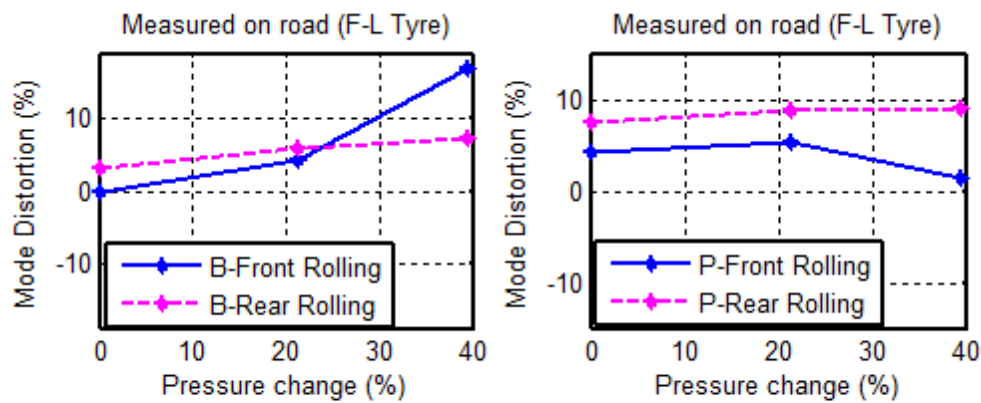


Figure 8-21: Modal energy differences corresponding to tyre pressure changes

### 8.6.3 Modal Shape Based Detection Technique for Damping Variation

The front left shock absorber only was changed in three cases as presented in Table 8-3. Figure 8-22 depicts the Modal Energy Differences (MED) versus the damping changes for the front and rear rolling of the vehicle body. In this figure, bouncing energy of front rolling (B), shows more fluctuations than the bouncing energy of rear rolling (B) modes which increased gradually. While, the pitching energy differences of front and rear rolling (P) modes show differently, with a little decrease on the rear modes and dramatic increase in the value of pitching energy for front rolling (P).

These significant changes due to a change in the damping system indicate that it is possible to detect a small fault and achieve a diagnosis. In addition, the key findings indicate that the experimental results of damping faults show acceptable agreements with the simulation results presented in Figure 4-4.

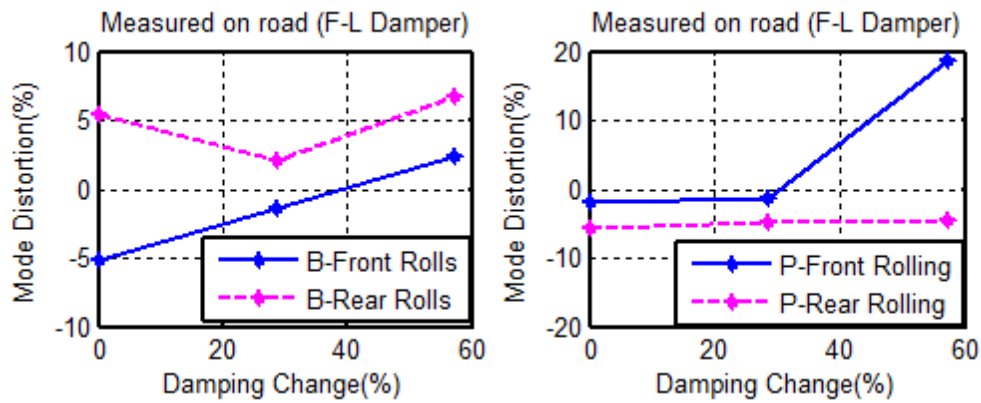


Figure 8-22: Modal Energy Differences (MED) versus the damping changes for modes of the vehicle body

From the above findings, it can be concluded that Modal shape based detection technique has been validated, and it has the potential to be used to diagnose suspension defects and to monitor suspension operating conditions with the application of suitable on-line operating conditions.

### 8.7 Summary of Experimental Studies based on Standard Roads

This experimental study can lead to following conclusions:

It is achievable to apply ACS-SSI approaches to vibration signals on the four corners to estimate suspension modal parameters though it may need a large amount data as long as 30minutes to obtain stable results.

The test results confirmed that either the modal frequency values or the damping amplitudes could not show a consistent result with the change in tyre pressures.

Fortunately, the mode shapes qualified by MED can give good indications on both the tyre pressure decreases and damping changes.

## **CHAPTER 9**

### **CONCLUSIONS AND FUTURE WORK**

*In this chapter the important results and conclusions of this research study have been presented. Furthermore, suggestions are also given for the future work in related research areas.*

## 9.1 Thesis Objectives and Achievements

The achievements and contributions of this research will be presented in this chapter. The study of on-line condition monitoring for vehicle suspension systems was the main focus of this research. It began with an initial overview of condition monitoring strategies, focusing particularly on the most methods used for suspension fault detection. The key to condition-based maintenance is the acquisition of accurate and up-to-date knowledge of the vehicle condition, which can be obtained through various techniques. Condition monitoring is known as how to use the measurement of data to detect the faults of a system or machine which is used to guide maintenance. It is concerned with gathering data to enable better understanding of the health or condition of an item of machinery. Fault detection method is used to monitor the current condition of vehicle suspension systems through simulations of vehicle models and analysis of measured signals.

Vehicle vibration signal has been analysed to characterise the vehicle parameters based on theoretical analysis and experimental studies. The key challenge and focus of this research has been the extraction of the vehicle modal parameters from the theoretical models, and from the vibration signals measured from a monitored suspension system.

The key achievement of this study is that a novel on-line condition monitoring technique has been developed for online monitoring suspension systems of four wheeled vehicles. The technique is based on the so-called modal shape based detection approach which is a novel and improved implementation of the recent ACS-SSI applied to vibration responses from the four corners of a vehicle.

Following this key achievement a number of further achievements are realised in this research, which can be outlined as:

**Objective 1:** To carry out a comprehensive literature review regarding to commonly used vibration analysis methods including methods for the detection of common faults occurring in suspension systems.

**Achievement 1:** Different relevant vibration analysis methods were fully understood and applied to characterise the system dynamics and behaviour, based on both simulations and experimental studies of the dynamic interactions between a vehicle and a road condition (see Chapter 2).

**Objective 2:** To develop a mathematical model of a full vehicle with (7-DOF), in order to understand the vehicle dynamics, leading to the characterisation of the modal parameters of the vehicle.

**Achievement 2:** the response of a vehicle has been analysed by using a 7-DOF model, and to analyse the time and frequency response of the vehicle in MATLAB (see Chapter 3). The vehicle parameters, including modal frequency, damping ratio and modal shapes, were simulated and presented using the 7-DOF full vehicle (see Section 4.2), which lead to subsequent development of modal based diagnostics.

**Objective 3:** Calibrate and verify the model offline and online so that the predicted vibration responses agree with that of real world measurements as much as possible.

**Achievement 3:** To calibrate the model offline, experimental work has been conducted by using a 4-post-test rig at the University of Huddersfield. The test was conducted to measure the response of the vehicle body and the vibration of the platform (shaker) in order to calculate the (FRF) of the vehicle, the objective of this test was to perform the calibration for the model using the actual values of the vehicle (see Section 7.5).

To evaluate the suspension model online, road tests were also conducted using a commercial vehicle operating in normal road conditions. The car was driven on typical UK suburban roads with speed limits from 20 to 40miles/h.

**Objective 4:** Investigate the behaviour of modal shapes under the influence of different suspension faults (damping coefficient, spring rate and under-inflation of the tyres), making use of the virtue that modal shapes are independent of vehicle load, speed and road excitation thereby developing modal shape-based approaches for monitoring suspension systems.

**Achievement 4:** The vehicle parameters of the vehicle and their characteristics were analysed under the condition of different suspension faults. These faults have been considered by reducing damping coefficient, spring stiffness and tyre pressure by various increments of approximately 10 %, 20 %, 30 %, and 40 % of their original values. The simulation results indicated that the shape of the bounce and pitch modes are less sensitive to vehicle load and road excitation, and more sensitive to the suspension parameters including stiffness, damping ratio and tyre inflation pressure. Therefore, the rolling modal energy differences for the front and rear of the bounce and pitch modes have been simulated and used as reliable detection parameters for suspension faults (see Section 4.3).

**Objective 5:** To investigate modal parameter identification technologies and develop stochastic subspace identification based approaches for the determination of the vehicle's modal parameters.

**Achievement 5:** The general Stochastic Subspace Identification (SSI) frameworks have been discussed. In particular, an average correlation signal-based stochastic subspace identification (ACS-SSI) method is identified to be the most potential one as it has been developed recently for online vehicle frame dynamics analysis by Chen et al. (2015) (see Chapter 5). It allows multiple data records and data frames to be combined through an averaging scheme in the correlation lag domain in which the optimal reference selection was proposed by using correlation functions rather than the raw spectra.

In addition, simulation validation studies were carried out for the SSI model. The output signals from the 7-DOF model have been generated to as the input of the SSI model, then the parameters obtained from the SSI model were compared to the theoretical modal parameters of the 7-DOF model. The simulation and validation process has been presented in Section 6.1.

**Objective 7:** Develop a wireless sensing system for on-line vibration and pressure measurement, which may serve to examine the under-inflation pressure effects on the suspension system performance.

**Achievement 7:** The experimental vehicle was driven in 'normal' driving conditions, with different tyre pressures in four cases (standard pressure 2.3 bars, and 1.5 bar for the passenger, driver and both front wheels respectively) and with two different vehicle speeds of 8 km/hr and 16 km/hr. The purpose of using the DTSPS was to synchronise the vibration and pressure signals, in order to specify the start point of the bump for more accurate analysis. The results indicate that, the signals of both vibration and pressure share the same starting time for all tests. The start point when the front wheels of the car pass over the bump can be specified in both the vibration and pressure data, enabling the synchronisation that offers more reliable and accurate analysis. The results also show a dramatic rise in the signal amplitude when the front wheels of the car pass over the bump, in both the vibration and the pressure.

The results also demonstrated that when the tyre pressure is lowered, the RMS value is increased. In addition, the change in the RMS was high in the tyre pressure of driver wheel, which can be referred to the mass change inside the vehicle. The influence of vehicle speed on the dynamic response of the suspension was investigated for the values of speed considered in

the test. It was found that the RMS of the vehicle body increases with increasing vehicle speed for all test conditions (see Section 8.2).

**Objective 8:** To evaluate experimentally the suspension models and the modal shape based detection technique proposed in this research, for different tyre pressures and damping coefficients.

**Achievement 8:** Road tests were conducted using a commercial vehicle operating in normal road conditions. Specifically, the vehicle was driven around typical UK suburban roads with speed limits from 20 to 40 mph. During the tests the car had two people in the front seats: the driver and a passenger who controlled the data collection system.

All data sets from on-road tests were processed in MATLAB, and an average correlation signal-based SSI method (ACS-SSI) was adopted to obtain measured modal shapes for each damping and tyre pressure case. The various data collected from road tests have been combined consistently to obtain the average correlation signals in order to implement singular value decomposition for parameter identification. The results show that the potential modes at about 1.4 Hz, 1.7 Hz and 2.0 Hz become more identifiable. Modal Energy Differences (MED) for the front and rear rolling of the bounce and pitch modes were simulated for damping reduction and the tyre pressure changes.

The experimental results showed that faults of suspension can be monitoring using the energy differences of the mode shape. Moreover, the rolling modal energy differences for the front and rear of the bounce and pitch modes can be used as reliable detection parameters. Detecting suspension faults in this way is thought to be more desirable than using the other modal parameters mentioned because it is independent of vehicle loads (see Section 8.6).

**Objective 9:** Verify and improve the proposed online condition monitoring approaches based on modal shape deformation characteristics.

**Achievement 9:** The validation of the model results against the experimental results shows acceptable agreement. Therefore, the proposed scheme combined with stochastic subspace identification methods is sensitive and reliable, allowing the detection and diagnosis of small changes in damping and tyre pressures when the vehicle operates on a standard road at different speeds. Therefore, on-line condition monitoring for suspension systems was investigated and presented in this research (see Section 8.6).

**Objective 10:** Provide recommendations for future research to improve the performance of suspension condition monitoring.

**Achievement 10:** Recommendations have been provided to continue for future work in this field (see Section 9.4), this based on using different devices to develop the condition monitoring of vehicle suspension. Furthermore, the full vehicle model is now ready to be used for more advanced examination of the suspension in each corner of the vehicle.

## **9.2 Conclusions on Characterisation of the Dynamics of an Automotive System for On-line Condition Monitoring**

The aim of this research was to investigate the vibration responses of suspension system and develop an on-line condition monitoring approach for automotive suspension systems based on cost-effective vibration measurement. The conclusions of this research can be summarised based on the theoretical and experimental studies which have been presented in the previous chapters.

### **9.2.1 Conclusions on Suspension System Models**

1. The fault detection of suspension has been discussed by using the vibration analysis for a mathematical simulation of the full vehicle. To achieve this purpose, a (7-DOF) model has been developed and solved by a standard state space method to: (i) understand the dynamics and behaviour of the vehicle; and (ii) extract the vehicle parameters including modal frequency, damping ratio and modal shapes for each corner of the vehicle.
2. The modal parameters of the vehicle, including modal frequency, damping ratio and modal shapes were identified theoretically and presented in this research.
3. The model has been calibrated offline and on line, so that the predicted vibration responses can be agreeable with that of measurements as much as possible.
4. From the modal parameters analysis, it can be concluded that, the modal frequency and damping are influenced by vehicle load and is not suitable for monitoring faults from suspension, see section 3-2.
5. Further parametric studies have found that the shape of the bounce and pitch modal are less sensitive to the vehicle load and speed but to the suspension parameters including stiffness, damping and tyre inflation pressures.
6. Following this, analyses were carried out on the energy differences for the mode shapes of the vehicle. For an ideal vehicle the bounce and pitch modes should have no rolling movement. Therefore, any difference between the two coordinates of the bounce and pitch modes can be a reliable indication of the asymmetry due to the abnormality in a suspension element.

7. Therefore, it can be concluded that the rolling modal energy differences for the front and rear of the bounce and pitch modes provide an effective method for fault diagnosis in suspension systems. Detecting suspension faults in this way is thought to be more desirable than using the other modal parameters mentioned because it is independent of vehicle loads.

### **9.2.2 Conclusions on Experimental Studies**

1. Multiple experiments were conducted to evaluate the model and the modal shape based detection technique which has been proposed for the condition monitoring of a suspension. Subsequently, the initial data was collected experimentally by driving the test vehicle over Bump 1 (within The University of Huddersfield). The acceleration response of the vehicle body, based on the model simulation, was validated using the experiments results. From these results, it can be concluded that, the comparison shows that the model predicts the suspension performance reasonably well.
2. Further experiments were conducted to evaluate the modal shape based detection technique which has been proposed for the condition monitoring of a suspension. This part included two different experiments to determine the effects of (i) a range of inflation tyre pressures, and (ii) a range of damping coefficients, using a commercial vehicle (the test vehicle) operating in normal road conditions.
3. All data sets from on-road tests were processed to obtain measured modal shapes of the vehicle for each tyre pressure and each damping case. The method used for this output-only modal parameter identification was an average correlation signal based stochastic subspace identification (ACS-SSI) for online vehicle dynamics analysis.
4. As it has been mentioned previously that, the modal frequency and damping are not suitable for monitoring faults from suspension. However, the mode shape of the bounce and pitch are less sensitive to the vehicle load and speed but to the suspension parameters including stiffness, damping and tyre inflation pressures.
5. Based on the previous facts, analyses were carried out on energy difference calculation for the rolling of the front and rear of the bounce and pitch modes of the vehicle.
6. Therefore, it can be concluded that, a suspension fault detection technique was developed based on observed changes in the mode shapes of the vehicle, allowing the detection and diagnosis of changes in tyre pressures and damping coefficients when the vehicle operates on standard roads at different speeds.

### **9.3 Novelties and Contribution to Knowledge**

This section summarises main aspects of novelty in developing on-line condition monitoring for automotive suspension systems, which have been presented a number of important advancements that are novel and not implemented in previous researchers. The following are the highlighted novel points.

#### **Novelty One:**

The author of this thesis believes that the modal shape based detection technique for on-line condition monitoring of suspension systems is a novel and reliable technique, by virtue of modal shapes being independent of vehicle loads. The same cannot however be said for the frequency and damping ratio as they are subject to changes dependent on the vehicle loads.

#### **Novelty Two:**

In the mathematical model, the way in which the vibration signal is calculated for each corner of the vehicle is a novel. That allows the translation of the vibration signals from centre of the model to each corner of the vehicle, in order to simulate each side of suspension and achieve a more reliable and accurate parameter identification.

#### **Novelty Three:**

With specific reference to the simulation, the way in which the rolling modal energy differences for the front and rear of the bounce and pitch modes have been calculated is entirely novel.

#### **Novelty Four:**

The vibration signal which has been analysed using an average correlation signal based stochastic subspace identification (ACS-SSI) for online vehicle dynamics analysis is novel, because the previous research has validated the effectiveness of ACS-SSI for the cases when the vibration responses are in a high frequency range ( $>10\text{Hz}$ ) and modal damping ratio is less than 10%, which are typical properties of vehicle frames. However, it has not been verified that the method is applicable to the scenarios of low frequency and high damping systems. Typically, the suspension damping ratios are about 10% to 30% and the frequency range is from 0.5 to 3 Hz. Therefore, this study has verified this new approach in conjunction with necessary improvements to the ACS-SSI in dealing with the low frequency high damping scenarios.

#### **9.4 Future Work Recommendations for On-Line Condition Monitoring of Suspension**

**Recommendation 1:** During the 4-post experimental work, it has been noted that the test vehicle has some horizontal movement which was combined with the vertical movement. In this case, a dual vibration sensor is recommended to be used in the future to collect all the vibration signals affecting the vehicle body.

**Recommendation 2:** Almost all modern vehicles have an Anti-lock Braking System (ABS), and this system has its own sensors. In future work, these sensors are recommended to be used in order to measure the acceleration of the vehicle at the four corners, reducing the cost of the measurement system.

**Recommendation 3:** The analysed fault handling strategies show promising results and encourage future research in this area including vehicle validation. This could be conducted in a simulation of other suspension types include semi-active and active suspensions. Different active and semi-active fault-tolerant control strategies that are applicable for real-time applications should be investigated and compared to one another.

**Recommendation 4:** Future investigation is needed to analyse the performance of suspension with different vehicles. This can be achieved by conducting road experiments for different vehicles, for example by testing active or semi-active suspension and then making a comparison with the passive systems.

**Recommendation 5:** Energy regeneration systems and active suspension schemes should be investigated and integrated with online condition monitoring systems to provide a more intelligent suspension system, for example by testing active or semi-active suspension and then making a comparison with the passive systems.

## References:

- Abdelghani, M., Verhaegen, M., Van Overschee, P., & De Moor, B. (1998). COMPARISON STUDY OF SUBSPACE IDENTIFICATION METHODS APPLIED TO FLEXIBLE STRUCTURES. *Mechanical Systems and Signal Processing*, 12(5), 679–692.
- Agharkakli, A., Sabet, G., & Barouz, A. (2012). Simulation and Analysis of Passive and Active Suspension System Using Quarter Car Model for Different Road Profile. *International Journal of Engineering Trends and Technology*-, 3(5).
- Ahmad Faheem, Fairoz Alam, & Thomas, V. (2006, December). The suspension dynamic analysis for a quarter car model and half car model. Retrieved 28 August 2013
- Al-Arbi, S. (2012, August). *Condition Monitoring of Gear Systems using Vibration Analysis* (doctoral). University of Huddersfield
- Al-Ghamd, A. M., & Mba, D. (2006). A comparative experimental study on the use of acoustic emission and vibration analysis for bearing defect identification and estimation of defect size. *Mechanical Systems and Signal Processing*, 20(7), 1537–1571.
- Al-Solihat, M. K., Rakheja, S., & Ahmed, A. K. W. (2010). Influence of tyre pressure on an urban bus transient and steady state handling performance. *Proceedings of the Institution of Mechanical Engineers, Part D: Journal of Automobile Engineering*, 224(7), 893–908.
- Aly, A. A., & Salem, F. A. (2013). Vehicle Suspension Systems Control: A Review. *Research Publisher Inc.*, 2.
- AMBEKAR, A. G. (2006). *MECHANICAL VIBRATIONS AND NOISE ENGINEERING*. PHI Learning Pvt. Ltd.
- Andersen, E. (2007, August 3). Multibody Dynamics Modeling and System Identification for a Quarter-Car Test Rig with McPherson Strut Suspension. Retrieved 13 May 2015
- Antonacci, E., De Stefano, A., Gattulli, V., Lepidi, M., & Matta, E. (2012). Comparative study of vibration-based parametric identification techniques for a three-dimensional frame structure. *Structural Control and Health Monitoring*, 19(5), 579–608
- Arıkan, K. B., Ünlüsoy, Y. S., Korkmaz, İ., & Çelebi, A. O. (2008). Identification of linear handling models for road vehicles. *Vehicle System Dynamics*, 46(7), 621–645.

- Austerlitz, H. (2002). *Data Acquisition Techniques Using PCs, Second Edition* (2 edition). Amsterdam: Academic Press.
- Bertram, T., Bekes, F., Greul, R., Hanke, O., Haß, C., Hilgert, J., ... Ward, D. (2003). Modelling and simulation for mechatronic design in automotive systems. *Control Engineering Practice*, *11*(2), 179–190
- Börner, M., Isermann, R., & Schmitt, M. (2002). *A Sensor and Process Fault Detection System for Vehicle Suspension Systems* (SAE Technical Paper No. 2002-01-0135). Warrendale, PA: SAE International
- Börner, M., Straky, H., Weispfenning, T., & Isermann, R. (2002). Model based fault detection of vehicle suspension and hydraulic brake systems. *Mechatronics*, *12*(8), 999–1010.
- Borutzky, W. (2014). *Bond Graph Model-based Fault Diagnosis of Hybrid Systems*. Springer.
- Breytenbach, B., & Els, P. S. (2011). Optimal vehicle suspension characteristics for increased structural fatigue life
- Carden, E. P., & Fanning, P. (2004). Vibration Based Condition Monitoring: A Review. *Structural Health Monitoring*, *3*(4), 355–377
- Chamseddine, A., & Noura, H. (2008). Control and Sensor Fault Tolerance of Vehicle Active Suspension. *IEEE Transactions on Control Systems Technology*, *16*(3), 416–433.
- Chang, C., & Sun, C. T. (1988). Acoustic emissions and transient elastic waves in an orthotropic laminate plate. *Composites Science and Technology*, *33*(3), 213–236.
- Chen, J., & Patton, R. J. (2012). *Robust Model-Based Fault Diagnosis for Dynamic Systems*. Springer Science & Business Media.
- Chen, Z., Wang, T., Gu, F., Zhang, R., Chen, Z., Wang, T., ... Zhang, R. (2015). Characterizing the Dynamic Response of a Chassis Frame in a Heavy-Duty Dump Vehicle Based on an Improved Stochastic System Identification. *Shock and Vibration*, *Shock and Vibration*, *2015*, 2015, e374083.
- Chiang, D.-Y., & Lin, C.-S. (2011a). Identification of modal parameters from ambient vibration data using eigensystem realization algorithm with correlation technique. *Journal of Mechanical Science and Technology*, *24*(12), 2377–2382

- Chiang, D.-Y., & Lin, C.-S. (2011b). Identification of modal parameters from ambient vibration data using eigensystem realization algorithm with correlation technique. *Journal of Mechanical Science and Technology*, 24(12), 2377–2382.
- Chouvion, B. (2010, January). *Vibration Transmission and Support Loss in MEMS Sensors*. University of Nottingham.
- Cornelius, S., & Paresh, G. B. (2004). *Practical Machinery Vibration Analysis and Predictive Maintenance*.
- Coulter, J. (2006, November 30). Process and method for safer vehicle navigation through facial gesture recognition and operator condition monitoring.
- Cronin, D. L. (1981). MacPherson strut kinematics. *Mechanism and Machine Theory*, 16(6), 631–644.
- Darryl Brian, P. (2008, June 3). *Estimation of Uncertain Vehicle Center of Gravity using Polynomial Chaos Expansions*. Virginia Polytechnic Institute and State University.
- Darus, R., & Sam, Y. M. (2009). Modeling and control active suspension system for a full car model. In *5th International Colloquium on Signal Processing Its Applications, 2009. CSPA 2009* (pp. 13–18)
- Davies, A. (1998). Visual inspection systems. In A. Davies (Ed.), *Handbook of Condition Monitoring* (pp. 57–77). Springer Netherlands
- Daws, J. (2010). Inflation Pressures for Plus - Size Fitments. *International Tire Exhibition and Conference*.
- DeCoursey, W. (2003). *Statistics and Probability for Engineering Applications*. Newnes.
- D. J. COLE, D. C. (1992). Validation of an Articulated Vehicle Simulation. *Vehicle System Dynamics - VEH SYST DYN*, 21(1), 197–223
- Döhler, M. (2011, October 10). *Subspace-based system identification and fault detection: Algorithms for large systems and application to structural vibration analysis* (phdthesis). Université Rennes 1.
- Döhler, M., Andersen, P., & Mevel, L. (2012). Operational Modal Analysis Using a Fast Stochastic Subspace Identification Method. In R. Allemang, J. D. Clerck, C. Niezrecki, & J. R. Blough (Eds.), *Topics in Modal Analysis I, Volume 5* (pp. 19–24). Springer New York.

- Dong, G., Chen, J., & Zhang, N. (2014). Investigation into on-road vehicle parameter identification based on subspace methods. *Journal of Sound and Vibration*, 333(24), 6760–6779.
- Efthymiou, K., Papakostas, N., Mourtzis, D., & Chryssolouris, G. (2012). On a Predictive Maintenance Platform for Production Systems. *Procedia CIRP*, 3, 221–226.
- Ertas, A. (2011). *Engineering Mechanics and Design Applications: Transdisciplinary Engineering Fundamentals*. CRC Press.
- Eslaminasab, N., Biglarbegian, M., Melek, W. W., & Golnaraghi, M. F. (2007). A neural network based fuzzy control approach to improve ride comfort and road handling of heavy vehicles using semi-active dampers. *International Journal of Heavy Vehicle Systems*, 14(2), 135–157.
- Eslaminasab, N., & Golnaraghi, F. (2009). A semi-active control strategy for vibration isolation to improve the ride comfort of vehicles. *International Journal of Modelling, Identification and Control*, 7(3), 282–293.
- Ewins, D. . J. (2000). *Modal Testing: Theory, Practice and Application* (Second Edition). Baldock, Hertfordshire, England: RESEARCH STUIES PRESS LTD.
- Eykhoff, P. (1974). *System Identification: Parameter and State Estimation*. Wiley-Interscience.
- Fan, W., & Qiao, P. (2011). Vibration-based Damage Identification Methods: A Review and Comparative Study. *Structural Health Monitoring*, 10(1), 83–111.
- Farrar, C. R., Doebling, S. W., & Nix, D. A. (2001). Vibration–based structural damage identification. *Philosophical Transactions of the Royal Society of London A: Mathematical, Physical and Engineering Sciences*, 359(1778), 131–149.
- Farrar, C. R., & James III, G. H. (1997). SYSTEM IDENTIFICATION FROM AMBIENT VIBRATION MEASUREMENTS ON A BRIDGE. *Journal of Sound and Vibration*, 205(1), 1–18
- Fenton, J. (1996). *Handbook of Vehicle Design Analysis*. Mechanical Engineering Publication Limited.
- Fijalkowski, B. T. (2011). *Automotive Mechatronics—Operational and Practical Issues*. Volumes I and II. *Automotive Mechatronics: Operational and Practical Issues Volume II*, 259.

- Fischer, D., Börner, M., Schmitt, J., & Isermann, R. (2007). Fault detection for lateral and vertical vehicle dynamics. *Control Engineering Practice*, 15(3), 315–324.
- Fischer, D., & Isermann, R. (2004). Mechatronic semi-active and active vehicle suspensions. *Control Engineering Practice*, 12(11), 1353–1367.
- Fitch, J. W. (1994). *Motor Truck Engineering Handbook*. Society of Automotive Engineers.
- Fleming, W. J. (2001). Overview of automotive sensors. *IEEE Sensors Journal*, 1(4), 296–308.
- Frank, P. M. (1990). Fault diagnosis in dynamic systems using analytical and knowledge-based redundancy: A survey and some new results. *Automatica*, 26(3), 459–474.
- Gáspár, P., & Nadai, L. (2007a). Estimation of dynamical parameters of road vehicles on freeways. In *Intelligent Systems and Informatics, 2007. SISY 2007. 5th International Symposium on* (pp. 107–112). IEEE.
- Gáspár, P., & Nadai, L. (2007b). Parameter estimation of coupled road-vehicle systems. In *Soft Computing Applications, 2007. SOFA 2007. 2nd International Workshop on* (pp. 199–204). IEEE.
- Gawade, T. R., Mukherjee, S., & Mohan, D. (2004). Wheel lift-off and ride comfort of three-wheeled vehicle over bump. *Journal of the Institution of Engineers(India), Part MC, Mechanical Engineering Division*, 85, 78–87.
- Gilles, T. (2005). *Automotive Chassis: Brakes, Suspension, and Steering*. Cengage Learning.
- Grieger, M., & Gutzmann, U. (2015). *From the Beetle of a Global Player: Volkswagen Chronicle*. Wolfsburg: VOLKSWAGEN.
- Gu, F., Li, W., Ball, A. D., & Leung, A. Y. T. (2000). *The Condition Monitoring of Diesel Engines Using Acoustic Measurements Part 1: Acoustic Characteristics of the Engine and Representation of the Acoustic Signals* (SAE Technical Paper No. 2000-01-0730). Warrendale, PA: SAE International.
- Guglielmino, E., Sireteanu, T., Stammers, C., Ghita, G., & Giuclea, M. (2008). *Semi-active Suspension Control*. London: Springer London.

- Hamed, M., Tesfa, B., Fengshou, G., & Ball, A. (2014). A study of the Suspension System for the Diagnosis of Dynamic Characteristics. *International Journal of Automation and Computing*, 11(3).
- Hamed, M., Tesfa, B., Gu, F., & Ball, A. (2013). A study of the influence of vehicle tyre pressure on suspension system response using a full car model. In G. Lucas (Ed.), *Proceedings of Computing and Engineering Annual Researchers' Conference 2013 : CEARC'13* (pp. 7–12). Huddersfield: University of Huddersfield.
- Hamed, M., Tesfa, B., Gu, F., & Ball, A. (2014, June). *Effects of Tyre Pressure on Vehicle Suspension Performance*. Conference presented at the World Symposium on Mechanics Engineering & Applied Physics ( WSMAEP'14), Sousse, Tunisia.
- Herlufsen, H. (2004). Modal Analysis using Multi-reference and Multiple-Input Multiple-Output Techniques. *Brüel & Kjær, Application Note*.
- Heydinger, G. J., Schwarz, C., Salaani, M. K., & Grygier, P. A. (2007). *Model Validation of the 2006 BMW 330i for the National Advanced Driving Simulator* (SAE Technical Paper No. 2007-01-0817). Warrendale, PA: SAE Technical Paper.
- Huang, W., & Su, X. (2015). Design of a Fault Detection and Isolation System for Intelligent Vehicle Navigation System. *International Journal of Navigation and Observation*, 2015, e279086.
- Hu, H.-X. (1993). *Experimental Validation of a Half-Vehicle Suspension Model* (SAE Technical Paper No. 931966). Warrendale, PA: SAE Technical Paper.
- Ikenaga, S., Lewis, F. L., Campos, J., & Davis, L. (2000). Active suspension control of ground vehicle based on a full-vehicle model. In *American Control Conference, 2000. Proceedings of the 2000* (Vol. 6, pp. 4019–4024 vol.6).
- International Energy Agency. (2006). World Energy Outlook 2006. Retrieved 20 August 2013,
- Irvine, T. (2000). an Introduction to Frequency Response Functions. *Rapport, College of Engineering and Computer Science*.
- Isermann, R. (1984). Process Fault Detection Based on Modeling and Estimation methods-A Survey. *Automatica*, 20(4), 387–404.

- Isermann, R. (2005). Model-based fault-detection and diagnosis – status and applications. *Annual Reviews in Control*, 29(1), 71–85.
- Isermann, R. (2011). *Fault-Diagnosis Applications*. Berlin, Heidelberg: Springer Berlin Heidelberg.
- Jain, K. K., & Asthana, R. B. (2002). *Automobile Engineering* (Fourth reprinte 2006). Tata McGraw-HILL
- Jardine, A. K. S., Lin, D., & Banjevic, D. (2006). A review on machinery diagnostics and prognostics implementing condition-based maintenance. *Mechanical Systems and Signal Processing*, 20(7), 1483–1510.
- Jayaswal, P., Wadhvani, A. K., & Mulchandani, K. B. (2008). Machine Fault Signature Analysis. *International Journal of Rotating Machinery*, 2008, e583982.
- J Chen, R. J. P. (1999). Robust Model-Based Fault Diagnosis for Dynamic Systems.
- Jemielniak, K. (2014). Commercial Tool Condition Monitoring Systems. *The International Journal of Advanced Manufacturing Technology*, 15(10), 711–721.
- Jeppesen, B. P., & Cebon, D. (2009). Application of observer-based fault detection in vehicle roll control. *Vehicle System Dynamics*, 47(4), 465–495.
- John, H. (2010). Good Garages. Retrieved 28 August 2013,
- Jorge de-J. Lozoya-Santos, J. C. T.-M. (2012). Fault Detection in an Automotive MR Damper.
- Juang, J.-N., Cooper, J. E., & Wright, J. R. (1987). An eigensystem realization algorithm using data correlations (ERA/DC) for modal parameter identification.
- Kashi, K., Nissing, D., Kesselgruber, D., & Soffker, D. (2006). Diagnosis of active dynamic control systems using virtual sensors and observers. In *2006 IEEE International Conference on Mechatronics* (pp. 113–118).
- Kim, C., Ro, P. I., & Kim, H. (1999). Effect of the suspension structure on equivalent suspension parameters. *Proceedings of the Institution of Mechanical Engineers, Part D: Journal of Automobile Engineering*, 213(5), 457–470.
- Kim, E. Y., Tan, A. C., Yang, B.-S., & Kosse, V. (2007). Experimental study on condition monitoring of low speed bearings: time domain analysis.

- Kim, H., & Lee, H. (2011). Model-based fault-tolerant control for an automotive air suspension control system. *Proceedings of the Institution of Mechanical Engineers, Part D: Journal of Automobile Engineering*, 0954407011418882.
- Kim, J., & Lynch, J. P. (2012). Subspace system identification of support-excited structures—part I: theory and black-box system identification. *Earthquake Engineering & Structural Dynamics*, 41(15), 2235–2251.
- Kutluay, E. (2013). *Development and Demonstration of a Validation Methodology for Vehicle Lateral Dynamics Simulation Models*. VDI-Verlag.
- Lajqi, S., & Pehan, S. (2012). Designs and optimizations of active and semi-active non-linear suspension systems for a terrain vehicle. *Strojniški Vestnik-Journal of Mechanical Engineering*, 58(12), 732–743.
- Lajqi, S., Pehan, S., Lajqi, N., Gjelaj, A., Pšeničnik, J., & Sašo, E. (2012). Design of independent suspension mechanism for a terrain vehicle with four wheels drive and four wheels steering. In *MOTSP Conference Proceedings* (pp. 230–237).
- Lau, J., Lanslots, J., P, B., & Auweraer, H. (2007). Automatic modal analysis: reality or myth? Presented at the IMAC 25, Orlando, USA, USA.
- Lew, J.-S., Juang, J.-N., & Longman, R. W. (1993). Comparison Of Several System Identification Methods For Flexible Structures. *Journal of Sound and Vibration*, 167(3), 461–480.
- Li, M. (2010). Structural Health Monitoring using Index Based Reasoning for Unmanned Aerial Vehicles. *ProQuest ETD Collection for FIU*, 1–163.
- Liu, Y. (2008). Recent Innovations in Vehicle Suspension Systems. *Recent Patents on Mechanical Engineering*, 1(3), 206–210.
- Londono, N. A., Desjardins, S. L., & Lau, D. T. (2004). Use of Stochastic Subspace Identification Methods for Post-Disaster Condition Assessment of Highway Bridges. In *Proceedings of 13th World Conference on Earthquake Engineering, Vancouver, BC, Canada*.
- Lu, F., Ishikawa, Y., Kitazawa, H., & Satake, T. (2010). Effect of vehicle speed on shock and vibration levels in truck transport. *Packaging Technology and Science*, 23(2), 101–109.

- Maher, D. (2011). *Combined Time and Frequency Domain Approaches to the Operational Identification of Vehicle Suspension Systems*. School of Mechanical and Manufacturing Engineering, Dublin City University, Dublin 9, Ireland.
- Maia, N. M. M. (1997). *Theoretical and Experimental Modal Analysis*. Wiley-Blackwell.
- Malekzadeh, S., & Ghaffari, A. (2015). Actuator fault reconstruction in an 8-DOF vehicle active suspension system using sliding mode observer. *International Journal of Vehicle Safety*, 8(2), 101
- Matschinsky, W. (2000). Road vehicle suspensions.
- Mba, D. (2006). Development of Acoustic Emission Technology for Condition Monitoring and Diagnosis of Rotating Machines: Bearings, Pumps, Gearboxes, Engines, and Rotating Structures. *The Shock and Vibration Digest*, 38(1), 3–16.
- McGrail, T. (1998). Condition monitoring-a user perspective. In *1998/448), IEE Colloquium on HV Measurements, Condition Monitoring and Associated Database Handling Strategies (Ref. No* (pp. 1/1–1/3).
- Mee, D. J. (2003). Dynamic calibration of force balances for impulse hypersonic facilities. *Shock Waves*, 12(6), 443–455.
- Metallidis, P., Verros, G., Natsiavas, S., & Papadimitriou, C. (2003). Fault Detection and Optimal Sensor Location in Vehicle Suspensions. *Journal of Vibration and Control*, 9(3-4), 337–359.
- Milliken, W. F., & Milliken, D. L. (1995). *Race car vehicle dynamics* (Vol. 400). Society of Automotive Engineers Warrendale.
- Ming, Y., Xiqiang, G., Zhang, J.-W., Guan, X.-Q., & Yuan, M. (2011). Application of subspace-based method in vehicle handling dynamic model identification and properties estimation. *International Journal of Vehicle Design*, 56(1), 125–145.
- Mitra, A., Benerjee, N., Khalane, H., Sonawane, M., Joshi, D., & Bagul, G. (2013). Simulation and Analysis of Full Car Model for various Road profile on a analytically validated MATLAB/SIMULINK model. *IOSR Journal of Mechanical and Civil Engineering (IOSR-JMCE)*, 22–33.

- Mohanty, P., & Rixen, D. J. (2005). Identifying mode shapes and modal frequencies by operational modal analysis in the presence of harmonic excitation. *Experimental Mechanics*, 45(3), 213–220.
- Moncada, H. B., & Marin, J. A. (2011). Fault Detection for a Bus Suspension Model Using an Utkin Observer. In *2011 IEEE Electronics, Robotics and Automotive Mechanics Conference (CERMA)* (pp. 246–251)
- Mondal, S., Chakraborty, G., & Bhattacharyya, K. (2008). Fault detection and isolation of vehicle suspension system using robust unknown input observers. *International Journal of Vehicle Systems Modelling and Testing*, 3(4), 331.
- NALECZ, A. G., LU, Z., & D'ENTREMONT, K. L. (1994). Development and Experimental Validation of Advanced Dynamic Vehicle Simulation (ADVS). *Vehicle System Dynamics*, 23(sup1), 390–410.
- Nandi, S., Toliyat, H. A., & Li, X. (2005). Condition monitoring and fault diagnosis of electrical motors-a review. *IEEE Transactions on Energy Conversion*, 20(4), 719–729.
- Ngigi, R. W., Pislaru, C., Ball, A., & Gu, F. (2012). Modern techniques for condition monitoring of railway vehicle dynamics. *Journal of Physics: Conference Series*, 364(1), 012016.
- Norton, M. P., & Karczub, D. G. (2003). *Fundamentals of Noise and Vibration Analysis for Engineers* (2 edition). Cambridge University Press.
- Nouby M Ghazaly, A. O. M. (2014). The Future Development and Analysis of Vehicle Active Suspension System. *IOSR Journal of Mechanical and Civil Engineering (IOSR-JMCE)*, 11(5), 19–25.
- Packard, H. (1997a). *Effective Machinery Measurements using Dynamic Signal Analysis* (Application Note 243-1 No. Application Note 243-1). Application Note 243-1.
- Packard, H. (1997b). *The fundamentals of modal testing*. application note 243-3.
- Paine, M., Griffiths, M., & Magedara, N. (2007). The role of tyre pressure in vehicle safety, injury and environment. *Heads of Compulsory Third Party Insurance in Australia and New Zealand*.
- Patil, K. S., Jagtap, V., Jadhav, S., Bhosale, A., & Kedar, B. (2013). Performance Evaluation of Active Suspension for Passenger Cars Using MATLAB. In *Second National Conference on*

- Recent Developments in Mechanical Engineering, IOSR Journal of Mechanical and Civil Engineering* (pp. 06–14).
- Patton, R. J., Frank, P. M., & Clark, R. N. (Eds.). (2000). *Issues of Fault Diagnosis for Dynamic Systems*. London: Springer London.
- Peden, M. (2004). World report on road traffic injury prevention. WHO Library Cataloguing.
- Peeters, B. (2000). System Identification and Damage Detection in Civil Engineering.
- Peeters, B., & De Roeck, G. (2001). Stochastic System Identification for Operational Modal Analysis: A Review. *Journal of Dynamic Systems, Measurement, and Control*, 123(4), 659–667.
- Peeters, B., De Roeck, G., Pollet, T., & Schueremans, L. (2000). Stochastic Subspace Techniques Applied To Parameter Identification Of Civil Engineering Structures.
- Persson, N., & Gustafsson, F. (2002). 2002-01-1250 Indirect Tire Pressure Monitoring Using Sensor Fusion. *Society of Automotive Engineers World Congress*.
- Peters, L., Beck, K., & Camposano, R. (1993). Adaptive fuzzy controller improves comfort. In *Fuzzy Systems, 1993., Second IEEE International Conference on* (pp. 512–515). IEEE.
- Petsounis, K. onstantinos, & Fassois, S. (2001). CRITICAL COMPARISON OF PARAMETRIC TIME DOMAIN METHODS FOR THE IDENTIFICATION OF VIBRATING STRUCTURES: *P Art of an in Vited Paper to Appear in the J Ournal of Mec Hanical Systems and Signal Pr Ocessing (Academic Press)*.
- Prawoto, Y., Ikeda, M., Manville, S. K., & Nishikawa, A. (2008). Failure Analysis of Automotive Suspension Coil Springs. *Iron & Steel Technology*, 5(9), 35–48.
- Pridham, B. A., & Wilson, J. C. (2003). A study of damping errors in correlation-driven stochastic realizations using short data sets. *Probabilistic Engineering Mechanics*, 18(1), 61–77.
- Prosser, S. J. (2007). Automotive sensors: past, present and future. *Journal of Physics: Conference Series*, 76(1), 012001.
- Qazi, A. J., de Silva, C. W., Khan, A., Khan, M. T., Qazi, A. J., de Silva, C. W., ... Khan, M. T. (2014). Performance Analysis of a Semiactive Suspension System with Particle Swarm Optimization and Fuzzy Logic Control, Performance Analysis of a Semiactive Suspension

- System with Particle Swarm Optimization and Fuzzy Logic Control. *The Scientific World Journal, The Scientific World Journal*, 2014, 2014, e174102.
- Rakheja, S., Cao, D., & Wang, Z. (2011). Urban bus driver ride and road–friendliness. Part I: Model development and role of operating parameters. *International Journal of Vehicle Design*, 57(4), 305–332.
- Randall, R. B. (2011). *Vibration-based Condition Monitoring: Industrial, Aerospace and Automotive Applications - Robert Bond Randall*. John Wiley & Sons
- Rao, R., Ram, T., Rao, k, & Rao, P. (2010, October). Analysis of passive and semi active controlled suspension systems for ride comfort in an omnibus passing over a speed bump. Retrieved 28 August 2013,
- Rao, S. S. (2004). *Mechanical Vibrations, Fourth International Edition*. Pearson Prentice Hall, Pearson Education, Inc. Upper Saddle River NJ07458.
- Rehnberg, A. (2008). Vehicle dynamic analysis of wheel loaders with suspended axles.
- Richardson, M. H., & Formenti, D. L. (1982). Parameter estimation from frequency response measurements using rational fraction polynomials. In *Proceedings of the International Modal Analysis Conference* (pp. 167–182).
- Rievaj, V., Vrabel, J., & Hudak, A. (2013). Tire Inflation Pressure Influence on a Vehicle Stopping Distances. Retrieved 28 August 2013
- Russo M, R. R. (2000). Car Parameters Identification by Handling Manoeuvres. *Vehicle System Dynamics*, 34(6), 423–436.
- Sabarirajan, S., Sarathkumar, K., Makesh Kumar, M., Bharanidharan, S., & Vinothkumar, C. (2015). Design and Analysis of Heavy Vehicle Leaf Spring Suspension System by Using FEA. *International Journal on Applications in Science, Engineering & Technology*, 1(4), pp.40–46.
- Saeed, A. (2008). *Online condition monitoring system for wind turbine*. Blekinge Institute of Technology.
- Sahoo, N., Babu, P. R., Sahoo, N., & Babu, P. R. (2014). Calibration Technique for Recovery of Short Duration Aerodynamic Force, Calibration Technique for Recovery of Short Duration

- Aerodynamic Force. *Journal of Aerodynamics, Journal of Aerodynamics*, 2014, 2014, e574520.
- Salaani, M. K., Schwarz, C., Heydinger, G. J., & Grygier, P. A. (2007). *Parameter Determination and Vehicle Dynamics Modeling for The National Advanced Driving Simulator of the 2006 BMW 330i* (SAE Technical Paper No. 2007-01-0818). Warrendale, PA: SAE Technical Paper.
- Sayers, M., & Karamihas, S. (1998). *The Little Book of Profiling Basic Information about Measuring and Interpreting Road Profiles*. The Regent of the University of Michigan.
- Sekulic, D., & Dedovic, V. (2011). The Effect of Stiffness and Damping of the Suspension System Elements on the Optimisation of the Vibrational Behaviour of a Bus. *International Journal for Traffic and Transport Engineering*, 1(4).
- Serridge, M., & Licht, T. R. (1987). *Piezoelectric accelerometers and vibration preamplifiers: theory and application handbook*.
- Shreve, D. H. (1995). *Signal processing for effective vibration analysis. IRD Mechanalysis Inc., Columbus, OH, USA*.
- Silva, L., Delarmelina, D., Junco, S., M'sirdi, N. K., & Noura, H. (2007). Bond Graph Based Fault Diagnosis of 4W-Vehicles Suspension Systems I: Passive Suspensions. SIMULATION COUNCILS, INC.
- Siringoringo, D. M., & Fujino, Y. (2008). System identification of suspension bridge from ambient vibration response. *Engineering Structures*, 30(2), 462–477.
- Smith, W. A., & Zhang, N. (2009). Recent developments in passive interconnected vehicle suspension. *Frontiers of Mechanical Engineering in China*, 5(1), 1–18.
- Sternberg, E. R. (1976). *Heavy-Duty Truck Suspensions* (SAE Technical Paper No. 760369). Warrendale, PA: SAE International. Retrieved from <http://papers.sae.org/760369/>
- Steven R Anton, H. A. S. (2007). A Review of Power Harvesting Using Piezoelectric Materials (2003-2006). *Smart Materials and Structures*, 16(3), R1.
- Thomson, W. (1996). *Theory of Vibration with Applications*. CRC Press.

- Tingtao, Z., Tianyu, L., Ke, C., & Xiaoguang, H. (2011). On-line monitoring system of insulator leakage current based on ARM. In *2011 6th IEEE Conference on Industrial Electronics and Applications (ICIEA)* (pp. 365–369).
- Tudon Martinez, V. S. (2013). Fault Tolerant Control with Additive Compensation for Faults in an Automotive Damper.
- Tyan, F., Hong, Y.-F., Tu, S.-H., & Jeng, W. S. (2009). Generation of random road profiles. *Journal of Advanced Engineering*, *4*(2), 1373–1378.
- Varrier, S., Morales-Menendez, R., Lozoya-Santos, J. D.-J., Hernandez, D., Molina, J. M., & Koenig, D. (2013). *Fault Detection in Automotive Semi-Active Suspension: Experimental Results* (SAE Technical Paper No. 2013-01-1234). Warrendale, PA: SAE International.
- Varrier, S., Vivas-Lopez, C. A., Lozoya-Santos, J. D.-J., Tudon M, J. C., Koenig, D., Martinez, J.-J., & Morales-Menendez, R. (2013). Applicative Fault Tolerant Control for semi-active suspension system: Preliminary results. In *Control Conference (ECC), 2013 European* (pp. 3803–3808).
- Venkatasubramanian, V., Rengaswamy, R., Yin, K., & Kavuri, S. N. (2003). A review of process fault detection and diagnosis: Part I: Quantitative model-based methods. *Computers & Chemical Engineering*, *27*(3), 293–311. [http://doi.org/10.1016/S0098-1354\(02\)00160-6](http://doi.org/10.1016/S0098-1354(02)00160-6)
- Vivekanandan, A. P. N., Gunaki, A., Acharya, C., Gilbert, S., & Bodake, R. (2014). DESIGN, ANALYSIS AND SIMULATION OF DOUBLE WISHBONE SUSPENSION SYSTEM. *IPASJ International Journal of Mechanical Engineering*, *2*(6).
- Wallentowitz, H. (2003). Vertical and Lateral Dynamics. *Kraftfahrwesen Aachen of RWTH Aachen University, Germany*.
- Wang, J. (2012). Nonlinear modeling and h-infinity model reference control of pneumatic suspension system.
- Wang, Q., McDaniel, J. G., & Wang, M. L. (2012). Dynamic tire pressure sensor for measuring ground vibration. *Sensors (Basel, Switzerland)*, *12*(11), 15192–15205.
- Wang, W. (2008). Condition-based Maintenance Modelling. In *Complex System Maintenance Handbook* (pp. 111–131). Springer London

- (Weidong), L., & Engineering, U. of M. M. S. of. (2000). *A Study of Diesel Engine Acoustic Characteristics*. University of Manchester.
- Weispfenning, T. (1997). Fault Detection and Diagnosis of Components of the Vehicle Vertical Dynamics. *Meccanica*, 32(5), 459–472.
- Wenzel, T. A., Burnham, K. J., Blundell, M. V., & Williams, R. A. (2006). Dual extended Kalman filter for vehicle state and parameter estimation. In *Vehicle system dynamics* (Vol. 44, pp. 153–171). Taylor & Francis.
- Williams, J. H., Davies, A., & Drake, P. R. (Eds.). (1994). *Condition-based Maintenance and Machine Diagnostics* (1994 edition). London: Springer.
- Wittbrodt, E., Adamiec, I., & Wojciech, S. (2006). *Dynamics of Flexible Multibody Systems - Rigid Finite Element Method*. Springer.
- Wong, J. Y. (2001). *Theory of Ground Vehicles*. John Wiley & Sons.
- Yang, X., Rakheja, S., & Stiharu, I. (1998). IDENTIFICATION OF LATERAL DYNAMICS AND PARAMETER ESTIMATION OF HEAVY VEHICLES. *Mechanical Systems and Signal Processing*, 12(5), 611–628.
- Yetendje, A., Seron, M., & Dona, D. (2007). Diagnosis and Actuator Fault Tolerant Control in Vehicle Active Suspension | San Francisco. Retrieved 9 March 2014,
- Zbiri, N., Rabhi, A., & M'Sirdi, N. K. (2004). Detection of critical situations for lateral vehicle control. *AVCS*, 4, 28–31.
- Zehsaz, M., Vakili-Tahami, F., & Paykani, A. (2014). Investigation on the Effects of Stiffness and Damping Coefficients of the Suspension System of a Vehicle on the Ride and Handling Performance, 76(1).
- Zhen, D. (2012, January). *A Study of Non-stationary Signal Processing for Machinery Condition Monitoring* (doctoral). University of Huddersfield.
- Zhu, X., Xia, Y., Chai, S., & Shi, P. (2014). A finite-frequency domain approach to fault detection filter design for vehicle active suspension systems. In *2014 11th World Congress on Intelligent Control and Automation (WCICA)* (pp. 485–490).

- Zohir, B. L. (2009). Ride Comfort Assessment in Off Road Vehicles using passive and semi-active suspension. Presented at the Asia pacific Conference on Defence & Security Technology.
- Zulkifli, N. (2012, June). Vibration investigation for passenger car with different damping characteristics on car suspension system [Undergraduates Project Papers]. Retrieved 16 August 2015,

# Appendixes

## Appendix A

### A-1. On road tests for repeatability

The experimental vehicle was driven on different road conditions. The data was collected from the four corners of the vehicle by using the vibration accelerometers as presented in Chapter 8. Figure A-1 shows the acceleration of the vehicle body for each side of the vehicle, these data was collected by driving the test vehicle on normal city road (Victoria road) in Huddersfield.

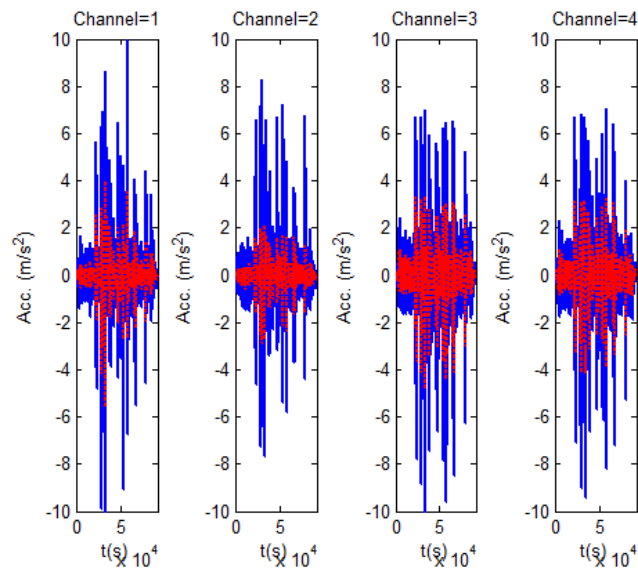


Figure A-1: Raw vibration signals of the four corner of the vehicle

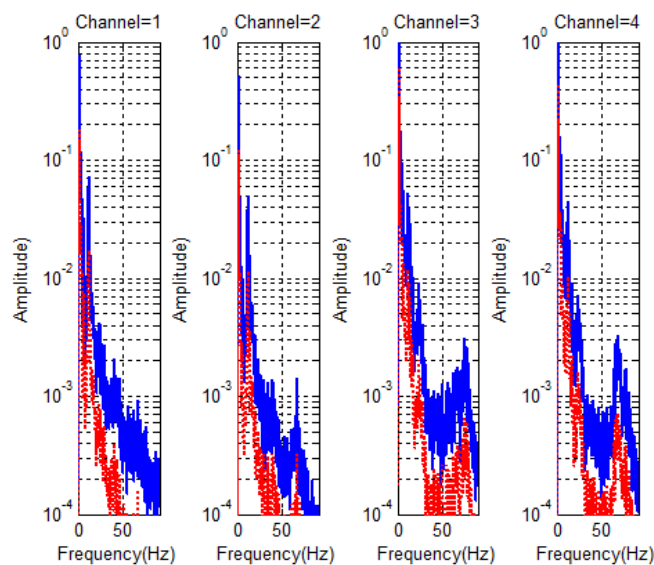


Figure A-2: Frequency Spectra of the collected signals

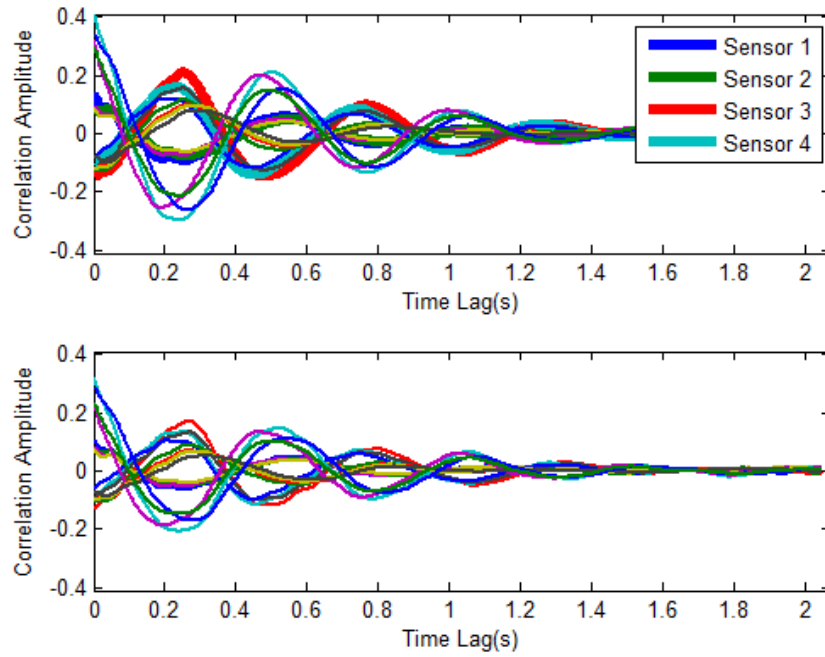


Figure A-3: Average scheme in the correlation lags domain for all sensors

The following data was collected by driving the test vehicle on rough road which is located within the premises of The University of Huddersfield. These tests have been conducted in order to examine the vibration responses of the vehicle when driven on different road conditions.

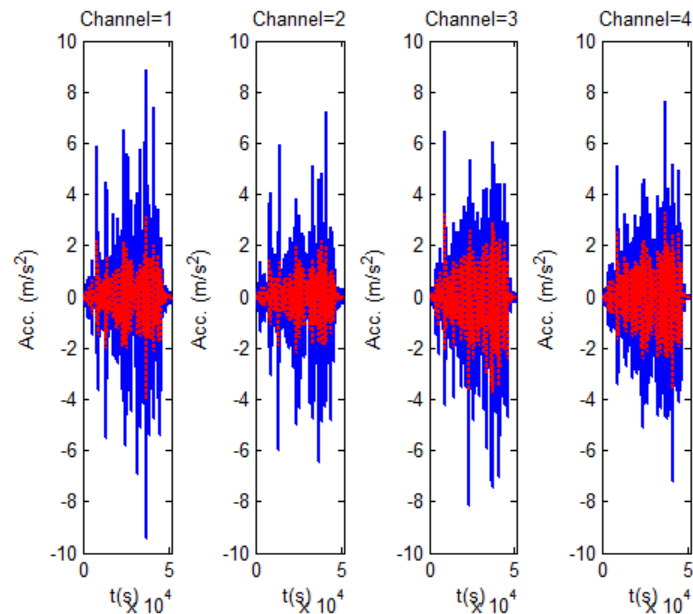


Figure A-4: Raw vibration signals of the four corner of the vehicle with different road conditions

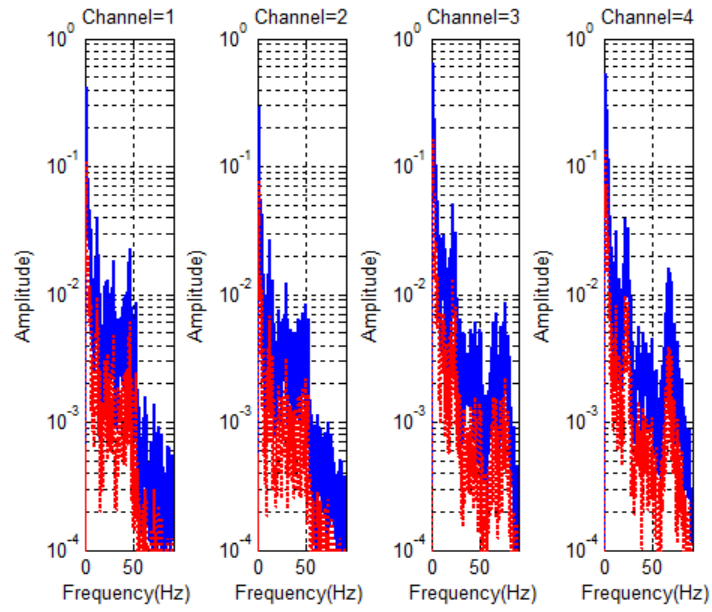


Figure A-5: Frequency Spectra of the signals

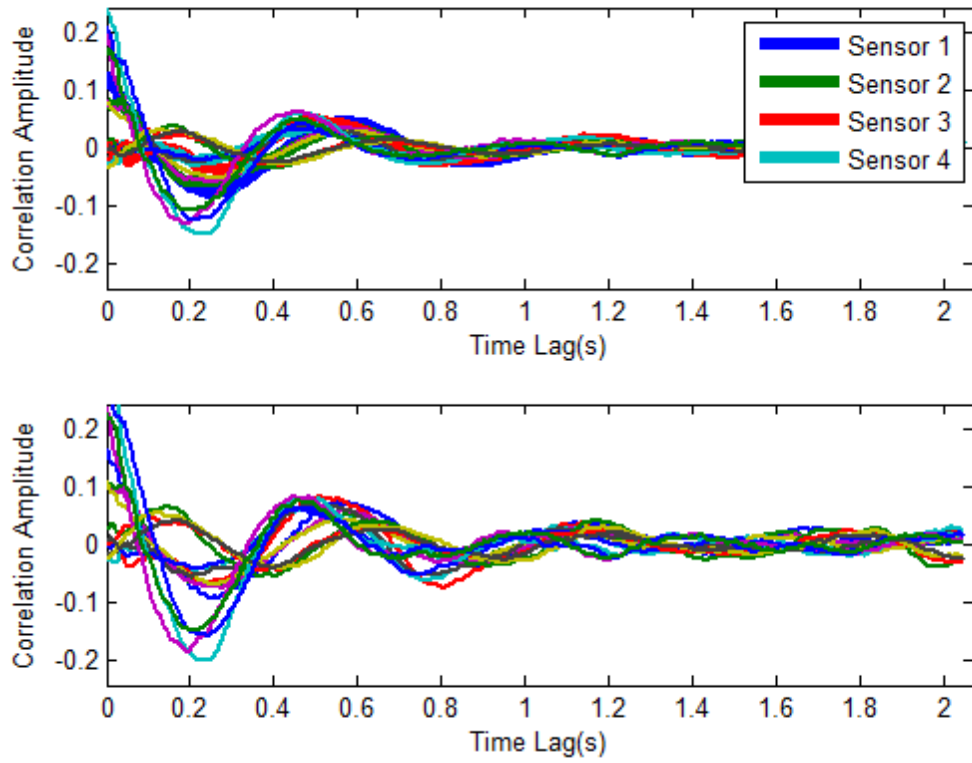


Figure A-6: Average scheme in the correlation lags domain for all sensors

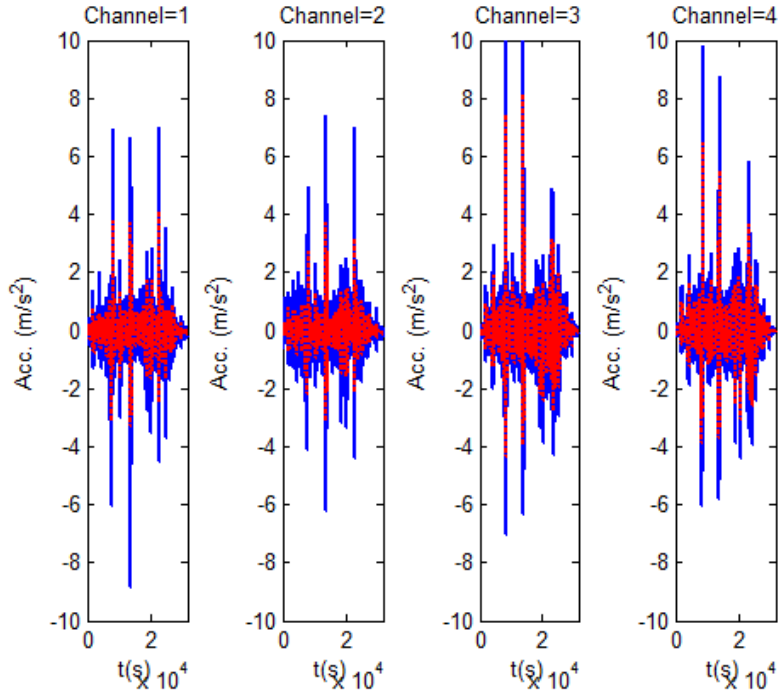


Figure A-7: Raw vibration signals of the four corner of the vehicle with different road conditions

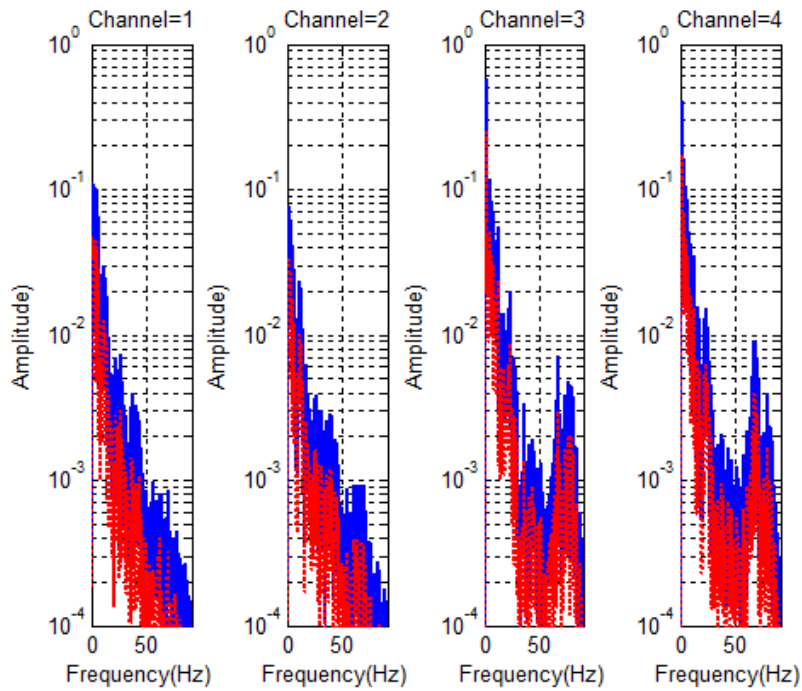


Figure A-8: Frequency Spectra of the signals

## Appendix B

### 4-POST TEST RIG



Figure B-1: 4-post rig at University of Huddersfield

### The main window and sub-windows in SERVO 4-post software

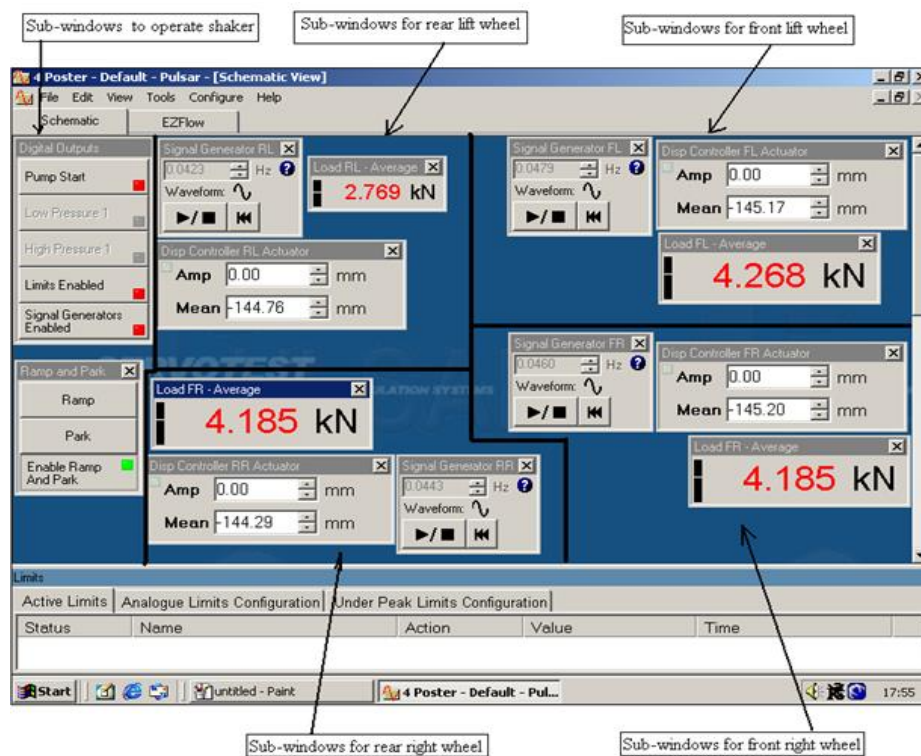


Figure B-2: the main window and sub-windows in SERVO 4-post software